

**NOVEL AZA-BODIPY DYES AND STUDY OF THEIR  
PHOTOPHYSICAL, PHOTODYNAMIC AND MOLECULAR  
RECOGNITION PROPERTIES**

THESIS SUBMITTED TO  
**THE UNIVERSITY OF KERALA**  
FOR THE DEGREE OF  
**DOCTOR OF PHILOSOPHY IN CHEMISTRY**  
UNDER THE FACULTY OF SCIENCE

*By*

**ADARSH N.**

**Photosciences and Photonics  
Chemical Sciences and Technology Division  
CSIR–National Institute for Interdisciplinary  
Science and Technology (CSIR–NIIST)  
Thiruvananthapuram-695 019, Kerala**

**MARCH 2015**

*Dedicated to my Appa, Amma, Ananthu and Chithra ....*

## **DECLARATION**

I hereby declare that the Ph. D. thesis entitled: **“NOVEL AZA-BODIPY DYES AND STUDY OF THEIR PHOTOPHYSICAL, PHOTODYNAMIC AND MOLECULAR RECOGNITION PROPERTIES”** is an independent work carried out by me and it has not been submitted anywhere else for any other degree, diploma or title.

**(ADARSH N.)**



डा. डी रमैया, एफ ए एससी  
निदेशक  
Dr. D. Ramaiah, F.A.Sc  
DIRECTOR

सीएसआईआर- उत्तर पूर्व विज्ञान तथा प्रौद्योगिकी संस्थान  
वैज्ञानिक तथा औद्योगिक अनुसंधान परिषद्  
जोरहाट-785006, आसाम, भारत

CSIR-NORTH EAST INSTITUTE OF SCIENCE & TECHNOLOGY  
COUNCIL OF SCIENTIFIC & INDUSTRIAL RESEARCH (CSIR)  
JORHAT-785006, ASSAM, INDIA



March 30, 2015

## CERTIFICATE

This is to certify that the work embodied in the thesis entitled: **“NOVEL AZA-BODIPY DYES AND STUDY OF THEIR PHOTOPHYSICAL, PHOTODYNAMIC AND MOLECULAR RECOGNITION PROPERTIES”** has been carried out by Mr. Adarsh N. under my supervision and guidance at the Photosciences and Photonics, Chemical Sciences and Technology Division of the CSIR-National Institute for Interdisciplinary Science and Technology (CSIR-NIIST), Trivandrum and the same has not been submitted elsewhere for a degree.

(D. Ramaiah)

Thesis Supervisor

*(Formerly, Head, Chemical  
Sciences and Technology Division,  
CSIR-NIIST, Trivandrum)*



## ACKNOWLEDGEMENTS

*It is my great pleasure to express my deep sense of gratitude to Dr. D. Ramaiah, my thesis supervisor, for suggesting the research problem and for his guidance, support and encouragement that led to the successful completion of this work.*

*I would like to express my sincere thanks to Professor M. V. George for being a source of motivation and encouragement during my stay at CSIR-NIIST.*

*I thank Dr. Suresh Das and Dr. B. C. Pai, former directors and Dr. Gangan Pratap, the Acting Director of the CSIR-National Institute for Interdisciplinary Science and Technology (CSIR-NIIST), Trivandrum, for providing the necessary facilities for carrying out this work.*

*I would like to thank Dr. A. Ajayaghosh, Dr. K. R. Gopidas, Dr. Joshy Joseph, Dr. K. George Thomas, Dr. A. Srinivasan, Dr. Narayan Unni, Dr. K. Yoosaf, Dr. C. Vijayakumar, Dr. B. Deb and Dr. V. Karunakaran, present and former Scientists of the Photosciences and Photonics, Chemical Sciences and Technology Division, for the help and support.*

*I sincerely thank Professor M. Radhakrishna Pillai, Dr. S. Asha Nair, Mr. P. S. Saneesh Babu, Rajiv Gandhi Centre for Biotechnology (RGCB), Trivandrum for the help in photobiological experiments.*

*I express my sincere thanks to Dr. Rekha Rachel Avirah for her generous support and care throughout my research career and I extend my thanks to Dr. Prakash, Dr. Jisha, Dr. Akhil, Dr. Suneesh, Dr. Sanju, Dr. Betsy, Mr. Nandajan, Ms. Dhanya, Mr. Albish, Mr. Hari Shankar, Mr. Shanmugasundaram, Ms. Viji, Mr. Shameel, Dr. Nidhi, Dr. Lavanya, Ms. Sreelekshmi, Ms. Rahi and Mr. Aswin for their valuable help.*

*I thank all the members of the Photosciences and Photonics and other Divisions of CSIR-NIIST for their help and cooperation. I would like to thank Mr. Robert Philip and Mr. Kiran for TEM and Mr. Chandran for SEM analysis. I also thank Mr. Adarsh, Ms. Saumini, Mr. Saran, Mr. Syam Ms. Viji, and Ms. Athira for NMR and mass spectral analyses.*

*Words are inadequate to express my gratitude to my family members who constantly stood as a source of encouragement and confidence. I take this opportunity to pay respect to all my teachers who guided and blessed me.*

*I thank Council of Scientific and Industrial Research (CSIR), UGC, and DST Government of India for financial assistance.*

**Adarsh N.**

# CONTENTS

	Page
<b>Declaration</b>	i
<b>Certificate</b>	ii
<b>Acknowledgements</b>	iii
<b>Contents</b>	iv
<b>Preface</b>	vii
<b>List of Figures</b>	xiii
<b>List of Tables</b>	xv
<b>List of Schemes</b>	xv
<b>List of Charts</b>	xvi
<b>List of Abbreviations</b>	xvii
<b>Chapter 1    Aza-BODIPY Dyes: Unveiling the Hidden Versatility</b>	
1.1            Introduction	1
1.2            BODIPY Dyes: Historical Developments	3
1.3            Aza-BODIPY -A Versatile Alternative to BODIPYs	10
1.3.1          Design and Synthetic Strategy of Aza-BODIPYs	11
1.3.2          Conformationally Restricted Aza-BODIPY Dyes	13
1.3.3          NIR Absorbing Aza-BODIPY Dyes	16
1.3.4          Aza-BODIPY Dyes as Singlet Oxygen Sensitizers	18
1.3.5          Aza-BODIPY Dyes as Chemosensors	20
1.3.6          Aza-BODIPY Dyes as Energy Transfer Cassettes	23
1.3.7          Aza-BODIPY Dyes as Therapeutic Agents	27
1.3.8          Photovoltaic Applications of Aza-BODIPY Dyes	29
1.4            Objectives of the Present Investigation	31

<b>Chapter 2</b>	<b>Design of Aza-BODIPY Dyes: Tuning of Triplet Excited State and Singlet Oxygen Generation Efficiencies</b>	
2.1	Abstract	33
2.2	Introduction	35
2.3.	Results and Discussion	38
2.3.1	Synthesis and Photophysical Properties	38
2.3.2	Quantification of Triplet Excited States	43
2.3.3	Quantification of Singlet Oxygen Generation	47
2.3.4	Halogenation vs Triplet Excited State and Singlet Oxygen Yields	55
2.4	Conclusions	57
2.5	Experimental Section	58
<b>Chapter 3</b>	<b>Selected Aza-BODIPY Dyes: Study of Photodynamic Therapeutic and Photooxygenation Applications</b>	
3.1	Abstract	70
3.2	Introduction	72
3.2.1	Basic Aspects of Photodynamic Therapy	72
3.2.2	Examples of Photooxygenation Reactions	74
3.3	Results and Discussion	76
3.3.1.	Preparation of DSPE-BODIPY Conjugates	76
3.3.1.1	Investigation of <i>In Vitro</i> Photobiological Properties	79
3.3.2	Photooxygenation Reactions Using Aza-BODIPY Derivatives	87
3.3.2.1	Efficiency of Aza-BODIPYs vs Standard Sensitizers	88
3.3.2.2	Photooxygenation of Substituted Naphthols	92
3.3.2.3	Photooxygenation of Thioanisole by Aza-BODIPYs	95
3.3.2.4	Photooxygenation of Furfural by Aza-BODIPYs	97

3.3.2.5	Photooxygenation on Polystyrene Support	98
3.4	Conclusions	99
3.5	Experimental Section	100
<b>Chapter 4</b>	<b>Novel Aza-BODIPY Dyes: Tuning of Photophysical and Molecular Recognition Applications</b>	
4.1	Abstract	106
4.2	Introduction	108
4.3	Results and Discussion	111
4.3.1	Synthesis and Photophysical Properties	111
4.3.2	Electrochemical and Theoretical Calculations	114
4.3.3	Aza-BODIPY ( <b>3b</b> ) as a Probe for Anions	117
4.3.3.1	Selectivity of Detection of Nitrite Ions	118
4.3.3.2	Estimation of Nitrite Ions in Natural Water Resources	119
4.3.3.3	Mechanism and Kinetics of Detection of Nitrite Ions	122
4.3.3.4	Estimation of Nitrate Ions by the Reduction Method	124
4.3.3.5	Direct Detection of Freshly Generated Nitric Oxide	126
4.3.3.6	Development of a “Dipstick” for Detection of Nitrite Ions	127
4.3.4	Aza-BODIPY ( <b>3a</b> ) as a Probe for Neutral Molecules	128
4.3.4.1	Selectivity of the Detection of H <sub>2</sub> S	131
4.3.4.2	Mechanism and Kinetics of Detection of H <sub>2</sub> S	133
4.4	Conclusions	134
4.5	Experimental Section	135
	<b>References</b>	144
	<b>List of Publications</b>	169

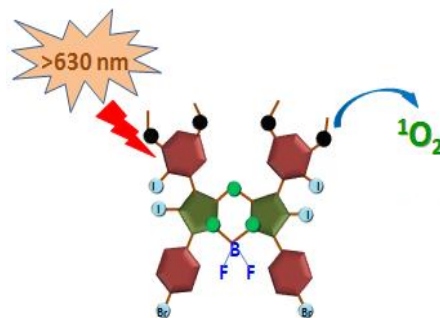
## PREFACE

The chemistry of dipyrromethene ligands has attracted much attention due to their inherent ability to form stable co-ordination complexes. The conjugated  $\pi$ -system of these ligands endowed their complexes with favorable optical properties such as intense absorption with high molar absorption coefficients ( $\epsilon > 10^4 \text{ M}^{-1}\text{cm}^{-1}$ ) and moderate to quantitative fluorescence quantum yields. Furthermore, these systems possessed long excited singlet-state lifetimes (1 to 10 ns), and versatile charge-transfer properties. Among these, the boron complexes such as 4,4-difluoro-4-bora-3a,4a-diaza-s-indacenes, abbreviated as BODIPYs have been well explored in the literature, however, the aza-dipyrromethenes and their boron complexes (aza-BODIPYs) attracted much less attention. The aza-BODIPY dyes showed around 100 nm bathochromic shifted absorption, when compared to BODIPYs. The nitrogen lone pair at the 8-position found to contribute to the orbital levels of the actual cyanine framework, reducing the HOMO–LUMO energy gap relative to BODIPY dyes bearing similar substituents. The electrochemical measurements and molecular-orbital calculations furthermore confirmed the observed red-shifted absorption and emission maxima in these systems.

The present thesis based on the aza-BODIPYs has been divided into four chapters and of which the first chapter presents an overview of the aza-BODIPY dyes, with a particular emphasis on their applications. Some of these aspects include the design strategy of the aza-BODIPY dyes with improved absorption properties, singlet

oxygen yields and a brief survey of their use as sensitizers in photodynamic, photovoltaic and molecular recognition applications. In addition, the specific objectives of the present thesis were briefly described at the end of this chapter.

The design of novel aza-BODIPY dyes and tuning of their excited state properties such as triplet excited state and singlet oxygen generation efficiencies through the judicious halogenation form the subject matter of 2nd Chapter. In this context, we have synthesized a series of novel aza-BODIPY derivatives **4a-c**, **5a,c** and **6b,c** by substituting with bromine and iodine atoms and have investigated their photophysical properties under different conditions. These derivatives showed strong NIR absorption in the range of 660-680 nm and exhibited fluorescence quantum yields ( $\Phi_F$ ) of *ca.* 0.05-0.08. The quantum yields of triplet excited state and singlet oxygen



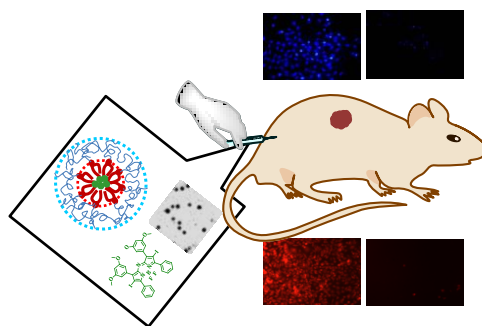
generation were determined and which showed significant dependence on the position and extent of halogenation of the parent dye and the heaviness of the substituent. For example, we observed negligible triplet excited state ( $\Phi_T$ ) and singlet oxygen yields ( $\Phi_\Delta$ ) for the parent unsubstituted aza-BODIPY, **4a** ( $\Phi_\Delta = 0.01$ ). However, upon peripheral bromination and iodination resulted in a marginal improvement as in the case of **4b** ( $\Phi_T = 0.07$ ,  $\Phi_\Delta = 0.012$ ) and **4c** ( $\Phi_T = 0.08$ ,  $\Phi_\Delta = 0.02$ ). Surprisingly, the core substituted dyes, **5a** ( $\Phi_T = 0.68$ ,  $\Phi_\Delta = 0.65$ ), **5c** ( $\Phi_T = 0.70$ ,  $\Phi_\Delta = 0.60$ ) **6b**, ( $\Phi_T = 0.78$ ,  $\Phi_\Delta = 0.70$ ) and **6c** ( $\Phi_T = 0.86$ ,  $\Phi_\Delta = 0.80$ ) showed significantly improved triplet excited state and singlet oxygen generation efficiencies,

when compared to the peripheral substituted systems. The dye **6c**, substituted with six iodine atoms at the core and peripheral phenyl rings showed quantitative quantum yield values of triplet excited state and singlet oxygen generation efficiency of *ca.* 86% and 80%, and these are the highest values reported in the literature for the aza-BODIPY derivatives. The results of these investigations demonstrated that these dyes exhibited favorable photophysical properties and high quantum yields of triplet excited state and singlet oxygen and hence can have potential as sensitizers for various applications.

The third chapter of the thesis deals with the investigation of *in vitro* photobiological properties of the selected aza-BODIPY derivatives, **5a,c** and **6b,c** as well as their efficacy as catalysts in singlet oxygen mediated photooxygenation reactions. To overcome the issue of water solubility, we have formulated the nanomicelles by the encapsulation of aza-BODIPY dyes **5a,c** and **6b,c** into the hydrophobic pocket of an amphiphilic lipid, 1,2-distearoyl-sn-glycero-3-phosphoethanolamine-N-[methoxy(polyethyleneglycol)-2000] (**DSPE**). Further, the *in vitro* photodynamic therapeutic applications

studies of the **DSPE-BODIPY** conjugates using MDA-MB-231 cells showed that these nanomicelles were cytotoxic only in presence of light with a low  $IC_{50}$  value of 2  $\mu$ M for the

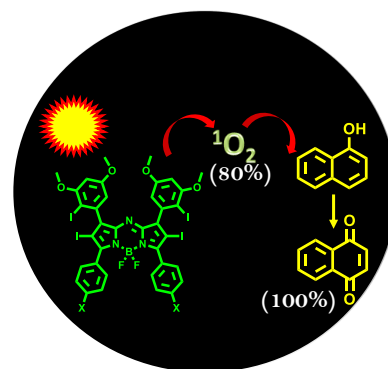
conjugate with the aza-BODIPY derivative, **5a** as the sensitizer. The mechanism of biological activity has been evaluated through FITC-Annexin V/propidium iodide staining experiments. We observed *ca.* 86% cell death in presence of 2  $\mu$ M of **DSPE-**



**BODIPY** conjugates and the mechanism of cell death was found to be through apoptosis. The apoptotic mediated cell destruction was further confirmed by morphological transformation, chromatin condensation, TMRM experiments and activation of caspase 3. The CM-H<sub>2</sub>DCFDA assay has further revealed the involvement of reactive oxygen species during the apoptotic mediated pathway.

We have further explored the potential use of these aza-BODIPY derivatives as catalysts for photooxygenation reactions. The aza-BODIPY dyes, **5a,c**, **6b,c** and the commonly used sensitizers such as tetraphenylporphyrin (**TPP**), Rose Bengal (**RB**) and Methylene Blue (**MB**) were used for the oxidation of 1-naphthol to 1,4-naphthoquinone under artificial light as well as sunlight irradiation conditions. Interestingly, the aza-BODIPY dye, **6b** showed *ca.* 100% conversion of 1-naphthol to 1,4-naphthoquinone in *ca.* 30 min. The versatility of the sensitizer was examined by employing the oxidation of different substrates such as thioanisole and furfural. We

observed efficient conversion in presence of the aza-BODIPY catalysts. Interestingly, these dyes can be uniformly loaded onto polystyrene matrix and can be used in the photooxidation of organic systems. The energy demand is low and the conditions used are

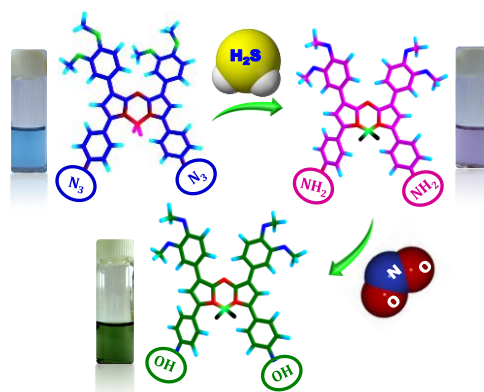


simple employing the aza-BODIPYs when compared to the standard laboratory oxidation reactions; hence such a conversion can be regarded as a green reaction. These results confirmed that the aza-BODIPY derivatives under irradiation, act as novel sensitizers in photodynamic therapy and also as “sustainable catalysts” for photooxygenation reactions.



Synthesis of the functional aza-BODIPY dyes and investigations of their photophysical properties and chemodosimetric applications are described in Chapter 4. We have synthesized the aza-BODIPY dyes, **3a-c** by changing the peripheral substitution with azido, amino and dimethylamino groups, and have investigated their photophysical properties. These dyes showed strong absorption in the range 700-800 nm, while the fluorescence maxima

were observed in the region 750-950 nm. We have investigated the interactions of the amino derivative, **3b**, with various anions and which showed selective recognition of nitrite ions ( $\text{NO}_2^-$ ). The successive addition of nitrite ions,



to the protonated form of the probe, **3b**, resulted in a hypochromicity in the absorbance at 570 nm, along with a gradual red shift in the maximum to 630 nm. The probe, **3b** showed selective recognition of the nitrite ions through a distinct visual color change from bright blue to intense green with a sensitivity of 20 ppb ( $0.5 \mu\text{M}$ ). Uniquely, this probe can be coated on a glass surface to fabricate a simple solid-state dipstick device. Such a dipstick device can be used for the visual detection of the nitrite ions in presence of other competing anions in distilled as well as natural water resources. This probe can be furthermore used for the sensitive detection of the nitrate ions ( $\text{NO}_3^-$ ) when coupled in a reduction step.

On the other hand, the azido-aza-BODIPY dye, **3a** showed selective interactions with hydrogen sulfide ( $\text{H}_2\text{S}$ ) through a color change from bright blue to purple with a detection limit of *ca.* 0.5 ppm. The gradual addition of  $\text{H}_2\text{S}$  to the probe

**3a** induced *ca.* 50% hypochromicity at 700 nm with a concomitant bathochromic shift of *ca.* 50 nm, through an isosbestic point at 726 nm. The observed purple color corresponds to the reduced amino aza-BODIPY dye, **3b**. The linearity of concentration dependent absorption changes supported its utility for the on-site analysis and estimation of H<sub>2</sub>S in the aqueous medium. In contrast, the dimethylamino-aza-BODIPY derivative, **3c** exhibited negligible affinity for the anions tested. Thus, by tuning the photophysical properties through the judicious functionalization, we have been successful in developing novel aza-BODIPY dyes for their use in the detection and analysis of biologically important molecules such as NO<sub>2</sub><sup>-</sup>, NO<sub>3</sub><sup>-</sup> and H<sub>2</sub>S.

In summary, we have synthesized novel aza-BODIPY dyes and have tuned their photophysical properties through appropriate substitution and explored their applications in photodynamic therapy, photooxygenation and molecular recognition. These systems showed good solubility in the organic media and exhibited high photostability, favorable absorption and fluorescence properties. The halogenated aza-BODIPY dyes showed excellent triplet excited state quantum yields and singlet oxygen generation efficiencies, thereby their use as sensitizers in photodynamic therapy as well as photooxygenation reactions. On the other hand, the amino and azido aza-BODIPY dyes showed selectivity for biologically important ions and demonstrating thereby their application as chemodosimeters. Overall, our results demonstrate that, the aza-BODIPY dyes reported in the thesis are the versatile systems, which can be further explored for their material and biological applications.

---

*Note: The numbers of various compounds given here correspond to those given under the respective chapters.*

<b>Sl. No</b>	<b>List of Figures</b>	<b>Page</b>
1.	Figure 1.1	2
2.	Figure 1.2	22
3.	Figure 1.3	25
4.	Figure 1.4	31
5.	Figure 2.1	41
6.	Figure 2.2	41
7.	Figure 2.3	44
8.	Figure 2.4	45
9.	Figure 2.5	46
10.	Figure 2.6	47
11.	Figure 2.7	48
12.	Figure 2.8	49
13.	Figure 2.9	50
14.	Figure 2.10	51
15.	Figure 2.11	52
16.	Figure 2.12	53
17.	Figure 2.13	54
18.	Figure 3.1	73
19.	Figure 3.2	77
20.	Figure 3.3	78
21.	Figure 3.4	79
22.	Figure 3.5	81
23.	Figure 3.6	82
24.	Figure 3.7	84
25.	Figure 3.8	84
26.	Figure 3.9	85
27.	Figure 3.10	86
28.	Figure 3.11	87

29.	Figure 3.12	90
30.	Figure 3.13	92
31.	Figure 3.14	94
32.	Figure 4.1	113
33.	Figure 4.2	114
34.	Figure 4.3	115
35.	Figure 4.4	116
36.	Figure 4.5	117
37.	Figure 4.6	118
38.	Figure 4.7	119
39.	Figure 4.8	120
40.	Figure 4.9	120
41.	Figure 4.10	122
42.	Figure 4.11	123
43.	Figure 4.12	124
44.	Figure 4.13	125
45.	Figure 4.14	126
46.	Figure 4.15	127
47.	Figure 4.16	128
48.	Figure 4.17	129
49.	Figure 4.18	130
50.	Figure 4.19	130
51.	Figure 4.20	131
52.	Figure 4.21	132
53.	Figure 4.22	132
54.	Figure 4.23	134

## **List of Tables**

1.	Table 2.1	42
2.	Table 2.2	53
3.	Table 3.1	81
4.	Table 3.2	91
5.	Table 3.3	94
6.	Table 3.4	96
7.	Table 3.5	98
8.	Table 4.1	114
9.	Table 4.2	121

## **List of Schemes**

1.	Scheme 1.1	4
2.	Scheme 1.2	9
3.	Scheme 1.3	11
4.	Scheme 1.4	12
5.	Scheme 1.5	14
6.	Scheme 1.6	19
7.	Scheme 1.7	21
8.	Scheme 2.1	39
9.	Scheme 2.2	40
10.	Scheme 2.3	56
11.	Scheme 2.4	67
12.	Scheme 3.1	75
13.	Scheme 3.2	80
14.	Scheme 3.3	88
15.	Scheme 3.4	93
16.	Scheme 3.5	95

17	Scheme 3.6	97
18.	Scheme 4.1	111
19.	Scheme 4.2	112
20.	Scheme 4.3	123
21.	Scheme 4.4	133

### **List of Charts**

1.	Chart 1.1	5
2.	Chart 1.2	6
3.	Chart 1.3	7
4.	Chart 1.4	8
5.	Chart 1.5	13
6.	Chart 1.6	15
7.	Chart 1.7	17
8.	Chart 1.8	17
9.	Chart 1.9	18
10.	Chart 1.10	20
11.	Chart 1.11	24
12.	Chart 1.12	26
13.	Chart 1.13	27
14.	Chart 1.14	28
15.	Chart 1.15	29
16.	Chart 1.16	30
17.	Chart 2.1	38
18.	Chart 3.1	76
19	Chart 3.2	88
20.	Chart 4.1	110

## List of Abbreviations

1. AFM- Atomic force microscopy
2. AcOH – Acetic acid
3. BHJ – Bulk heterojunction
4.  $\text{BF}_2^+$  - Boron difluoride cation
5.  $\text{BF}_3\text{O}(\text{Et})_2$  - Boron trifluoride diethyletherate
6. BODIPY - 4,4-Difluoro-4-bora-3a, 4a-diaza-s-indacene
7. B3LYP – Becke, three-parameter, Lee-Yang-Parr
8.  $\beta$ -CD –  $\beta$ -cyclodextrin
9.  $^\circ\text{C}$  – Degree celsius
10. *ca.* – *circa*
11. CAK1 – Cdk-Activating kinase
12. CrEL – Cremophor EL
13. CV – Cyclic voltammetry
14. CT – Charge transfer
15.  $\text{CDCl}_3$  – Deuterated chloroform
16.  $\text{CD}_3\text{COCD}_3$  – Deuterated acetone
17.  $\text{CHCl}_3$  – Chloroform
18.  $\text{CH}_3\text{CN}$  – Acetonitrile
19.  $\text{CH}_3\text{OH}$  – Methanol
20.  $\text{CH}_3\text{NO}_2$  – Nitro methane
21.  $\text{C}_2\text{H}_5\text{OH}$  – Ethanol
22. Calcd. – Calculated

23. CM-H<sub>2</sub> DCFDA- 5-(and-6)-Chloromethyl-2',7'-dichlorodihydrofluorescein diacetate acetyl ester
24. Cu – Copper
25. CH<sub>3</sub>I – Methyl iodide
26. CO<sub>3</sub><sup>2-</sup> – Carbonate ion
27. CH<sub>3</sub>COO<sup>-</sup> - Acetate ion
28. DAPI – 4',6-Diamidino-2-phenylindole
29. DCM – Dichloromethane
30. DLS – Dynamic light scattering
31. DPBF – 1,3-Diphenylisobenzofuran
32. DMEM – Dulbecco's modified eagle medium
33. DMSO – Dimethylsulphoxide
34. [d<sub>6</sub>] DMSO – Deuterated dimethylsulphoxide
35. DMF – N,N-Dimethylformamide
36. DLR – Dual lifetime referencing
37. DSPE – 1,2-Distearoyl-sn-glycero-3-phosphoethanolamine
38. DEA – Diethylamine
39. DSPE-PEG<sub>2000</sub>-MeO – 1,2-Distearoyl-sn-glycero-3-phosphoethanolamine-N-[methoxy(polyethylene glycol)-2000]
40. DIEA – Diisopropylethylamine
41. DFT – Density functional theory
42. DIC – Differential interference contrast
43. d – Hydrodynamic diameter
44. *et al.* – *Et alii/alia*



45. ET – Energy transfer
46.  $\epsilon$  – Molar extinction coefficient
47. EC<sub>50</sub> – Half maximal effective concentration
48. EPA – Environmental protection agency
49. E<sub>gap</sub> – Energy gap (bandgap)
50. E<sub>HOMO</sub> – Energy of HOMO
51. E<sub>LUMO</sub> – Energy of LUMO
52. ESI-MS – Electrospray ionisation mass spectrometry
53. EtOH - Ethanol
54. eV – Electron volt
55. °E – Degree East
56. FAB-MS – Fast atom bombardment mass spectrometry
57. FITC – Fluorescein isothiocyanate
58. FT-IR – Fourier transform infrared
59. FACS – Fluorescence-activated cell sorting
60. g - Gram
61. GM – Goepfert Mayer
62. GC – Gas chromatography
63. h – Hour
64. HOMO – Highest occupied molecular orbital
65. HeLa – Human cervical cancer cell line
66. Hg (II) – Mercury (II) ion
67. HEK 293T – Human embryonic kidney 293 cells

68. HpD – Hematoporphyrin derivative
69. Hg lamp – Mercury lamp
70. H<sub>2</sub>S – Hydrogen sulfide
71. HSO<sub>3</sub><sup>-</sup> – Bisulfite ion
72. HCO<sub>3</sub><sup>-</sup> – Bicarbonate ion
73. HPO<sub>4</sub><sup>2-</sup> – Hydrogen phosphate ion
74. HCl – Hydrochloric acid
75. ICT – Intramolecular charge transfer
76. IC<sub>50</sub> – Half inhibitory concentration
77. ISC – Intersystem crossing
78. IR – Infrared
79. K<sup>+</sup> – Potassium ion
80. k' – Rate constant
81. kV – Kilovolt
82. kVA – Kilovolt amps
83. kDa – Kilodalton
84. KBr – Potassium bromide
85. K<sub>2</sub>CO<sub>3</sub> – Potassium carbonate
86. LED – Light emitting diode
87. LUMO – Lowest unoccupied molecular orbital
88. λ<sub>max</sub> – Wavelength maximum
89. LOD – Limit of detection
90. LP – Long pass
91. MB – Methylene blue

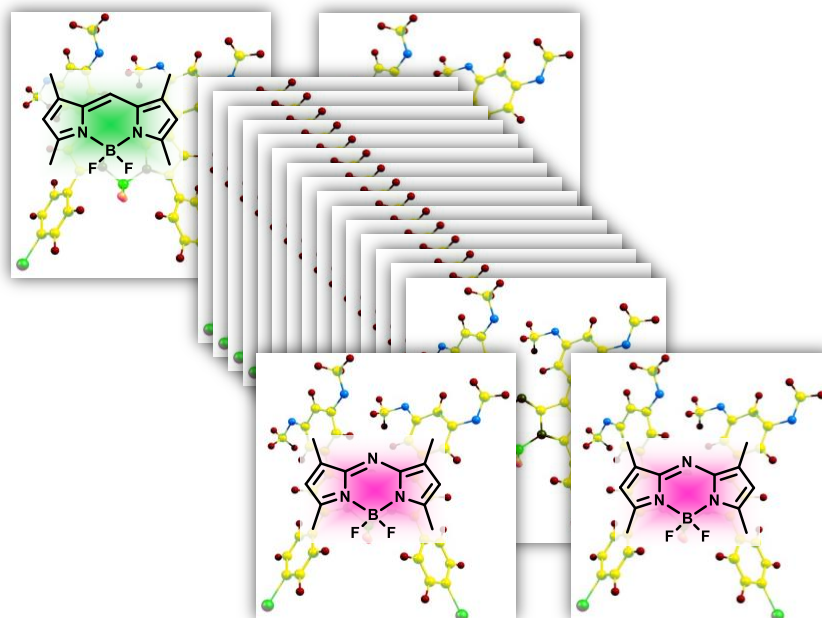
92. MCF-7 – Human breast cancer cells
93. MDA-MB-231 – Aggressive human breast cancer cells
94. mg – Milligram
95. MHz – Megahertz
96. mJ – Millijoule
97. mW – Milliwatt
98. mL – Millilitre
99.  $\mu\text{M}$  – Micromolar
100.  $\mu\text{s}$  – Microseconds
101.  $\mu\text{m}$  – Micrometer
102. mM – Millimolar
103. mmol – Millimole
104. mp – Melting point
105. MRC5-SV40 – Immortalized human fibroblasts
106. MO – Molecular orbital
107. MALDI-TOF-MS – Matrix-assisted laser desorption ionization-time of flight- mass spectrometry
108. MCL – Maximum contaminant level
109. MTT – (3-(4,5-Dimethylthiazol-2-yl)-2,5-diphenyl tetrazolium bromide
110. °N – Degree north
111.  $\text{NH}_4\text{OAc}$  – Ammonium acetate
112.  $\text{NH}_4^+$  – Ammonium ion
113.  $\text{NO}_2^-$  – Nitrite ion
114.  $\text{NO}_3^-$  – Nitrate ion

- 115. NO – Nitric oxide
- 116. NaNO<sub>2</sub> – Sodium nitrate
- 117. NaN<sub>3</sub> – Sodium azide
- 118. Na<sub>2</sub>S – Sodium sulfide
- 119. N<sub>3</sub><sup>-</sup> – Azide ion
- 120. NLO – Nonlinear optics
- 121. NIS – *N*-Iodosuccinimide
- 122. Nd:YAG – Neodymium-doped yttrium aluminum garnet
- 123. NIR – Near infrared
- 124. nm – Nanometer
- 125. nM – Nano molar
- 126. NMR – Nuclear magnetic resonance
- 127. ns – Nanosecond
- 128.  $\nu_{\max}$  – Frequency maximum
- 129. vs – Versus
- 130. <sup>1</sup>O<sub>2</sub> – Singlet oxygen
- 131. OD – Optical density
- 132. OLED – Organic light emitting diode
- 133. OFET – Organic field effect transistor
- 134. •OH – Hydroxyl radical
- 135. PDT – Photodynamic therapy
- 136. pH – Hydrogen ion concentration at logarithmic scale
- 137. PET – Photo induced electron transfer

138. PCE – Power conversion efficiency
139. Pd (0) – Palladium (0)
140. pKa – Acid dissociation constant at logarithmic scale
141. PPABs – Pyrrolopyrrole aza-BODIPY analogues
142. P3HT – Poly(3-hexylthiophen-2,5-diyl)
143. PCBM – Phenyl- C61-butyrac acid methyl ester
144. PL – Photoluminescence
145. ppb – Parts per billion
146. ppm – Parts per million
147. PI – Propidium iodide
148.  $\Phi_F$  – Quantum yields of fluorescence
149.  $\Phi_{UC}$  – Quantum yields of upconversion
150.  $\Phi_T$  – Quantum yields of triplet excited state
151.  $\Phi_\Delta$  – Singlet oxygen quantum yield
152. RT – Room temperature
153. ROS – Reactive oxygen species
154.  $[\text{Ru}(\text{bpy})_3]^{2+}$  – Tris(2,2'-bipyridine)ruthenium(II)
155. s – Seconds
156. S<sub>N</sub>Ar – Aromatic nucleophilic substitution
157. SWNT – Single-wall carbon nanotube
158. SEC – Spectroelectrochemistry
159. SD – Standard deviation
160.  $\text{S}_2\text{O}_3^{2-}$  – Thiosulphate ion
161.  $\text{S}^{2-}$  – Sulfide ion

- 162. SEM – Scanning electron microscopy
- 163. TLC – Thin layer chromatography
- 164. TMRM – Tetramethylrhodamine methyl ester
- 165.  $T_1$  – Triplet excited state
- 166. TPA – Two photon absorption
- 167. TAS – Transient absorption spectroscopy
- 168. THF – Tetrahydrofuran
- 169. TEA – Triethylamine
- 170. TEM – Transmission electron microscopy
- 171. TMS – Tetramethylsilane
- 172. TPP – Tetraphenylporphyrin
- 173.  $\tau_T$  – Triplet lifetime
- 174. USA – United States of America
- 175. UV – Ultraviolet
- 176. Vis – Visible
- 177. W – Watt
- 178. WHO – World Health Organization
- 179. XPS – X-ray photoelectron spectroscopy

# AZA-BODIPY DYES: UNVEILING THE HIDDEN VERSATILITY



## 1.1. INTRODUCTION

Myriad classes of highly fluorescent organic compounds are available in the literature for various applications. Among these, 4,4-difluoro-4-bora-3a,4a-diaza-s-indacene, abbreviated as BODIPY, has gained much attention as being one of the most versatile fluorophores. The BODIPY dyes were synthesized for the first time by Treibs and Kreuzer, (Treibs *et al.*, 1968) but not much explored until the end of the 1980s. The potential fluorescence properties of these dyes were explored only late 1980s and which has resulted in synthesis of new and novel BODIPY based dyes and their

commercialization for labeling applications (Monsma *et al.*, 1989; Haughland *et al.*, 1988; Worries *et al.*, 1985). The fundamental aspects on the chemical reactivity and the photophysical properties of the BODIPY dyes have been well explored since then as reflected in the publication of papers and patents in the literature (Figure 1.1A).

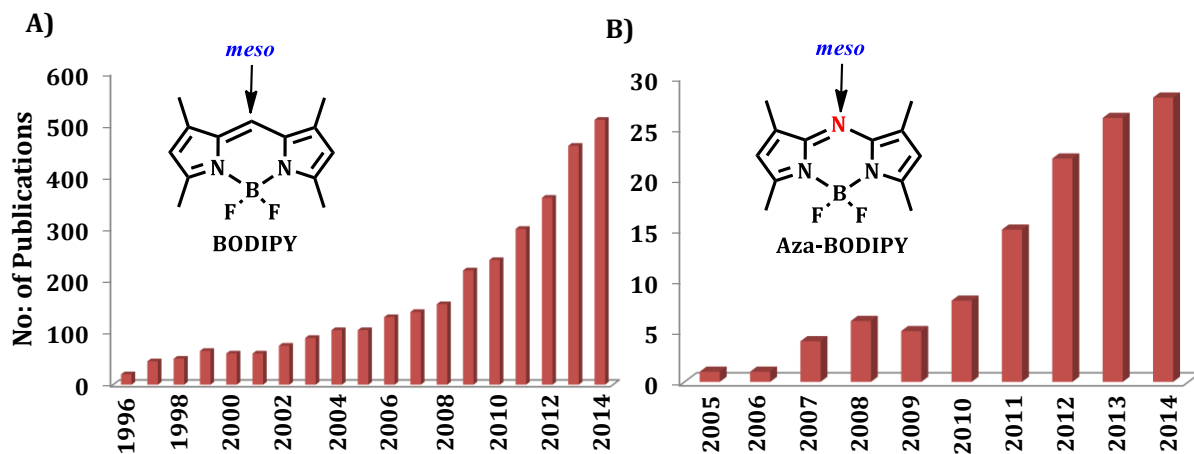


**Figure 1.1.** Statistical survey of the number of publications on A) BODIPY and B) aza-BODIPY dyes appeared in the literature up to 2014.

Unlike BODIPY dyes, aza-dipyrrromethenes and their boron complexes (aza-BODIPYs), which differ only at the meso carbon atom, have been rarely explored in the literature due to their negligible fluorescence and synthetic difficulty, when compared to the BODIPY dyes. Though these compounds were first reported in 1940s but have been remained unexplored for applications since that time (Rogers, 1943; Knott, 1947). However, this class of dyes has attracted considerable attention from the beginning of 21<sup>st</sup> century with the report from O'Shea and co-workers (Killoran *et al.*, 2002).

The first chapter of the present thesis gives an overview of the scope and applications of this neglected class of chromophore, aza-BODIPY dyes. Furthermore, it

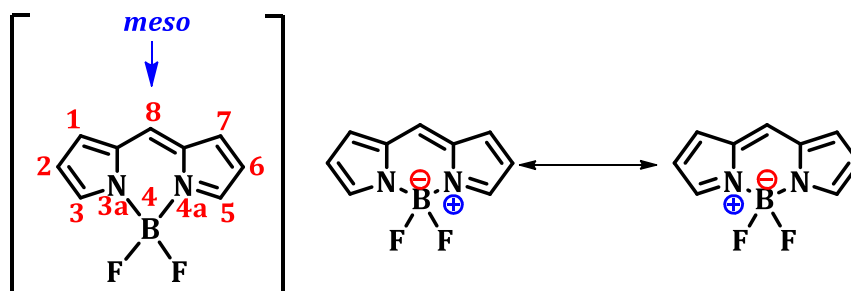


also includes a brief discussion on the parent BODIPY dyes and their limitations followed by the development of aza-BODIPY dyes and their use as the sensitizers for biological and molecular recognition applications. In addition, the objectives of the present thesis are also briefly described at the end of this chapter.

## 1.2. BODIPY DYES: HISTORICAL DEVELOPMENTS

Of the various fluorophores reported, 4,4-difluoro-4-bora-3a,4a-diaza-s-indacene (BODIPY) dyes, display favorable properties, and hence attracted much attention during the last three decades. Although the first example of this class of dyes was reported in 1968, the possible applications of BODIPY-based dyes as biological labeling agents, electroluminescent devices, tunable laser dyes, solid-state solar concentrators, and fluorescent switches were fully recognized only in the mid-1990s (Ulrich *et al.*, 2008; Loudet *et al.*, 2007). The huge appeal of these dyes in the recent times may be due to their stability, relatively high molar absorption coefficients ( $\epsilon_{\max}$ ) and fluorescence quantum yields ( $\Phi_F$ ), and good solubility in various solvents. The excitation/emission wavelengths in the visible spectral region (500-600 nm), and fluorescence lifetimes in the nanosecond range added to their use in biological applications (Boens *et al.*, 2012; Diring *et al.*, 2009; Cakmak *et al.*, 2009; Goze *et al.*, 2006; Yilmaz *et al.*, 2006; Rohand *et al.*, 2005). In addition, the spectroscopic and photophysical properties of BODIPY dyes can be fine-tuned by the attachment of different functional groups at the appropriate positions of the BODIPY core (Scheme 1.1). These dyes were synthesized from the pyrrole derivatives and the corresponding aldehydes through an *in situ* multi-step reaction. Using this synthetic strategy,

numerous BODIPY systems have been prepared from readily available pyrrole derivatives (Peters *et al.*, 2007; Golovkova *et al.*, 2005; Trieflinger *et al.*, 2005; Turfan *et al.*, 2002; Haugland *et al.*, 1996).



**Scheme 1.1.** The mode of numbering of BODIPY dyes and their resonance structures.

Urano *et al.*, have reported a BODIPY based probe **1** for imaging acidic endosomes in cancer cells (Chart 1.1). These systems were non-fluorescent in the non-protonated form ( $\Phi_F = 0.002$ ), but upon protonation, exhibited strong fluorescence ( $\Phi_F = 0.55-0.60$ ). Based on this, a selective strategy for *in vivo* tumor visualization was developed in which the pH-triggerable fluorescent probes were conjugated to a cancer targeting monoclonal antibody (trastuzumab) (Urano *et al.*, 2009). Detailed confocal spectroscopy studies have revealed that the probe-antibody conjugates were not fluorescent outside tumor cells at neutral pH. After internalization by endocytosis, the probe-antibody conjugates were highly fluorescent after accumulation (after 4 h) in endosomes or lysosomes (pH=5-6) because of acidic pH of the tumor cells. In another report, Boens and co-workers have synthesized BODIPY-linked aza-crown ether sensor, **2** having high selectivity for potassium over other alkali ions. This was the first example of a probe synthesized using SNAr of 3,5-dichloroBODIPY. The authors have attributed the observed significant blue shift in the absorption and emission spectra

due to the large conformational change of the sensor upon binding with  $K^+$  ions (Baruah *et al.*, 2005).

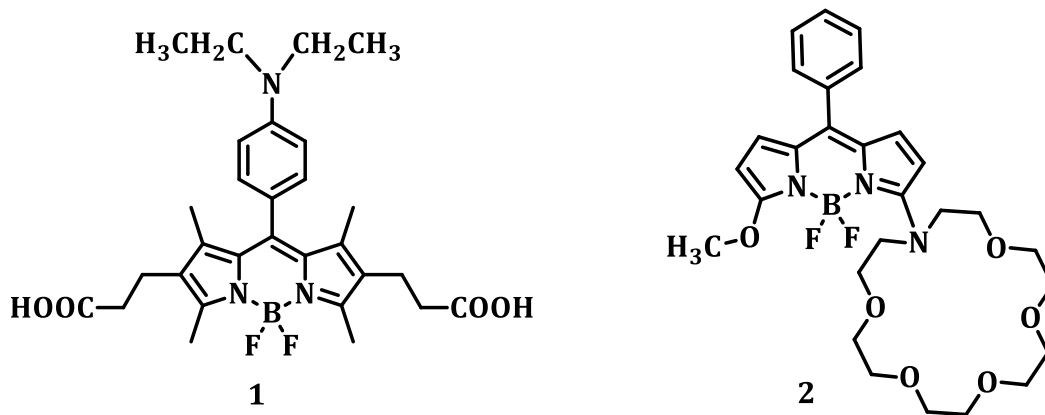


Chart 1.1

Akkaya and co-workers, have described the formation of the distyryl-BODIPY dyes *via* Knoevenagel condensation reaction since 2,7-methyl substituents on BODIPYs were found to be reasonably acidic for such a reaction. The authors have synthesized the brominated BODIPY dye, **3** having oligoethylene glycol fragments to promote water-solubility (Chart 1.2) and have investigated the photodynamic therapeutic (PDT) properties. The compound **3** exhibited an  $EC_{50}$  (conc. required for 50% of the maximal effect) of 200 nM under low fluence rate LED irradiation and the cytotoxicity was attributed to cell-membrane damage as indicated *via* fluorescence microscopy (Atilgan *et al.*, 2006). In a similar study, Ng and co-workers have developed a series of unsymmetrical distyryl-BODIPY dyes and have observed that the N-methylated derivative, **4** was found to be highly photocytotoxic with  $IC_{50}$  value of 15 nM (Chart 1.2). The high potency was attributed to their low aggregation tendency, high efficiency in generating singlet oxygen and high cellular uptake (He *et al.*, 2011).

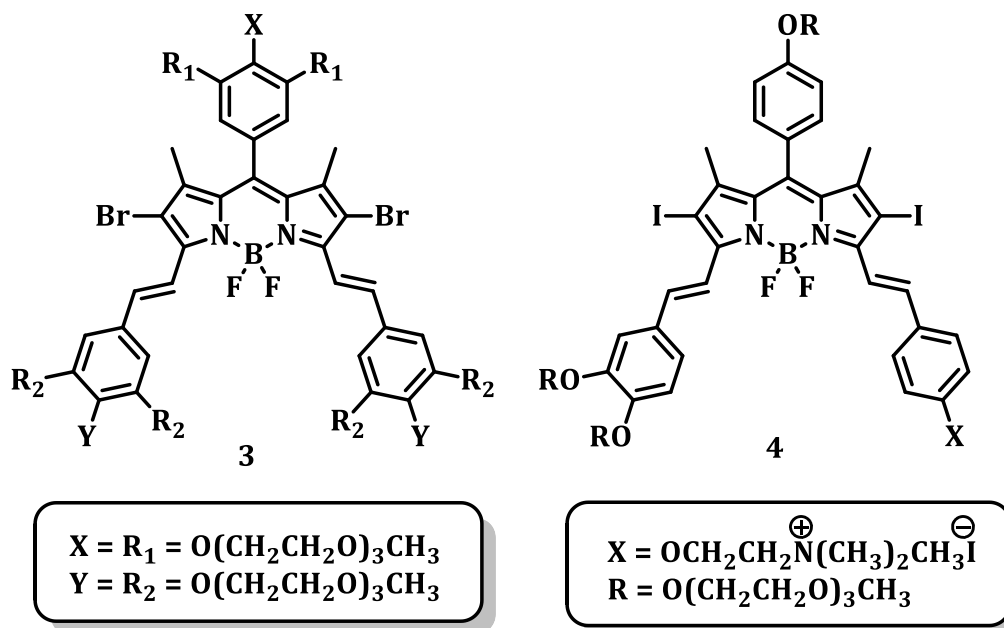


Chart 1.2

Apart from the molecular recognition and photodynamic therapeutic applications, the BODIPY derivatives were widely used as energy transfer cassettes, initially conceptualized by Ziessel and co-workers. Various synthetic strategies have been developed by covalent attachment of an ancillary light absorber to the BODIPY core to form the conjugates **5-7** (Chart 1.3) (Ziessel *et al.*, 2005; Wan *et al.*, 2003). An important feature of these systems was that the two chromophores remained electronically isolated because of the orthogonal arrangement around the connecting linkage. The rate of energy transfer depended on the structure of the dual-dye system and which decreased with the increasing center-to-center separation in line with a dipole-dipole transfer mechanism. The overall energy-transfer efficiency exceeded *ca.* 90%, even in the most extended system, **5**. Significantly, the faster energy transfer was observed when the anthracene donor was attached to the long axis of the BODIPY acceptor, as in **6**, than when the donor was coupled to the short axis, as in **7** (Chart 1.3).

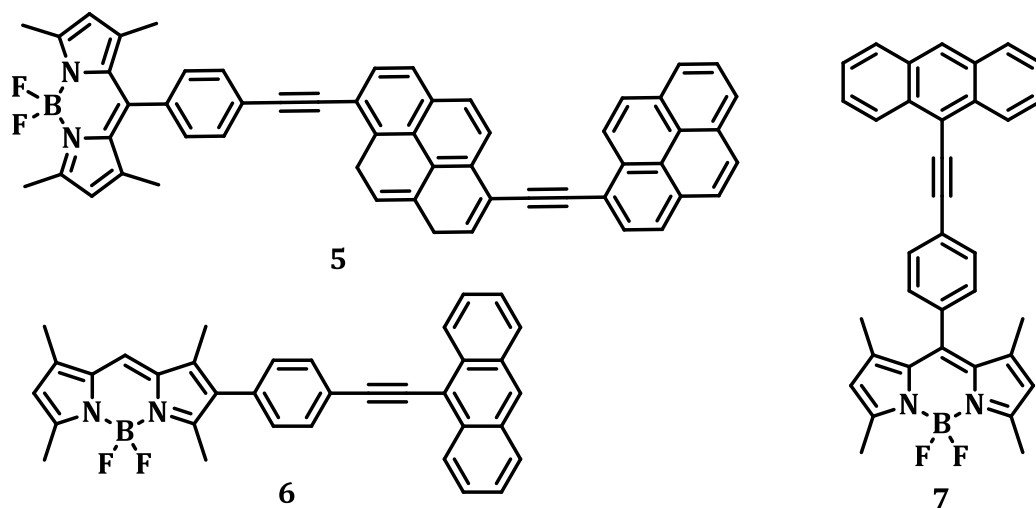
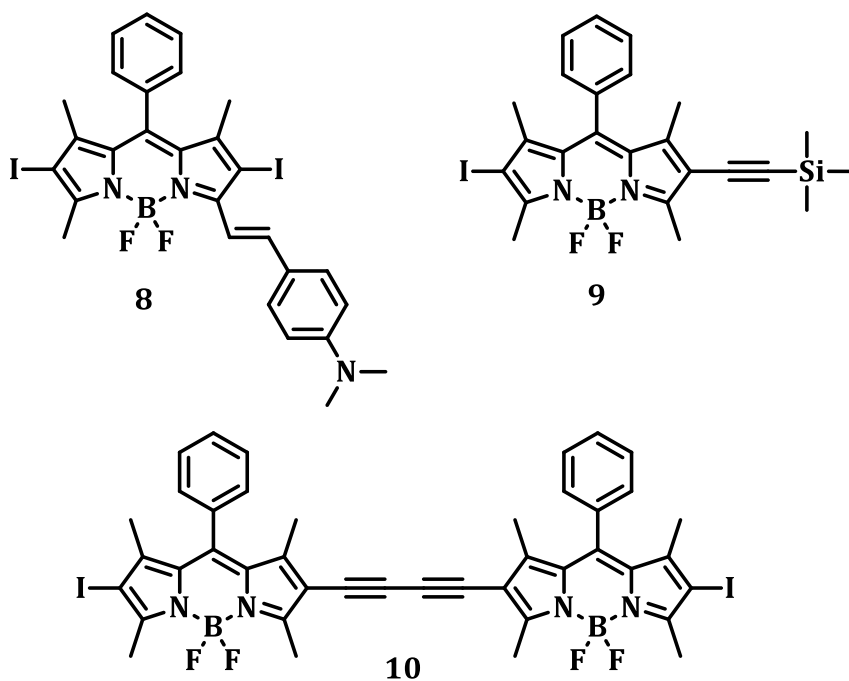


Chart 1.3

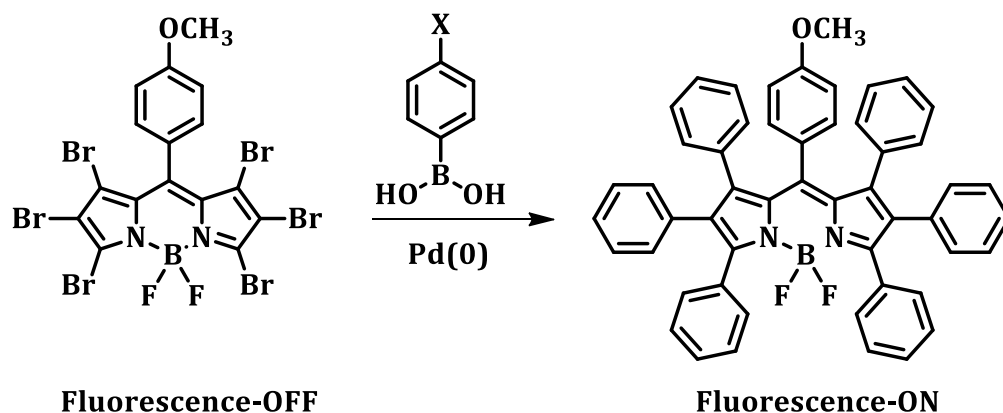
Recently, Zhao and co-workers have designed a small library of BODIPY based organic triplet sensitizers **8-10** (Chart 1.4) and have investigated the phenomenon of triplet-triplet annihilation based fluorescence upconversion. The absorption of the sensitizers exhibited a broad range of 510–630 nm and the variation of the absorption wavelength of the sensitizers was accomplished by extension of  $\pi$ -conjugation framework of the molecules. These molecules showed relatively weak fluorescence and the exhibited the lifetimes of the triplet excited states in the range of 66  $\mu$ s. The derivative, **8** showed a much lower T1 energy level than the other sensitizers which was rationalized due to its spin density distribution. With perylene or 1-chloro-9,10-bis(phenylethynyl)anthracene as the triplet acceptor, significant upconversion ( $\Phi_{UC}$  up to 6.1%) was observed in solution samples and polymer matrix. The authors have attributed the efficient upconversion with **8-10** was due to the iodo substitution, which were directly substituted on the BODIPY core. This hypothesis was confirmed by

comparing with a model compound that lacks iodine atoms at the core (Wu *et al.*, 2011; Zhao *et al.*, 2011).



**Chart 1.4**

Ravikanth and co-workers have developed a short and rapid synthetic route for the polyarylated BODIPY dyes, avoiding the use of aryl-substituted pyrroles. The authors have utilized hexabromo-BODIPY as the key synthon in their strategy to prepare a set of aryl-substituted BODIPYs by coupling with arylboronic acids through Pd(0) coupling conditions. The X-ray analysis showed that the structure was distorted with a propeller like conformation, and electrochemical studies have indicated that these compounds exhibit reversible oxidation and reduction potentials. The absorption and emission bands of the aryl substituted derivatives showed large red shifts with significant fluorescence quantum yields as well as lifetimes as compared to the unsubstituted BODIPYs (Scheme 1.2) (Lakshmi *et al.*, 2011).



**Scheme 1.2.** Schematic representation of the fluorescence OFF-ON switching during the formation of hexaaryl-BODIPY dye from the corresponding hexa-bromo synthon.

The aforementioned literature reports have demonstrate that the applications of BODIPY dyes range from the fields of fluorescence labeling, light harvesting, to therapeutic applications. However, these dyes suffer from some undesirable characteristics such as poor solubility and unfavorable optical properties for applications in biology. For example, most of the BODIPY derivatives reported showed absorption in the short wavelength and emission less than 600 nm. In this context, several attempts have been made by Ziessel, Burgess and Akkaya groups in the literature to improve the absorption properties of the BODIPY dyes (Haefele *et al.*, 2010; Cakmak *et al.*, 2009; Yilmaz *et al.*, 2006; Atilgan *et al.*, 2008; Goze *et al.*, 2006). However, most of these explored strategies were to extend the conjugation through the introduction of styryl arms at the peripheral positions of the BODIPY chromophore. Thus, the core modification of the BODIPY framework was largely unrealized, which otherwise can lead to the development of molecules that can be efficiently utilized for molecular recognition and in therapeutic applications. The most promising alternative to BODIPY derivative was obtained by replacing the meso carbon atom with a nitrogen

atom, named 'aza-BODIPY' dye, which showed significantly bathochromic shifted strong NIR absorption in the region of 600-800 nm.

### 1.3. AZA-BODIPY- A VERSATILE ALTERNATIVE TO BODIPYS

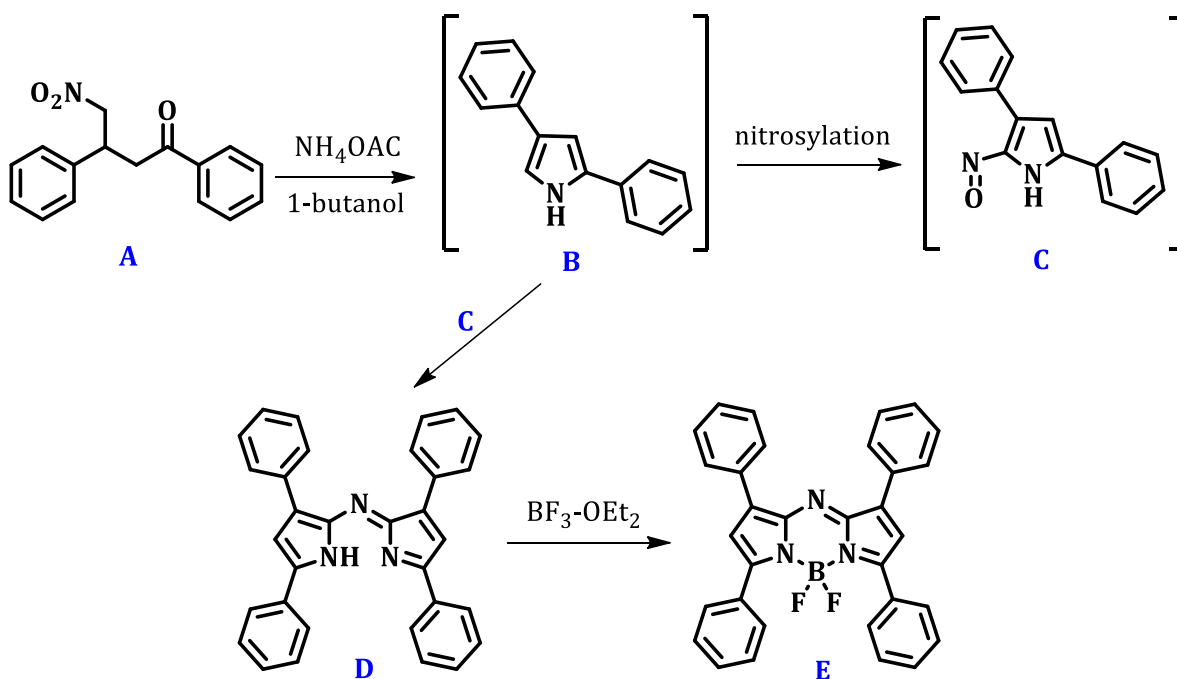
Very recently, an increasing interest has been focused on 4-bora-3a,4a,8-triazaindacene dyes (commonly referred to as aza-BODIPY dyes) owing to their absorption and fluorescence in the far-red and near-IR regions of the spectrum. Notably, the aza-BODIPY dyes show absorbance and fluorescence around 650 and 700 nm respectively, and further bathochromic shift in these properties can be achieved through judicious substitution. The nitrogen lone pair at the 8-position in these systems has been found to be responsible for the reduction in the HOMO-LUMO energy gaps relative to the normal BODIPY dyes bearing similar substituents. Results of electrochemical measurements as well as the molecular-orbital calculations were in supportive of this hypothesis (Ulrich *et al.*, 2008).

The synthesis of the aza-BODIPY dyes involves the intermediate precursor, aza-dipyrromethene, which was obtained by the condensation of hydroxylamine with 1-oxopropionitrile followed by  $\text{BF}_3 \cdot \text{OEt}_2$  complexation (Oki *et al.*, 1995; Sathyamoorthi *et al.*, 1993). In this context, serious efforts have been made to obtain the symmetric and asymmetric aza-BODIPY dyes primarily by the groups of O'Shea and Carreira, motivated by their potential applications as biological labels, sensitizers for photodynamic therapy and as luminescent proton sensors (Carreira *et al.*, 2006; Zhao *et al.*, 2005; Killoran *et al.*, 2002).



### 1.3.1. Design and Synthetic Strategy of Aza-BODIPYs

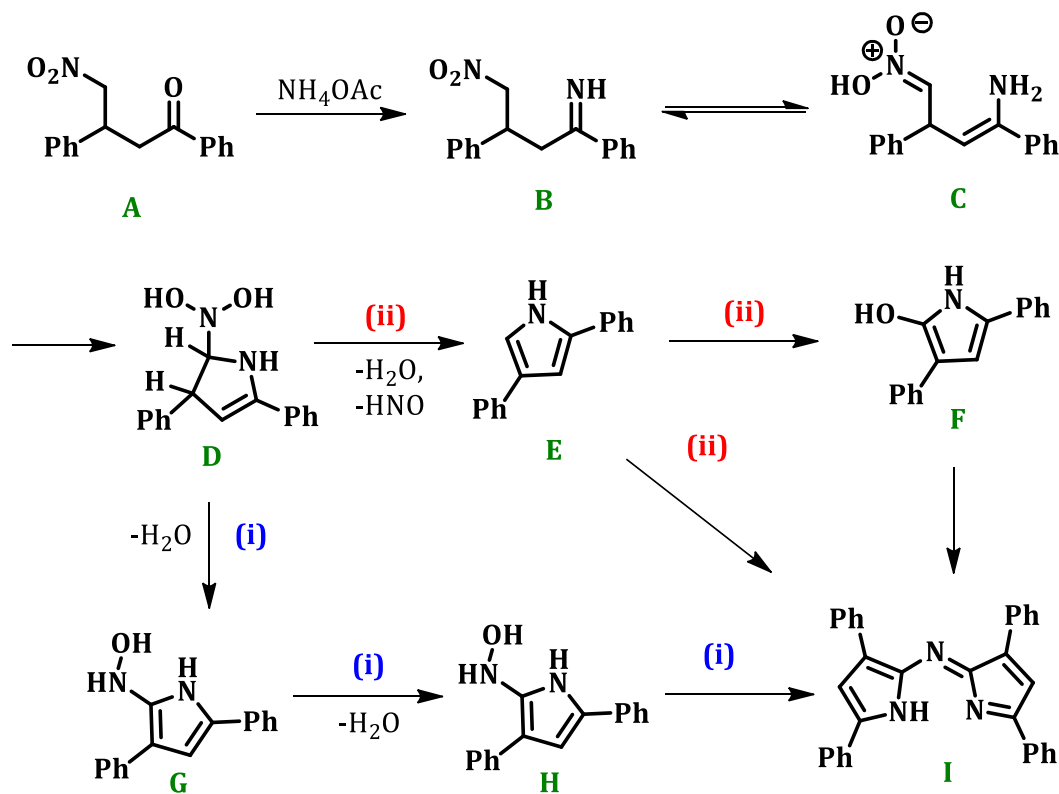
One-pot synthetic route towards the aza-dipyrrens was established as early as in 1943s (Knott, 1947; Davies *et al.*, 1944; Rogers, 1943), but their complexation to yield the aza-BODIPY dyes was reported only in 1994. As shown in Scheme 1.3, the one-pot sequence comprises condensation of the nitromethane adducts of chalcones (**A**) at elevated temperatures with a nitrogen source to form the pyrrole derivatives (**B**), which were partially nitrosated to yield (**C**) in the reaction mixture. A cross-condensation of these two pyrrole moieties then resulted in the formation of aza-dipyrromethene (**D**). Unfortunately, such aza-BODIPY dyes can only be synthesized from the heavily substituted pyrrole derivatives, such as 2,4-diarylpyrroles or ring annulated pyrroles (Zhao *et al.*, 2006; Zhang *et al.*, 2005). Several groups have attempted to synthesize the corresponding alkyl aza-BODIPY dyes without any success.



**Scheme 1.3.** Synthesis of aza-BODIPY dyes through the formation of nitrosopyrrole.

Recent synthetic evidence also confirmed the instability of the alkylated pyrroles and nitrosopyrroles under previously established reaction conditions (Liras *et al.*, 2007).

The most direct synthetic route for the aza-dipyrromethenes was reported by O'shea *et al.*, which involves the heating of 4-nitro-1,3-diarylbutan-1-ones with an ammonium source in an alcohol solvent (Scheme 1.4). Even though the synthesis was relatively simple; but the reaction mechanism was not clearly understood. The authors have proposed a mechanism for the formation of aza-dipyrromethenes from the corresponding nitromethane adducts using  $^{15}\text{N}$  labelling methods. A study of the dimerization pathway of the pyrroles revealed an unprecedented nitrogen rearrangement in the final stages involving a ring-opening/closing of the pyrrole ring.



**Scheme 1.4.** Proposed mechanism and pathways for the formation of the aza-dipyrromethene from their corresponding nitromethane derivatives.

Evidence has been provided to support the formation of a key intermediate (**H**), which subsequently undergoes dimerization with a loss of ammonia to yield (**I**) or it can also react with 2,4-diphenylpyrrole (**E**) to yield the product. Both reaction pathways have been proposed for the transformation of (**A**) to the final product (**I**) (Grossi *et al.*, 2012).

### 1.3.2. Conformationally Restricted Aza-BODIPY Dyes

It may be mentioned that the widespread applications of the aza-BODIPY dyes, when compared to BODIPYs have been limited due to their low fluorescence quantum yields. The weak fluorescence observed for the aza-BODIPY dyes has been attributed to the free rotation of the phenyl rings around the BODIPY chromophore. Carreira and coworkers in 2005 have developed a novel strategy for the synthesis of the structurally rigidified aza-BODIPY dyes. It was speculated that the rigidified aza-BODIPY core would offer a bathochromic shifted absorption, high extinction coefficients, and enhanced fluorescence quantum yields. The authors have synthesized a conformationally restricted NIR aza-BODIPY dye, **11**, which expectedly showed intense absorption and exhibited high fluorescence quantum yields ( $\epsilon = 159000 \text{ M}^{-1}\text{cm}^{-1}$ ;  $\Phi_F = 0.28$ ) (Chart 1.5) (Zhao *et al.*, 2005, 2006).

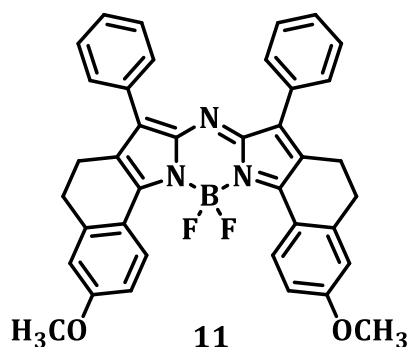
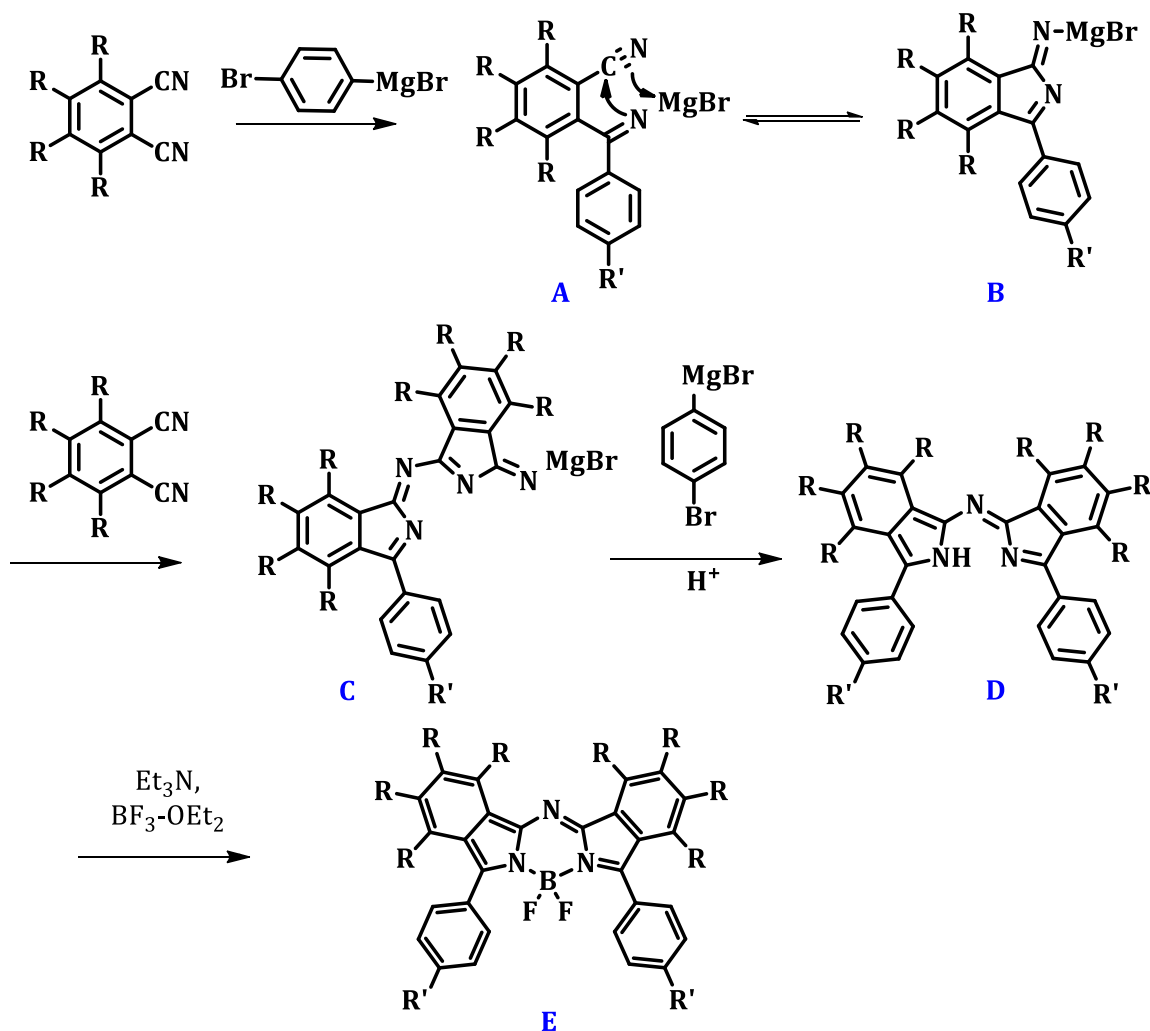


Chart 1.5

The synthesis and theoretical analysis of a series of fused-ring-expanded aza-BODIPY dyes have been described by Kobayashi *et al.* using substituted phthalonitriles and aryl magnesium bromides. The synthetic strategy adopted for the conformationally restricted aza-BODIPY dyes was simple when compared to the conventional reaction (Scheme 1.5). An initial nucleophilic attack by the Grignard reagent at the carbon atom of the nitrile moiety yielded the intermediate [(2-cyanoaryl)(aryl)methylene]-amide (**A**), which subsequently underwent ring cyclization to form the isoindol derivative (**B**). The reaction of the magnesium salt of **B** with phthalonitrile gave (**C**), which on further



**Scheme 1.5.** Synthesis of conformationally restricted aza-BODIPY dyes.

reaction with a Grignard reagent and followed by complexation with  $\text{BF}_3\text{-OEt}_2$  yielded the corresponding aza-BODIPY derivatives. Interestingly, the benzo and 1,2-naphthofused aza-BODIPY dyes displayed markedly red-shifted absorption and emission bands ( $>700\text{ nm}$ ), when compared to the tetraaryl-aza-BODIPYs (Lu *et al.*, 2011).

Kobayashi *et al.* have synthesized novel pyrrolopyrrole aza-BODIPY analogues (PPABs), **12-14** from diketopyrrolopyrrole and heteroaromatic amines using titanium tetrachloride (Chart 1.6). These systems interestingly showed intense absorption in the lower-energy visible region and exhibited significant fluorescence quantum yields of  $\Phi_F = 0.80$  (Chart 1.6). A significant perturbation of the energy levels of the frontier orbitals by the heteroaromatic units was inferred from the red-shifted absorption bands of the PPABs. The inclusion of the aryl substituent at the  $\alpha$ -positions also found to play a major role in their absorption properties through alteration of the planarity (Shimizu *et al.*, 2013).

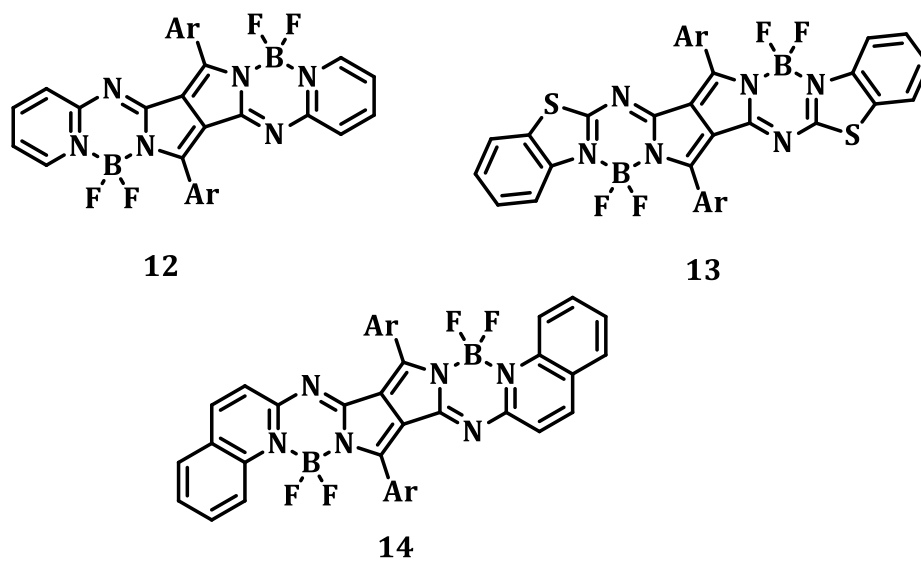


Chart 1.6

### 1.3.3. NIR Absorbing Aza-BODIPY Dyes

The typical aza-BODIPY derivatives showed absorption and emission maxima in the region 600-700 nm. To improve their absorption properties in the NIR region, two common approaches were adopted. One of these strategies was to modify the peripheral phenyl groups through introducing the electron donating group and extending the conjugation length (Bellier *et al.*, 2011; Gorman *et al.*, 2004). The other strategy was to fuse the 3- and 5-phenyl groups to the aza-BODIPY core to form the six membered rings (Loudet *et al.*, 2008; Zhao *et al.*, 2006). The synthesized systems showed significant NIR bathochromic shifts and which was ascribed to the better electron delocalization due to the enhancement of coplanarity of the aza-BODIPY core (Zhang *et al.*, 2012).

Xiao *et al.* have developed a feasible strategy to extend the absorption and fluorescence properties of the aza-BODIPY dyes, **16-17** by replacing the phenyl rings with thiophene in the parent aza-BODIPY dye, **15** (Chart 1.7). The thienyl bearing dyes **16** and **17** showed bathochromic shifts in the range of 60–90 nm in both the absorption and emission spectra, when compared to that of **15**. The X-ray crystallographic data, DFT calculations and electrochemical investigations of these systems have confirmed that the origin of the bathochromic shift was due to the smaller torsion angles, and higher electron donating capability of thienyl against phenyl units. For example, the thiophene substituted aza-BODIPY derivative **16**, exhibited strong NIR fluorescence with a quantum yield of 0.46 in acetonitrile, indicating its potential as a very competitive NIR fluorophore (Zhang *et al.*, 2012).

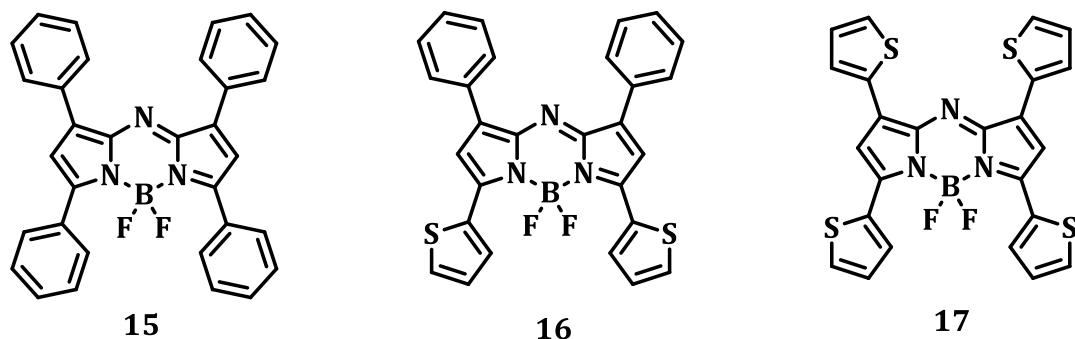


Chart 1.7

In another report, Andraud and co-workers have investigated the effect of position of the thiophene substitution on the photophysical properties of the aza-BODIPY dyes (Chart 1.8). The substitution of thiophene at 3, 5 (**18**) or 1, 7-positions (**19**) induced a significant bathochromic shift in the absorption and emission compared to their parent phenyl substituted derivatives. For example, the derivative **19** showed relatively a broad absorption spectrum, while the aza-BODIPY dye **18**, substituted with

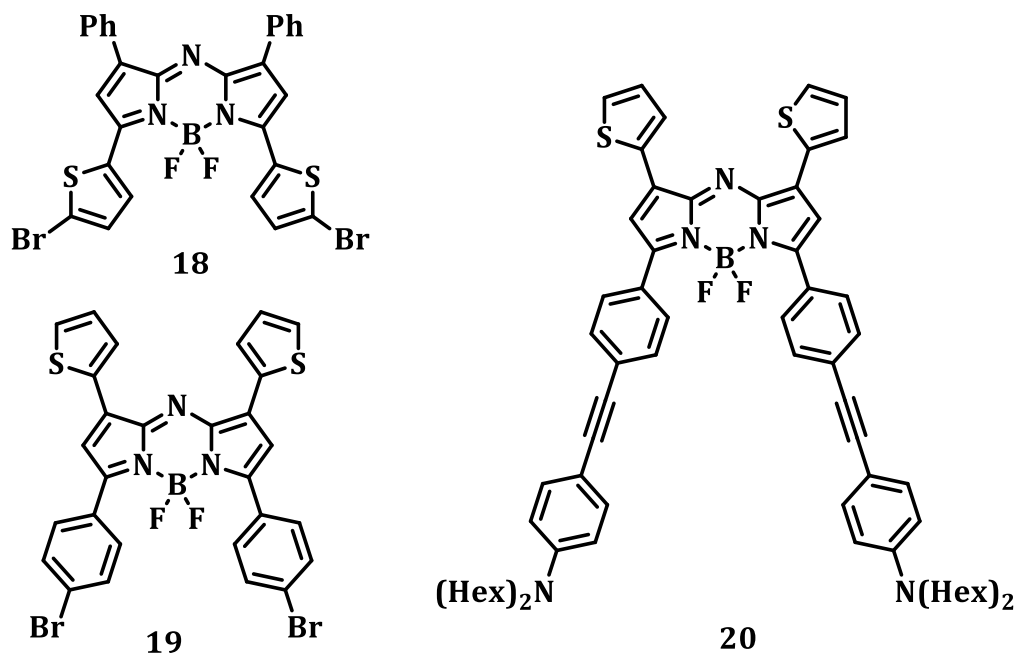


Chart 1.8

thiophene at 3, 5-positions, showed relatively red-shifted absorption and emission spectra and significant fluorescence quantum yields. Similarly, the incorporation of electron donating aniline moiety at 3, 5-positions as in the case of **20** resulted in significant bathochromic shifts both in the absorption and emission maxima (Bellier *et al.*, 2012). These results have been attributed to the increased electron-donating effect of the thiophene and aniline moieties, when compared to the parent dye.

### 1.3.4. Aza-BODIPY Dyes as Singlet Oxygen Sensitizers

The substitution of the meso-carbon of BODIPY dyes with the nitrogen atom in the aza-BODIPYs dyes led to some surprising effects in their photophysical properties as we discussed earlier in this chapter. Interestingly, the heavy atom substitution at 2,6-positions of the aza-BODIPY resulted in a reduction in the fluorescence quantum yields, and simultaneously an increased population of the triplet excited states was observed. For example, O'Shea and co-workers have reported the aza-BODIPY dyes, **21-22** with and without the bromo substitution at the core position (Chart 1.9). Of these systems, the bromo derivatives, **22a** and **22b** exhibited triplet excited states and

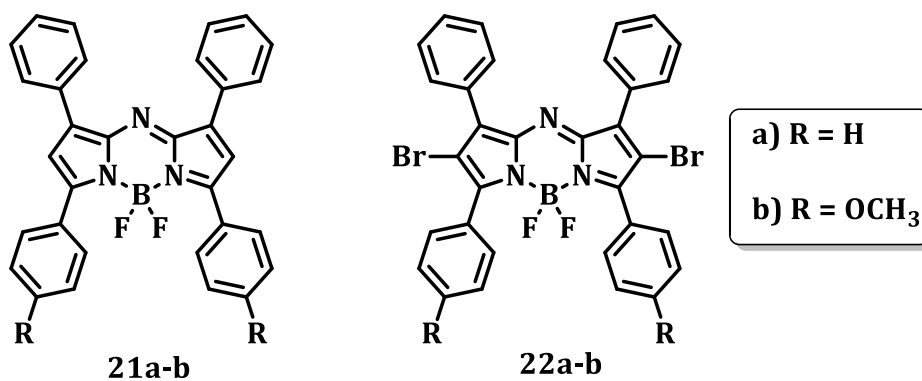
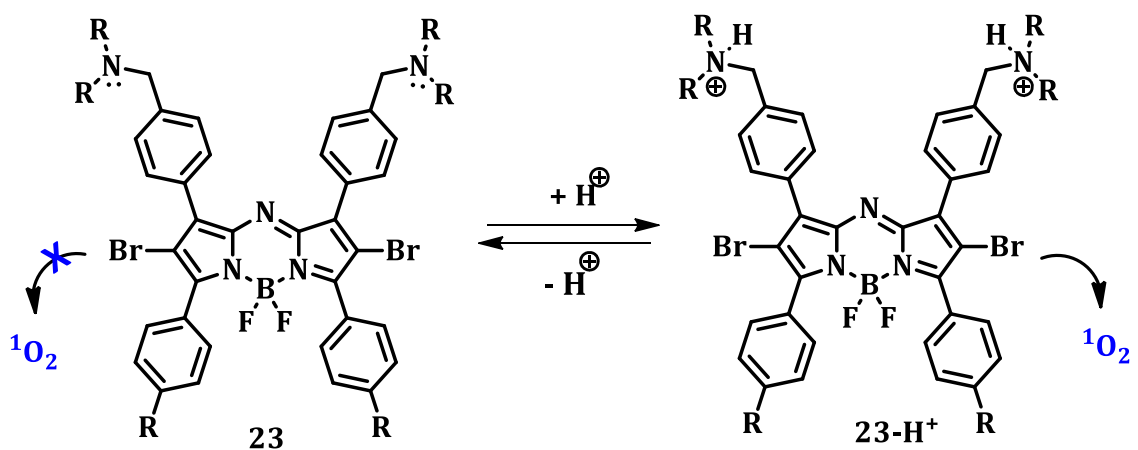


Chart 1.9



increased singlet oxygen generation, when compared to the non-halogenated systems **21a** and **21b** (Killoran *et al.*, 2002). In 2005, the same group had reported the effect of acid on the generation of singlet oxygen by the aza-BODIPY dyes. The ability of these dyes to regulate the generation of singlet oxygen in response to an acidic environmental stimulus was studied by trapping with 1,3-diphenylisobenzofuran (DPBF) (Scheme 1.6). In DMF alone, **23** exhibited negligible generation of singlet oxygen, however by the addition of an acid, singlet oxygen generation by the derivative **23** was found to be enhanced significantly when compared to the parent derivative. By comparing singlet oxygen generation rates of **23** in the presence and absence of acid gave a relative rate enhancement of *ca.* 8.5. These observations have been attributed to the control of singlet oxygen by the Photo-induced Electron Transfer (PET) mechanism (McDonnal *et al.*, 2005). Even though, there were a few more reports on singlet oxygen generation by the aza-BODIPY dyes, a systematic tuning of the triplet excited state and singlet oxygen generation were not explored in the literature.



**Scheme 1.6.** Schematic representation of singlet oxygen generation switching in the aza-BODIPY dyes through protonation.

### 1.3.5. Aza-BODIPY Dyes as Chemosensors

The development of organic chromophores having absorption in the near-infrared (NIR) and visible spectral regions has been an attractive area since such systems can have potential use as optical probes. In this context, O'Shea and co-workers have reported the aza-BODIPY derivative **24** (Chart 1.10), which showed excellent sensor performance with significant OFF-ON fluorescence intensity responses and low microenvironment polarity effects. Upon protonation, the fluorescence spectrum of **24** showed a strong proton induced fluorescence enhancement (Killoran *et al.*, 2006). In 2008, the same group has reported an intrinsic dual chemosensor based on the aza-BODIPY dye which can be used for monitoring of the pH changes. For example, **25** having two intrinsically connected amine donors exhibited pronounced spectral changes in response to acid analyte (Chart 1.10). The authors have made the aqueous solutions of the chemosensor, **25**, using the emulsifier Cremophor EL (CrEL), which showed a complete quenching of the fluorescence in the pH range, where the amine receptor remained un-protonated and upon protonation,

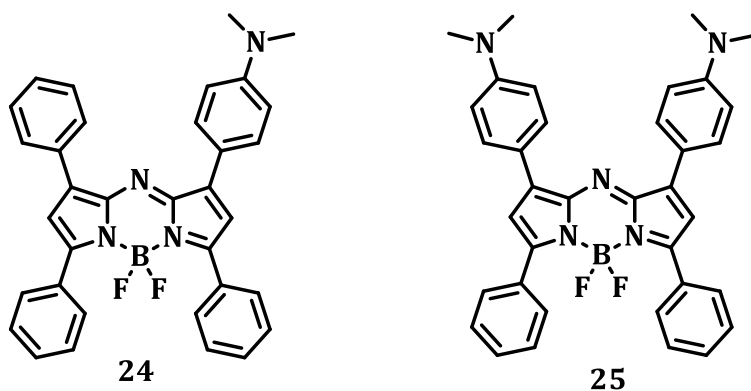
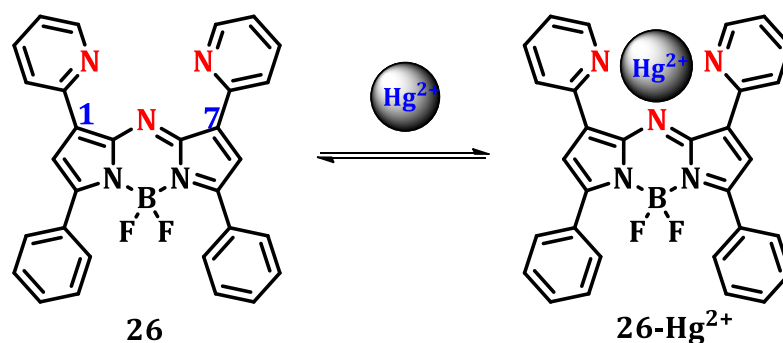


Chart 1.10

the fluorescence spectrum showed a strong proton induced fluorescence enhancement at 685 nm (Killoran *et al.*, 2008).

Akkaya *et al.* have reported the first application of an aza-BODIPY dye in metal ion recognition. The authors have synthesized a pyridyl substituted aza-BODIPY dye, **26**, having the pyridyl substituents at positions 1 and 7 which acted as a well-defined pocket for the metal ion binding (Scheme 1.7). This aza-BODIPY derivative showed effective interaction with Hg(II) ions, when compared to other ions and signaled the event through changes in both absorption and emission properties. Of the various metal ions, the mercuric ions produced the largest spectral changes in both the absorption and emission spectra, thereby demonstrating their selective detection. On mercuric ion addition, the absorption maximum of **26** shifted from 655 to 690 nm through a clear isosbestic point at 672 nm (Coskun *et al.*, 2007).



**Scheme 1.7.** Schematic representation of the recognition of mercuric ions (Hg<sup>2+</sup>) in the well-defined pocket of aza-BODIPY dye **26**.

Kobayashi and co-workers have reported a novel aza-BODIPY, **27**, containing two fused pyrazine rings from the pyrazine phthalonitrile precursors (Figure 1.2). This derivative was found to be highly selective for the NH<sub>4</sub><sup>+</sup> ions and has exhibited

pronounced spectral changes from green to pink enabling their facile naked-eye detection. This observed  $\text{NH}_4^+$  mediated color change and fluorescent quenching was attributed to the formation of H-aggregates of the aza-BODIPY. Upon addition of the  $\text{NH}_4^+$  ions, there was a marked decrease in the molar absorption coefficient and which was associated with a quenching of the fluorescence intensity (Liu *et al.*, 2011).

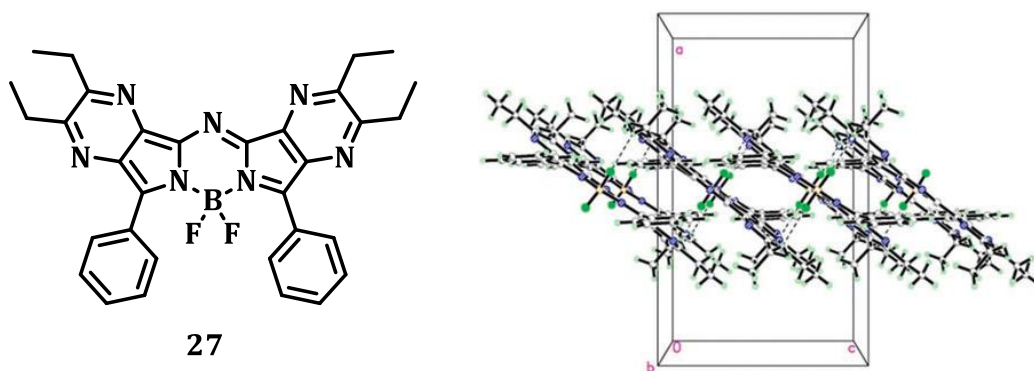


**Figure 1.2.** Structure of the aza-BODIPY based chemosensor, **27** and its one-dimensional crystal arrangement viewed along the c axis. (Adapted from the reference Liu *et al.*, 2011).

The chemosensors based on the aza-BODIPY dyes, thus discussed in this section were some of the important representative examples of each category reported in the literature so far. As indicated, most of these systems were limited to either metal cations or to detect the changes in pH of the medium. There were no scientific reports which deal with the detection of environmentally important toxic anions as well as biologically important neutral molecules by using the aza-BODIPY derivatives. In this context, a well and designed chemodosimetric approach based on the novel aza-BODIPY based probes would be highly useful for the development of selective probes for biologically relevant anions and neutral molecules.

### 1.3.6. Aza-BODIPY Dyes as Energy Transfer Cassettes

Many biological experiments involve irradiating a mixture of different fluorescent probes with a single excitation source. To be effective in such multiplexing experiments, the fluorophore must have intense and well resolved fluorescence emission peaks. The applications of the dyes that emit close to the excitation wavelength will be limited due to the resolution problems, while for the dyes that emit far from the excitation wavelength will suffer from the reduction in intensity (Ulrich *et al.*, 2008). To overcome these issues, radiationless electronic energy transfer has been used in such multiplexing experiments. In these systems, the energy of a donor dye (that absorbs at relatively short wavelengths) transferred to an acceptor dye that emits at longer wavelengths. Therefore, the development of ‘energy transfer cassettes,’ in which the donor and acceptor components are introduced simultaneously as a single unit, has received intense attraction during the last decade. In this context, the BODIPY derivatives have been widely used as energy transfer antennas, but their analogues, the aza-BODIPYs have not been explored despite the fact that they have intriguing spectroscopic and excited-state dynamics in the NIR region (Batat *et al.*, 2011).

Fukuzumi and co-workers have developed a ‘molecular clip’ featuring an NIR emitting aza-BODIPY which was covalently linked to two zinc-porphyrins to host a three dimensional electron acceptor fullerene, **28** via a ‘two-point’ metal–ligand axial coordination (Chart 1.11). In this case, an efficient singlet-singlet energy transfer from the excited porphyrin moiety to the aza-BODIPY part was observed in the dyad and triad in nonpolar solvents. In contrast, both the electron and energy transfer processes

were observed in polar solvents. Furthermore, these supramolecular polyads were utilized to build photoelectrochemical cells and the presence of the aza BODIPY and fullerene entities of the tetrad improved their overall light energy conversion efficiency. An incident photon-to-current conversion efficiency was observed to be *ca.* 17% for the tetrad modified electrode (D'Souza *et al.*, 2012).

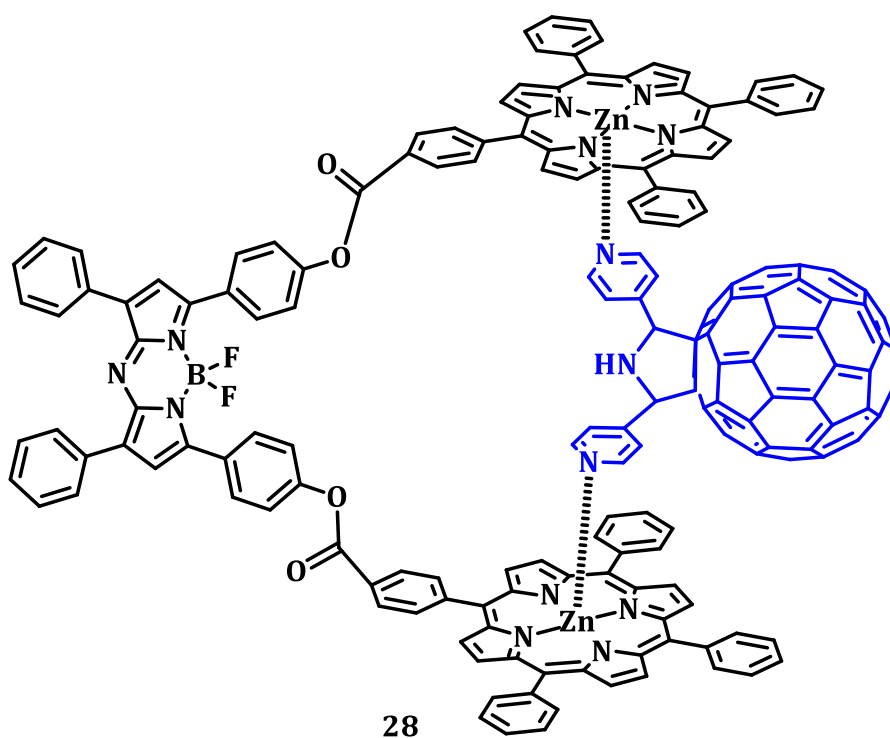


**Chart 1.11**

In another report, Ng and co-workers have described a  $\beta$ -cyclodextrin conjugated aza-BODIPY dyad, which formed stable complexes with metal-free and zinc (II) tetrasulfonated porphyrins in water (Figure 1.3). The UV-Vis studies have revealed formation of a 1:1 host-guest complex between aza-BODIPY- $\beta$ -CD conjugate and the porphyrin guest molecules. The resulting complexes exhibited predominantly a photoinduced energy or electron transfer processes depending on the nature of

porphyrin chromophore. When the porphyrin center was changed from metal-free to zinc (II), there was a switch over of the photoinduced process from the energy transfer to the electron transfer in the complex, and which was confirmed through time-resolved fluorescence and picosecond transient measurements (Shi *et al.*, 2013).

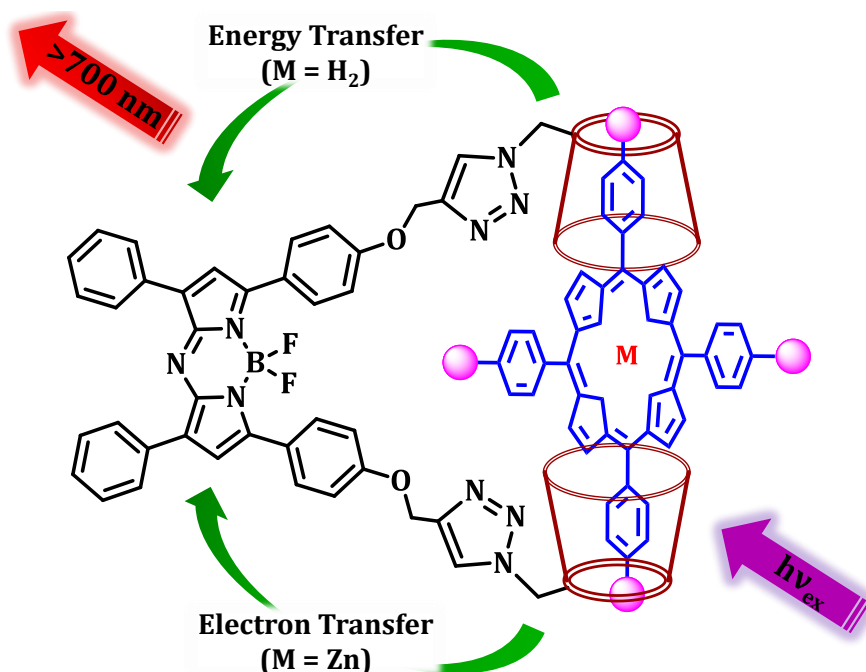


**Figure 1.3.** The schematic representation of the switching of electron transfer and energy transfer processes in  $\beta$ -CD-aza-BODIPY-porphyrin conjugates.

Andraud and co-workers have reported the two photon absorption (TPA) properties of the two extended  $\pi$ -conjugated aza-BODIPY dyes, **29-30** having O-hexyl and N, N-dialkyl chains (Chart 1.12). For example, the O-hexyl derivative, **29** showed relatively less non-linear optical (NLO) activity, when compared to the N-alkyl derivative, **30** which exhibited significant TPA cross section values (around 600 GM) over the broad 1300–1450 nm spectral range. Furthermore, at lower wavelengths, a significant increase was observed with a maximal two-photon cross-section of 1070

GM at 1220 nm. Thus the versatile nature of these of chromophores can be explored further to optimize properties in the NIR region by functionalization and to develop novel and efficient TPA systems based on aza-BODIPY dyes (Bouit *et al.*, 2009).

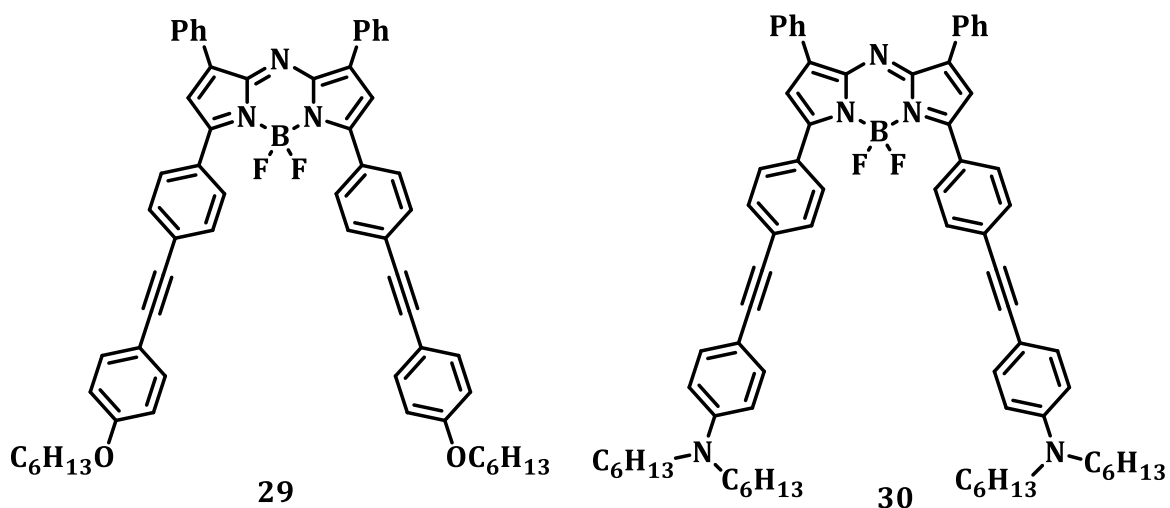


Chart 1.12

Maury and co-workers have introduced few novel conjugated aza-BODIPY dyes, **31-32** having pendant nitrofluorenylethynyl substituents at the peripheral phenyl arms (Chart 1.13). This functionalization allows for moving the absorption and luminescence of these dyes in the NIR region (*ca.* 650-750 nm), conserving a good quantum yield. These marked red shift in the absorption and fluorescence spectra observed for these dyes were attributed to the extension of conjugation and charge transfer character, whereas the large emission Stokes-shift observed was due to the excited state reorganization. The authors have successfully achieved the bathochromic shift in the photophysical properties of the aza-BODIPY dyes and extended into the NIR region alternatively through peripheral substitution (Bellier *et al.*, 2011).



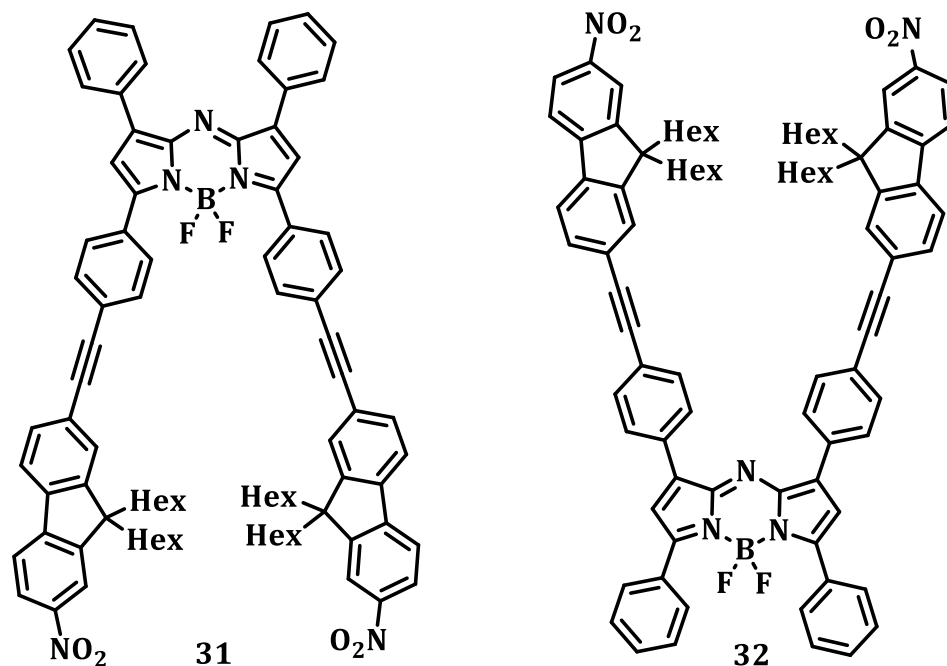


Chart 1.13

### 1.3.7. Aza-BODIPY Dyes as Therapeutic Agents

Investigation of the non-porphyrin photosensitizers for the development of novel photodynamic therapeutic (PDT) agents has been an active area of research in recent years. Among these sensitizers, the aza-BODIPY derivatives show favorable strong absorption in the NIR region, resistance to photobleaching, and higher light-dark toxicity ratios than the conventional PDT sensitizers. O'Shea and co-workers have reported a few water soluble aza-BODIPY dyes, **33-35** bearing sulfonic acid, carboxylic acid or quaternary amine moieties (Chart 1.14). The *in vitro* photobiological properties using DMEM solutions of **33-35** indicated their efficient internalization in MDA-MB-231 cells at a relatively short incubation period. The nuclear co-staining with 4,6-diamidino-2-phenylindole (DAPI) showed that the sub-cellular localization of these dyes in the cytoplasm (Tasior *et al.*, 2010).

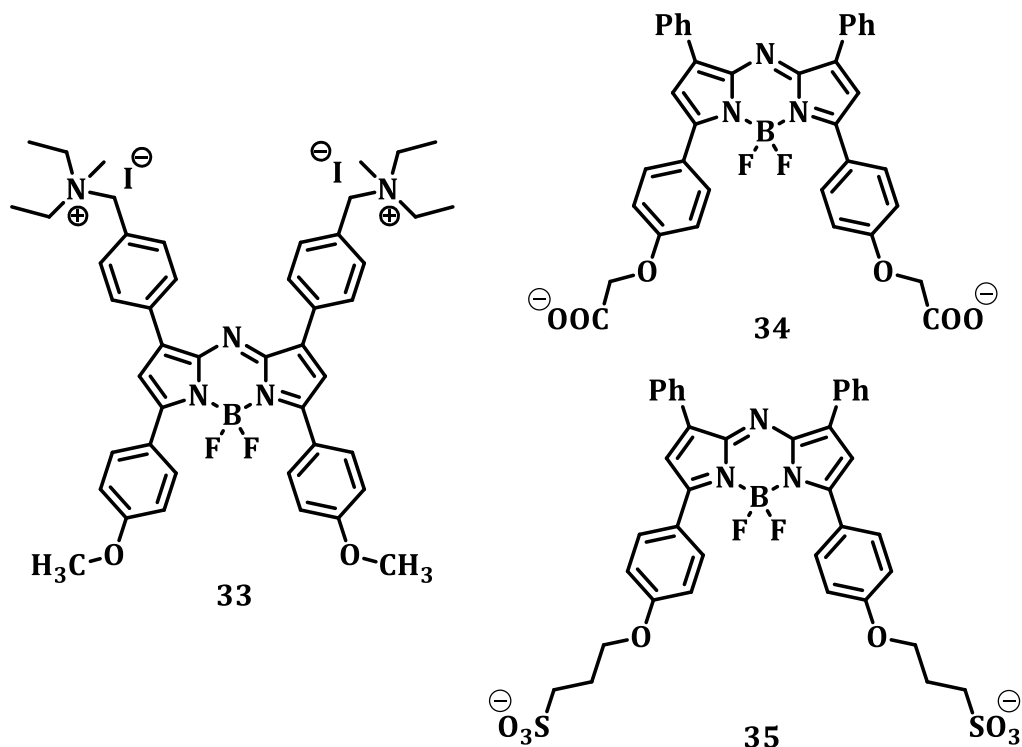


Chart 1.14

Similarly, the same group developed few aza-BODIPY based nanoparticles systems that switch their fluorescence ON following cellular uptake but remained as fluorescence OFF in the extracellular environments (Chart 1.15). The mechanism was based on the control of molecular fluorophore aggregates at the particle surface. The reason for the fluorescence OFF state in the aqueous environment was assigned due to the aggregation of the hydrophobic fluorophore. However, in the presence of a micelle forming disaggregating agents, the fluorophore molecules were far from the surface of the particles and hence exhibited enhancement of the fluorescence intensity. Furthermore, the authors have explored the conjugate, **36** as a real time *in vitro* imaging agent using MDA-MB-231 (breast cancer), HEK293T (kidney), and CAKI-1 (renal cancer) cell lines. Interestingly, this system showed OFF-ON fluorescence

switching by the uptake of cells (Palma *et al.*, 2011). As these systems exhibit strong NIR absorption and high cellular uptake, the appropriately substituted aza-BODIPY based sensitizers can have application as effective PDT and imaging agents.

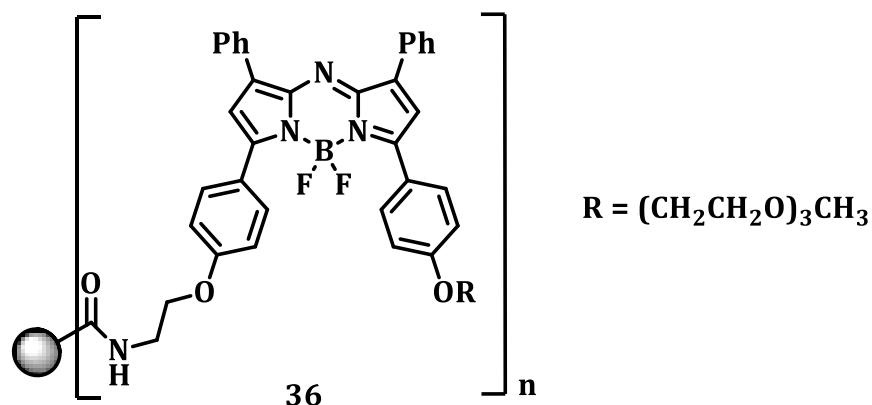


Chart 1.15

### 1.3.8. Photovoltaic Applications of Aza-BODIPY Dyes

Development of organic electronic devices, such as organic light-emitting diodes (OLEDs), dye sensitized solar cells, organic field effect transistors (OFETs), and organic memory devices, has been an active area of research in recent years (Dou *et al.*, 2013; Grimsdale *et al.*, 2009; McCulloch *et al.*, 2006; Möller *et al.*, 2003; Burroughes *et al.*, 1990). Of the various chromophores, the aza-BODIPY dyes have attracted much interest owing to their high molecular extinction coefficients and better photostability. These dyes have been investigated as p-type or donor materials in solution-processed bulk heterojunction (BHJ) solar cells (Mueller *et al.*, 2012; Rousseau *et al.*, 2009; Hong *et al.*, 2009). For example, Giordani and co-workers have described an amine functionalized donor-acceptor system, **37** containing aza-BODIPY dye as the donor and functionalized single-wall carbon nanotube (SWNT) as the acceptor (Chart 1.16). The

transient absorption measurements have confirmed the efficient electron transfer from the photoexcited aza-BODIPY to SWNT resulting in the formation of radical ion pair state with a lifetime of 1.2 ns (Flavin *et al.*, 2011).

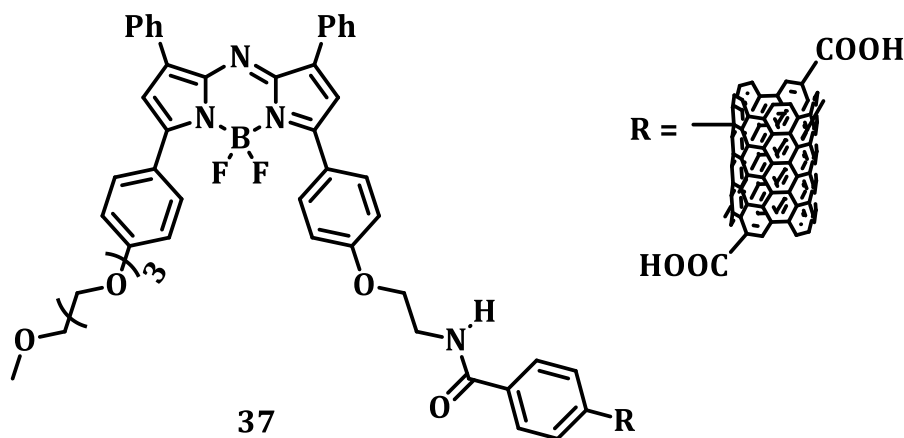
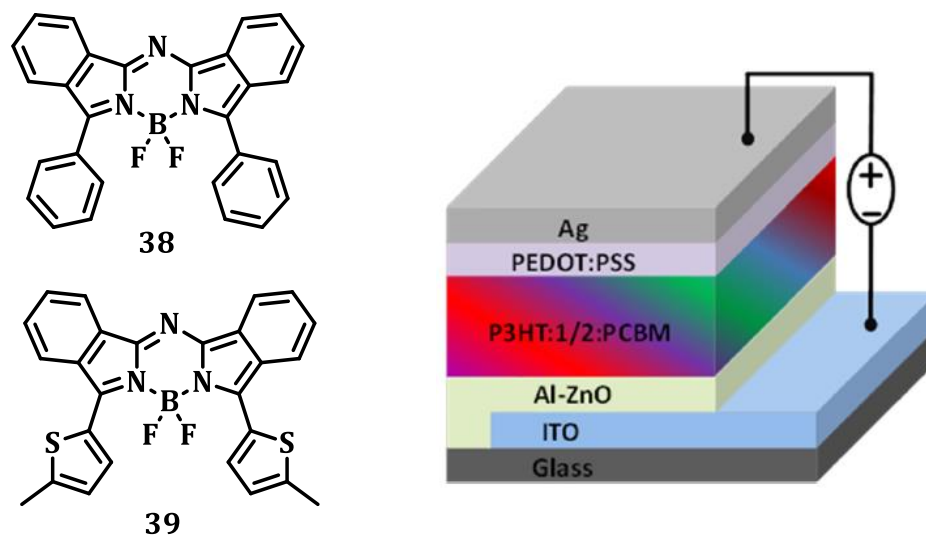


Chart 1.16

In another report, the inverted organic solar cells based on poly(3-hexylthiophen-2,5-diyl) (P3HT) and phenyl-C61-butyric acid methyl ester (PCBM) blended with two different NIR absorbing benz-annulated aza-BODIPY dyes, **38** and **39** were constructed (Min *et al.*, 2013). The amount of these two aza-BODIPY dyes, **38** and **39** within the P3HT and PCBM matrix, was systematically varied, and the characteristics of the respective devices were recorded. Although the addition of both the aza-BODIPY dyes enhanced the absorption of the blends, only the addition of phenyl substituted aza-BODIPY dye, **38** showed improved overall power conversion efficiency (PCE) in the NIR region when comparative to the thiophenyl derivative, **39** (Figure 1.4). These results paved the way for the integration of NIR absorbing aza-BODIPY derivatives as sensitizers in the fabrication of ternary composite solar cells.



**Figure 1.4.** The structure of the aza-BODIPY dyes **38** and **39**, and the schematic illustration of P3HT:aza-BODIPY:PCBM solar cell architecture (Adapted from the reference Min *et al.*, 2013).

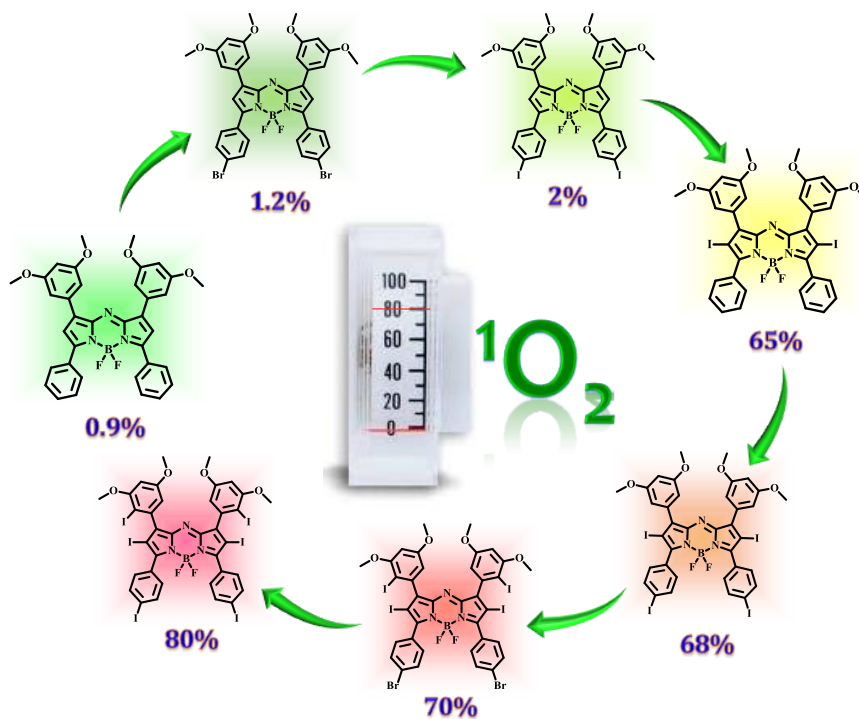
## 1.4. OBJECTIVES OF THE PRESENT INVESTIGATION

The aza-dipyrromethenes and their boron complexes (aza-BODIPY), which differ from the widely exploited BODIPY dyes by the substitution at the meso position (8<sup>th</sup> position), have not been well explored in the literature. As these aza-BODIPY dyes exhibit high photostability and strong absorption in the NIR region, the appropriately substituted systems can be investigated for their use as effective sensitizers for biological and material applications. In this context, our main goal was to design novel aza-BODIPY systems and explore their scope and applications in photodynamic therapy, photooxygenation reactions and molecular recognition. One of our objectives was to design sensitizers based on the aza-BODIPY dyes and investigation of their excited state properties such as triplet excited state quantum yields and singlet oxygen

generation efficiency. It was also of our interest to investigate the effect of heavy atom substitution on the photophysical properties of various aza-BODIPYs including their efficacy as singlet oxygen generators. Another objective of the present thesis has been to investigate *in vitro* photobiological properties of the aza-BODIPY derivatives thus synthesized as well as their efficacy as catalysts in the singlet oxygen mediated green photooxygenation reactions. Yet another objective of our study was to design functionalized novel aza-BODIPY derivatives and evaluation of their potential as efficient probes for environmentally and biologically important analytes.

We have synthesized novel few halogenated aza-BODIPY dyes and have tuned their quantum yields of triplet excited states as well as their singlet oxygen generation efficiency. Our detailed studies indicated that these systems exhibit good solubility in common organic solvents, strong absorption in the NIR region and excellent photostability. Moreover, through proper halogenations, we have been successful in tuning their triplet excited state and singlet oxygen quantum yields from *ca.* 1% to 90%. *In vitro* photobiological studies of the selected aza-BODIPY dyes using the amphiphilic lipid, **DSPE** have revealed that these conjugates effectively induced apoptosis mediated cancerous cell destruction. Furthermore, we have demonstrated that the selected aza-BODIPY dyes were found to be quite efficient as green catalysts for photooxidation of aromatic alcohols (phenol and thiophenol) to their corresponding oxidized products in both solution and also when coated on the polymer matrix. Lastly, the aza-BODIPY dyes substituted with azido and amino functional groups were found to act as selective and sensitive probes for the on-site analysis and detection of biologically important analytes such as H<sub>2</sub>S and nitrite ions in the aqueous medium.

## DESIGN OF AZA-BODIPY DYES: TUNING OF TRIPLET EXCITED STATE AND SINGLET OXYGEN GENERATION EFFICIENCIES



### 2.1. ABSTRACT

We synthesized a new series of aza-BODIPY derivatives (**4a-c**, **5a,c** and **6b,c**) with appropriate substitution of heavier halogen atoms such as bromine and iodine, and have investigated their photophysical properties. These derivatives showed strong NIR absorption in the range of 660-680 nm and have exhibited good solubility in the common organic solvents such as  $\text{CHCl}_3$ ,  $\text{CH}_3\text{CN}$ , THF, DMSO, and DMF. Fluorescence quantum yields ( $\Phi_F$ ) of these derivatives were determined and the values are found to be in the range of 0.05-0.08. The triplet excited state and singlet oxygen generation

quantum yields of these dyes were tuned by the proper substitution of halogen atoms. The effect of substitution has been studied in detail by varying the position and number of halogen atoms in the aza-BODIPY dyes. The quantum yields of triplet excited state ( $\Phi_T$ ) and singlet oxygen generation ( $\Phi_\Delta$ ) showed significant dependence on the position of halogenation of the parent dye and the heaviness of the halogen substituent. For example, we observed negligible triplet excited state and singlet oxygen yields of *ca.* 0.01 for the parent unsubstituted aza-BODIPY, **4a**, which upon peripheral bromination and iodination resulted in a marginal improvement as in the case of **4b** ( $\Phi_T = 0.07$ ,  $\Phi_\Delta = 0.012$ ) and **4c** ( $\Phi_T = 0.08$ ,  $\Phi_\Delta = 0.02$ ). In contrast, the core substituted dyes **5a** ( $\Phi_T = 0.68$ ,  $\Phi_\Delta = 0.65$ ), **5c** ( $\Phi_T = 0.70$ ,  $\Phi_\Delta = 0.60$ ) **6b**, ( $\Phi_T = 0.78$ ,  $\Phi_\Delta = 0.70$ ) and **6c** ( $\Phi_T = 0.86$ ,  $\Phi_\Delta = 0.80$ ) showed high triplet excited state yields and singlet oxygen generation efficiencies when compared to the peripheral substituted systems.

For example, the dye **6c**, substituted with six iodine atoms at the core and peripheral phenyl rings showed significant quantum yields of triplet excited state ( $\Phi_T = 0.86$ ) and singlet oxygen generation efficiency ( $\Phi_\Delta = 0.80$ ). As far as we know, these are the highest values so far reported in the literature for the triplet excited state and singlet oxygen generation quantum yields for aza-BODIPY derivatives. The uniqueness of these aza-BODIPY systems is that they are quite stable under irradiation conditions and possess strong NIR absorption. Moreover, by the judicious substitution of bromine and iodine atoms, we could successfully tune the triplet excited state and singlet oxygen yields from almost zero to *ca.* 86%, thereby demonstrating their potential as novel sensitizers for biological applications.



## 2.2. INTRODUCTION

Singlet oxygen,  $O_2 (^1\Delta_g)$ , is the lowest excited electronic state of molecular oxygen, which has a characteristic chemistry that sets it apart from the triplet ground state of molecular oxygen,  $O_2 (^3\Sigma_g^-)$  (Ogilby, 2010). Singlet oxygen, is a reactive species in a broad range of chemical and biological processes, like photodynamic therapy (PDT) (Dougherty *et al.*, 2001; Lindsey, 2000; Bonnett *et al.*, 1995), age related macular degeneration (Kelkar *et al.*, 2011; Johan *et al.*, 2009), waste-water treatment in environmental chemistry and photooxygenation reactions in fine chemical industry (Griesbeck *et al.*, 2012; Fudickar *et al.*, 2011; Timothy *et al.*, 2011; Greer *et al.*, 2006). The chemistry of singlet oxygen differs from that of molecular oxygen since it is an efficient electrophilic oxidant to several electron rich organic substrates. The presence of unpaired valence electrons in the ground state configuration of molecular oxygen is unusual and possesses high chemical reactivity. This typical electronic configuration of molecular oxygen gives rise to three different energetically close lying electronic states such as the triplet ground state ( $^3\Sigma_g^-$ ), the excited singlet state ( $^1\Delta_g$ ), and the singlet ground state ( $^1\Sigma_g^+$ ) (Skovsen *et al.*, 2005). The “classic” and most commonly cited reactions of singlet oxygen with an organic molecule invariably produces a peroxide as an initial product. Although, many of these peroxides can be isolated and characterized at low temperature (Kang *et al.*, 2002; Orfanopoulos *et al.*, 1990), they are often stable precursors to other products in systems of functional importance (e.g., a live cell). Specifically, the peroxide O–O bond has low dissociation energy and as such readily cleaved to yield oxygen-based radicals (e.g.,  $\cdot OH$  from a hydroperoxide). These radicals

can then propagate to generate a wide range of other reactive intermediates and, ultimately, a variety of reaction products (Halliwell *et al.*, 1999). Hence, singlet oxygen has the ability to interrupt the cellular functions in living organisms and exhibits high chemical reactivity towards most of the organic molecules due to the spin-allowed nature of its reactions.

Although singlet oxygen can be produced in a variety of ways such as chemical reaction, gas phase discharge etc., a convenient and most common method is through the sensitization reaction due to its extensive applications. The photosensitization is a light induced chemical process wherein the photosensitizer upon irradiation gets excited to its singlet excited state. This excited state of the photosensitizer can undergo intersystem crossing to the triplet excited state, where it can transfer its energy to molecular oxygen to produce singlet oxygen (Kamkaew *et al.*, 2013; Avirah *et al.*, 2012; Awuah *et al.*, 2012). The quantitative generation of singlet oxygen ( $\Phi_{\Delta}$ ) is one of the most essential requirements with regard to its applications. For the efficient generation of singlet oxygen in quantitative yields, the sensitizer should have high intersystem crossing efficiency and as well as high triplet quantum yields.

The main strategy adopted to enhance the intersystem crossing efficiency of a sensitizer is based on “heavy atom effect” by introducing heavy atoms such as bromine, iodine and transition metal ions (Scott *et al.*, 2010; Ramaiah *et al.*, 1997; Detty *et al.*, 1990; Turro, 1978). An electronic transition from a singlet to a triplet excited state within a molecule is a spin-forbidden process and as such occurs inefficiently for many compounds. In order for a transition between states of different spin multiplicities to occur effectively, a spin-orbit perturbation is generally required (Lower *et al.*, 1966).

Enhanced spin-orbit perturbations can be achieved by the attachment of a heavy atom directly onto the molecule (internal heavy atom effect) or placing the molecule in a surrounding environment containing heavy atoms (external heavy-atom effect) (Koziar *et al.*, 1978; McClure, 1949; Yuster *et al.* 1949). A series of photosensitizers have been reported in the literature as singlet oxygen generators, which include Methylene Blue, Rose Bengal, porphyrins, chlorins, bacteriochlorins, phthalocyanines, and squaraines (Marydasan *et al.*, 2013; Karunakaran *et al.*, 2013; Ishii *et al.*, 2012; Randy *et al.*, 2011; Jisha *et al.*, 2010; Ribeiro *et al.*, 2006; Pushpan *et al.*, 2002; Bonnett *et al.*, 2001).

Recently, the boron complexes such as 4,4-difluoro-4-bora-3a,4a-diaza-s-indacenes, abbreviated as BODIPYs have been reported to hold great promise as ideal sensitizers owing to their favorable properties (Ozlem *et al.*, 2009; Ziessel *et al.*, 2009; Loudet *et al.*, 2007). These systems exhibit strong absorption in the range 500-600 nm, and significant fluorescence quantum yields and high photostability. In contrast, the aza-dipyrrromethenes and their boron complexes (aza-BODIPYs) showed around 100 nm bathochromic shifted absorption, when compared to BODIPYs; but have attracted less attention (Gallagher *et al.*, 2005; Gorman *et al.*, 2004). In this context, we designed a series of novel aza-BODIPY derivatives **4a-c**, **5a,c** and **6b,c** (Chart 2.1), and have investigated their photophysical properties under different conditions. Our results demonstrate that, the triplet excited state as well as singlet oxygen generation efficiencies of these aza-BODIPY derivatives can be successfully tuned from around *ca.* 1% to 86% through proper heavy atom substitution.

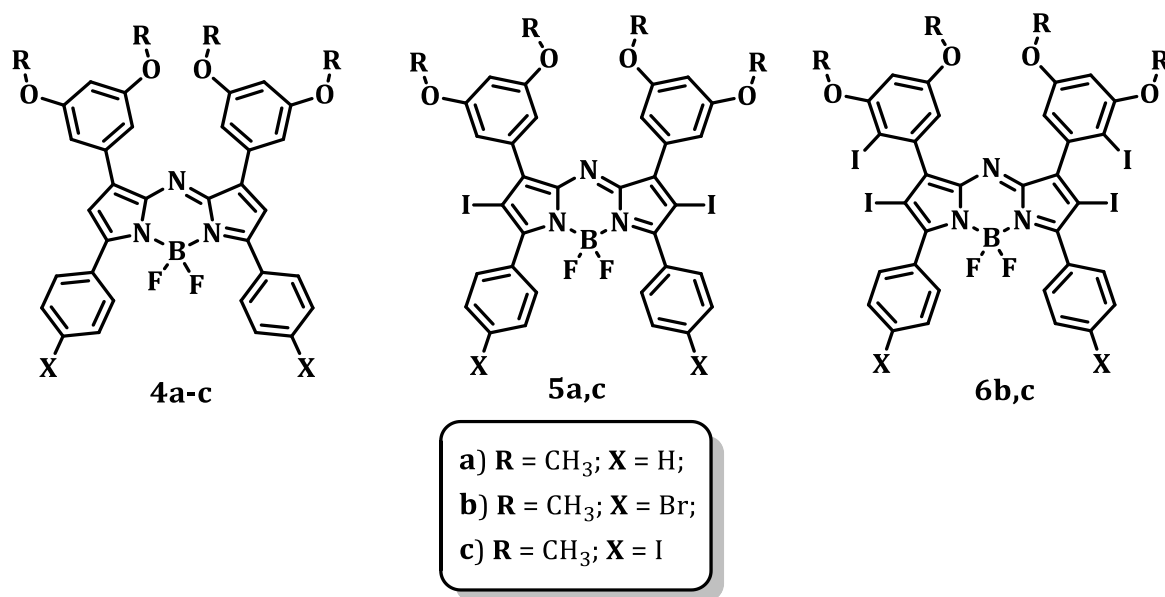


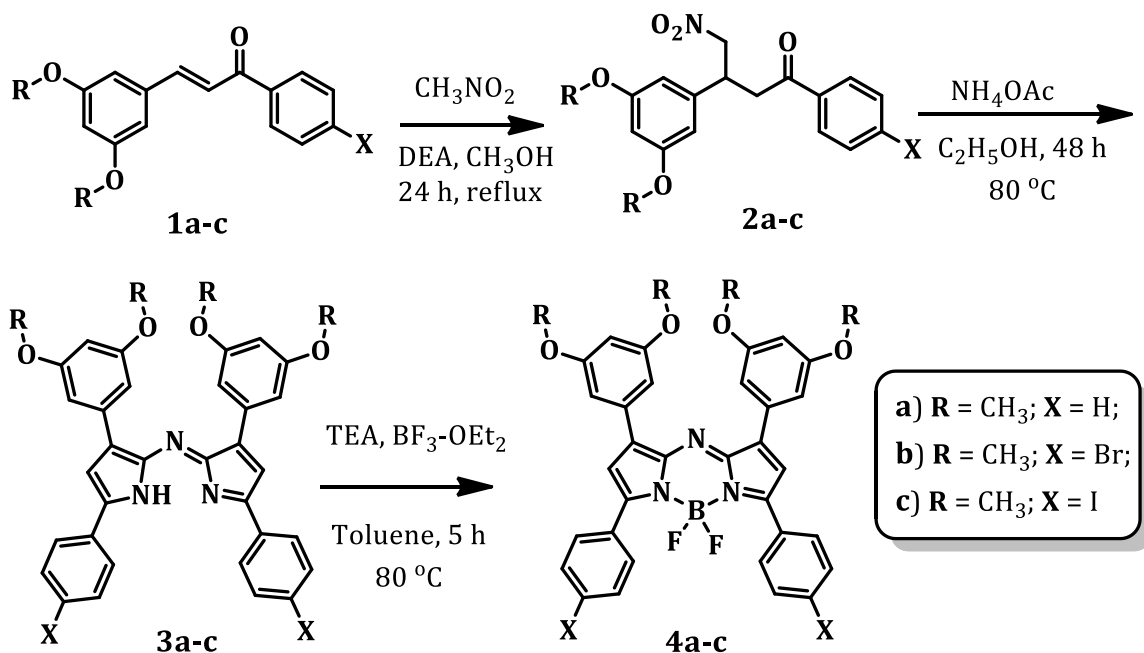
**Chart 2.1.** Structures of the aza-BODIPY derivatives **4-6** synthesized.

## 2.3. RESULTS AND DISCUSSION

### 2.3.1. Synthesis and Photophysical Properties

The synthesis of the aza-BODIPY derivatives **4a-c**, **5a,c** and **6b,c** was achieved as shown in Scheme 2.1. The compounds **4a-c** were synthesized in a facile three-step route starting from the chalcones **1a-c**, which in turn were synthesized by aldol condensation reaction between the corresponding aldehyde and acetophenone. Addition of nitromethane to the chalcone in presence of diethylamine in methanol gave the addition products **2a-c** in *ca.* 75-80% yields. Subsequently, the condensation products **3a-c** were prepared by refluxing **2a-c** with ammonium acetate in ethanol for 48 h. The product precipitated during the course of the reaction was filtered and recrystallized to yield the aza-dipyrromethenes, **3a-c** (40-50%) having violet metallic luster. Subsequently, **3a-c** were converted to the targeted aza-BODIPY derivatives **4a-c**

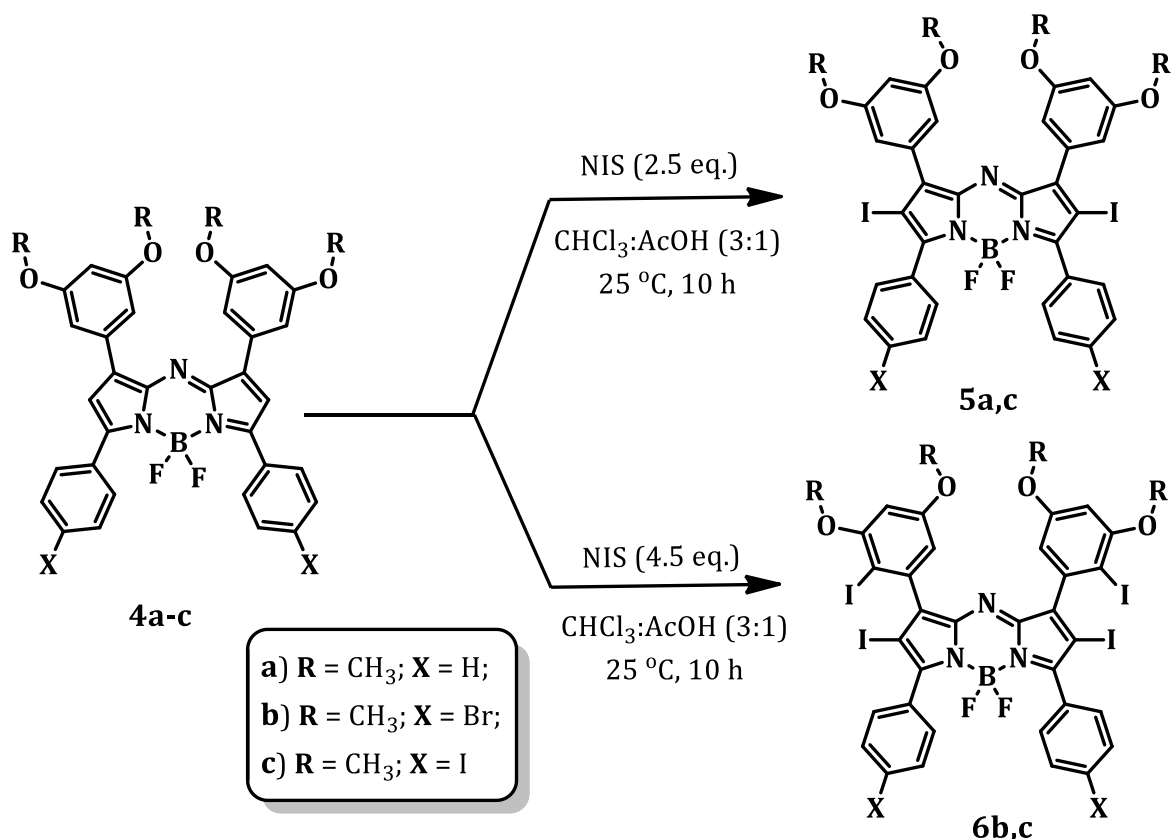
(65-70%) by refluxing with boron trifluoride diethyl etherate and triethylamine in toluene for 5 h. The products **4a-c** formed were isolated, purified through column chromatography and were characterized on the basis of spectral and analytical evidence (Scheme 2.1).



**Scheme 2.1.** Synthesis of the aza-BODIPY derivatives **4a-c**.

The iodination of the aza-BODIPY derivatives **4a-c** was achieved using *N*-iodosuccinimide (NIS) in a mixture (3:1) of chloroform and acetic acid. The selective iodination can be done by controlling the equivalents of NIS. When 2.5 equivalents of NIS was used, we could isolate the compounds **5a,c** in 60-65% yields having iodine atoms only at the core of the pyrrole ring. On the other hand, when the iodination was carried out using 4.5 equivalents of NIS under similar conditions gave the tetraiodo derivatives **6b,c**. The reaction mixture after column chromatography yielded the aza-BODIPY derivatives **6b,c** in 65-68% yields (Scheme 2.2). All these products were

recrystallized from toluene and characterized on the basis of spectral and analytical evidence.



**Scheme 2.2.** Synthesis of the aza-BODIPY derivatives **5a,c** and **6b,c**.

The starting aza-dipyrromethenes **3a-c**, showed absorption in red region (610-625 nm) having molar extinction coefficients in the range  $3 \times 10^4 - 7 \times 10^4 \text{ M}^{-1}\text{cm}^{-1}$  (Figure 2.1A). The attachment of the lewis acid  $\text{BF}_2^+$  to the ligand induced a red-shift in the absorption spectra of the aza-BODIPY derivatives. In the case of the aza-BODIPY derivatives **4a-c**, we observed a bathochromic shift in the absorption of *ca.* 50-60 nm as compared to its corresponding dipyrromethene derivatives (Figure 2.2A). Notably, in the case of the iodinated systems, the core substituted derivatives **5a** and **5c** showed blue shifted absorption maximum at 660 and 670 nm, respectively, while the

derivatives **6b,c** having substitution both at the peripheral and core positions, exhibited absorption maximum at 666 and 676 nm, respectively. All these aza-BODIPY derivatives showed good solubility and exceptional stability in common organic solvents such as  $\text{CHCl}_3$ ,  $\text{CH}_3\text{CN}$ , THF, DMSO, and DMF.

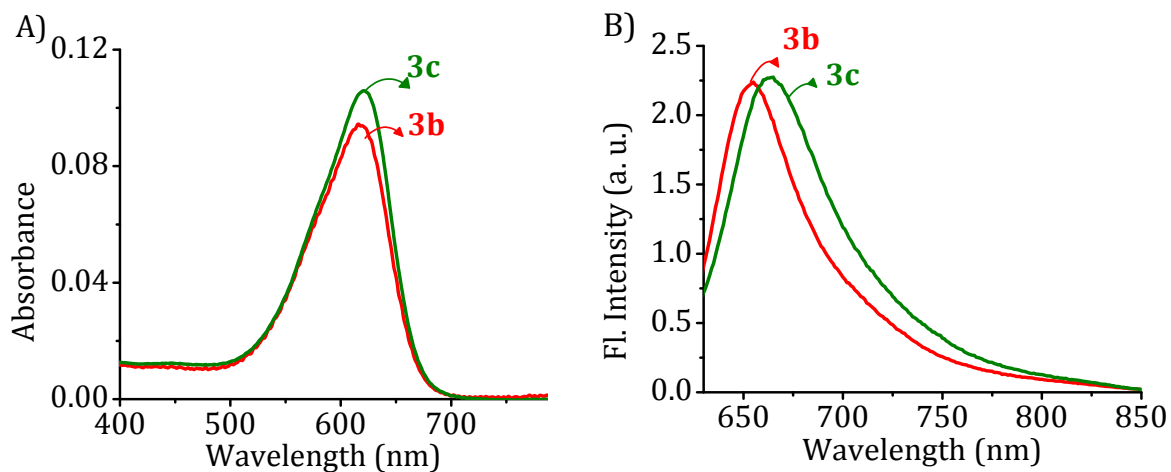


**Figure 2.1.** Representative A) absorption and B) fluorescence spectra of the aza-dipyromethenes **3b** (10  $\mu\text{M}$ ), and **3c** (10  $\mu\text{M}$ ) in DMSO,  $\lambda_{\text{ex}} = 610$  nm.

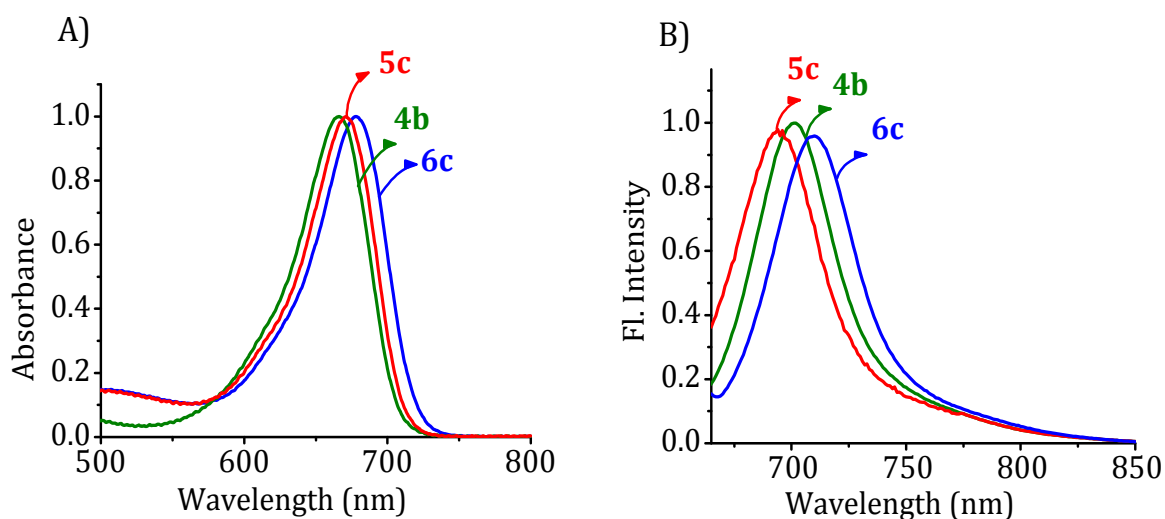


**Figure 2.2.** Normalized A) absorption and B) fluorescence spectra of the aza-BODIPY dyes **4b** (5  $\mu\text{M}$ ), **5c** (5  $\mu\text{M}$ ), and **6c** (5  $\mu\text{M}$ ) in DMSO,  $\lambda_{\text{ex}} = 650$  nm.

The fluorescence properties of the aza-dipyrromethenes and aza-BODIPY dyes were investigated in DMSO. Upon excitation of aza-dipyrromethenes, **3a-c** at 610 nm we observed the fluorescence spectra having bands in the range of 650-670 nm (Figure 2.1B). The aza-BODIPY derivatives **4-6** exhibited emission maximum in the range 690-770 nm region with a large Stoke shift of *ca.* 530-1730  $\text{cm}^{-1}$  (Figure 2.2B). The fluorescence quantum yields of these derivatives were determined by using Nile blue as the reference ( $\Phi_F = 0.27$  in methanol) (Sens *et al.*, 1981) and the values are found to be in the range 0.05-0.08. The relatively low quantum yields exhibited by these derivatives can be attributed to the enhanced intersystem crossing (ISC) because of the presence of heavy atoms such as bromine and iodine. The photophysical properties of these aza-BODIPY dyes are summarized in Table 2.1.

**Table 2.1.** Photophysical characteristics of **4a-c**, **5a,c** and **6b,c**.<sup>a,b</sup>

Compound	$\lambda_{\text{max}}$ , nm	$\epsilon$ , $10^4 \text{M}^{-1}\text{cm}^{-1}$	$\lambda_{\text{em}}$ , nm	$\tau_T$ , $\mu\text{s}$	$\Phi_T$ <sup>[c]</sup>
<b>4a</b>	680	$5.9 \pm 0.06$	772	28	$0.01 \pm 0.002$
<b>4b</b>	664	$3.8 \pm 0.15$	701	44	$0.07 \pm 0.002$
<b>4c</b>	675	$5.2 \pm 0.04$	710	7.8	$0.08 \pm 0.001$
<b>5a</b>	660	$8.3 \pm 0.02$	706	1.9	$0.68 \pm 0.02$
<b>5c</b>	670	$7.1 \pm 0.11$	695	1.8	$0.70 \pm 0.03$
<b>6b</b>	666	$6.9 \pm 0.05$	694	1.5	$0.78 \pm 0.02$
<b>6c</b>	676	$4.9 \pm 0.07$	712	1.6	$0.86 \pm 0.03$

<sup>[a]</sup> Average of more than three experiments, <sup>[b]</sup> in DMSO, <sup>[c]</sup> yields calculated through triplet-triplet energy transfer method.



### 2.3.2. Quantification of Triplet Excited States

The aza-BODIPY derivatives due to their strong absorption in the NIR region can have immense potential as efficient sensitizers in photodynamic therapy (PDT). Since the photodynamic activity of the photosensitizers is expected to involve in the generation of singlet oxygen, it is our objective to study the excited state properties of the synthesized compounds. In order to characterize the transient intermediates such as triplet excited states in these systems, we have carried out nanosecond laser flash photolysis of aza-BODIPY derivatives under different conditions. All the derivatives have sufficient absorption at 355 nm making it possible to excite them directly with the third harmonic of the Nd:YAG laser. Figure 2.3A shows the transient absorption spectrum of **6b** in DMSO obtained after 355 nm laser excitation (10 ns, 50 mJ/pulse). Upon excitation of **6b** gave the formation of fairly strong transient absorption having peaks at 320 and 510 nm, with a bleach in the region corresponding to its ground state absorption. The transient formed from **6b** within the laser pulse, decayed by a first-order process and led to the recovery of the ground state absorption (Figure 2.3B), thereby ruling out the formation of any permanent products or degradation of the dye under these conditions. To characterize the transients involved, we have checked the transient absorption after purging with oxygen under similar conditions. We observed that the transient absorption was readily quenched by dissolved oxygen, suggesting that the absorption may be due to the formation of triplet excited state (Ramaiah *et al.*, 1997). Further, the formation of triplet excited state was confirmed and quantified by quenching the transients using  $\beta$ -carotene, a well-known triplet excited state quencher.

Upon addition of  $\beta$ -carotene, which possesses a low energy level triplet excited state, led to a quenching of the transient absorption, and was accompanied by a growth of a new transient absorption at 515 nm, corresponding to  $\beta$ -carotene triplet excited state. Since the intersystem crossing efficiency in  $\beta$ -carotene is negligible, the formation of the  $\beta$ -carotene triplet excited state upon laser excitation of **6b** clearly confirms the involvement of triplet excited states of the aza-BODIPY dye, **6b**. Furthermore, the triplet excited state quantum yield ( $\Phi_T$ ) of **6b** was measured by employing the method of energy transfer to  $\beta$ -carotene using tris(bipyridyl)-ruthenium(II) complex as the reference. The quantum yield value was found to be  $0.78 \pm 0.02$  with a lifetime of  $1.5 \mu\text{s}$ .

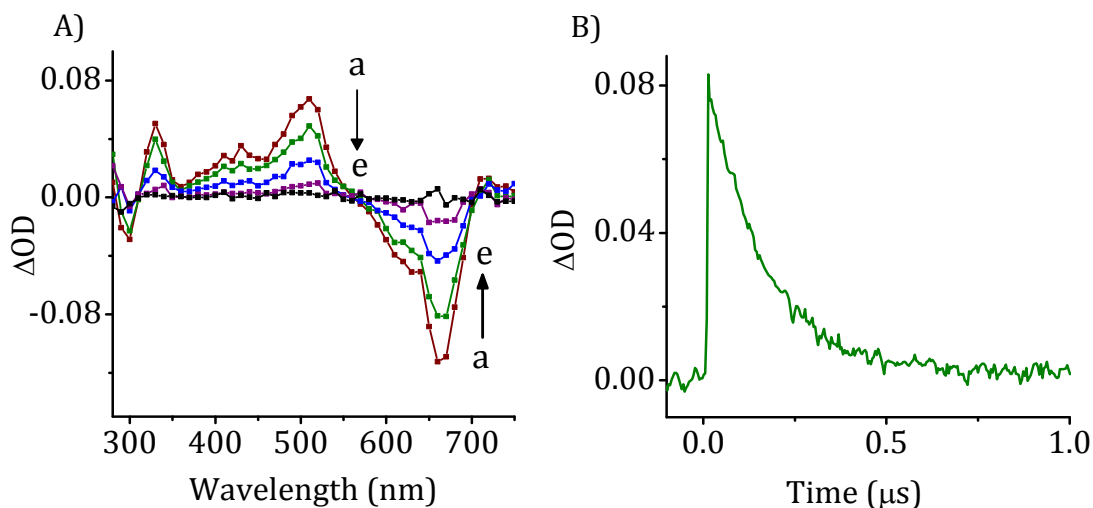


**Figure 2.3.** A) Transient absorption spectra of **6b** (10  $\mu\text{M}$ ) following 355 nm laser pulse excitation; time-resolved absorption spectra recorded at (a) 0.1, (b) 0.4, (c) 1, (d) 2, and (e) 4  $\mu\text{s}$ . B) The transient decay of **6b** (10  $\mu\text{M}$ ) at 510 nm.

Similarly, upon excitation of **6c**, having six iodine atoms, with 355 nm laser pulse in DMSO led to the formation of a transient absorption having peaks at 330 and

520 nm, with a bleach in the region corresponding to its ground state absorption (Figure 2.4). The transient having absorptions at both the wavelengths were fitted through the single exponential decay fitting and was confirmed as triplet excited state by the oxygen quenching experiments. The triplet excited state quantum yield ( $\Phi_T$ ) for **6c** showed a higher value of  $0.86 \pm 0.03$  with a triplet lifetime of 1.6  $\mu\text{s}$ , determined by the energy transfer to  $\beta$ -carotene using tris(bipyridyl)ruthenium(II) complex as the reference. Notably, this is the highest triplet excited state quantum yield value, reported for the aza-BODIPY systems so far in the literature.

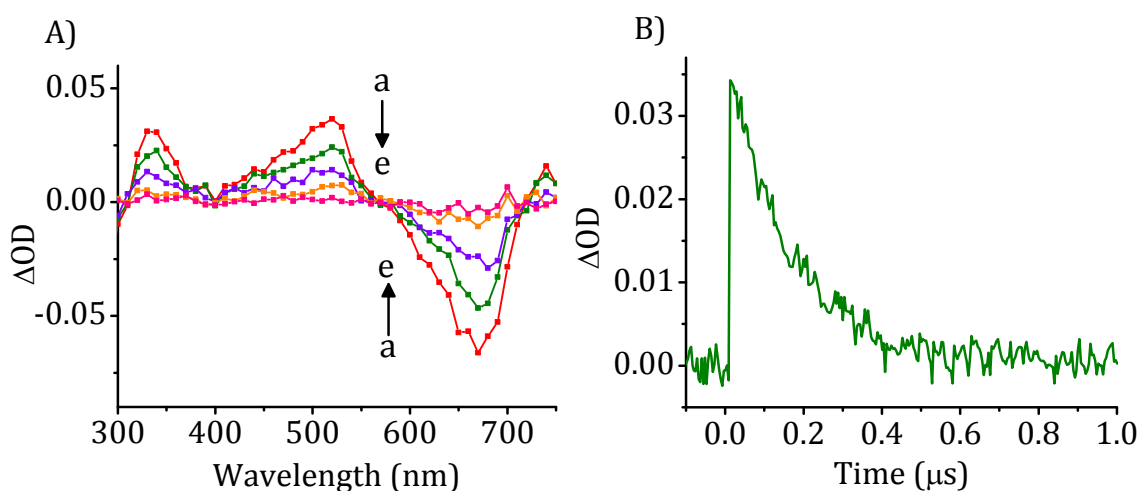


**Figure 2.4.** A) Transient absorption spectra of **6c** (12  $\mu\text{M}$ ) following 355 nm laser pulse excitation; time-resolved absorption spectra recorded at (a) 0.1, (b) 0.5, (c) 1, (d) 2, and (e) 5  $\mu\text{s}$ . B) The transient decay of **6c** (12  $\mu\text{M}$ ) at 520 nm.

The core only iodinated derivative **5a**, on the other hand, showed transient absorption maximum at 460 nm, with a bleach in the region 560-700 nm, where it has strong ground state absorption (Figure 2.5). The triplet excited state of **5a** was confirmed by quenching with molecular oxygen and the quantum yield of triplet excited state was calculated to be  $0.68 \pm 0.02$  with a triplet lifetime of 1.9  $\mu\text{s}$ . Another

core iodinated aza-BODIPY derivative **5c** having two additional peripheral iodine atoms, showed similar transient absorption spectra with a maximum at 520 nm and a bleach in the region 650-670 nm (Figure 2.6). The triplet excited state quantum yield of **5c** was found to be  $0.70 \pm 0.03$ , with a triplet lifetime of 1.8  $\mu\text{s}$  because of the presence of peripheral iodine atoms when compared to **5a**.

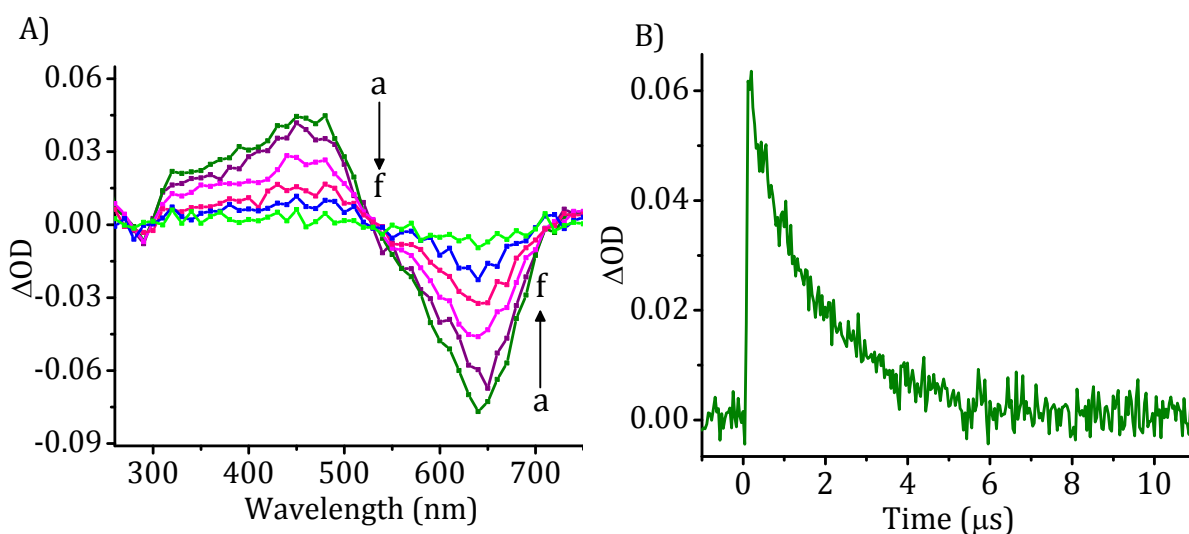


**Figure 2.5.** A) Transient absorption spectra of **5a** (10  $\mu\text{M}$ ) following 355 nm laser pulse excitation; time-resolved absorption spectra recorded at (a) 0.1, (b) 1, (c) 2, (d) 3, (e) 4 and (f) 10  $\mu\text{s}$ . B) Transient decay of **5a** (10  $\mu\text{M}$ ) at 460 nm.

In contrast, the non-core iodinated aza-BODIPY dyes **4a-c** showed transient maxima at 450, 430 and 460 nm, respectively. The parent non-halogenated dye **4a** exhibited low quantum yield of triplet excited state ( $\Phi_T = 0.01 \pm 0.002$ ) with a triplet lifetime of 28  $\mu\text{s}$ . The bromo substituted aza-BODIPY dye, **4b** on the other hand, showed a relatively better triplet quantum yield of *ca.*  $0.07 \pm 0.002$  with a lifetime value of 44  $\mu\text{s}$ , whereas the iodo derivative, **4c** exhibited almost similar triplet excited state quantum yield value of *ca.*  $0.08 \pm 0.001$ , with a lifetime of 7.8  $\mu\text{s}$ , when compared

to **4b**. Notably, when the pyrrole ring was iodinated (core substitution), we observed excellent yields of the triplet excited states as we have obtained  $\Phi_T = 0.68$  and  $0.70$  for **5a** and **5c**, respectively. Interestingly, when the core of the pyrrole as well as the peripheral phenyl ring was substituted with iodine atoms, we observed significant enhancement in the triplet quantum yields of  $\Phi_T = 0.78$  and  $0.86$  for **6b** and **6c** respectively. Thus through proper substitution, we could tune the triplet excited state quantum yields from *ca.* 1% to as high as 86% for the aza-BODIPY derivatives for their potential applications (Table 2.1).

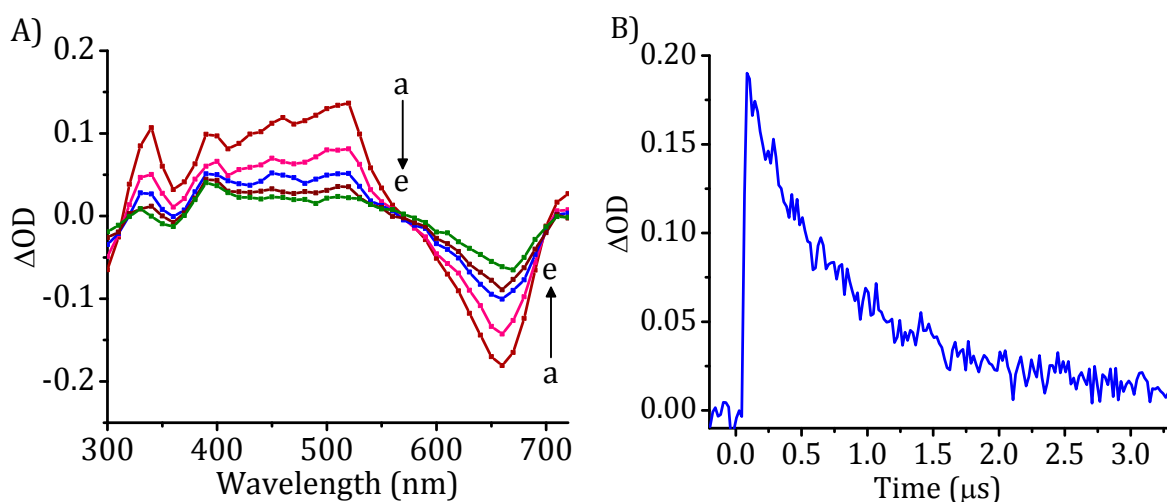


**Figure 2.6.** A) Transient absorption spectra of **5c** (8 μM) following 355 nm laser pulse excitation; time resolved absorption spectra recorded at (a) 0.1, (b) 1, (c) 2, (d) 3 and (e) 12 μs. B) The transient decay of **5c** (8 μM) at 460 nm.

### 2.3.3. Quantification of Singlet Oxygen Generation

Enhanced triplet quantum yields are favorable for the efficient generation of singlet oxygen and hence we have examined the efficacy of the photosensitized singlet oxygen generation by these aza-BODIPY systems. The quantum yields of singlet oxygen

generation were determined indirectly by monitoring the photooxidation of 1,3-diphenylisobenzofuran (DPBF) through absorption spectroscopy (Mirenda *et al.*, 2010; Rossi *et al.*, 2008; Morone *et al.*, 2006) as well as by directly monitoring the luminescence intensity at 1270 nm (Mark *et al.*, 2002; Quimby *et al.*, 1975). For the indirect method, a solution of the aza-BODIPY derivative and DPBF was irradiated using 630 nm long pass over a period of 6-600 s depending on the derivatives, and the decrease in the absorption band ( $\sim 10\%$ ) of DPBF at 418 nm was monitored (Figure 2.7A). The same experiment was repeated with a reference sensitizer such as Methylene Blue (**MB**,  $\Phi_{\Delta} = 0.52$ ), under similar conditions (Ogilby *et al.*, 1983; Nemoto *et al.*, 1969). Yields for the generation of singlet oxygen were calculated by plotting the reduction in absorbance ( $\Delta OD$ ) of DPBF in presence of the aza-BODIPY as well as Methylene Blue (**MB**), against the irradiation time (Figure 2.7B). The plot followed a

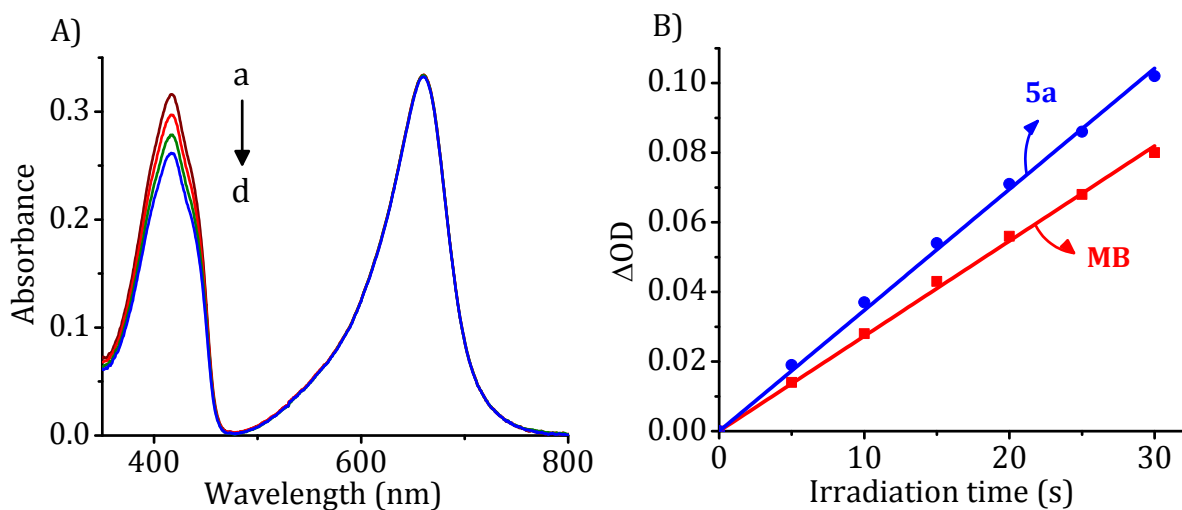


**Figure 2.7.** A) Absorption spectra of DPBF upon irradiation in the presence of **5a** (4  $\mu\text{M}$ ) for 15 s, (a) 0 s to (d) 15 s (recorded at 5 s interval). B) Plot of change in absorbance of DPBF at 418 nm vs irradiation time ( $\lambda_{\text{irr}} = 630 \text{ nm}$ ) in the presence of **5a** (4  $\mu\text{M}$ ) against methylene blue (**MB**) (3  $\mu\text{M}$ ) as the standard in DMSO.

good linearity. From the slope and by knowing the singlet oxygen generation quantum yields ( $\Phi_{\Delta}$ ) of the reference sensitizer, we have calculated the quantum yields of singlet oxygen generation for the aza-dipyrromethenes and aza-BODIPY derivatives.

The aza-dipyrromethenes **3a-c** showed negligible singlet oxygen generation efficiency. In contrast, when they were complexed with  $\text{BF}_2$ , non-negligible singlet oxygen quantum yields were observed for the dyes **4a-c** due to the formation of the triplet excited states in these dyes as evidenced from laser flash photolysis studies. The singlet oxygen generation quantum yields were determined by DPBF trap degradation experiments and the values are found to be in the range of *ca.*  $0.009 \pm 0.001$  and  $0.012 \pm 0.003$  for **4a** and **4b**, respectively. The yields were increased to *ca.*  $0.02 \pm 0.003$  by the replacement of bromine with iodine, as in the case of **4c**. Unlike the core free derivatives **4a-c**, the aza-BODIPY dyes **5a,c** and **6b,c** having the core iodo substitution

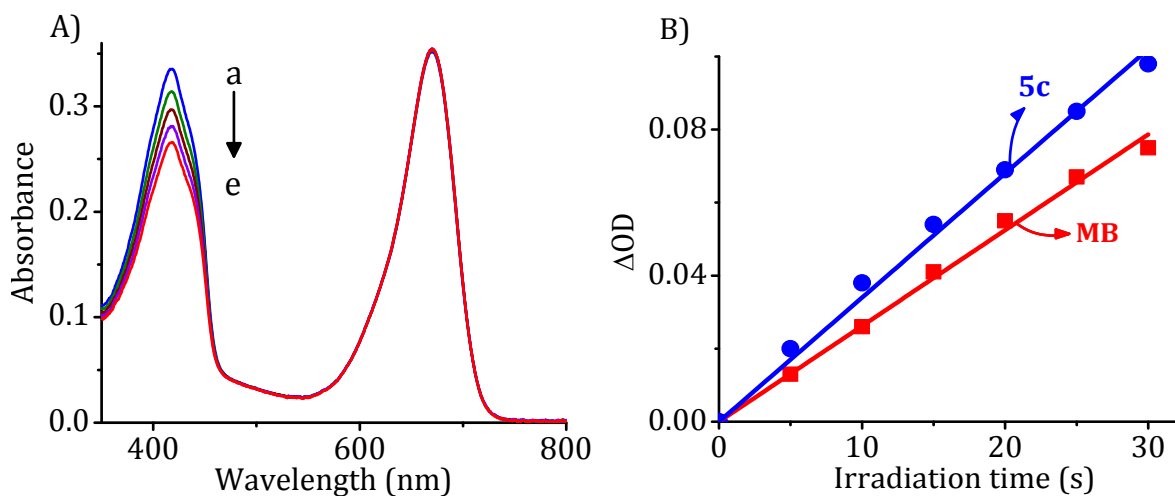


**Figure 2.8.** A) Absorption spectra of DPBF upon irradiation in presence of **5c** ( $5 \mu\text{M}$ ). (a) 0 and (e) 20 s (recorded at 5 s interval). B) Plot of change in absorbance of DPBF at 418 nm vs irradiation time ( $\lambda_{\text{irr}} = 630 \text{ nm}$ ) in the presence of **5c** ( $5 \mu\text{M}$ ) and methylene blue (**MB**) ( $3 \mu\text{M}$ ) as the standard in DMSO.

showed expectedly good to quantitative yields of singlet oxygen generation efficacy. For example, when the derivative **5a**, having only two iodine atoms at the core of the pyrrole was irradiated in the presence of DPBF, showed a considerable decrease (>10%) in absorbance at 418 nm within 10-15 s. The singlet oxygen quantum yield of **5a** was calculated with respect to **MB** and the value is found to be *ca.*  $0.65 \pm 0.02$  (Figure 2.7B). Similarly, the derivative, **5c** with four iodine atoms in the core and peripheral positions also exhibited enhanced singlet oxygen generation efficiency as compared to its parent derivative **4c**. DPBF trap experiments using the derivative **5c** enabled us to quantify its efficiency of generation of singlet oxygen and we obtained the quantum yield values of *ca.*  $0.68 \pm 0.03$  (Figure 2.8).

On the other hand, the derivatives **6b** and **6c**, which showed the highest triplet excited state quantum yields of *ca.* 80% and 86%, exhibited the maximum efficiency of singlet oxygen generation. The aza-BODIPY dye **6b**, having four iodine atoms and two

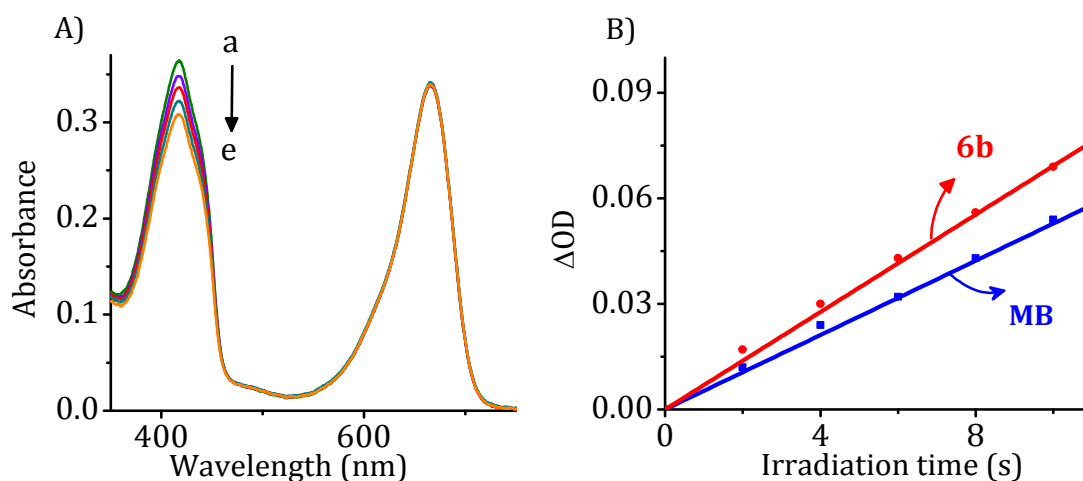


**Figure 2.9** A) Absorption spectra of DPBF upon irradiation in presence of **6b** (5 μM) for 8 s, (a) 0 s to (e) 8 s (recorded at 2 s interval). B) Plot of change in absorbance of DPBF at 418 nm vs irradiation time ( $\lambda_{\text{irr}} = 630 \text{ nm}$ ) in the presence of **6b** (5 μM) against methylene blue (**MB**) (3 μM) as the standard in DMSO.



bromine atoms, when irradiated with 630 nm long pass filter, led to the drastic reduction in the absorbance of DPBF within *ca.* 4-6 s. Singlet oxygen generation quantum yield was calculated to be *ca.*  $0.70 \pm 0.03$  for **6b** (Figure 2.9). Interestingly, in the case of **6c** with six iodine atoms at both core as well as in the peripheral positions showed highest quantum yield of *ca.*  $0.80 \pm 0.02$ , when compared to the standard **MB** (Figure 2.10). To the best of our knowledge, these are the highest singlet oxygen generation quantum yield values reported so far in the literature for the aza-BODIPY dyes (Table 2.2).

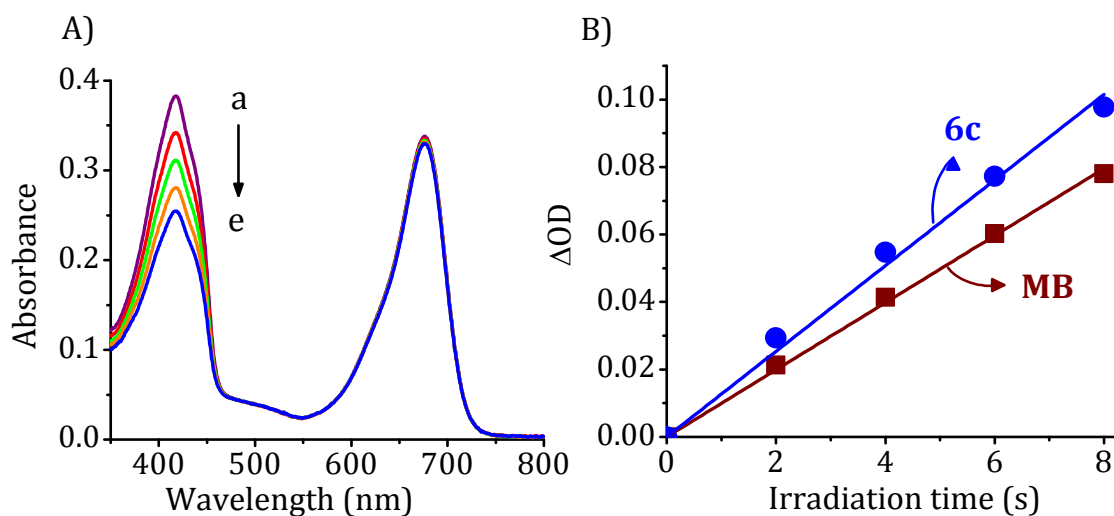


**Figure 2.10.** A) Absorption spectra of DPBF upon irradiation in presence of **6c** (5 μM). (a) 0 and (e) 8 s (recorded at 2 s interval). B) Plot of change in absorbance of DPBF at 418 nm vs irradiation time ( $\lambda_{\text{irr}} = 630$  nm) in the presence of **6c** (5 μM) and methylene blue (**MB**) (3 μM) as the standard in DMSO.

From these investigations, it can be confirmed that, the triplet excited state and singlet oxygen quantum yields of the aza-BODIPY dyes strongly depend on the number and position of heavier halogen atoms such as bromine and iodine. Further, to check the resistance of these dyes towards photo-bleaching, we have carried out the

control experiments by the continuous irradiation of an oxygen saturated solution of these dyes for 0-2 h. We observed negligible changes in their absorption spectra, confirming thereby the stability of the aza-BODIPY derivatives under these conditions (Figure 2.11).

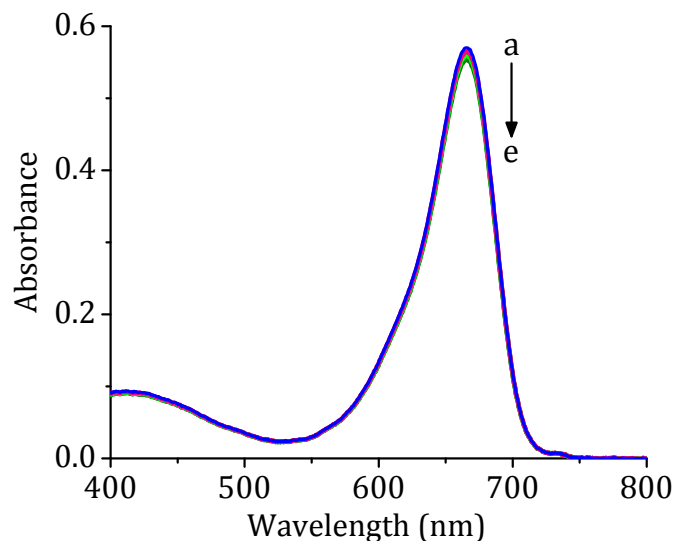


**Figure 2.11.** Representative absorption spectra of the aza-BODIPY dye **6b** (8  $\mu\text{M}$ ) showing the changes before and after the continuous irradiation using 630 nm long pass filter for a) 0 and e) 2 h.

To further confirm the quantum yields of singlet oxygen generation, we have employed the direct method by monitoring singlet oxygen luminescence at 1270 nm. For the direct measurement of singlet oxygen through NIR luminescence method, we used Fluorolog-3 spectrofluorimeter connected with an NIR detector and 450 W Xenon lamp as the light source. To obtain the singlet oxygen luminescence at 1270 nm in the steady-state, we prepared optically matched solutions of the selected aza-BODIPY dyes and a common reference sensitizer, Rose Bengal (**RB**). The aza-BODIPY dye, **6b** was excited at different wavelengths so as to obtain the maximum intensity of the signal. It

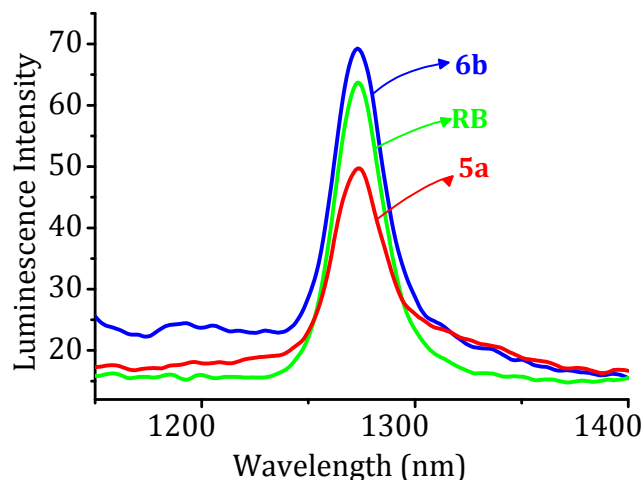


**Figure 2.12.** Singlet oxygen luminescence spectra of representative aza-BODIPY dyes **5a** (10  $\mu\text{M}$ ), **6b** (10  $\mu\text{M}$ ) and **RB** (10  $\mu\text{M}$ ) in acetonitrile after the excitation at 630 nm.

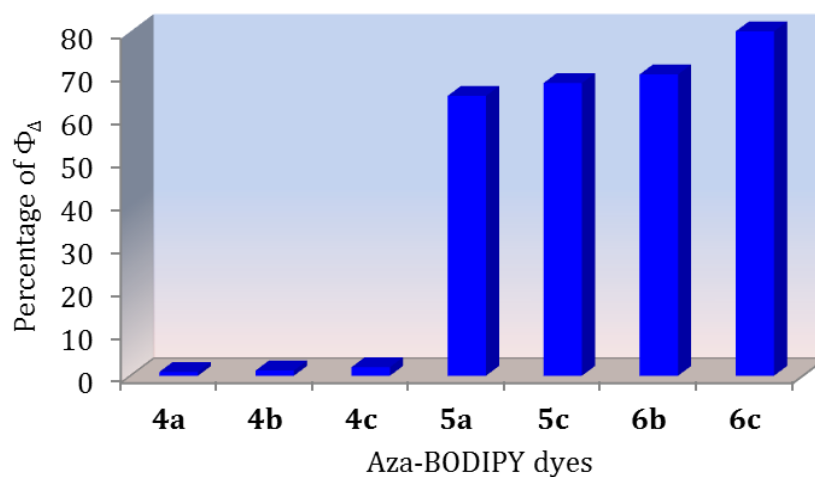
**Table 2.2.** Quantum yields of singlet oxygen generation of aza-BODIPY dyes.<sup>[a]</sup>

Compound	$\Phi_{\Delta}$ by DPBF trap <sup>[b]</sup>	$\Phi_{\Delta}$ by 1270 emission <sup>[c]</sup>
<b>4a</b>	0.009 $\pm$ 0.001	[d]
<b>4b</b>	0.012 $\pm$ 0.003	[d]
<b>4c</b>	0.02 $\pm$ 0.003	[d]
<b>5a</b>	0.65 $\pm$ 0.02	0.50 $\pm$ 0.04
<b>5c</b>	0.68 $\pm$ 0.03	0.70 $\pm$ 0.02
<b>6b</b>	0.70 $\pm$ 0.03	0.80 $\pm$ 0.03
<b>6c</b>	0.80 $\pm$ 0.02	0.90 $\pm$ 0.04

<sup>[a]</sup>Average of more than three experiments, <sup>[b]</sup>quantified through scavenging of  $^1\text{O}_2$  by DPBF, <sup>[c]</sup>yields calculated by a relative method with respect to RB ( $\Phi_{\Delta} = 0.79$ ) (Esser *et al.*, 1994), <sup>[d]</sup>not determined.

was observed that when **6b**, was excited using 630 nm, we observed the maximum intensity of the singlet oxygen luminescence (Figure 2.12). We have carried out the

similar trials with all other aza-BODIPY derivatives as well as **RB** and observed the signal at 1270 nm with difference in intensities, which correspond to singlet oxygen luminescence. By comparing the emission intensities of the aza-BODIPY dyes and **RB**, singlet oxygen quantum yields ( $\phi_{\Delta}$ ) were determined by a relative method (Mathai *et al.*, 2007) following the literature protocol. The quantum yields obtained were in good agreement with the values obtained through the DPBF trap degradation method as summarized in Table 2.2.



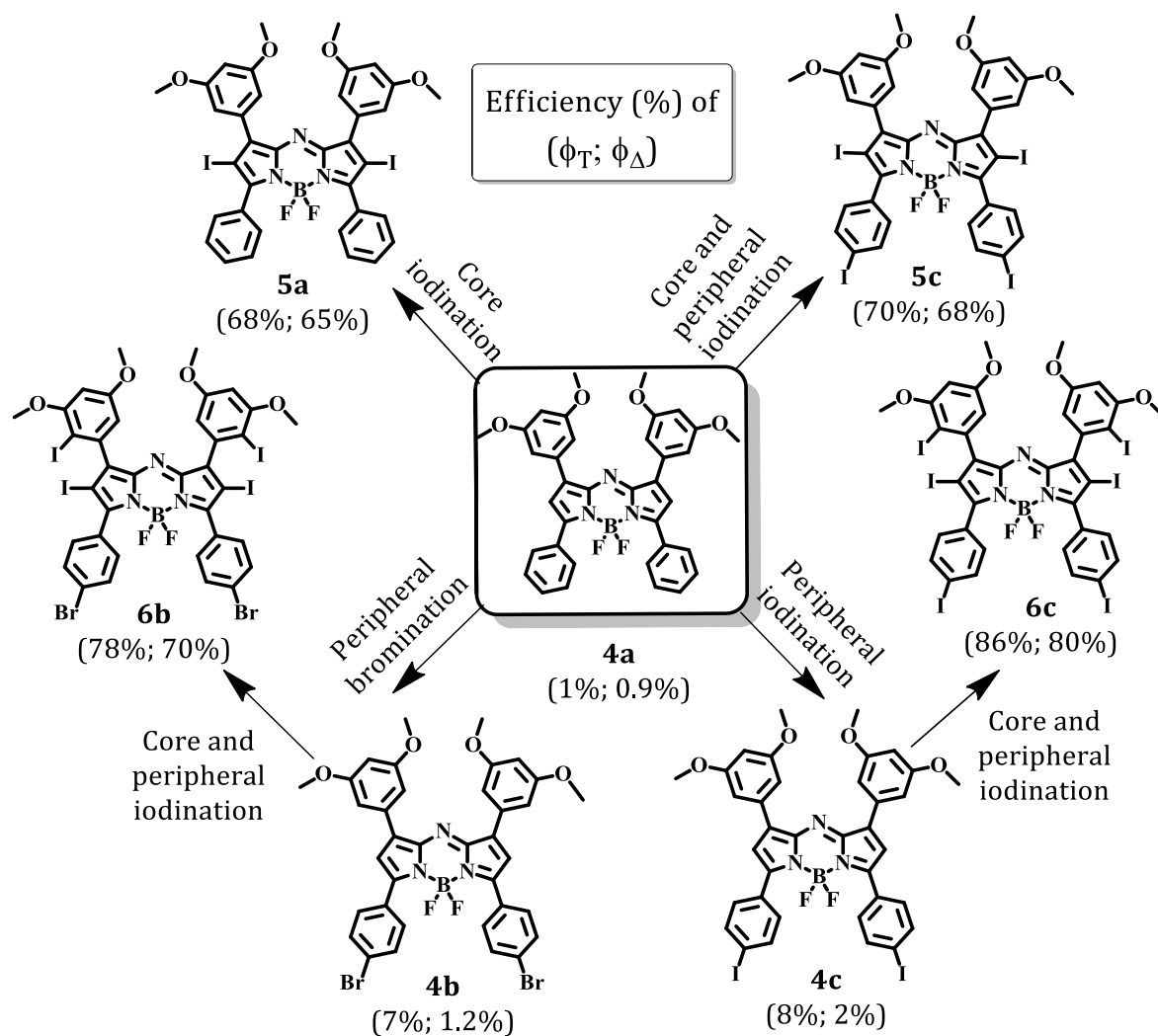
**Figure 2.13.** Bar diagram showing the percentage of singlet oxygen generated by the aza-BODIPY derivatives, **4a-c**, **5a,c** and **6b,c**.

Figure 2.13 shows the relative percentage quantum yields of singlet oxygen generation of all the aza-BODIPY derivatives **4a-c**, **5a,c** and **6b,c** synthesized. We observed a marginal increase in the singlet oxygen generation of the aza-BODIPY dyes with peripheral substitution of halogen atoms, **4b-c** and a significant enhancement was observed in the case of the core substituted systems, **5a**, **5c**, **6b** and **6c**. These results demonstrate that by proper substitution of halogen atoms, the systematic tuning of

triplet excited state as well as singlet oxygen generation of aza-BODIPY derivatives can be achieved.

### 2.3.4. Halogenation vs Triplet Excited State and Singlet Oxygen Yields

It has been reported that the triplet excited state quantum yields as well as singlet oxygen generation efficiencies of a sensitizer can be altered by suitably incorporating heavy atoms onto the molecular structure (Ramaiah *et al.*, 1997; Detty *et al.*, 1990; Turro, 1978). In the present case, in order to investigate the effect of halogenation in aza-BODIPY dyes, we have substituted the halogen atoms such as bromine and iodine at the core as well as peripheral phenyl rings. We observed a low singlet oxygen generation for the unsubstituted aza-BODIPY **4a**, indicating that this derivative showed negligible triplet excited state yields. However, upon bromination and iodination resulted in the improved triplet excited state and singlet oxygen generation yields as observed in the case of **4b-c**. The enhancement of quantum yields of triplet excited state and singlet oxygen generation was found to depend on the position of halogenation of the parent dye and the heaviness of the halogen substituent. The comparison between the peripheral halogenated aza-BODIPY dyes **4b** and **4c** and that of the unsubstituted dye **4a** showed a marginal improvement of *ca.* 6-7% in triplet excited state quantum yields and *ca.* 0.3% and 1.1%, in the efficiency of singlet oxygen generation, respectively (Scheme 2.3). In contrast, the core substitution of the aza-BODIPY dyes showed a significant influence on the triplet excited state and singlet oxygen generation efficiency. For example, the core iodinated aza-BODIPY dyes **5a** and **5c** showed *ca.* 64% and 66% enhancement in the singlet oxygen yields as compared to



**Scheme 2.3.** Triplet excited state and singlet oxygen generation efficiencies of various aza-BODIPY derivatives synthesized.

the parent dyes **4a** and **4c**, respectively. An interesting observation is the additive effect observed on iodination at the core as well as at the peripheral rings. For example, **6b** having substitution at the core and also at the two peripheral phenyl rings showed *ca.* 70% and *ca.* 68% of enhancement in the triplet excited state and singlet oxygen generation yields, respectively, as compared to the bromo substituted dye, **4b**. Similar observations were made with **6c** having two iodine atoms in the core and four iodine atoms in the peripheral phenyl rings. This compound showed the maximum additive

effect and exhibited an enhancement of *ca.* 78% in both triplet excited state and singlet oxygen generation efficiencies as compared to **4c**.

When compared between **6b** and **6c** that differ only in the peripheral halogen atoms (bromine to iodine), we observed *ca.* 10% enhancement in the singlet oxygen yields of **6c** as compared to **6b**. Similarly *ca.* 10-12% difference was observed between **5c** and **6c** (Scheme 2.3). These results demonstrate that the halogenation of the peripheral phenyl rings of the aza-BODIPYs has only marginal improvement (*ca.* 10-15%) on the quantum yields of triplet excited state and singlet oxygen generation. In contrast, significant enhancement of *ca.* 65-70% was observed, when the core pyrrole rings of the aza-BODIPYs were substituted with halogen atoms.

## 2.4. CONCLUSIONS

In summary, we have designed and synthesized a series of novel aza-BODIPY derivatives **4a-c**, **5a,c** and **6b,c** through a high yielding synthetic route and have investigated their photophysical properties as well as tuned their excited state properties such as quantum yields of triplet excited state and singlet oxygen generation efficiency. All these derivatives showed strong absorption in the region 660-680 nm with high molar extinction coefficient values. Moreover these dyes exhibited good solubility and exceptional photostability in all the organic solvents. The substitution of these derivatives with heavy atoms at the core as well as the peripheral positions resulted in significant enhancement in their triplet excited state and singlet oxygen generation yields.

The excited state studies have revealed that the non-halogenated aza-BODIPY derivative **4a** showed a triplet and singlet oxygen generation quantum yield of *ca.* 1%, while the quantum yields were found to be enhanced with the substitution of halogen atoms due to internal 'heavy atom effect'. Interestingly, the aza-BODIPY derivative **6c** having six iodine atoms at the core and peripheral positions exhibited quantitative triplet excited state quantum yield of *ca.*  $0.86 \pm 0.03$  and singlet oxygen generation efficiency of *ca.*  $0.80 \pm 0.02$ , which are the highest values so far reported for the aza-BODIPY systems. Thus, the triplet excited state and singlet oxygen generation efficiency of these systems could be tuned from *ca.* 1% to as high as 86% by the judicious substitution of bromine and iodine atoms. Our results demonstrate that these novel aza-BODIPY derivatives exhibit favorable photophysical properties including strong NIR absorption and excellent singlet oxygen generation efficiency and hence can have potential applications as sensitizers in photodynamic therapy as well as green photooxygenation catalysts.

## 2.5. EXPERIMENTAL SECTION

### 2.5.1. General Techniques

Melting points were determined on a Mel-Temp II melting point apparatus. The electronic absorption spectra were recorded on a Shimadzu UV-3101 or 2401PC UV-Vis-NIR scanning spectrophotometer. The fluorescence spectra were recorded on a SPEX-Fluorolog F112X spectrofluorimeter.  $^1\text{H}$  and  $^{13}\text{C}$  NMR spectra were recorded on a 500 MHz Bruker advanced DPX spectrometers with chemical shifts reported relative to



TMS. Photophysical studies were carried out using spectroscopic grade solvents. IR spectra were recorded on a PRESTIGE-21 FTIR-84005 IR spectrometer. MALDI-TOF MS analysis was performed with a Shimadzu Biotech Axima CFR plus instrument equipped with a nitrogen laser in the linear mode using 2,5-dihydroxybenzoic acid (DHB) as the matrix. The transient absorption studies were carried out using a nanosecond laser flash photolysis system by employing an Applied Photophysics model LKS-20 laser kinetic spectrophotometer using OCR-12 Series Quanta Ray Nd:YAG laser. The analyzer and laser beams were fixed at right angles to each other. The laser energy was 60-65 mJ at 355 nm. Quantum yields of fluorescence were measured by the relative method using optically matching solutions. All experiments were carried out at room temperature (25 °C).

### 2.5.2. Materials and Methods

*Starting materials.* 3,5-Dimethoxybenzaldehyde, 4-bromoacetophenone, 4-iodoacetophenone, nitromethane, diethylamine, ammonium acetate, borontrifluoride diethyl etherate, triethylamine, N-iodosuccinimide, Methylene Blue, Rose Bengal,  $\beta$ -carotene were purchased from Aldrich and S. D. Fine Chemicals, India. 1,3-Diphenylisobenzofuran (DPBF) was recrystallized from a mixture (1:1) of ethanol and chloroform.  $\beta$ -carotene was used after recrystallizing from a mixture (1:1) of ethanol and chloroform. All the solvents used were purified and distilled before use by standard methods. 3-(3,5-Dimethoxyphenyl)-1-phenylprop-2-en-1-one (**1a**), mp 81-82 °C (mixture mp 80-82 °C), 4-bromophenyl-3-(3,5-dimethoxyphenyl)prop-2-en-1-one (**1b**), mp 86-87 °C (mixture mp 86-88 °C), and 4-iodophenyl-3-(3,5-dimethoxyphenyl)-

prop-2-n-1-one (**1c**), mp 86-87 °C (mixture mp 86-88 °C), were synthesized by modifying the literature reported procedures (Lv *et al.*, 2010).

### 2.5.3. Synthesis of the Aza-BODIPY Derivatives 4-6

**General procedure for the synthesis of 2a-c:** To a solution of **1a-c** (2 g, 5.76 mmol) dissolved in 80 mL of methanol was added diethylamine (4 mL) and nitromethane (2 mL) and refluxed for 24 h. The mixture was neutralized using 1N HCl and extracted with chloroform. Removal of the solvent gave a residue, which was separated by column chromatography over silica gel. Elution of the column with a mixture (1:9) of ethyl acetate and hexane gave **2a-c** in good yields.

**3-(3,5-Dimethoxyphenyl)-4-nitro-1-phenylbutan-1-one (2a):** 75%, IR (KBr)  $\nu_{\max}$  1680, 1562, 1280  $\text{cm}^{-1}$ ;  $^1\text{H}$  NMR ( $\text{CDCl}_3$ , 500 MHz)  $\delta$  7.88 (2H, d,  $J = 8.5$  Hz), 7.73 (2H, d,  $J = 8.5$  Hz), 7.70 (1H, s), 7.41 (1H, s), 6.77 (2H, s), 4.20 (1H, s), 4.11 (1H, s), 4.05 (1H, t,  $J = 7$  Hz), 3.84 (6H, s), 3.05 (2H, s);  $^{13}\text{C}$  NMR ( $\text{CDCl}_3$ , 125 MHz)  $\delta$  161.1, 145.4, 137.9, 137.4, 136.5, 129.9, 122.0, 106.4, 102.9, 100.6, 55.5; FAB-MS  $m/z$  Calcd for  $\text{C}_{18}\text{H}_{19}\text{NO}_5$ : 329.35; Found: 329.36 ( $\text{M}^+$ ).

**1-(4-Bromophenyl)-3-(3,5-dimethoxyphenyl)-4-nitrobutan-1-one (2b):** 78%, IR (KBr)  $\nu_{\max}$  1683, 1595, 1298, 1205  $\text{cm}^{-1}$ ;  $^1\text{H}$  NMR ( $\text{CDCl}_3$ , 500 MHz)  $\delta$  7.67 (2H, d,  $J = 8.5$  Hz), 7.49 (2H, d,  $J = 8.5$  Hz), 6.31 (2H, s), 6.25 (1H, s), 4.70 (1H, t,  $J = 8$  Hz), 4.58 (1H, s), 4.05 (1H, t,  $J = 7$  Hz), 3.66 (6H, s), 3.35 (2H, q,  $J = 6.5$  Hz);  $^{13}\text{C}$  NMR ( $\text{CDCl}_3$ , 125 MHz)  $\delta$  194.8, 160.1, 140.3, 134.0, 130.9, 128.4, 127.7, 104.6, 98.1, 78.3, 54.2, 40.3, 38.3; FAB-MS  $m/z$  Calcd for  $\text{C}_{18}\text{H}_{18}\text{BrNO}_5$ : 408.24; Found: 408.23 ( $\text{M}^+$ ).

**3-(3,5-Dimethoxyphenyl)-1-(4-iodophenyl)-4-nitrobutan-1-one (2c):** 75%, IR (KBr)  $\nu_{\max}$  1685, 1586, 1208  $\text{cm}^{-1}$ ;  $^1\text{H}$  NMR ( $\text{CDCl}_3$ , 500 MHz)  $\delta$  7.83 (2H, d,  $J = 8.5$  Hz), 7.62 (2H, d,  $J = 8.5$  Hz), 6.40 (2H, d,  $J = 2$  Hz), 6.39 (1H, t,  $J = 2.5$  Hz), 4.79 (1H, q,  $J = 8$  Hz), 4.67 (1H, q,  $J = 8$  Hz), 4.15 (1H, m), 3.76 (6H, s), 3.43 (2H, m);  $^{13}\text{C}$  NMR ( $\text{CDCl}_3$ , 125 MHz)  $\delta$  196.2, 161.2, 141.3, 138.1, 135.6, 129.4, 101.7, 99.3, 79.3, 53.4, 41.4, 39.3; FAB-MS  $m/z$  Calcd for  $\text{C}_{18}\text{H}_{18}\text{INO}_5$ : 456.03; Found: 456.51 ( $\text{M}^+$ ).

**General procedure for the synthesis of 3a-c:** The nitromethane derivatives **2a-c** (2.45 mmol) and ammonium acetate (7.6 g, 95 mmol) were dissolved in ethanol (20 mL) and heated under reflux for 48 h. The precipitated product was filtered, washed with cold ethanol, dried and recrystallized from chloroform to give **3a-c** as violet crystals with a metallic luster.

**(Z)-3-(3,5-Dimethoxyphenyl)-N-(3-(3,5-dimethoxyphenyl)-5-phenyl-2H-pyrrol-2-ylidene)-5-phenyl-1H-pyrrol-2-amine (3a):** 40%, mp 220-221  $^{\circ}\text{C}$ ; IR (KBr)  $\nu_{\max}$  3062, 1597, 1537, 1348  $\text{cm}^{-1}$ ;  $^1\text{H}$  NMR ( $\text{CDCl}_3$ , 500 MHz)  $\delta$  7.97 (4H, d,  $J = 8$  Hz), 7.62 (2H, d,  $J = 8$  Hz), 7.56 (6H, d,  $J = 7$  Hz), 7.49 (2H, d,  $J = 7$  Hz), 7.11 (2H, s), 6.94 (2H, d,  $J = 8.5$  Hz), 3.95 (6H, s), 3.76 (6H, s);  $^{13}\text{C}$  NMR ( $\text{CDCl}_3$ , 125 MHz)  $\delta$  154.8, 149.5, 149.3, 148.8, 142.7, 132.2, 129.9, 129.1, 127.0, 126.5, 121.9, 114.0, 112.3, 111.0, 56.0, 55.8; FAB-MS  $m/z$  Calcd for  $\text{C}_{36}\text{H}_{31}\text{N}_3\text{O}_4$ : 570.23; Found: 570.23 ( $\text{M}^+$ ).

**(Z)-5-(4-Bromophenyl)-N-(5-(4-bromophenyl)-3-(3,5-dimethoxyphenyl)-2H-pyrrol-2-ylidene)-3-(3,5-dimethoxyphenyl)-1H-pyrrol-2-amine (3b):** 50%, mp 245-246  $^{\circ}\text{C}$ ; IR (KBr)  $\nu_{\max}$  2999, 1589, 1456, 1338, 1278  $\text{cm}^{-1}$ ;  $^1\text{H}$  NMR ( $\text{CDCl}_3$ , 500 MHz)  $\delta$  7.77 (4H, d,  $J = 8.5$  Hz), 7.67 (4H, d,  $J = 8.5$  Hz), 7.10 (2H, s), 7.08 (4H, m), 6.48

(2H, t, J = 2.5 Hz), 3.69 (12H, s);  $^{13}\text{C}$  NMR ( $\text{CDCl}_3$ , 125 MHz)  $\delta$  161.4, 160.6, 156.4, 154.0, 149.7, 143.3, 140.8, 138.1, 135.2, 132.4, 131.8, 130.9, 128.6, 127.8, 124.5, 123.6, 117.22, 115.5, 106.9, 105.5, 100.9, 100.6, 55.5; FAB-MS m/z Calcd for  $\text{C}_{36}\text{H}_{29}\text{Br}_2\text{N}_3\text{O}_4$ : 727.44; Found: 727.45 ( $\text{M}^+$ ).

**(Z)-3-(3,5-Dimethoxyphenyl)-N-(3-(3,5-dimethoxyphenyl)-5-(4-iodophenyl)-2H-pyrrol-2-ylidene)-5-(4-iodophenyl)-1H-pyrrol-2-amine (3c):** 40%, mp 236-237 °C; IR (KBr)  $\nu_{\text{max}}$  2997, 1681, 1591, 1454  $\text{cm}^{-1}$ ;  $^1\text{H}$  NMR ( $\text{CDCl}_3$ , 500 MHz)  $\delta$  7.87 (4H, d, J = 8.5 Hz), 7.63 (4H, d, J = 8.5 Hz), 7.10 (2H, s), 7.08 (4H, d, J = 2.5), 6.48 (2H, s), 3.69 (12H, s);  $^{13}\text{C}$  NMR ( $\text{CDCl}_3$ , 125 MHz)  $\delta$  161.4, 156.6, 137.9, 128.8, 117.2, 105.5, 95.6, 55.6, 55.3; FAB-MS m/z Calcd for  $\text{C}_{36}\text{H}_{29}\text{I}_2\text{N}_3\text{O}_4$ : 823.03; Found: 823.14 ( $\text{M}^+$ ).

**General procedure for the synthesis of aza-BODIPY dyes 4a-c:** The compounds **3a-c** (0.45 mmol) dissolved in dry toluene (80 mL) were treated with triethylamine (0.8 mL, 4.6 mmol) and stirred for 10 min at 30 °C. To this reaction mixture, boron trifluoride diethyl etherate (1 mL, 8.13 mmol) was added and heated at 80 °C for 4 h. The solvent was evaporated, washed with water (2 × 50 mL) and extracted with chloroform. Removal of the solvent gave a residue, which was separated by column chromatography over silica gel. Elution of the column with a mixture (1:1) of dichloromethane and hexane gave the products **4a-c** as metallic brown solids.

**1,9-Bis(3,5-dimethoxyphenyl)-5,5-difluoro-3,7-diphenyl-5H-dipyrrolo[1,2-c:2',1'-f][1,3,5,2]triazaborinin-4-ium-5-uide (4a):** 75%, mp 239-240 °C; IR (KBr)  $\nu_{\text{max}}$  1595, 1500, 1452, 1267, 1122  $\text{cm}^{-1}$ ;  $^1\text{H}$  NMR ( $\text{CDCl}_3$ , 500 MHz)  $\delta$  8.09 (4H, s), 7.85 (2H, q, J = 8.5 Hz), 7.67 (2H, s), 7.57 (6H, s), 7.50 (2H, s), 7.14 (2H, d, J = 8.5 Hz), 3.87

(6H, s), 3.78 (6H, s);  $^{13}\text{C}$  NMR ( $\text{CDCl}_3$ , 125 MHz)  $\delta$  158.1, 150.8, 148.9, 144.7, 143.5, 131.1, 130.9, 129.3, 128.5, 124.7, 122.9, 118.9, 112.5, 55.7, 55.6; FAB-MS  $m/z$  Calcd for  $\text{C}_{36}\text{H}_{30}\text{BF}_2\text{N}_3\text{O}_4$ : 617.45; Found: 617.45 ( $\text{M}^+$ ).

**3,7-Bis(4-bromophenyl)-1,9-bis(3,5-dimethoxyphenyl)-5,5-difluoro-5H-dipyrrolo[1,2-c:2',1'-f][1,3,5,2]triazaborinin-4-ium-5-uide (4b):** 80%, mp 284-285 °C; IR (KBr)  $\nu_{\text{max}}$  1587, 1473, 1398, 1261  $\text{cm}^{-1}$ ;  $^1\text{H}$  NMR ( $\text{CDCl}_3$ , 500 MHz)  $\delta$  7.90 (4H, d,  $J = 8.5$  Hz), 7.63 (4H, d,  $J = 8.5$  Hz), 7.12 (4H, s), 6.96 (2H, s), 6.54 (2H, s), 3.76 (12H, s);  $^{13}\text{C}$  NMR ( $\text{CDCl}_3$ , 125 MHz)  $\delta$  160.8, 158.2, 145.7, 144.9, 133.8, 132.0, 131.0, 130.2, 126.0, 119.6, 107.3, 102.3, 99.9, 55.5; FAB-MS  $m/z$  Calcd for  $\text{C}_{36}\text{H}_{28}\text{BBr}_2\text{F}_2\text{N}_3\text{O}_4$ : 775.24; Found: 775.24 ( $\text{M}^+$ ).

**1,9-Bis(3,5-dimethoxyphenyl)-5,5-difluoro-3,7-bis(4-iodophenyl)-5H-dipyrrolo[1,2-c:2',1'-f][1,3,5,2]triazaborinin-4-ium-5-uide (4c):** 82%, mp 259-261 °C; IR (KBr)  $\nu_{\text{max}}$  1585, 1512, 1489, 1284  $\text{cm}^{-1}$ ;  $^1\text{H}$  NMR ( $\text{CDCl}_3$ , 300 MHz)  $\delta$  7.85 (4H, d,  $J = 8.7$  Hz), 7.76 (4H, d,  $J = 8.7$  Hz), 7.12 (4H, d,  $J = 2.1$  Hz), 6.96 (2H, s), 6.54 (2H, s), 3.75 (12H, s);  $^{13}\text{C}$  NMR ( $\text{CDCl}_3$ , 125 MHz)  $\delta$  160.9, 158.4, 145.8, 144.9, 137.9, 133.9, 131.0, 130.9, 130.8, 119.6, 107.3, 102.3, 98.5, 55.3; FAB-MS  $m/z$  Calcd for  $\text{C}_{36}\text{H}_{28}\text{BF}_2\text{I}_2\text{N}_3\text{O}_4$ : 869.02; Found: 869.36 ( $\text{M}^+$ ).

**General Procedure for the synthesis of 5a,c:** To a solution of **4a,c** (0.26 mmol) in a mixture (40 mL, 3:1) of chloroform and acetic acid, N-iodosuccinimide (0.15 g, 0.65 mmol) was added and stirred at 30 °C for 4-5 h. The reaction mixture was washed with sodium thiosulphate followed by sodium bicarbonate solution and extracted with chloroform. Removal of the solvent gave a residue, which was separated by column

chromatography over silica gel. Elution of the column with a mixture (1:9) of methanol and chloroform gave 60-65% of **5a,c**.

**1,9-Bis(3,5-dimethoxyphenyl)-5,5-difluoro-2,8-diiodo-3,7-diphenyl-5H-dipyrrolo[1,2-c:2',1'-f][1,3,5,2]triazaborinin-4-ium-5-uide (5a):** 60%, mp 236-237 °C; IR (KBr)  $\nu_{\max}$  1598, 1485, 1379, 1263  $\text{cm}^{-1}$ ;  $^1\text{H}$  NMR ( $\text{CDCl}_3$ , 500 MHz)  $\delta$  7.55 (4H, m), 7.44 (2H, dd,  $J = 2$  Hz), 7.40 (6H, m), 7.29 (2H, d,  $J = 2$  Hz), 6.89 (2H, d,  $J = 8.5$  Hz), 3.89 (6H, s), 3.64 (6H, s);  $^{13}\text{C}$  NMR ( $\text{CDCl}_3$ , 125 MHz)  $\delta$  160.05, 149.6, 147.4, 146.5, 143.9, 130.2, 129.5, 129.2, 126.9, 123.8, 123.2, 113.1, 109.5, 55.0, 54.7; FAB-MS  $m/z$  Calcd for  $\text{C}_{36}\text{H}_{28}\text{BF}_2\text{I}_2\text{N}_3\text{O}_4$ : 870.03; Found: 871.20 ( $\text{M}+1^+$ ).

**1,9-Bis(3,5-dimethoxyphenyl)-5,5-difluoro-2,8-diiodo-3,7-bis(4-iodo phenyl)-5H-dipyrrolo[1,2-c:2',1'-f][1,3,5,2]triazaborinin-4-ium-5-uide (5c):** 65%, mp 263-264 °C; IR (KBr)  $\nu_{\max}$  1579, 1508, 1423, 1321  $\text{cm}^{-1}$ ;  $^1\text{H}$  NMR ( $\text{CDCl}_3$ , 500 MHz)  $\delta$  7.86 (4H, d,  $J = 8.5$  Hz), 7.79 (4H, d,  $J = 9$  Hz), 7.13 (2H, s), 6.68 (2H, d,  $J = 2.5$  Hz), 6.44 (2H, d,  $J = 2.5$  Hz), 3.88 (6H, s), 3.67 (6H, s);  $^{13}\text{C}$  NMR ( $\text{CDCl}_3$ , 125 MHz)  $\delta$  159.5, 158.1, 156.7, 146.3, 145.3, 137.4, 137.0, 137.1, 129.7, 123.1, 108.3, 98.9, 98.6, 97.7, 79.3, 55.6, 54.7; FAB-MS  $m/z$  Calcd for  $\text{C}_{36}\text{H}_{26}\text{BF}_2\text{I}_4\text{N}_3\text{O}_4$ : 1121.04; Found: 1121.38 ( $\text{M}^+$ ).

**General procedure for the synthesis of 6b-c:** To a solution of **4b-c** (0.26 mmol) in a mixture (40 mL, 3:1) of chloroform and acetic acid, N-iodosuccinimide (260 mg, 1.16 mmol) was added and stirred at 30 °C for 10 h. The reaction mixture was washed with sodium thiosulphate followed by sodium bicarbonate solution and extracted with chloroform. Removal of the solvent gave a residue which was separated by column

chromatography over silica gel. Elution of the column with a mixture (1:9) of methanol and chloroform gave 65-70% of **6b-c**.

**3,7-Bis(4-bromophenyl)-5,5-difluoro-2,8-diiodo-1,9-bis(2-iodo-3,5-dimethoxyphenyl)-5H-dipyrrolo[1,2-c:2',1'-f][1,3,5,2]triazaborinin-4-ium-5-uide (6b):** 65%, mp 308-310 °C; IR (KBr)  $\nu_{\max}$  1587, 1506, 1477, 1336, 1278  $\text{cm}^{-1}$ ;  $^1\text{H}$  NMR ( $\text{CDCl}_3$ , 500 MHz)  $\delta$  7.93 (3H, d,  $J = 8.5$  Hz), 7.63 (5H, d,  $J = 11.5$  Hz), 6.64 (1H, s), 6.37 (2H, s), 5.30 (1H, s), 3.89 (12H, s);  $^{13}\text{C}$  NMR ( $\text{CDCl}_3$ , 125 MHz)  $\delta$  159.0, 157.9, 153.0, 144.3, 142.7, 132.0, 129.5, 125.6, 80.2, 56.9; FAB-MS  $m/z$  Calcd for  $\text{C}_{36}\text{H}_{24}\text{BBr}_2\text{F}_2\text{I}_4\text{N}_3\text{O}_4$ : 1279.64; Found: 1279.63 ( $\text{M}^+$ ).

**5,5-Difluoro-2,8-diiodo-1,9-bis(2-iodo-3,5-dimethoxyphenyl)-3,7-bis(4-iodophenyl)-5H-dipyrrolo[1,2-c:2',1'-f][1,3,5,2]triazaborinin-4-ium-5-uide (6c):** 68%, mp 305-307 °C; IR (KBr)  $\nu_{\max}$  1556, 1462, 1409, 1261  $\text{cm}^{-1}$ ;  $^1\text{H}$  NMR ( $[d_6]\text{DMSO}$ , 500 MHz)  $\delta$  7.97 (4H, t,  $J = 2.5$  Hz), 7.79 (2H, d,  $J = 8.5$  Hz), 7.39 (2H, d,  $J = 8$  Hz), 7.27 (1H, s), 6.70 (2H, d,  $J = 9.5$  Hz), 5.76 (1H, s), 3.89 (12H, s);  $^{13}\text{C}$  NMR ( $\text{CDCl}_3$ , 125 MHz)  $\delta$  159.4, 159.3, 154.9, 153.7, 145.6, 143.8, 143.1, 137.6, 137.4, 136.5, 131.8, 130.9, 125.0, 101.5, 94.7, 78.9, 78.5, 55.6, 55.5; FAB-MS  $m/z$  Calcd for  $\text{C}_{36}\text{H}_{24}\text{BF}_2\text{I}_6\text{N}_3\text{O}_4$ : 1373.62; Found: 1373.92 ( $\text{M}^+$ ).

#### 2.5.4. Determination of Triplet Excited State Quantum Yields ( $\Phi_T$ )

Nanosecond laser flash photolysis studies were carried out by employing an Applied Photophysics model LKS-20 laser kinetic spectrometer using OCR-12 Series Quanta Ray Nd:YAG laser. The analyzing and laser beams were fixed at right angles to each other. The laser energy was 64 mJ at 355 nm. The triplet excited state yields ( $\Phi_T$ )

of the aza-BODIPY derivatives were measured employing an earlier described method of energy transfer to  $\beta$ -carotene using  $\text{Ru}(\text{bpy})_3^{2+}$ , as the reference. For these experiments, optically matched (355 nm) solutions of  $\text{Ru}(\text{bpy})_3^{2+}$  or the aza-BODIPY derivatives were mixed with a known volume of  $\beta$ -carotene solution (end concentration of  $\beta$ -carotene was  $2.0 \times 10^{-4}$  M). The transient absorbance ( $\Delta A$ ) of the  $\beta$ -carotene triplet excited state, formed by the energy transfer from  $\text{Ru}(\text{bpy})_3^{2+}$  or the aza-BODIPY triplet, was monitored at 510 nm. By substituting the quantum yield of the reference sensitizer and from the comparison of plateau absorbance following the completion of sensitized triplet excited state formation, properly corrected for the decay of the donor triplets in competition with energy transfer to  $\beta$ -carotene, enabled us to estimate  $\Phi_T$  of the aza-BODIPY derivatives based on eq. 2.1,

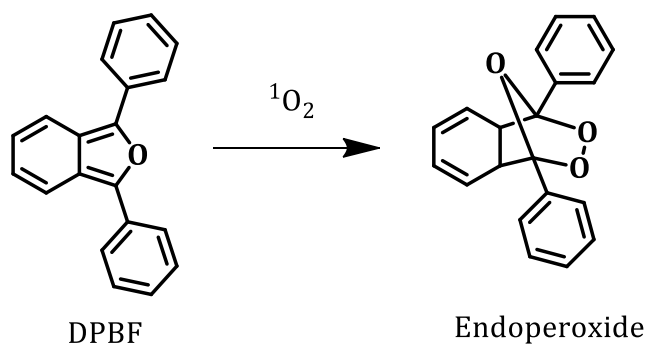
$$\Phi_T^{bod} = \Phi_T^{ref} \frac{\Delta A_{bod}}{\Delta A_{ref}} \frac{k_{obs}^{bod}}{k_{obs}^{bod} - k_0^{bod}} \frac{k_{obs}^{ref} - k_0^{ref}}{k_{obs}^{ref}} \dots \dots \dots \text{(Eq. 2.1)}$$

where superscripts '*bod*' and '*ref*' designate the different aza-BODIPY derivatives and  $\text{Ru}(\text{bpy})_3^{2+}$ , respectively,  $k_{obs}$ , is the pseudo-first-order rate constant for the growth of the  $\beta$ -carotene triplet and  $k_0$  is the rate constant for the decay of the donor triplets, in the absence of  $\beta$ -carotene, observed in solutions containing  $\text{Ru}(\text{bpy})_3^{2+}$  or aza-BODIPY dye at the same optical density (OD) as those used for sensitization. The direct excitation of  $\beta$ -carotene did not result in any significant triplet formation under these experimental conditions, because of negligible triplet yield. The  $\Phi_T^{ref}$  in methanol for  $\text{Ru}(\text{bpy})_3^{2+}$  was taken to be unity (Kumar *et al.*, 1984). The  $\Phi_T$  data obtained in this manner are reliable to the extent to which the assumption regarding 100% efficiency of energy transfer to  $\beta$ -carotene is valid.



### 2.5.5. Estimation of Singlet Oxygen Generation

**Indirect Method-Degradation of DPBF:** Singlet oxygen generation studies were carried out with a light source 200 W mercury lamp (model 3767) on an Oriel optical bench (model 11200) with a grating monochromator (model 77250). The intensity of light was maintained constant throughout the irradiations by measuring the output using an Oriel photodiode detection system (model 7072). The quantum yields for singlet oxygen generation in DMSO were determined by monitoring the photooxidation of DPBF sensitized by the aza-BODIPY derivatives. DPBF is a convenient acceptor since it absorbs in a region of dye transparency and rapidly scavenges singlet oxygen to give colorless endoperoxide products (Scheme 2.4).



**Scheme 2.4.** Singlet oxygen mediated photooxidation of DPBF.

This reaction occurs with little or no physical quenching. Singlet oxygen quantum yields were measured at low dye concentrations (optical density 0.2-0.3 at the irradiation wavelengths >630 nm) to minimize the possibility of singlet oxygen quenching by the dyes. The photooxidation of DPBF was monitored between 2 s to 2 min, depending on the efficiency of the dye sensitizer. No thermal recovery of DPBF (from a possible decomposition of endoperoxide product) was observed under the

conditions of these experiments. The quantum yields of singlet oxygen generation ( $\Phi_{\Delta}$ ) were calculated by a relative method using optically matched solutions and comparing the quantum yield of photooxidation of DPBF sensitized by the dye of interest to the quantum yield of MB ( $\Phi_{\Delta} = 0.52$ ) as the reference (Nemoto *et al.*, 1969). The following eq. 2.2 was used,

$$\Phi_{\Delta}^{bod} = \Phi_{\Delta}^{MB} \frac{m^{bod} F^{MB}}{m^{MB} F^{bod}} \dots\dots\dots \text{(Eq. 2.2)}$$

where superscripts 'bod' and 'MB' designate aza-BODIPY derivatives and MB, respectively,  $\Phi_{\Delta}$  is the quantum yield of singlet oxygen, 'm' is the slope of a plot of difference in change in absorbance of DPBF (at 418 nm) with the irradiation time and 'F' is the absorption correction factor, which is given by  $F = 1 - 10^{-OD}$  (OD at the irradiation wavelength).

**Direct Method-Singlet Oxygen Luminescence at 1270 nm:** In the direct method, we monitored the singlet oxygen emission intensity generated by the aza-BODIPY derivatives and reference Rose Bengal (**RB**) by using Fluorolog 3 spectrofluorimeter (FL3-221) connected with a NIR detector (Hamamatsu H10330A-45) with 450 W Xenon lamp as excitation source. To obtain the direct singlet oxygen luminescence intensity by steady-state method, we prepared optically matching solutions of the aza-BODIPY dyes and **RB** ( $0.1 \leq x \leq 0.15$ ) in acetonitrile and used excitation wavelength of 630 nm. We collected the emission from 1100 nm to 1400 nm region with an integration time of 0.5 s per nanometer using 12 nm band pass through Hamamatsu H10330A-45. The singlet oxygen luminescence maximum was observed normally in the region 1268-1273 nm and obtained the luminescence maximum at

1270 nm. From the luminescence intensities obtained in the presence of the compounds **4-6**, and the standard **RB** using the optically matched solutions under identical conditions, we calculated the singlet oxygen quantum yields employing the equation 2.3,

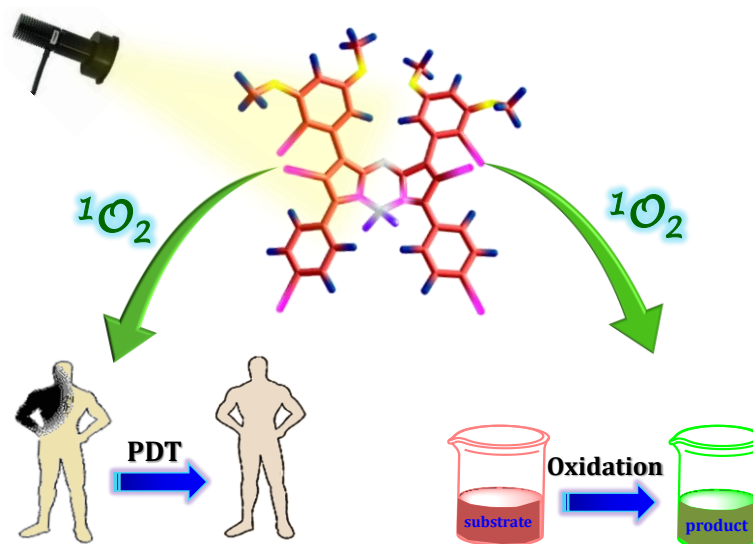
$$\Phi_{\Delta}^{bod} = \Phi_{\Delta}^{RB} \frac{I_{RB} I_{\Delta}^{bod} \tau_{RB}}{I_{bod} I_{\Delta}^{RB} \tau_{bod}} \dots\dots\dots (\text{Eq. 2.3})$$

where  $I_{RB}$  and  $I_{bod}$  denote for the incident light intensities on the reference and the aza-BODIPY samples,  $I_{\Delta}^{bod}$  and  $I_{\Delta}^{RB}$  represent singlet oxygen luminescence intensity at 1270 nm for the aza-BODIPY dyes and the reference, respectively.  $\tau_{RB}$  and  $\tau_{bod}$  represent the lifetime of singlet oxygen in particular solvent and  $\Phi_{\Delta}^{RB}$  is the singlet oxygen quantum yield of the reference, **RB**.

---

**SELECTED AZA-BODIPY DYES: STUDY OF PHOTODYNAMIC THERAPEUTIC AND PHOTOOXYGENATION APPLICATIONS**

---



### 3.1. ABSTRACT

With an objective to explore the applications of the aza-BODIPY systems, we have investigated their use in photodynamic therapy and green photooxygenation reactions. We have selected the aza-BODIPY derivatives **5a,c** and **6b,c** as these dyes exhibited excellent singlet oxygen generation and have formulated their nanoconjugates with an amphiphilic lipid, 1,2-distearoyl-sn-glycero-3-phosphoethanolamine-N-[methoxy(polyethylene glycol)-2000] (**DSPE**) to improve their solubility in the aqueous medium. The **DSPE-BODIPY** nanospheres, thus synthesized were characterized using spectroscopic and morphological techniques. Further, we have investigated *in vitro* PDT activity of the **DSPE-BODIPY** conjugates in MDA-MB-231,

MCF-7 and HeLa cells. We observed favorable IC<sub>50</sub> values of 2, 7, 9 and 12  $\mu$ M, respectively, for the DSPE conjugates of the aza-BODIPY derivatives **5a**, **5c**, **6b** and **6c** in MDA-MB-231 cell lines. The mechanism of biological activity has been evaluated through Annexin V-FITC/ propidium iodide staining experiments, which revealed that the **DSPE** conjugate with aza-BODIPY dye, **5a** effectively induced apoptosis mediated cell death. Tetramethylrhodamine methyl ester assay and chromatin condensation experiments revealed *ca.* 80% and 85% decrease, respectively, in mitochondrial inner membrane potential upon PDT treatment. Notably, we observed the activation of caspase-3 and significant production of ROS as confirmed by CM-H<sub>2</sub>DCFDA assay, furthermore confirmed ROS mediated apoptotic cell death.

As these aza-BODIPY dyes exhibited quantitative singlet oxygen generation, we explored their catalytic activity in singlet oxygen mediated photooxygenation reactions. We have employed naphthols, thioanisole and furfural as the substrates for photooxygenation in presence of different aza-BODIPY sensitizers, **5a,c** and **6b,c** and compared with the standard sensitizers such as tetraphenylporphyrin (**TPP**), Rose Bengal (**RB**) and Methylene Blue (**MB**). Of all these sensitizers, the aza-BODIPY dye, **6b**, showed *ca.* 100% conversion using both artificial light and normal sunlight irradiation conditions. Uniquely, these dyes can be uniformly adsorbed onto polystyrene matrix and can be used for the photooxidation of organic molecules. The energy demand of the entire reaction was low compared to the standard oxidation reactions carried out in laboratory and using photochemical reactors. Therefore, the aza-BODIPY derivatives under investigation act as attractive “sustainable catalysts” for efficient green photooxygenation reactions.

## 3.2. INTRODUCTION

### 3.2.1. Basic Aspects of Photodynamic Therapy

Photodynamic therapy (PDT) has been attracting much attention as an alternative to the traditional cancer treatments due to its high selectivity in the destruction of tumor cells over normal cells (Bonnet, 2000). PDT involves the generation of highly toxic and reactive oxygen species (ROS) upon excitation of a photosensitizer (Patrice, 2003; Sharman *et al.*, 1999) which ultimately destroy the tumor tissue. PDT comprises various four stages, in which the first stage involves the administration of the sensitizer into the body. The sensitizer then selectively found to accumulate around the tumor tissue when allowed for a suitable period of incubation in the stage 2. When the target tissue was irradiated in the stage 3, the light acts as a stimulus, and the cytotoxic agents such as ROS were generated due to the excitation of the sensitizer. These species react with the biological targets such as proteins, amino acids, lipids, nucleotides and nucleic acids thereby disrupt the normal functions of the cell and causing cell death in stage 4. A sensitizer in PDT can, therefore, be regarded as a 'stimuli-responsive system', being inactive in dark but becomes active only when irradiated with light of an appropriate wavelength.

Two main reaction pathways were proposed to be involved in the PDT action (Wainwright, 2009). The first pathway, called the type I mechanism, which involves the generation of radical species through either hydrogen abstraction or redox processes between a sensitizer in the excited state and the biomolecules. The second pathway is called, the type II mechanism, wherein the sensitizer in the triplet excited state

generates singlet oxygen ( $^1\text{O}_2$ ) from the ground-state molecular oxygen ( $^3\text{O}_2$ ) through an energy transfer process (Greer, 2006; Schmidt, 2006) (Figure 3.1). It has been postulated that singlet oxygen was responsible for the photoinactivation of tumor cells by a majority of the reported photosensitizers.

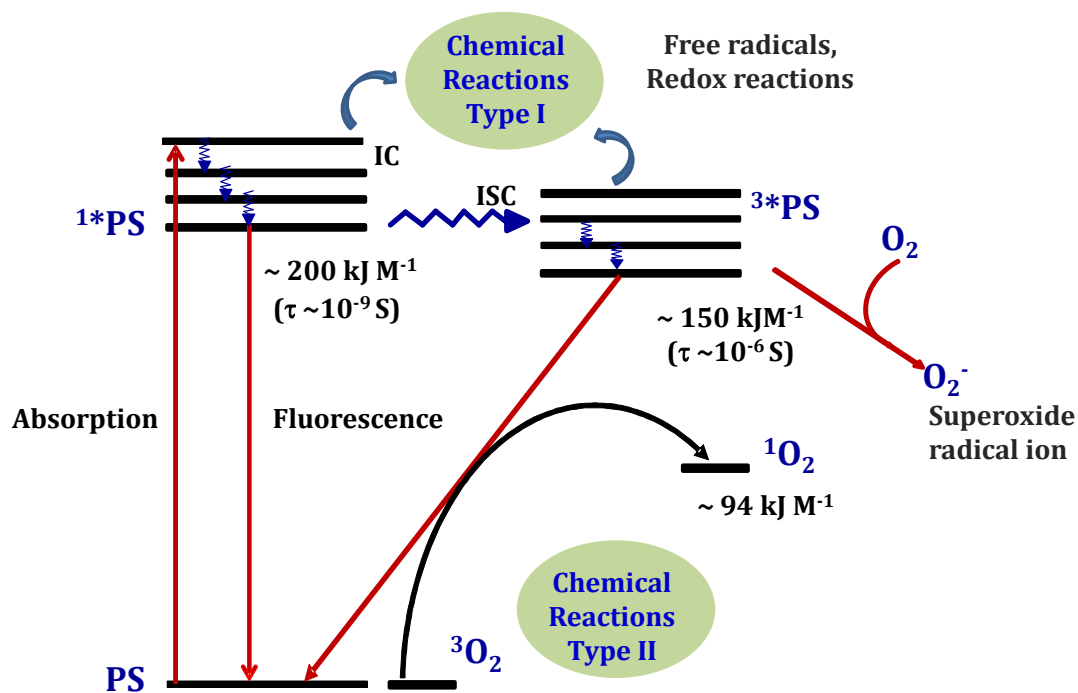


**Figure 3.1.** Modified Jablonski diagram illustrating the various photophysical processes occur upon excitation of a photosensitizer (PS) in PDT treatment.

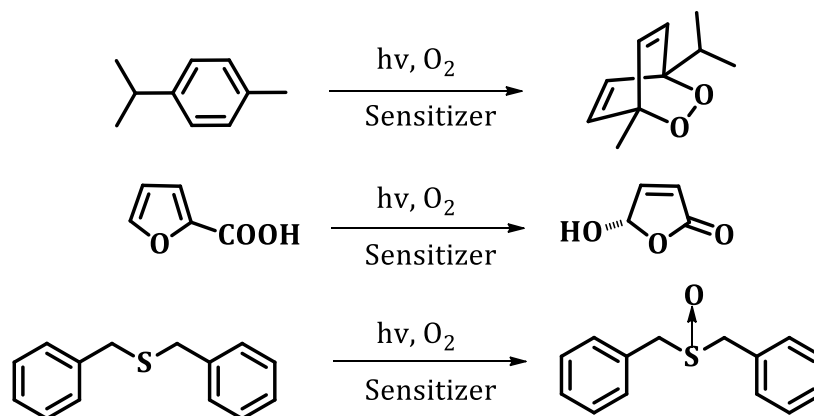
The most desirable photosensitizer should have strong absorption in the longer wavelength region, ideally in the 600-850 nm region, which is known as the 'photodynamic window', wherein the tissue penetration by light is very high (Lovell *et al.*, 2010; Dougherty *et al.*, 1992). The sensitizer should also exhibit high triplet excited state yields with long lifetimes and should be able to generate reactive species such as singlet oxygen in quantitative yields. In addition, the sensitizer should have minimal dark toxicity and only be cytotoxic in the presence of light. It should also be

preferentially retained by the target tissue and be rapidly excreted from the body. Several compounds from the simple aromatics to complex macrocycles have been proposed as sensitizers in PDT including porphyrins, phthalocyanines, chlorins, bacteriochlorins, cyanines, Rose Bengal, Methylene Blue, squaraines, 5-aminolevulinic acid and their derivatives (Karunakaran *et al.*, 2013; Avirah *et al.*, 2012; Thomas *et al.*, 2012; Devi *et al.*, 2008; Dougherty *et al.*, 1992; Foote, 1991). The most extensively studied sensitizer was Photofrin®, a hematoporphyrin derivative (HpD), for which first regulatory authorizations for the clinical use were obtained in a number of countries. Most of the sensitizers based on porphyrins exhibit slow metabolic degradative pathways and, unfortunately, were activated by light of wavelength below 600 nm, which cannot penetrate more than a few millimeters into the skin (Basu *et al.*, 2012; Wainwright, 2008). Due to this reason, recently, there has been increased interest in the development of dyes that possess absorption in the red to NIR region (Avirah *et al.*, 2008, 2007; de Rosa *et al.*, 2002).

### 3.2.2. Examples of Photooxygenation Reactions

The singlet oxygen mediated photooxygenation reactions have attracted much attention in recent years due to their importance in stereoselective synthesis, industrial processes and material science (Ribeiro *et al.*, 2013; Fudickar *et al.*, 2011; Ravelli *et al.*, 2009; Hoffmann, 2008; Griesbeck *et al.*, 2008; 2004; Palmisano *et al.*, 2007; Protti *et al.*, 2007; Albini *et al.*, 2004). These reactions can be classified under the well known ene reaction, [4+2] and [2+2] cycloaddition as well as heteroatom oxidation (e.g., sulfide to sulfoxide) (Li *et al.*, 2013; Takaguchi *et al.*, 2004) (Scheme 3.1).





**Scheme 3.1.** Representative examples of singlet oxygen mediated reactions.

The generation of singlet oxygen for the practical purpose can be achieved in solution by the decomposition of an endo-peroxide or by the photochemical triplet-triplet sensitization from an appropriate sensitizer. A variety of sensitizers have been reported in the literature, which differ with respect to their chemical stability and singlet oxygen quantum yields (Griesbeck *et al.*, 2005). Moreover, most of these singlet oxygen mediated reactions have been studied extensively by using artificial light sources such as mercury or halogen lamps, limiting their industrial use due to the high energy demand. To overcome these disadvantages, sunlight as a sustainable light source has been explored with limited success for such applications (Hajimohammadi *et al.*, 2011; Haggiage *et al.*, 2009; Oelgemoller *et al.*, 2005; Esser *et al.*, 1994). In this context, we have explored the potential of the aza-BODIPY derivatives **5a**, **5c**, **6b** and **6c** in PDT as well as singlet oxygen mediated catalytic organic transformation reactions (Chart 3.1). Our results demonstrate that these derivatives exhibit favorable photophysical and photobiological properties and hence can have use as sensitizers in PDT and photooxygenation reactions, and are worth for further explorations.

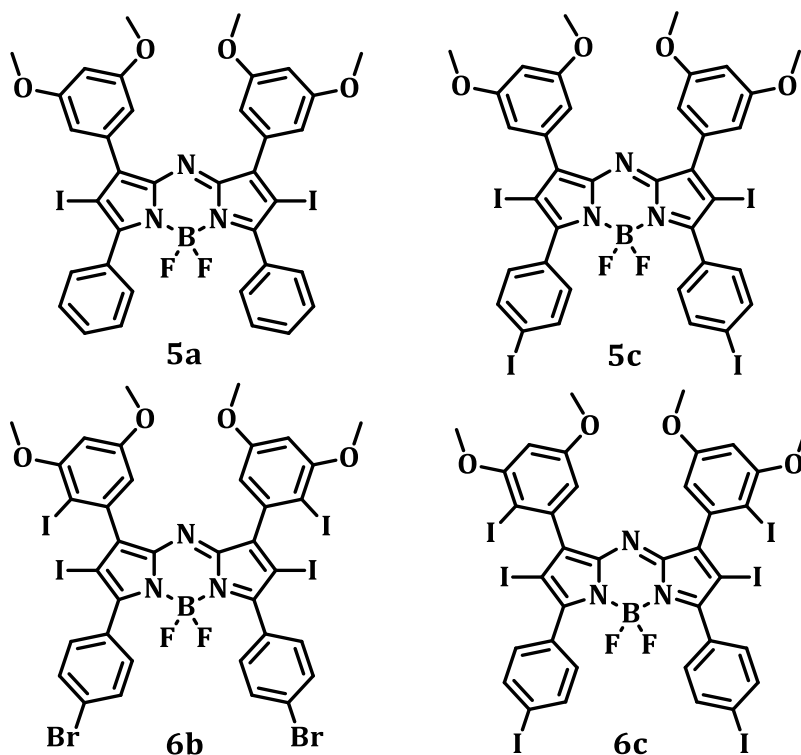


**Chart 3.1.** Structures of the aza-BODIPY derivatives under investigation.

### 3.3. RESULTS AND DISCUSSION

#### 3.3.1. Preparation of DSPE-BODIPY Conjugates

The aza-BODIPY derivatives **5a**, **5c**, **6b**, and **6c**, which were described in Chapter 2 of the thesis, have been selected for investigations since these derivatives have exhibited favorable photophysical properties including singlet oxygen generation efficiency. To carry out the biological studies in the aqueous medium, we have encapsulated these dyes into amphiphilic nanoparticle systems derived from lipids. Encapsulation of hydrophobic dyes into nanoparticles not only solubilizes them in the aqueous medium but also known to aid their specific accumulation in the tumor tissue (Kim *et al.*, 2004; Adams *et al.*, 2003; Perkins *et al.*, 2000). For the preparation of

nanomicelles, we have chosen an amphiphilic lipid, namely, 1,2-distearoyl-sn-glycero-3-phosphoethanol amine-N-[methoxy(polyethylene glycol)-2000] (**DSPE**), which has an ability to spontaneously form micelles with hydrophobic core upon dispersion in the aqueous solutions (Wang *et al.*, 2011; Torchilin, 2007).

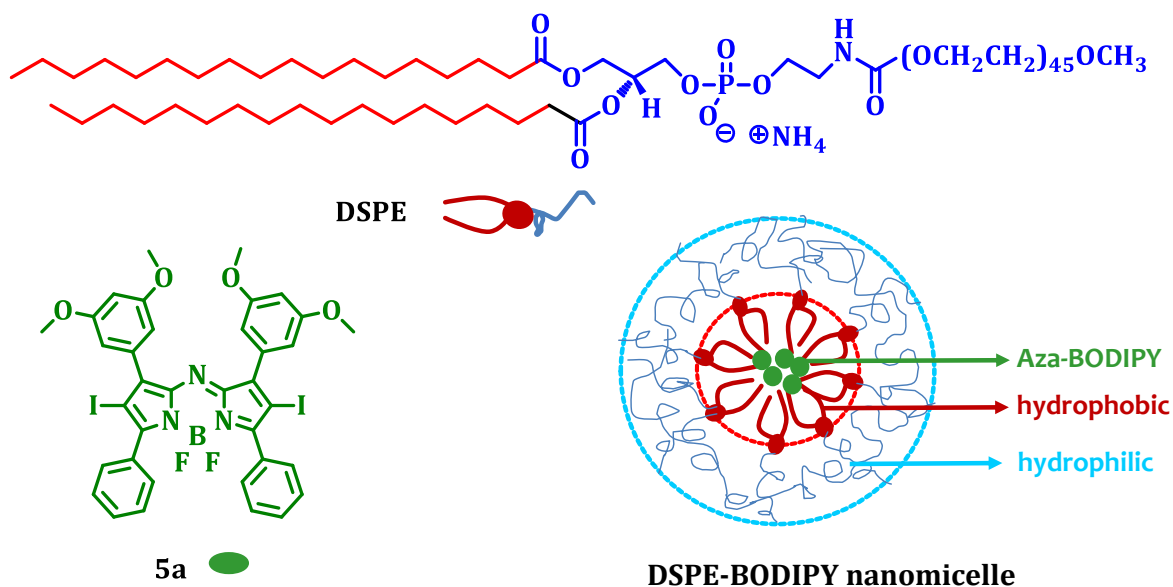


**Figure 3.2.** Schematic representation of the nanomicelle formed from 1,2-distearoyl-sn-glycero-3-phosphoethanolamine-N-[methoxy(polyethylene glycol)-2000] (**DSPE**) and a representative aza-BODIPY dye, **5a**.

The encapsulation of aza-BODIPY dyes into **DSPE** nanomicelles were carried out using the lipid-hydration method, wherein, the lipid-PEG conjugates form amphiphilic micellar structures consisting of a hydrophilic polymer shell and an organic lipidic core (Figure 3.2). The aza-BODIPY dyes were solubilized within the lipid-rich area and incorporated into nanosized structures that can aid their accumulation at the tumor sites (Maeda *et al.*, 2010; Nasongkla *et al.*, 2006; Lukyanov *et al.*, 2002). At concentrations above the reported critical micelle concentration of DSPE (1  $\mu\text{M}$ ) (Ashok *et al.*, 2004), various drug-to-lipid ratios were examined for their drug

encapsulation efficiency. By keeping the concentration of aza-BODIPY dyes constant and increasing the concentration of **DSPE**, it was found that highest encapsulation efficiencies were obtained for the ratio of 3:1 (DSPE/aza-BODIPY). The amount of encapsulation of aza-BODIPY dyes into the **DSPE** micelles were determined using UV-Vis spectroscopy and found to be *ca.* 95%. As a control and to understand the effect of variable concentration of **DSPE** on the nanomicelle formation, we have analyzed the size of nanomicelles formed through dynamic light scattering (DLS) technique. By varying the concentration of **DSPE** from 100  $\mu\text{M}$  to 1 mM in the aqueous medium, we observed that the formation of micelles having uniform spherical shape with a hydrodynamic diameter of *ca.*  $20 \pm 0.5$  nm (Kastantin *et al.*, 2009; Ashok *et al.*, 2004).

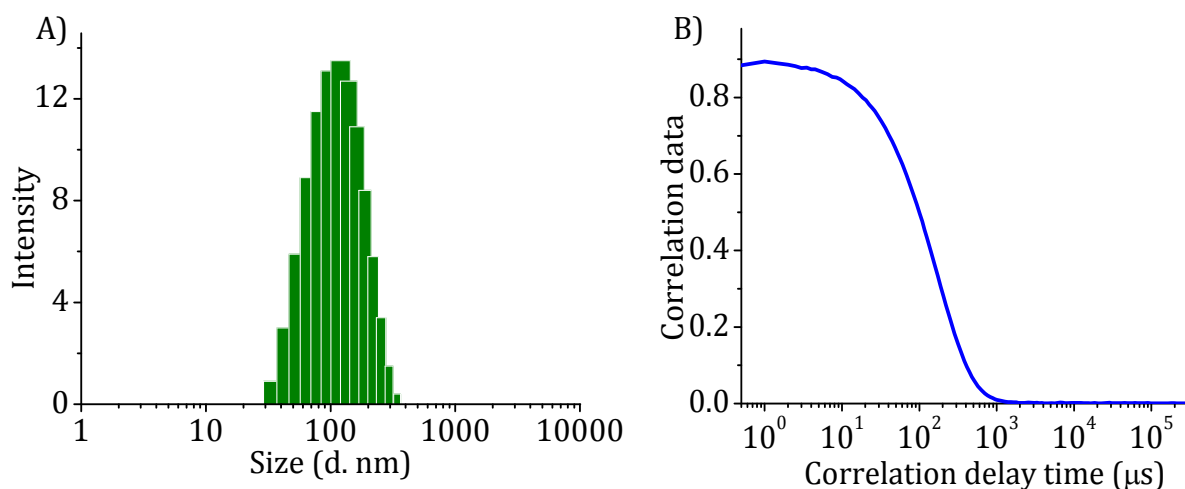


**Figure 3.3.** Representative example of A) size distribution and B) correlogram of the dynamic light scattering experiments corresponding to **DSPE-BODIPY** nanomicelles (200  $\mu\text{M}$ ) formed from the aza-BODIPY derivative **5a** and **DSPE**.

The assembled **DSPE-BODIPY** structures were characterized using various spectroscopic and morphological analyses. DLS measurements revealed that the nanomicelles formed were in the uniform spherical shape with hydrodynamic

dimensions of  $150 \pm 30$  nm in diameter (Figure 3.3). The smooth correlation evidenced the uniformity of the assembled spherical shaped nanomicelles in the solution. Furthermore, the evidence for the synthesized nanomicelles was obtained through transmission electron microscopy (TEM) experiments, which confirmed the formation of spherical nanomicelles having a diameter of  $150 \pm 30$  nm (Figure 3.4). These nanosized spheres with a potent sensitizer, the aza-BODIPY **5a** have been used for the *in vitro* biological investigations.

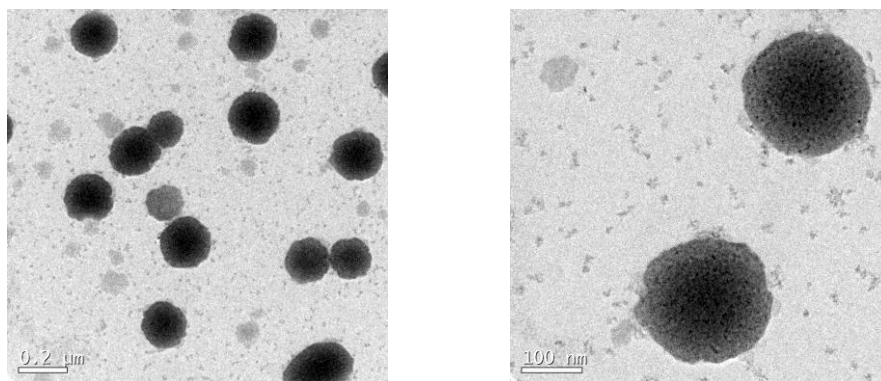
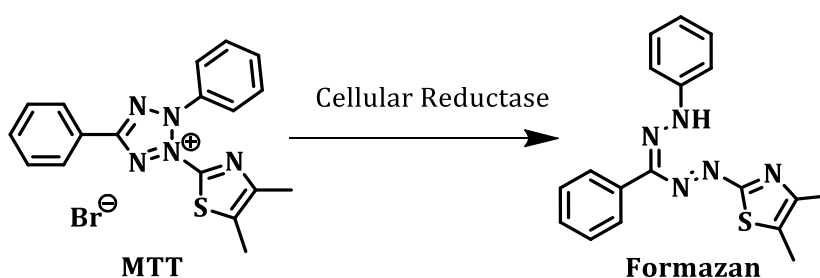


**Figure 3.4.** Transmission electron microscopic (TEM) images of **DSPE-BODIPY** nanomicelles ( $200 \mu\text{M}$ ) formed from the aza-BODIPY derivative **5a** and **DSPE**.

### 3.3.1.1. Investigation of *In Vitro* Photobiological Properties

To investigate the *in vitro* photodynamic efficacy of the **DSPE-BODIPY** nanomicelles in cells, we have employed 3-(4,5-dimethylthiazol-2-yl)-2,5-diphenyl-tetrazolium bromide (MTT) assay, which is a standard colorimetric technique used for the measurement of cellular proliferation (cell growth). MTT is yellow in color, but when reduced, it transforms to purple formazan by cellular reductase enzymes present in living cells (Scheme 3.2). To determine the photocytotoxicity of the **DSPE-BODIPY** conjugates, we have carried out the MTT assay in three different cancer cell lines; MCF-

7 (human breast cancer), HeLa (cervical cancer) and MDA-MB-231 (aggressive human breast cancer). The light source used for the irradiations was a commercially available VINVISH PDT laser with the excitation wavelength at 630 nm (10 mW/cm<sup>2</sup>, 15 min). The IC<sub>50</sub> value, which is a direct measurement of cytotoxicity, was quantified by measuring the absorbance of the formazan formed in the region 500-600 nm, under different conditions such as with and without irradiation.



**Scheme 3.2.** Enzymatic conversion of MTT (yellow) to formazan (purple).

The percentage of growth inhibition of cells in the presence of **DSPE-BODIPY** conjugates formed from different aza-BODIPY derivatives **5a**, **5c**, **6b**, **6c** and the control samples such as **DSPE** alone, and aza-BODIPYs alone were determined using MTT assay with and without irradiation (Figure 3.5). The **DSPE-BODIPY** conjugate formed from the aza-BODIPY dye, **5a** showed highest photocytotoxicity and exhibited an IC<sub>50</sub> value of 2 μM in MDA-MB-231 cells. Similar experiments were carried out for the conjugates prepared using **5c**, **6b** and **6c** under similar conditions and IC<sub>50</sub> values obtained are 7, 12 and 9 μM, respectively (Table 3.1). To evaluate the cell selectivity, we employed other two different cancer cell lines, namely, MCF-7 and HeLa. As summarized in Table 3.1, we have made similar observations albeit with little difference in IC<sub>50</sub> values. Among the various nanoconjugates screened, the conjugate

derived from the aza-BODIPY dye, **5a** was found to be most efficient and hence we have investigated this system for further detailed photobiological investigations to understand the mechanism of its biological activity.

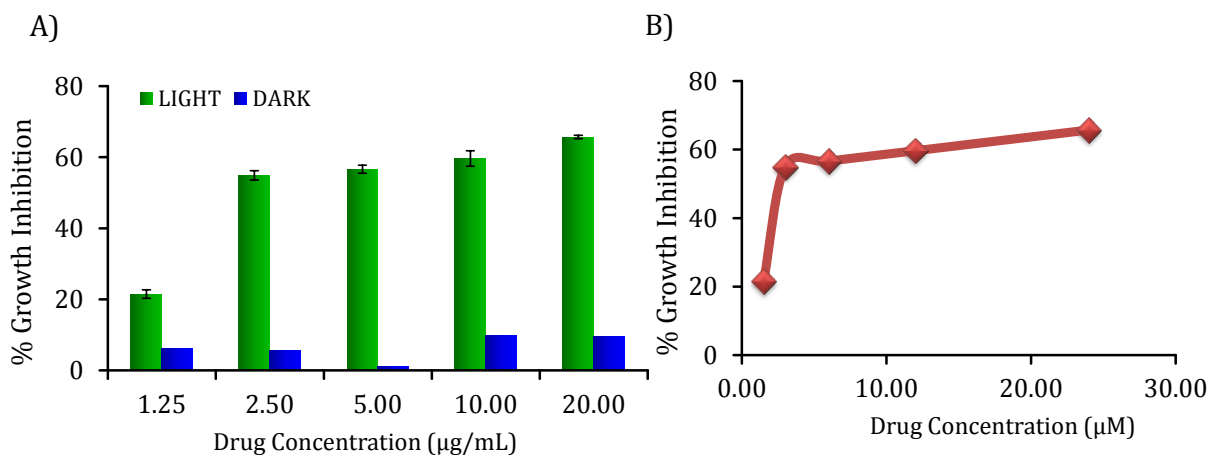


**Figure 3.5.** A) Histogram depicting the cytotoxicity of the **DSPE-BODIPY** conjugate of **5a** in light (green) and dark (blue) in MDA-MB-231 cells. B) Plot showing the percentage of growth inhibition in presence of **DSPE-BODIPY** in MDA-MB-231 cells upon irradiation using VINVISH PDT laser (600-720 nm, 50 mJ/cm<sup>2</sup>, 1 h).

**Table 3.1.** The IC<sub>50</sub> values of **DSPE-BODIPY** conjugates in different cell lines.\*

Aza-BODIPY used for <b>DSPE-BODIPY</b> conjugates	Half inhibitory concentration (IC <sub>50</sub> ) values in µM		
	MDA-MB-231	MCF-7	HeLa
<b>5a</b>	2.0	2.5	3.5
<b>5c</b>	7.0	6.0	7.0
<b>6b</b>	9.0	8.0	10.0
<b>6c</b>	12.0	10.0	9.0

\*The values are the average of more than three independent experiments.

To understand the mechanism of the PDT activity and cellular damage induced by the **DSPE-BODIPY** conjugates, we performed Annexin V-FITC/PI assay using flow cytometric analysis. For this, Annexin V-FITC was used together with propidium iodide (PI), which was another fluorescent probe to distinguish viable cells from the dead cells. The former can penetrate through the intact and viable cells, whereas the propidium iodide can only pass through dead cells (Figure 3.6). The cell populations at different phases of cell death, namely, viable (Annexin V-FITC (-ve)/PI (-ve)), early

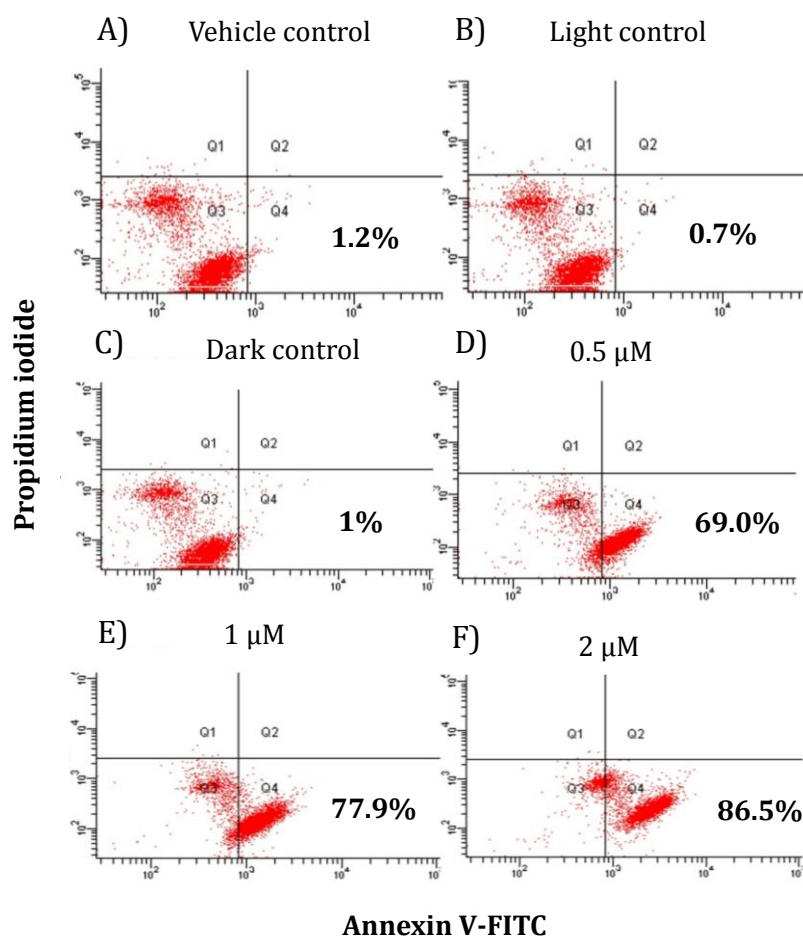


**Figure 3.6.** Flow cytometric analysis of MDA-MB-231 cells after PDT treatment with A) vehicle control, B) light control, C) dark control and D) in presence of **DSPE-BODIPY**, 0.5 μM, E) 1 μM and F) 2 μM.



apoptotic (Annexin V-FITC (+ve)/PI (-ve)) and necrotic or late-stage apoptotic (Annexin V-FITC (+ve)/PI (+ve)) were examined at different drug doses. The lower left quadrant (Q3) of each panel showed the viable cells, since they were negative for both Annexin V-FITC and PI, whereas the lower right quadrants (Q4) represent the apoptotic cells (Annexin V-FITC (+ve)/PI (-ve)). We observed that most of the cells were negative for both Annexin V-FITC and PI with **DSPE-BODIPY** (2  $\mu$ M) in the dark, which indicates that this conjugate shows negligible toxicity in MDA-MB-231 cells under these conditions. However, upon illumination, the percentage of cells in the lower right quadrant (Q4), *i.e.*, in the early apoptotic stage (*i.e.*, externalization of phospholipid phosphatidylserine but not membrane leakage, Annexin V-FITC (+ve)/PI (-ve)) increased from 1.2% to 86.5%, when the concentration of **DSPE-BODIPY** was increased from 0 to 2  $\mu$ M. These results clearly indicate that the photoactivated **DSPE-BODIPY** conjugates induce cancer cell death predominantly through apoptosis.

The nature of cell death induced by the **DSPE-BODIPY** conjugate was evidenced through the phase contrast microscopic morphological analysis of the cells in the presence and absence of light (Figure 3.7). The MDA-MB-231 cells were irradiated before and after incubating with the **DSPE-BODIPY** and also with the lipid **DSPE** alone as a vehicle control. We observed significant changes in cell morphology only after treatment with **DSPE-BODIPY** followed by irradiation. These morphological transformations indicate good cell cytotoxicity towards MDA-MB-231 cells. In contrast, the light controls (where the cells were only irradiated), dark controls (where cells were treated with the photosensitizers in the dark) and the vehicle control (**DSPE** alone) showed negligible changes in the cell morphology confirming thereby the

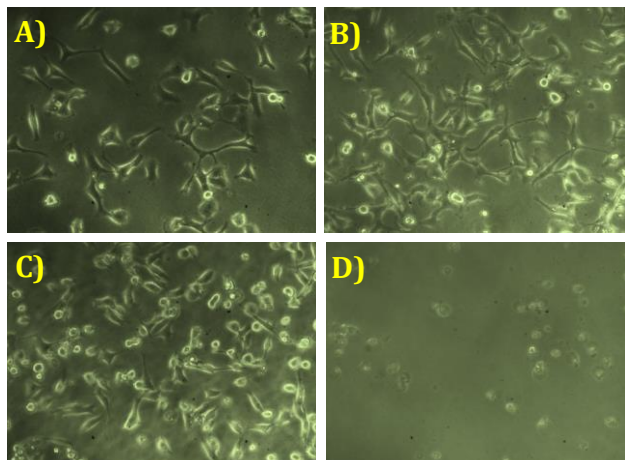


**Figure 3.7.** Morphological changes of MDA-MB-231 cell lines, A) light control B) dark control and after PDT with **DSPE-BODIPY**, plus light C) 0.5  $\mu\text{M}$  and D) 1  $\mu\text{M}$ .

apoptotic mediated cell death caused by the nanoconjugate, **DSPE-BODIPY** in the presence of light. Further, the cells were treated with the **DSPE-BODIPY** nanoconjugates together with the staining agent, Hoechst (Figure 3.8). It was found that PDT with **DSPE-BODIPY** in MDA-MB-231 cells at 2  $\mu\text{M}$ , resulted in *ca.* 85% decrease in fluorescence intensity of the Hoechst dye to nuclear condensation.

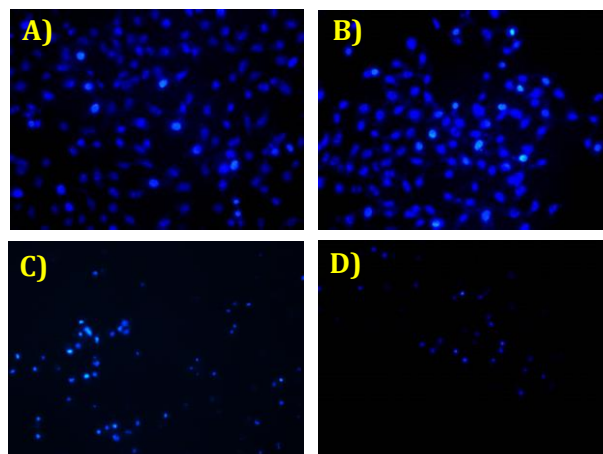


**Figure 3.8.** Confirmation of chromatin condensation by Hoechst staining in MDA-MB-231 cells; A) light control, B) dark control, and in the presence of **DSPE-BODIPY**, plus light C) 1  $\mu\text{M}$ , D) 2  $\mu\text{M}$ .

In contrast, the control experiments (dark and light only) showed negligible nuclear condensation, which clearly confirm a gradual concentration dependent destruction of the cancerous tissue due to the PDT activity of the **DSPE-BODIPY** nanoconjugates.

The apoptosis mediated cell death was furthermore evidenced through tetramethylrhodaminemethyl ester (TMRM) treatment. TMRM is a cell-permeable cationic, red-orange fluorescent dye that is readily sequestered by the active mitochondria. The changes in mitochondrial membrane potential via apoptosis were monitored through imaging of TMRM fluorescence intensity. The photodynamic treatment of MDA-MB-231 cells with **DSPE-BODIPY** nanoconjugates at 2  $\mu\text{M}$  resulted in about *ca.* 80% decrease in membrane potential. In contrast, the controls showed negligible decrease in mitochondrial membrane potential. These observations suggest that the **DSPE-BODIPY** induces cell death during PDT treatment predominantly through apoptotic pathway (Figure 3.9).

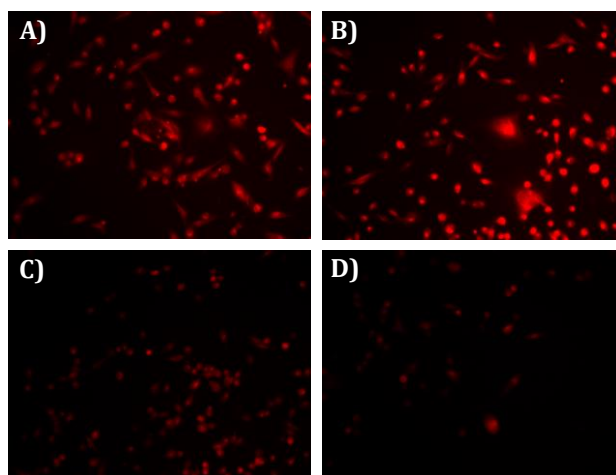


**Figure 3.9.** Reduction in fluorescence intensity of tetramethylrhodaminemethyl ester (TMRM) showing the decrease in mitochondrial membrane potential in MDA-MB-231 cells; A) light control, B) dark control, in presence of **DSPE-BODIPY**, plus light C) 1  $\mu\text{M}$ , D) 2  $\mu\text{M}$ .

The cell death through apoptotic pathway was accomplished by a conserved intracellular machinery of execution, which was mainly attributed to the activation of the caspase family of cysteine proteases. Caspase-3 is a common effector of most of the apoptotic pathways, expressed as a proenzyme of 32 kDa that in response to several stimuli gets cleaved, generating two subunits of 17 and 12 kDa. Detection of active caspase-3 in cells and tissues can be achieved by several methods, and one of the important methods is Western blotting. We observed the cleavage of caspase-3 in the presence of 2  $\mu\text{M}$  of **DSPE-BODIPY** conjugate, which unambiguously confirmed the apoptotic mediated cell death during PDT (Figure 3.10) using aza-BODIPY dyes.

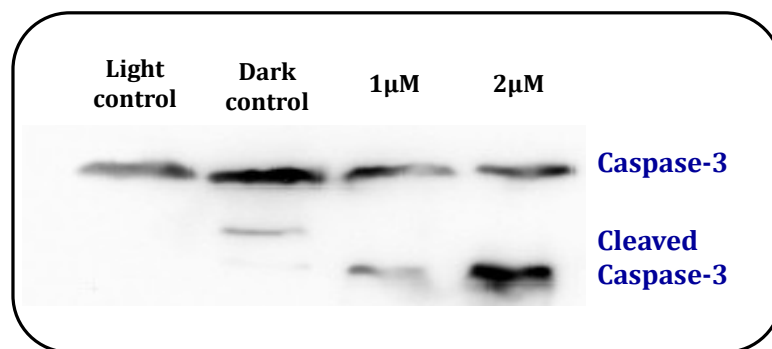


**Figure 3.10.** Western blot analysis showing the caspase-3 activity in presence of **DSPE-BODIPY** plus light (1  $\mu\text{M}$  and 2  $\mu\text{M}$ ) and the controls under similar conditions.

To understand the involvement of reactive oxygen species (ROS), we quantified the generation of ROS in cells during the PDT treatment with **DSPE-BODIPY** conjugates, using 5-(and-6)-chloromethyl-2',7'-dichlorodihydrofluorescein diacetate acetyl ester (CM-H<sub>2</sub>DCFDA) assay. In the reduced form, CM-H<sub>2</sub>DCFDA is non-fluorescent, but after cellular oxidation followed by esterases mediated hydrolysis of acetate groups results in a green fluorescent derivative. When MDA-MB-231 cells were treated with **DSPE-**

**BODIPY** (2  $\mu\text{M}$ ) and irradiation followed by the addition of CM-H<sub>2</sub>DCFDA, we observed fluorescence in *ca.* 80% of cells (Figure 3.11). In contrast, light alone and **DSPE-BODIPY** in the dark, showed only background values of *ca.* 10% and *ca.* 5%, respectively. These results demonstrate that only **DSPE-BODIPY** conjugates upon excitation generate concentration dependent ROS, which are primarily involved in the apoptosis mediated cell death.

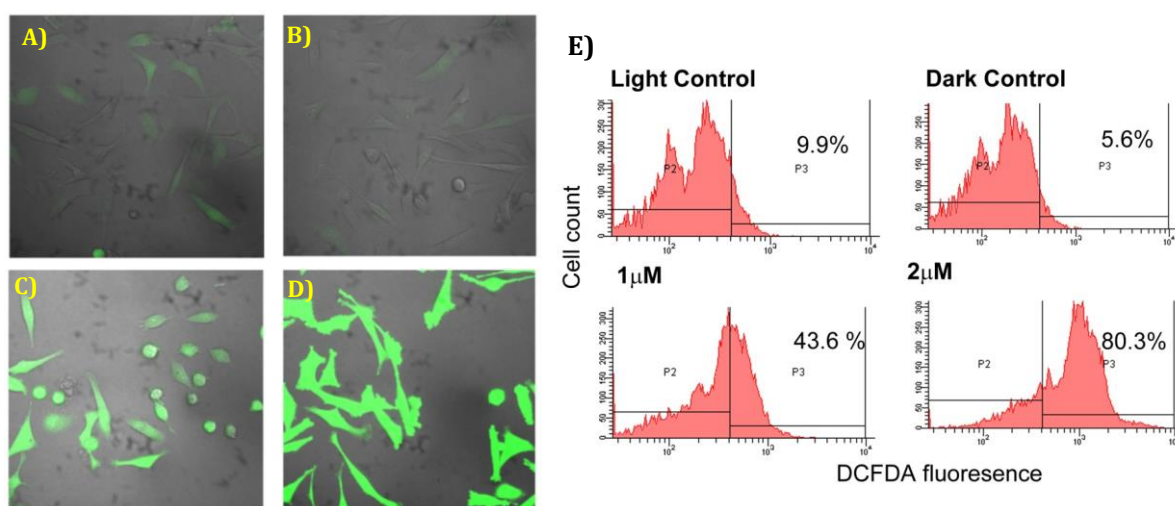


**Figure 3.11.** Confocal microscopy images showing concentration dependent green fluorescence in MDA-MB-231 cells after PDT with **DSPE-BODIPY** and incubation with CM-H<sub>2</sub>DCFDA at A) light control, B) dark control, in presence of **DSPE-BODIPY** plus light, C) 1  $\mu\text{M}$ , D) 2  $\mu\text{M}$ , and E) quantification of ROS generation by FACS analysis.

### 3.3.2. Photooxygenation Reactions Using Aza-BODIPY Derivatives

As the aza-BODIPY derivatives showed high singlet oxygen generation efficiency, it was of our interest to explore their use as photooxygenation catalysts. The different aza-BODIPY dyes (**5a**, **5c**, **6b** and **6c**) and three commonly used standard sensitizers such as tetraphenylporphyrin (**TPP**), Rose Bengal (**RB**) and Methylene Blue (**MB**) were

employed for the photooxygenation reactions (Chart 3.2). To screen the sensitizer efficiency, we have used the most common reaction of i.e., the oxidation of 1-naphthol to 1,4-naphthoquinone (Scheme 3.3). 1,4-Naphthoquinones are important natural products and serve as valuable building blocks in the synthesis of several biologically active compounds (Suchard *et al.*, 2006; Thomson, 1997; Wakamatsu *et al.*, 1984; Crouse *et al.*, 1981).

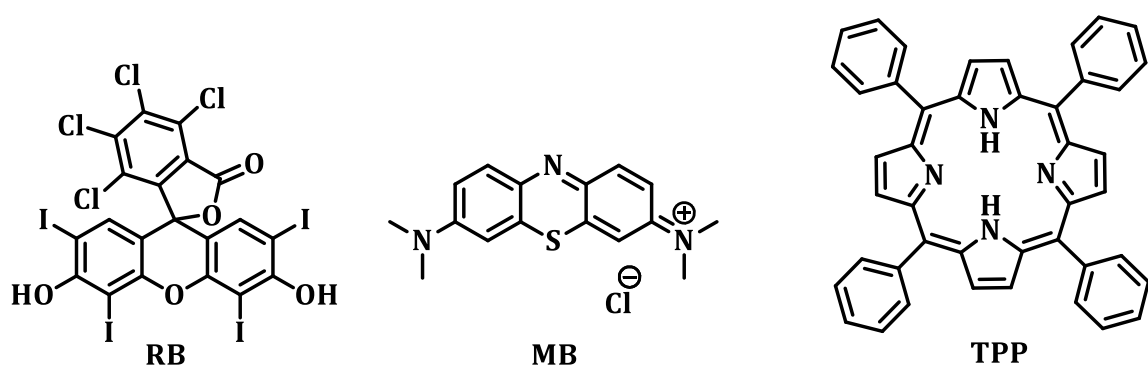
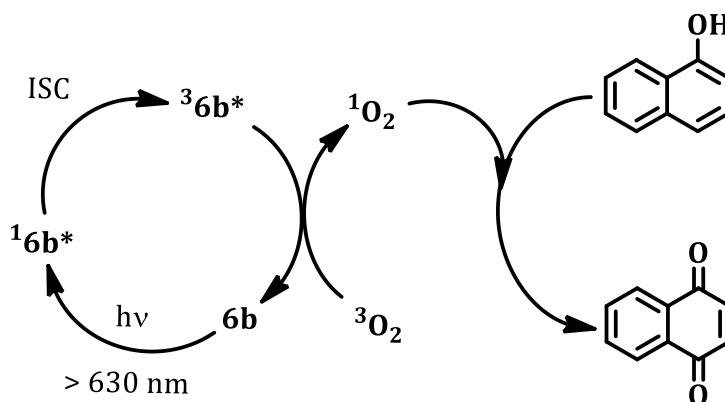


Chart 3.2



Scheme 3.3. Photooxygenation of 1-naphthol using the aza-BODIPY 6b.

### 3.3.2.1. Efficiency of Aza-BODIPYs vs Standard Sensitizers

The photooxygenation reaction using various sensitizers and the aza-BODIPY dyes was carried out under identical conditions and using three different irradiation

light sources, namely, i) 200 W Hg lamp (energy of output light *ca.* 6-8 mJ); ii) direct sunlight (Trivandrum, India, November-December 2011, 8.5°N 76.9°E, 5 m above sea level, energy of output light *ca.* 20-25 mJ) and iii) focused sunlight using convex lens (location as above and energy of output light *ca.* 200-220 mJ). The progress of the photooxygenation reaction was analyzed by thin layer chromatography (TLC), NMR and gas chromatography (GC) in all the cases. We have selected the aza-BODIPY dye, **6b** as the lead molecule for further photooxygenation reactions. We chose **6b** due to its high photostability and good solubility in common organic solvents among the various aza-BODIPY dyes and also due to its comparable singlet oxygen generation efficiency as that of the standard sensitizers like **TPP**, **MB** and **RB** (Hajimohammadi *et al.*, 2011; Haggiage *et al.*, 2009; Oelgemoller *et al.*, 2005; Esser *et al.*, 1994). The preparative photooxygenation reactions were carried out by irradiating a solution of 1-naphthol (0.2 mM) in CH<sub>3</sub>CN (3 mL) in the presence of sensitizers (2 μM) and the analysis of the reaction mixture was carried out by GC, TLC and <sup>1</sup>H NMR. We observed *ca.* 100% conversion of 1-naphthol to 1,4-naphthaquinone in the presence of aza-BODIPY dye, **6b** as the sensitizer. We have monitored the conversion through UV-Vis spectroscopy and we could observe a regular decrease in the absorption of 1-naphthol at 295 nm, with the concomitant formation of a new band at 320 nm, corresponding to 1,4-naphthoquinone (Figure 3.12). In contrast, the standard sensitizers such as **TPP**, **MB** and **RB**, under similar irradiation conditions, showed very low conversion efficiency of *ca.* 40%, 26% and 20%, respectively (Table 3.2). The low conversion efficiency of standard sensitizers could be due to their poor photostability under the irradiation conditions. As reported in the literature, **TPP**, **MB** and **RB** showed non-negligible

decrease in absorbance with the irradiation time (Griesbeck *et al.*, 2007). The aza-BODIPY derivative **6b**, on the other hand, showed high efficiency and exceptionally high photostability for more than 8 h and thereby demonstrating its superiority over the currently used sensitizers for photooxygenation reactions.

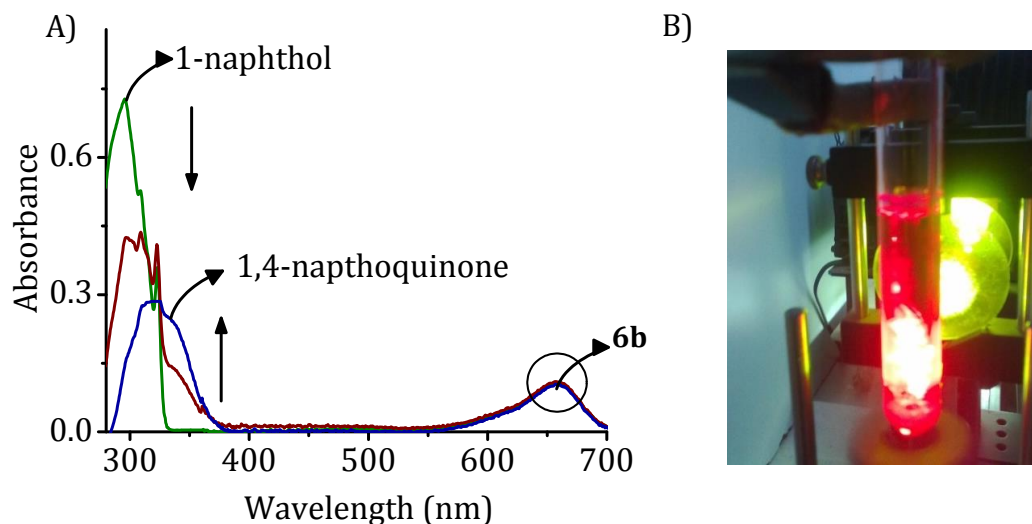


**Figure 3.12.** A) Absorption spectra indicating the formation of 1,4-naphthoquinone from 1-naphthol by the irradiation using 200 W mercury lamp in presence of the dye, **6b** (2  $\mu$ M). B) Photograph showing the method of irradiation using Oriel lamp.

With an objective to develop a ‘green’ and ‘sustainable’ procedure for the photooxygenation reaction, we have carried out the conversion of 1-naphthol to 1,4-naphthoquinone using normal sunlight as the light source (energy of the output light is *ca.* 20-25 mJ). Interestingly, we observed that the reaction required around *ca.* 1 h for *ca.* 100% conversion in the presence of the dye **6b**. The commonly used sensitizers such as **TPP**, **MB** and **RB** showed less than *ca.* 50% conversion efficiency under similar conditions. These observations demonstrate that the aza-BODIPY dyes having high photostability and ideal absorption makes them attractive photooxygenation catalysts.



**Table 3.2.** Photooxygenation of 1-naphthol to 1,4-naphthoquinone using various sensitizers and light sources in acetonitrile.

Sensitizer	$\Phi_{\Delta}$	Yield (%) <sup>[a]</sup>		
		200 W Hg lamp <sup>[b]</sup>	Sunlight (direct) <sup>[c]</sup>	Sunlight (focused) <sup>[d]</sup>
<b>5a</b>	0.65	85	80	85
<b>5c</b>	0.68	80	80	90
<b>6c</b>	0.80	90	85	90
<b>6b</b>	0.70	100	100	100
<b>TPP</b>	0.74	40	40	60
<b>MB</b>	0.52	26	38	40
<b>RB</b>	0.79	20	24	20

<sup>[a]</sup> Average of more than three experiments. Singlet oxygen generation yields of **TPP**, **MB** and **RB** were taken from the literature. Energy of outputs light measured by Oriel photodiode (Model 7072) were <sup>[b]</sup> 8 h, 6-8 mJ; <sup>[c]</sup> 1 h, 20-25 mJ; <sup>[d]</sup> 0.5 h, 200-220 mJ.

Further to understand the effect of intensity of sunlight on the efficiency of the reaction, we have carried out the photooxygenation reaction using focused sunlight as reported in the literature (Wurm *et al.*, 1985; Durchstein *et al.*, 1984; Griffiths *et al.*, 1976). We have used acetonitrile as the solvent because of the solubility and non-volatility. Following this strategy, various solutions of sensitizers were exposed in a quartz tube and purged with a gentle stream of oxygen. The sunlight was focused on the quartz tube using a convex lens and a 570 nm long pass filter (energy of the focused light was around 200-220 mJ) (Figure 3.13). All experiments gave satisfactory yields in reasonable periods of time without any noticeable side products. The known sensitizers **MB**, **RB** and **TPP** showed almost similar yields in acetonitrile as previously

discussed in the literature. Interestingly, the aza-BODIPY derivative **6b** exhibited much improved efficiency and required only *ca.* 30 min irradiation to achieve *ca.* 100% conversion to 1,4-naphthoquinone. The results with both artificial light, as well as sunlight as the irradiation source suggest that the aza-BODIPY derivatives can catalyze the singlet oxygen mediated photooxygenation reactions quite efficiently.

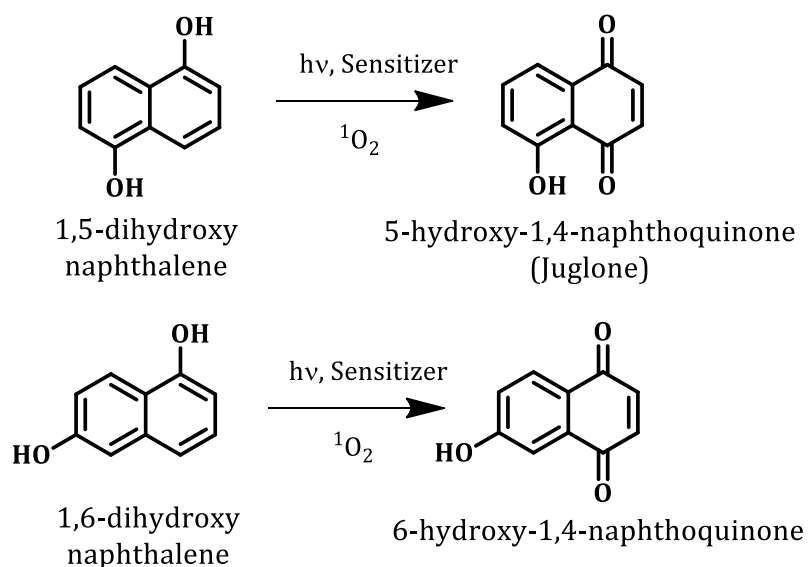


**Figure 3.13.** Photographs showing the photooxygenation reaction of 1-naphthol (0.2 mM) in the presence of the aza-BODIPY catalyst, **6b** (2  $\mu$ M) under direct sunlight (Trivandrum, India, November-December 2011, 8.5°N 76.9°E, 5 m above sea level).

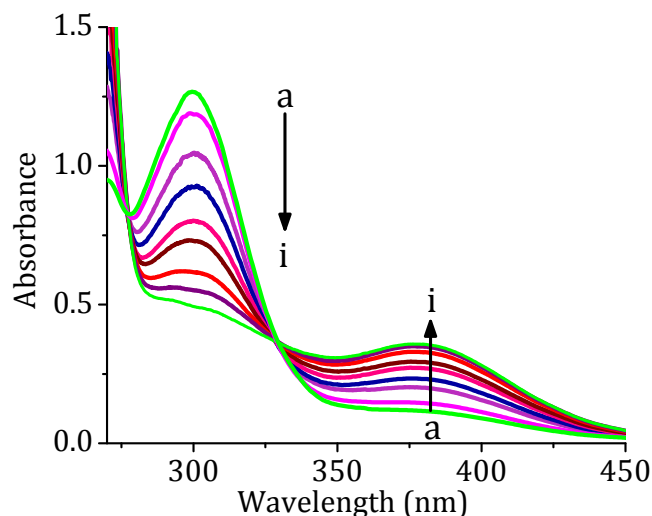
### 3.3.2.2. Photooxygenation of Substituted Naphthols

To investigate the generality of the aza-BODIPY as efficient sensitizers towards photooxygenation reactions, we have carried out the conversion of two more naphthol derivatives such as 1,5-dihydroxynaphthalene and 1,6-dihydroxynaphthalene (Scheme 3.4). The naphthoquinone derivatives based on 5-hydroxy-1,4-naphthoquinone (Juglone) represent an important class of natural products (Suchard *et al.*, 2006). The photooxygenation reactions were carried out by the similar procedure as for 1-naphthol and the progress of the reactions was monitored by TLC at each 15 min intervals and quantified by  $^1\text{H}$  NMR and GC-MS. After an illumination time of 5 h using

200 W Hg lamp, the naphthols showed *ca.* 100% conversion to their corresponding 1,4-naphthoquinones in the presence of aza-BODIPY dye, **6b** as the sensitizer, whereas the standard dyes showed less than *ca.* 50% conversion efficiency. We have monitored these reactions through UV-Vis spectroscopy (Figure 3.14). For example, 1,6-dihydroxynaphthalene showed an absorption maximum at 300 nm, which upon irradiation and in the presence of the sensitizer exhibited hyperchromicity at 380 nm, due to the formation of the product, 6-hydroxy-1,4-naphthoquinone. Similar observations were made with 1,5-dihydroxynaphthalene to yield Juglone in *ca.* 100% yield. The conversion efficiency was found to be fast when we changed the irradiation source from artificial Hg lamp to sunlight. Notably, we observed *ca.* 100% conversion for both of these reactions in 30 min by the irradiation using ordinary sunlight in the presence of continuous stream of oxygen as summarized in Table 3.3.

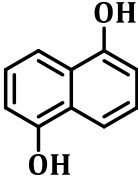
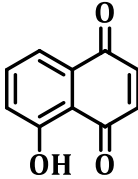
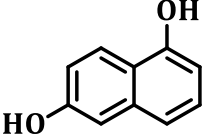
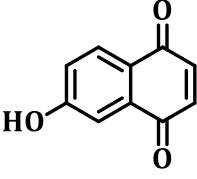


**Scheme 3.4.** Conversion of 1,5-dihydroxynaphthalene and 1,6-dihydroxynaphthalene to the corresponding naphthoquinones by the irradiation in presence of sensitizers.



**Figure 3.14.** A) Absorption spectra showing the conversion of 1,6-dihydroxynaphthalene to 6-hydroxy-1,4-naphthaquinone by the irradiation using 200 W mercury lamp in the presence of **6b** ( $2 \mu\text{M}$ ); a) 0 h, i) 5 h.

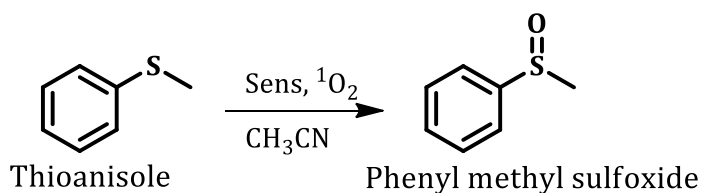
**Table 3.3.** Photooxygenation of naphthols using various sensitizers and light sources.\*

Substrate	Product	Photooxygenation reactions		
		Sensitizer	Hg Lamp, 5 h Yield (%)	Sunlight, 30 min Yield (%)
		<b>6b</b>	100	100
		<b>TPP</b>	40	40
		<b>MB</b>	15	15
		<b>RB</b>	10	10
		<b>6b</b>	100	100
		<b>TPP</b>	38	55
		<b>MB</b>	20	25
		<b>RB</b>	10	20

[<sup>a</sup>] Average of more than three experiments; energy of output light measured by Oriel photodiode (Model 7072), [<sup>b</sup>] 8 h, 6-8 mJ; [<sup>c</sup>] 1 h, 20-25 mJ; [<sup>d</sup>] 0.5 h, 200-220 mJ.

### 3.3.2.3. Photooxygenation of Thioanisole by Aza-BODIPYs

We have further explored the efficiency of the sensitizers as photocatalysts by employing the conversion of thioanisole to sulfoxides. Sulfoxides are important intermediates in pharmaceutical and fine chemical industry (Fernandez *et al.*, 2003; Carreno *et al.*, 1995). The selective oxidation of sulfides to sulfoxides has been one of the important transformations from a synthetic point of view (Chen *et al.*, 2010). Photocatalytic oxidation of sulfide to sulfoxide was reported using Ru(bpy)<sub>3</sub><sup>2+</sup> in acetonitrile by Zen and coworkers (Zen *et al.*, 2003). More recently, it was reported that the BODIPYs can be used as photocatalysts for the aerobic oxidation of thioanisole with an efficacy of *ca.* 89% (Li *et al.*, 2011). In another report, Cibulka and Albin have described the photooxidation of thioanisole to sulfoxide using flavin as the sensitizer (Dadova *et al.*, 2012). Furthermore, Li and coworkers have improved the rate of oxidation reaction and have achieved *ca.* 100% conversion efficiency by modifying the BODIPYs by incorporating with iodine atoms (Li *et al.*, 2013).



**Scheme 3.5.** Conversion of thioanisole to methylphenylsulfoxide by the sensitizers.

In this context, it was our interest to explore the utility of aza-BODIPYs as catalysts in the conversion of thioanisole to sulfoxide in presence of both artificial light and sunlight irradiation (Scheme 3.5). The concentration of aza-BODIPY catalyst used in the conversion was *ca.* 1 mol% of the substrate, thioanisole. A 200 W mercury lamp

with a bandpass filter ( $\lambda = 570$  nm) was used as the visible light source (ranges from 400 to 700 nm). The conversion of the reaction was determined through GC-MS by integrating the peaks of the reaction mixtures assigned to the sulfide substrate and sulfoxide product. We observed *ca.* 100% conversion of thioanisole to methylphenylsulfoxide in 3 h by using aza-BODIPY dye, **6b** as the catalyst (Table 3.4). To examine the effect of light source, we have replaced the artificial light with normal sunlight (energy of the output light was maintained as *ca.* 25±5 mJ throughout the reaction) and the thioanisole oxidation was found to take place efficiently, in *ca.* 1 h. Interestingly, no sulfones were detected in the reaction mixture even after 10 h irradiation demonstrating a high degree of selectivity of this reaction. These results clearly demonstrate the aza-BODIPY sensitizers have advantages over the conventional oxidizing agents as well as common sensitizers in the selective oxidation of thioanisole to methylphenylsulfoxide.

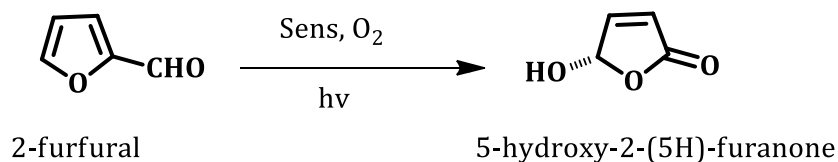
**Table 3.4.** Photooxygenation of thioanisole to methylphenylsulfoxide using various sensitizers and light sources.\*

Sensitizer	$\Phi(^1O_2)$	Yield (%)	
		200 W Hg lamp Irradiation (3 h)	Sunlight Irradiation (3 h)
<b>6b</b>	0.70	80	100
<b>TPP</b>	0.74	15	20
<b>MB</b>	0.52	10	15
<b>RB</b>	0.79	5	15

\*Average of more than three independent experiments in acetonitrile.

### 3.3.2.4. Photooxygenation of Furfural by Aza-BODIPYs

To investigate the versatility of the aza-BODIPY catalysts, we have chosen furfural for singlet oxygen photooxygenation reaction (Scheme 3.6). Furan and its derivatives are among the most reactive substrates for singlet oxygen leading to 5-hydroxy-2-(5H)-furanone, which is a key constituent of the potent analgesic and anti-inflammatory agent manolide and many other natural and unnatural products of medicinal importance (Lattmann *et al.*, 1996; Kanazawa *et al.*, 1975; Heather *et al.*, 1974; Meyers *et al.*, 1974). The photosensitizer (1% mol of the substrate) was added to a solution of 2-furfural in CH<sub>3</sub>CN. The resultant mixture contained in a Pyrex vessel was vigorously stirred at room temperature under O<sub>2</sub> and irradiated with a 200 W mercury lamp through a UV-cut-off filter (Scheme 3.6). GC analysis indicated the complete oxidation of furfural after 3 h of irradiation using aza-BODIPY dye, **6b** as the catalyst.



**Scheme 3.6.** Conversion of furfural to furanone by the irradiation in the presence of sensitizers.

Removal of the sensitizer by filtration, and removal of the solvent under vacuum gave the product, 5-hydroxy-2-(5H)-furanone, which was characterized using various spectroscopic techniques. We have further carried out these reactions in presence of sunlight as the light source. We observed that the aza-BODIPY **6b** was efficient in the conversion of furfural to furanone under these conditions (Table 3.5).

**Table 3.5.** Photooxygenation of 2-furfural using various sensitizers and light sources.\*

Sensitizer	Yield (%)	
	200 W Hg lamp (3h)	Sunlight (3h)
<b>6b</b>	100	100
<b>TPP</b>	80	80
<b>RB</b>	70	50
<b>MB</b>	50	45

\*Average of more than three independent experiments in acetonitrile.

### 3.3.2.5. Photooxygenation on Polystyrene Support

To demonstrate the potential applications of singlet oxygen mediated photooxygenation reactions, recently efforts have been made to adsorb the sensitizers on various matrices. We have performed the singlet oxygen photooxygenation with the sensitizers adsorbed on commercially available raw polystyrene beads. The aza-BODIPY sensitizer dissolved in dichloromethane was transferred in catalytic amounts into the polystyrene network by dissolving the polystyrene in a solution of dichloromethane and subsequent evaporation of the solvent. The substrate (1-naphthol) was transferred onto the polymer beads by the same procedure as in the case of the sensitizers. After evaporation of the excess solvent, a layer of sandy solid was obtained, which was irradiated in a loosely covered petri dish under sunlight without external cooling or purging with oxygen. After irradiation, the product was extracted from the polymer beads by repeatedly washing with hexane, in which the aza-BODIPY dyes were not soluble. We have observed *ca.* 50% conversion of



1-naphthol to 1,4-naphthoquinone in the presence of the aza-BODIPY, **6b**, while **TPP** gave around *ca.* 20% under similar conditions.

### 3.4. CONCLUSIONS

In summary, the aza-BODIPY dyes under investigation exhibited good solubility and excellent photostability. The conjugates of these dyes with an amphiphilic lipid, **DSPE** gave the formation of nanospheres having diameter of *ca.* 150±30 nm. The *in vitro* PDT efficacy of these nanospheres using MDA-MB-231 cells revealed that the conjugate with the aza-BODIPY derivative, **5a** showed high photocytotoxicity with an IC<sub>50</sub> value of 2 µM. The *in vitro* studies have indicated that the biological activity of these nanomicelles can be attributed predominantly to the generation of reactive species such as singlet oxygen. The mechanism of cell death induced by these conjugates was determined to be apoptotic pathway, as evidenced through Annexin V-FITC/PI flow cytometric analysis, morphological transformation, nuclear condensation, and activation of caspase-3.

Of the various dyes investigated, the aza-BODIPY, **6b** was found to be the most efficient catalyst in the photooxygenation reactions under both artificial light as well as sunlight irradiation conditions. Furthermore, these dyes can be uniformly loaded onto the polystyrene matrix and can be used in the photooxidation reactions. This simple and convenient strategy using the aza-BODIPY dyes represents a practical alternative to the standard oxidizing agents. Our results have demonstrated that the aza-BODIPY dyes under investigation can act not only as efficient green photooxygenation catalysts but also as sensitizers in photodynamic therapy.

## 3.5. EXPERIMENTAL SECTION

### 3.5.1. General Techniques

The melting points of various compounds were determined using Mel-Temp melting point apparatus and compared with the authentic samples, reported in the previous chapter. The electronic absorption spectra were recorded on a Shimadzu UV-3101 or 2401PC UV-Vis-NIR scanning spectrophotometer. <sup>1</sup>H NMR spectroscopy was performed on a 500 MHz Bruker advanced DPX spectrometer. Yields of the reactions were obtained using Shimadzu QP2010 Gas chromatograph mass spectrometer. The photoactivation was done using VINVISH PDT laser (600-720 nm, 200J cm<sup>-2</sup>, 50 mW cm<sup>-2</sup>). Flow cytometric analysis was carried out in a BD FACS Aria 2 machine. Gel electrophoresis was carried out using a BIO-RAD Gel DOC XR.

#### 3.5.1.1. Transmission Electron Microscopy (TEM) Analysis

TEM analysis was performed on JEOL 100 kV high resolution transmission electron microscope. The **DSPE-BODIPY** nano conjugates (3:1, 200 μM) in PBS buffer were drop casted on the top of carbon-coated Cu grid. The samples were dried by a vacuum pump under reduced pressure for 1 h at room temperature. The accelerating voltage of the transmission electron microscope was 100 kV and the beam current was 65 A. Samples were imaged using a Hamamatsu ORCA CCD camera.

#### 3.5.1.2. Scanning Electron Microscopy (SEM) Analysis

The SEM studies were carried out using ZEISS EVO MA and LS series scanning electron microscope. The operating range was between 100-230V at 50-60Hz single

phase with a consumption of 2.5 kVA. The sample solution (200  $\mu\text{M}$ ) in PBS buffer was drop casted directly on the top of the aluminium grid and the solvents were allowed to evaporate at ambient conditions. The obtained sample was coated with copper in order to attain the easy passage flow of electrons.

### **3.5.1.3. Dynamic Light Scattering (DLS) Analysis**

The DLS studies were carried out on a Nano Zeta Sizer, Malvern instruments. The samples were prepared in water/PBS buffer at required concentrations. The light scattering experiments were performed under low polydispersity index by using glass cuvettes. The hydrodynamic diameters and polydisperse indices of the samples were determined using a Malvern Zeta Nano-ZS system.

## **3.5.2. Materials and Methods**

Tetramethylrhodaminemethyl ester, hoechst, propidium iodide, FITC-Annexin V, 3(4,5-dimethylthiazol-2-yl)-2,5-diphenyltetrazolium bromide (MTT), Methylene Blue (**MB**), Rose Bengal (**RB**), naphthols, thioanisole, furfural were purchased from S.D. Fine chemicals, India; Sigma-Aldrich; U.S.A Merk Chemicals, Germany. DSPE was purchased from Avanti polar lipid, USA. CM-H<sub>2</sub>DCFDA was purchased from Invitrogen. The aza-BODIPY derivatives, **5a**, **5c**, **6b** and **6c** were synthesized as described in Chapter 2 of the thesis and characterized using different spectroscopic and analytical techniques. All the solvents used were purified and distilled before use by standard methods.

### **3.5.2.1. Determination of Cytotoxicity (IC<sub>50</sub> value)**

3(4,5-Dimethylthiazol-2-yl)-2,5-diphenyltetrazolium bromide (**MTT**) assay is a standard colorimetric assay for measuring cellular proliferation (cell growth). The

cancer cells (5 x 10<sup>3</sup> cells per well) were added to wells of two 96 well microliter plate. One for dark cytotoxicity and another for light cytotoxicity with 150 µL Dulbecco's Modified Eagle Medium (DMEM) with 10% serum and incubated for 24 h. Then added 0.625 to 10 µM of the various **DSPE-BODIPY** conjugates in serial dilution (stock 100 mM diluted using DMEM for test) for control and incubated for 24 h and irradiated in one plate using VINVISH PDT lamp (70 W for 15 min) while the other plate was kept in dark. After 24 h of incubation, the plates were removed from the incubator and added 10 µL of MTT (5 mg/mL stock) to each well. After 4 h, the supernatant was removed taking care that the formazan crystals formed were not being removed and added 100 µL of isopropyl alcohol to each well. The plates were covered with aluminium foil and kept on a shaker until crystals were dissolved. The absorbance at 570 nm was monitored and the percentage growth inhibition was calculated using the equation 3.1,

$$\% \text{Growth inhibition} = (\text{control-test}) / \text{control} \times 100 \dots\dots\dots (\text{Eq. 3.1})$$

### 3.5.2.2. Flow Cytometric Analysis with Annexin V-FITC/PI Assay

After appropriate treatments, the cells were harvested by gentle scraping followed by their re-suspension in PBS. Annexin V-FITC/PI staining was done using Invitrogen (USA) kit, following manufacturer's protocol. Viable cells were not stained with Annexin V-FITC/PI (bottom left quadrant). After PDT, with the **DSPE-BODIPY** nanomicelles (2 µM), a significant number of cells were stained positive by Annexin V-FITC, indicating apoptosis mediated cell death.

### 3.5.2.3. Tetramethylrhodamine Methyl Ester (TMRM) Assay

Tetramethylrhodamine, methyl ester (TMRM) is a cell-permeate, cationic, red-

orange fluorescent dye that is readily sequestered by active mitochondria. For this assay we seeded MDA-MB-231 cells in a 75 cm<sup>2</sup> flask and incubated for 24 h. Stock solution of the **DSPE-BODIPY** nanomicelles was prepared and it is further diluted to two different concentrations such as 1 μM and 2 μM in order to carry out the concentration dependent analysis. The nanoconjugate was then injected to the MDA-MB-231 cancerous cell lines at two different concentrations and was analyzed using fluorescent microscopic technique.

#### **3.5.2.4. Chromatin Condensation Assay by Hoechst Staining**

To study chromatin condensation, approximately 10<sup>5</sup> MDA-MB-231 cells were seeded in 96 well culture dishes and incubated for 24 h. Then, cells were incubated with 1 μM and 2 μM **DSPE-BODIPY** for 24 h followed by photoirradiation using VINVISH PDT lamp. Light and Dark control were taken as previously described. After 24 h of treatment MDA-MB-231 cells were rinsed twice with PBS and stained with 5 μg/ml Hoechst dye for 15 min at room temperature. Cells were then washed twice with PBS and visualized under an inverted fluorescence microscope.

#### **3.5.2.5. Detection of Reactive Oxygen Species**

For the detection of the reactive oxygen species (ROS) produced, approximately 10<sup>6</sup> MDA-MB-231 cells were plated in 60 mm and 96 well (BD falcon) plates with serum containing media. After 24 h, the cells were treated with 2 μM of **DSPE-BODIPY** for 24 h and irradiation was carried out for 30 min. To one of the plates, **DSPE-BODIPY** was added and kept in dark as the dark control. Immediately after PDT, cellular ROS content was determined using CM-H<sub>2</sub>DCFDA probe according to the manufacturer's

instructions (Invitrogen). Confocal images and differential interference contrast (DIC) images were acquired using Nikon A1R microscope system. Images were merged and processed using Nikon Imaging Software (NIS-Elements AR).

### **3.5.3. Photooxygenation Reactions**

#### **3.5.3.1. Irradiation with Artificial Light (200 W mercury lamp)**

Photolysis was carried out with a light source 200 W Mercury lamp (model 3767). The intensity of the output light was maintained constant (5-6 mJ) throughout the irradiations by measuring the output using an Oriel photodiode detection system (model 7072). Appropriate filters were used to avoid the photobleaching of the dyes due to direct UV exposure. The substrate was dissolved in 5-10 mL of the solvent. The sensitizer was added (1 mol percent) and the solution was irradiated at room temperature, while purging with a gentle stream of oxygen. The progress of the reaction was monitored by UV, TLC or GC analysis. All experiments gave satisfactory results in reasonable periods of time without any noticeable side products.

#### **3.5.3.2. Irradiation with Sunlight**

Oriel photodiode detection system (model 7072) was used for measuring the output intensity of the sunlight. The substrate and sensitizer were dissolved in suitable solvent and the solution was exposed to direct sunlight with a gentle stream of air. The progress of the reaction was monitored by TLC or GC analysis. The same sets of reactions were carried out simultaneously to maintain the intensity of the sunlight uniform. The convex lenses and suitable filters were used for the experiments with concentrated sunlight.

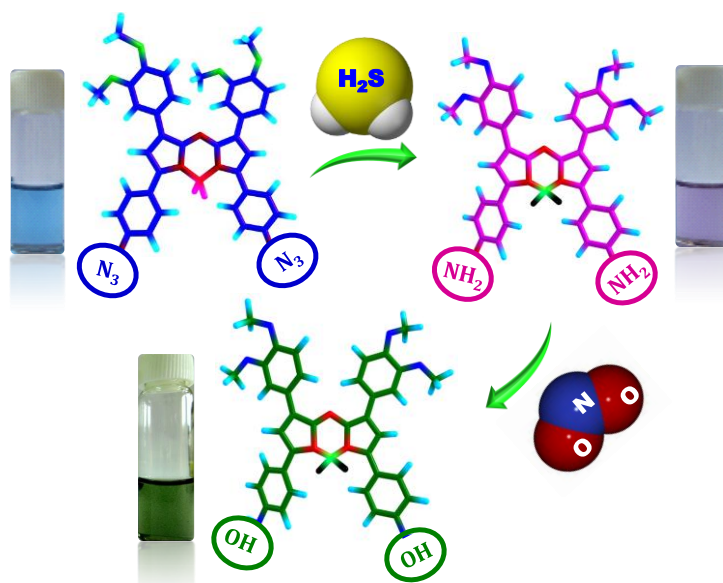
### **3.5.3.3. Photooxygenation on Polystyrene Support**

The aza-BODIPY and the reference sensitizers were transferred in catalytic amounts onto the polystyrene network by dissolving the raw polystyrene in a solution of the sensitizer in dichloromethane in a petri dish. The solvent was subsequently evaporated at room temperature. The substrate was also transferred in the same procedure and evaporated to get a sandy solid. The petri dish was further subjected to sunlight irradiation in open air for about 3 to 5 h. The product thus obtained was washed out using hexane and the petri dish with sensitizer encapsulated polystyrene was reused for next reaction.

---

## NOVEL AZA-BODIPY DYES: TUNING OF PHOTOPHYSICAL AND MOLECULAR RECOGNITION APPLICATIONS

---



### 4.1. ABSTRACT

With an objective to develop optical probes based on aza-BODIPY dyes, we synthesized a few novel N-substituted NIR absorbing dyes **3a-c** and have investigated their photophysical and molecular recognition properties under different conditions. These dyes showed strong absorption in the range of 700-800 nm with fluorescence in the region 750-950 nm. We observed a profound red shift in the absorption and fluorescence spectra of the aza-BODIPY dyes with the substitution from azido to amino to dimethylamino groups. Electrochemical and theoretical calculations have confirmed a consistent decrease in HOMO-LUMO gap in the case of **3a-c**, which is in agreement with the observed spectral changes.



We have investigated the interactions of the amino derivative, **3b**, with various biologically relevant anions. This aza-BODIPY dye exhibited selective interactions with nitrite ions ( $\text{NO}_2^-$ ) when compared to other anions and showed a distinct visual color change from bright blue to intense green with a sensitivity of 20 ppb ( $0.5 \mu\text{M}$ ). Successive addition of nitrite ions, to the protonated form of the probe, **3b** resulted in a hypochromicity in absorbance at 570 nm along with a gradual red shift in the maximum to 630 nm. Uniquely, this probe can be coated on a glass surface to fabricate a simple solid-state dipstick device that can be used for the visual detection of the  $\text{NO}_2^-$  ions in presence of other competing anions in distilled as well as natural water resources. This probe can be furthermore used for the sensitive detection of the nitrate ( $\text{NO}_3^-$ ) ions through a reduction step and freshly generated nitric oxide (NO) in aqueous medium.

On the other hand, the azido aza-BODIPY dye, **3a** showed selective interactions with hydrogen sulfide ( $\text{H}_2\text{S}$ ), when compared to other anions and neutral molecules. The detection of  $\text{H}_2\text{S}$  can be visualized through a color change from bright blue to purple with a detection limit of 0.5 ppm. The sensitivity of the probe was observed to be *ca.* 20-fold higher than the allowed exposure limits of  $\text{H}_2\text{S}$  as defined by US-EPA. The linear behavior of concentration dependent absorption changes confirmed the utility of the dye **3a** as a probe for the on-site analysis and estimation of  $\text{H}_2\text{S}$  in the aqueous medium. In contrast to the dyes **3a** and **3b**, the dimethylamino-aza-BODIPY derivative, **3c** exhibited negligible affinity for all the anions tested. These results demonstrate that the functional aza-BODIPY dyes, **3a** and **3b** can have potential use as probes for the detection and on-site analysis of biologically important anions and neutral molecules.

## 4.2. INTRODUCTION

The BODIPY dyes hold great promise as ideal materials owing to their favorable optical and electronic properties (Bozdemir *et al.*, 2010; Loudet *et al.*, 2007). In recent years, there has been increased interest in tuning of optical properties of these dyes by the appropriate substitution. The tuning of absorption as well as emission properties of these dyes, can be achieved through extending conjugation and by the use of fused pyrrole rings (Haefele *et al.*, 2010; Cakmak *et al.*, 2009; Yilmaz *et al.*, 2006; Atilgan *et al.*, 2008; Goze *et al.*, 2006; Baruah *et al.*, 2005). Alternatively, O'Shea, Akkaya and Kobayashi have achieved the synthesis of 8-aza-boradiazaindacenes (aza-BODIPYs), which exhibited around 100 nm bathochromic shift in absorption in the region 600-800 nm, when compared to BODIPYs (Shimizu *et al.*, 2013; Lu *et al.*, 2011; Liu *et al.*, 2011; Ozlem *et al.*, 2009; McDonnell *et al.*, 2006, 2005; Gorman *et al.*, 2004). Furthermore, the optical properties of the aza-BODIPYs can be tuned by substituting with electron donating groups at the peripheral positions. Such dyes having NIR absorption can have potential applications as chemosensors for various anions, cations and neutral molecules. In this context, the interaction of aza-BODIPY dyes with metal ions at different pH have been reported in the literature by different research groups (Killoran *et al.*, 2008; Coskun *et al.*, 2007; Killoran *et al.*, 2006). However, the recognition of anions and neutral molecules by the aza-BODIPY dyes are less explored.

Among the various ions, the nitrite ( $\text{NO}_2^-$ ) ions are considered to be type A inorganic contaminants in drinking water, and have proven to be of significant threat to human health (Chen *et al.*, 2012; Xiao *et al.*, 2010; Daniel *et al.*, 2009). The nitrite ions,

upon interaction with proteins, act as important precursors for the generation of highly carcinogenic N-nitrosamines (Ye *et al.*, 2011; Kilfoy *et al.*, 2011; Greer *et al.*, 2005). Excessive consumption of  $\text{NO}_2^-$  can lead to a number of medical issues such as esophageal cancer, infant methemoglobinemia (blue baby syndrome), spontaneous abortion and birth defects in the central nervous system (Manassaram *et al.*, 2006; Brender *et al.*, 2004; Hanajiri *et al.*, 2002). The maximum contaminant levels (MCL), legislated by the U.S. Environmental Protection Agency (EPA), of  $\text{NO}_2^-$  ions is 1 ppm (21.7  $\mu\text{M}$ ) and analogous guideline values set by the World Health Organization (WHO) is 3 ppm (World Health Organization, 2008; Focazio *et al.*, 2006; Buldt *et al.*, 1999; Hill, 1996; United States Environmental Protection Agency, 1995). Therefore, the determination of  $\text{NO}_2^-$  levels is essential for monitoring drinking water quality and clinical diagnosis. On the other hand, among the variety of neutral species, hydrogen sulfide ( $\text{H}_2\text{S}$ ) and the development of  $\text{H}_2\text{S}$  sensors has gained much attraction due to its toxicity (Tanizawa *et al.*, 2011; Boehning *et al.*, 2003; Abe *et al.*, 1996). The rapid detection of  $\text{H}_2\text{S}$  is imperative because of its high reactivity and adverse effects on human health. Higher levels of  $\text{H}_2\text{S}$  can induce shock, convulsions, coma, and death. Moreover,  $\text{H}_2\text{S}$  prevents cellular respiration due to complexation with cytochromes which ultimately can lead to death (Chen *et al.*, 2007).

The most common techniques used for the detection of these toxic species were electrochemical methods (Lin *et al.*, 2011; Wang *et al.*, 2010; Lawrence *et al.*, 2004; 2000), gas chromatography (Moorcroft *et al.*, 2001; Richardson *et al.*, 2000; Radford-Knaery *et al.*, 1993; Kim *et al.*, 1989), fluorescence and colorimetric methods (Lippert *et al.*, 2011; Peng *et al.*, 2011; Qian *et al.*, 2011). Of the various optical methods reported,

the spectrophotometric technique is simple and can be used for the visual on-site analysis. The spectrophotometric techniques are more reliable and accurate since they offer a fast response. The commercially used nitrite sensor, Griess reagent, is based on this technique, which involves the diazotization of sulphanilamide by nitrous acid under acidic conditions. The coupling of *in situ* generated diazonium ion with *N*-(1-naphthyl)ethylenediamine, leads to the formation of azochromophore (European Standard, 1993, EN 26777; Fox J. B., 1979). However, a special attention is required for the preparation and storage of these reagents because of the usage of high concentrations of three different components. Besides, the way of detection makes it difficult in the fabrication of a simple strip or dipstick for the practical applications.

Herein, we designed and synthesized three novel aza-BODIPY derivatives, **3a-c** and tuned their photophysical properties by changing the substitution at peripheral phenyl rings with azido, amino and dimethylamino moieties and investigated their interactions with various anions, cations and neutral molecules. Interestingly, the azido aza-BODIPY, **3a** showed high selectivity and sensitivity towards H<sub>2</sub>S, whereas the amino derivative **3b** showed selective interactions with nitrite ions (NO<sub>2</sub><sup>-</sup>) in aqueous medium.

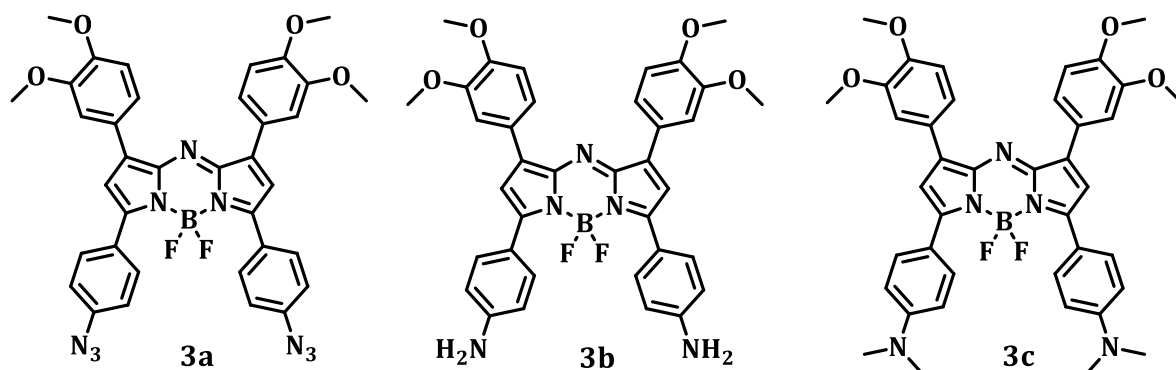
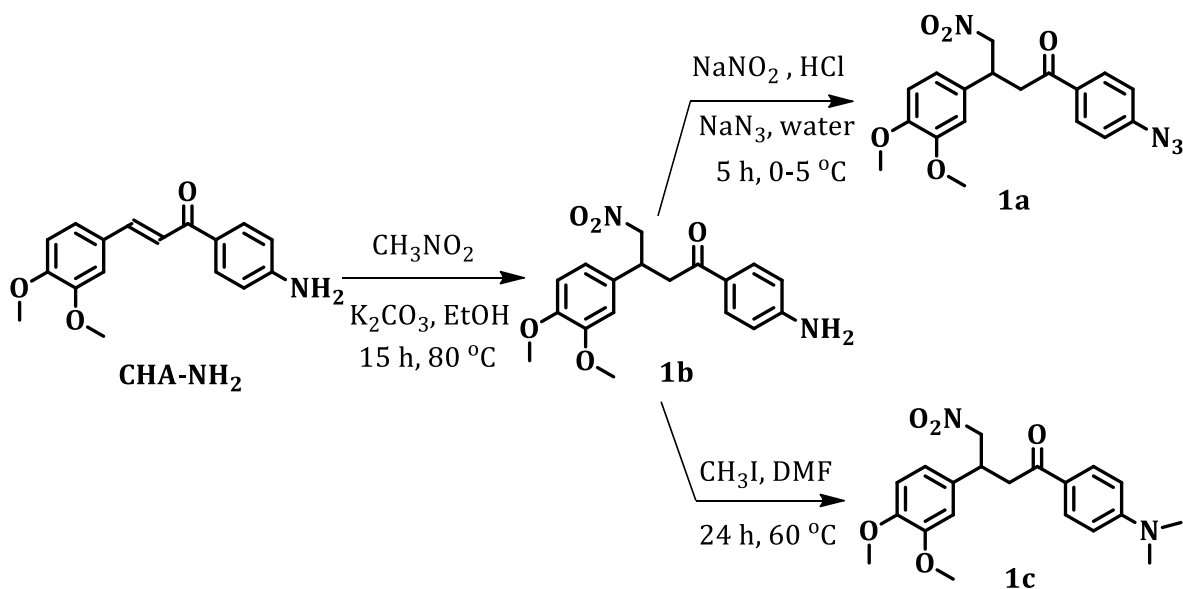


**Chart 4.1.** Structures of the aza-BODIPY derivatives **3a-c**.

## 4.3. RESULTS AND DISCUSSION

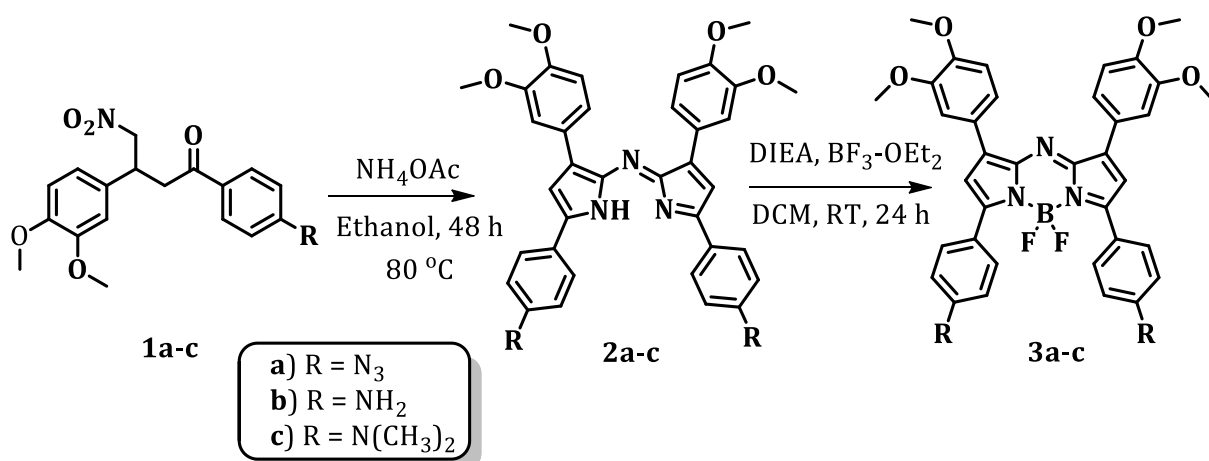
### 4.3.1. Synthesis and Photophysical Properties

The synthesis of the aza-BODIPY dyes **3a-c** was achieved in a facile three step route by modifying the reported procedures. All the three derivatives were synthesized from their corresponding nitromethane adducts **1a-c**. The parent amino adduct, **1b** was synthesized by the Michael addition reaction of nitromethane to the amino chalcone, which was prepared by the aldol condensation reaction between 4-aminoacetophenone and 3,4-dimethoxybenzaldehyde. The derivative **1b** was subsequently converted to azido and dimethylamino adducts **1a** and **1c** by the diazotization reaction with sodium azide and N-alkylation with methyl iodide, respectively (Scheme 4.1). The condensation products **2a-c** were generated by refluxing **1a-c** with ammonium acetate in ethanol for 48 h. The crude product was isolated and purified through column chromatography to



**Scheme 4.1.** Synthesis of the nitromethane adducts **1a-c**.

yield the aza-dipyrromethenes, **2a-c** in *ca.* 40-50% yields. These aza-dipyrromethenes **2a-c** were converted to the targeted aza-BODIPY dyes **3a-c** by the treatment with boron trifluoride diethyletherate and N, N-diisopropylethylamine in DCM for 24 h at room temperature (*ca.* 75-80%) (Scheme 4.2). All these derivatives were purified and were characterized by various spectroscopic and analytical techniques.



**Scheme 4.2.** Synthesis of the aza-BODIPY derivatives **3a-c**.

The synthesized aza-BODIPY derivatives, **3a-c** showed good photostability and solubility in most of the organic solvents such as CHCl<sub>3</sub>, DCM, CH<sub>3</sub>CN and THF. These dyes were characterized by their intense absorption in the NIR region. For example, the azido aza-BODIPY, **3a** showed a sharp absorption band at 700 nm with a molar extinction coefficient value of  $5.66 \times 10^4 \text{ M}^{-1}\text{cm}^{-1}$  in THF. When the azido group was replaced with more electron rich amino group, the absorption maximum was red shifted to 750 nm with an extinction coefficient value of  $4.80 \times 10^4 \text{ M}^{-1}\text{cm}^{-1}$ . Furthermore, the dimethylamino substitution at para position of the peripheral phenyl group, **3c** resulted in a 40 nm red-shift in the absorption spectrum and showed a

maximum at 790 nm with an extinction coefficient value of  $1.16 \times 10^4 \text{ M}^{-1}\text{cm}^{-1}$ . In these cases, we observed a regular bathochromic shift of *ca.* 40-50 nm in the absorption spectrum of the aza-BODIPY dyes, when substituted with azido to amino to dimethylamino groups (Figure 4.1). The absorption properties of these systems are summarized in Table 4.1.

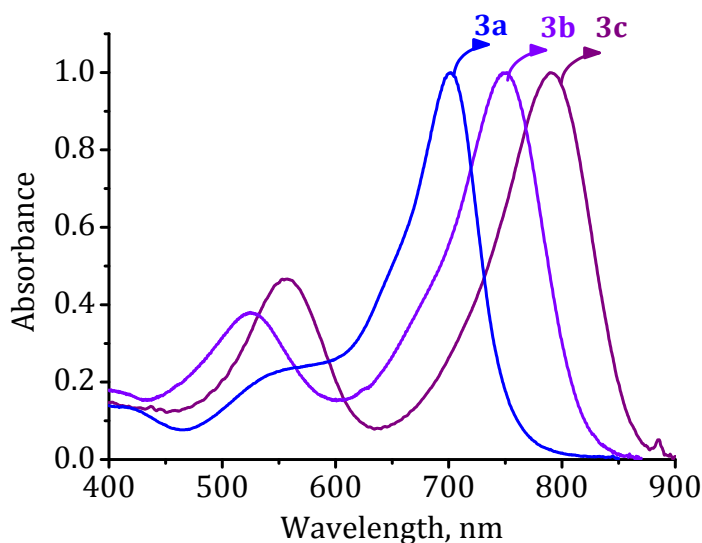


**Figure 4.1.** Normalized UV-Vis absorption spectra of the aza-BODIPY derivatives **3a** (2  $\mu\text{M}$ ), **3b** (2  $\mu\text{M}$ ) and **3c** (2  $\mu\text{M}$ ) in THF.

We observed the similar trend in the fluorescence spectra of the dyes, **3a-c** (Figure 4.2). The azido aza-BODIPY, **3a** showed an emission maximum at 750 nm with a quantum yield of  $\Phi_{\text{F}} = 0.07$ , wherein we have used indotricarbocyanine dye as the reference ( $\Phi_{\text{F}} = 0.28$ ) (Samtsov *et al.*, 2009). On the other hand, the fluorescence maximum of the amino derivative, **3b** shifted to 815 nm and showed reduction in the fluorescence quantum yields ( $\Phi_{\text{F}} = 0.02$ ) (IR-125 was used as the reference,  $\Phi_{\text{F}} = 0.13$ ) (Rurack *et al.*, 2011). Interestingly, the dimethylamino derivative, **3c** exhibited large Stokes shift with an emission maximum of 945 nm in THF.

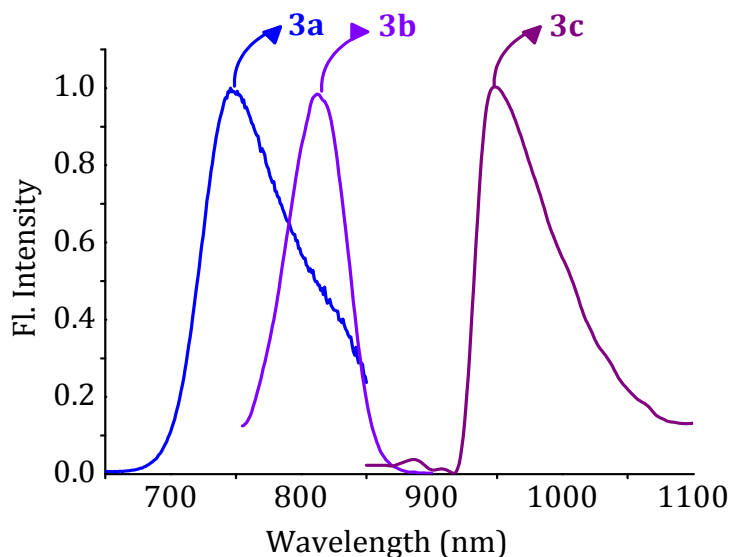


**Figure 4.2.** Normalized fluorescence spectra of the aza-BODIPY derivatives **3a** (2  $\mu\text{M}$ ), **3b** (2  $\mu\text{M}$ ), **3c** (2  $\mu\text{M}$ ) in THF.  $\lambda_{\text{ex}}$  680, 740 and 800 nm for **3a**, **3b** and **3c**, respectively.

**Table 4.1.** Summary of photophysical properties of **3a-c**.

Compound	$\lambda_{\text{max}}$ (nm) ( $\epsilon, 10^4$ $\text{M}^{-1}\text{cm}^{-1}$ ) <sup>[a]</sup>	$\lambda_{\text{em}}$ (nm)	$E_{\text{HOMO}}^{\text{[b]}}$ (eV)		$E_{\text{LUMO}}^{\text{[b]}}$ (eV)		$E_{\text{gap}}^{\text{[b]}}$ (eV)	
			Theoretical	Experimental	Theoretical	Experimental	Theoretical	Experimental
<b>3a</b>	700 (5.66 $\pm$ 0.06)	750	-5.52	-5.13	-3.49	-3.54	2.03	1.59
<b>3b</b>	750 (4.80 $\pm$ 0.08)	815	-4.97	-4.96	-3.01	-3.46	1.96	1.49
<b>3c</b>	790 (1.16 $\pm$ 0.18)	945	-4.75	-4.85	-2.88	-3.45	1.87	1.40

<sup>[a]</sup>Average of more than three independent experiments, <sup>[b]</sup>calculated by using B3LYP/6-31g\* method (theoretical) and by cyclic voltammetry (experimental).

#### 4.3.2. Electrochemical and Theoretical Calculations

The cyclic voltammetry was used to investigate the electronic effects of the substituents at peripheral phenyl rings of the aza-BODIPY dyes **3a-c**. These



electrochemical investigations provided information with regard to the HOMO and LUMO levels of the molecules. The first oxidation potential ( $E_{\text{ox}}$ ) of these derivatives were measured using cyclic voltammetry and the measurements were carried out with  $10^{-3}$  M of the dyes in  $\text{CH}_3\text{CN}$  using  $\text{Fc}/\text{Fc}^+$  as the external standard. HOMO energy levels of the dyes in eV can be derived from Equation 4.1 (Djurovich *et al.* 2009). The oxidation potential values were obtained for  $\text{Fc}/\text{Fc}^+$  vs  $\text{Ag}/\text{AgCl}$  and are found to be of 0.44 V.

$$E_{\text{HOMO}} = -[E_{\text{ox}}(\text{BODIPY vs Ag/AgCl}) - E_{\text{ox}}(\text{Fc/Fc}^+ \text{ vs Ag/AgCl})] - 4.8 \dots\dots (\text{Eq. 4.1})$$

$E_{\text{ox}}$  determined from the cyclic and square wave voltammograms of the aza-BODIPY dye, **3b** (Figure 4.3) was found to be 0.598 V vs  $\text{Ag}/\text{AgCl}$  and the corresponding HOMO energy level was found to be at  $-4.96$  eV. The LUMO levels of these dyes were determined from the difference of HOMO energy value and the optical transition energy ( $E_{0-0}$ ).  $E_{0-0}$  was determined by employing the optical transition wavelength ( $\lambda_{0-0}$ ) obtained from the offset values of the normalized absorption spectra of these dyes in

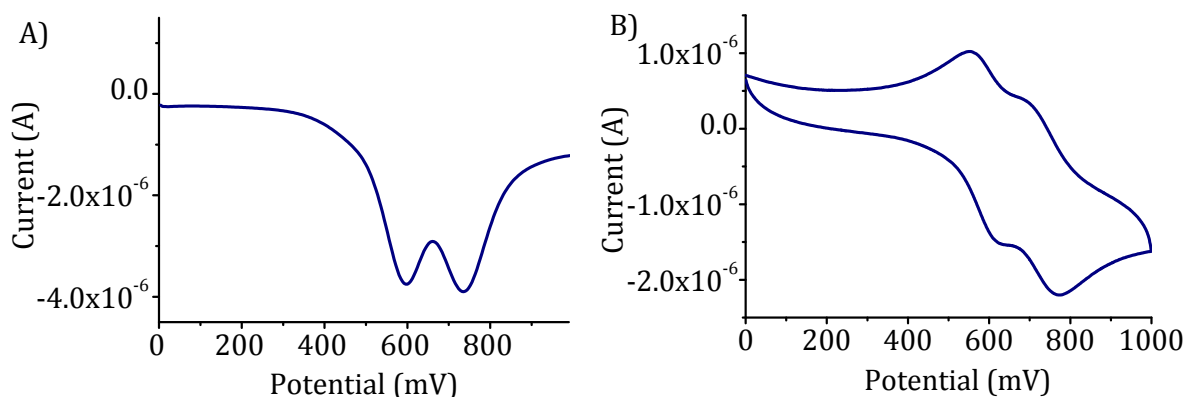


**Figure 4.3.** A) Square wave and B) cyclic voltammograms of **3b** (1 mM) in acetonitrile using tetrabutylammonium hexafluorophosphate as supporting electrolyte at a scanning rate of 100 mV/sec.

acetonitrile. The LUMO energy of the derivative, **3b** was found to be at -3.46 eV. Similarly, the azido and dimethylamino aza-BODIPY dyes **3a** and **3c** were also subjected to electrochemical characterizations and the energy level values obtained are summarized in Table 4.1.

The theoretical calculations of **3a-c** were carried out using density functional theory (DFT) method used for similar systems by the application of B3LYP/6-31g\* level of theory. The HOMO-LUMO gaps (band gap) for these dyes were determined theoretically and are found to be 2.03, 1.96 and 1.87 eV for **3a**, **3b** and **3c**, respectively. These values are in agreement with those obtained through the experimental measurements (Figure 4.4). The band gap values of the aza-BODIPY dyes were found to decrease from azido (**3a**) to amino (**3b**) to dimethylamino (**3c**) derivatives (Table 4.1).

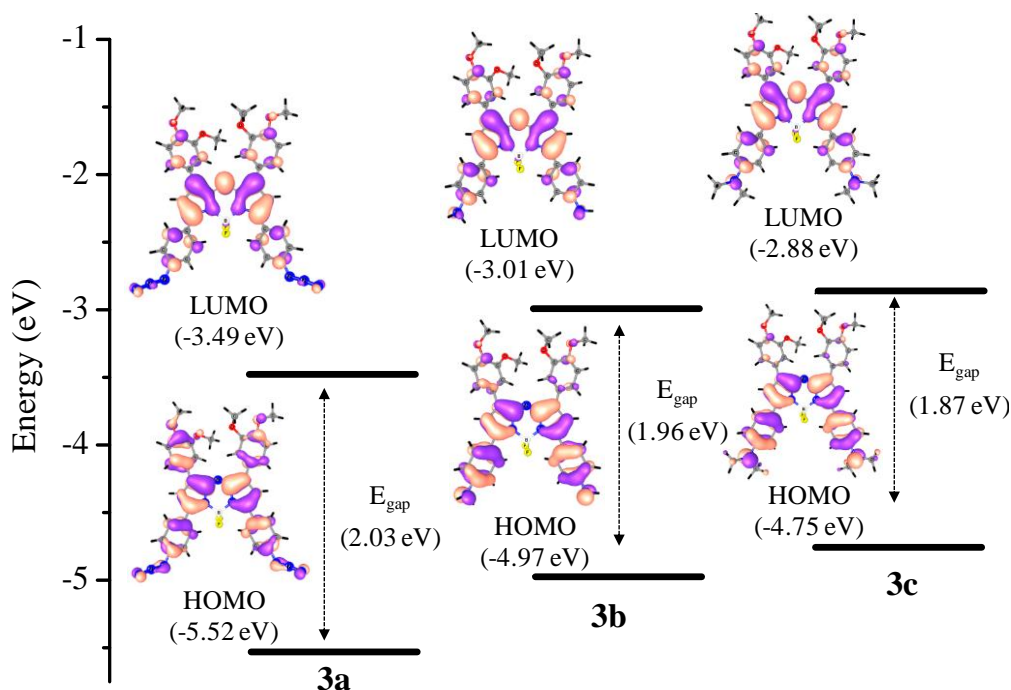


**Figure 4.4.** Energy level diagram containing the HOMO and LUMO levels, A) **3a**, B) **3b**, and C) **3c**, calculated by using B3LYP/6-31g\* method.

### 4.3.3. Aza-BODIPY (3b) as a Probe for Anions

To investigate the potential of aza-BODIPY derivative **3b** as the molecular probe, we have studied its interactions with various anions at different conditions. Uniquely, the successive addition of the  $\text{NO}_2^-$  ions to the protonated form of the probe **3b** resulted in a hypochromicity in absorbance at 570 nm along with a gradual red shift in the maximum. With the addition of 2 ppm (43  $\mu\text{M}$ ) of the nitrite ions, we observed *ca.* 70% hypochromicity at 570 nm with a concomitant bathochromic shift of 60 nm and a change in color from blue to green (Figure 4.5A). Analysis of the concentration dependent absorbance revealed a linear response of the aza-BODIPY, **3b** for nitrite ions

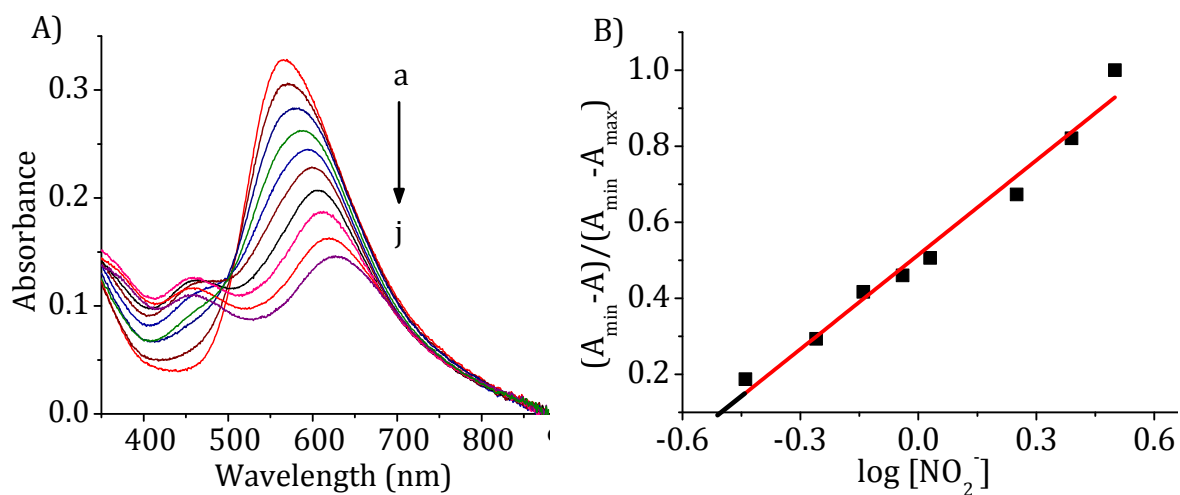


**Figure 4.5.** A) Changes in absorption spectra of the aza-BODIPY probe **3b** (20  $\mu\text{M}$ ) in 1N HCl by the successive addition of nitrite ( $\text{NO}_2^-$ ) ions in water a) 0 ppm, j) 2 ppm. B) The linear plot for the estimation of limit of detection.

in the range of 0–2 ppm (Figure 4.5B). The limit of detection (LOD) of the probe **3b** towards the nitrite ions was found to be 20 ppb (0.5  $\mu\text{M}$ ), which is far more sensitive than the maximum contaminant levels of nitrite ions (MCL = 1 ppm, 21.7  $\mu\text{M}$ ) as per the

US-EPA. The deep green colored species generated in the assay was visible, demonstrating the utility of aza-BODIPY, **3b** for the visual detection of nitrite ions.

#### 4.3.3.1. Selectivity of Detection of Nitrite Ions

To investigate the selectivity of the aza-BODIPY probe, **3b** towards  $\text{NO}_2^-$  ions, similar titration experiments were carried out with other biologically relevant anions such as  $\text{SO}_4^{2-}$ ,  $\text{Cl}^-$ ,  $\text{HSO}_3^-$ ,  $\text{CO}_3^{2-}$ ,  $\text{CH}_3\text{COO}^-$ ,  $\text{NO}_3^-$ ,  $\text{S}_2\text{O}_3^{2-}$ , and  $\text{N}_3^-$ . We observed negligible changes in the absorption spectra of the probe **3b** even at 100-fold higher concentrations of these ions when compared to the  $\text{NO}_2^-$  ions (Figure 4.6). It is evident

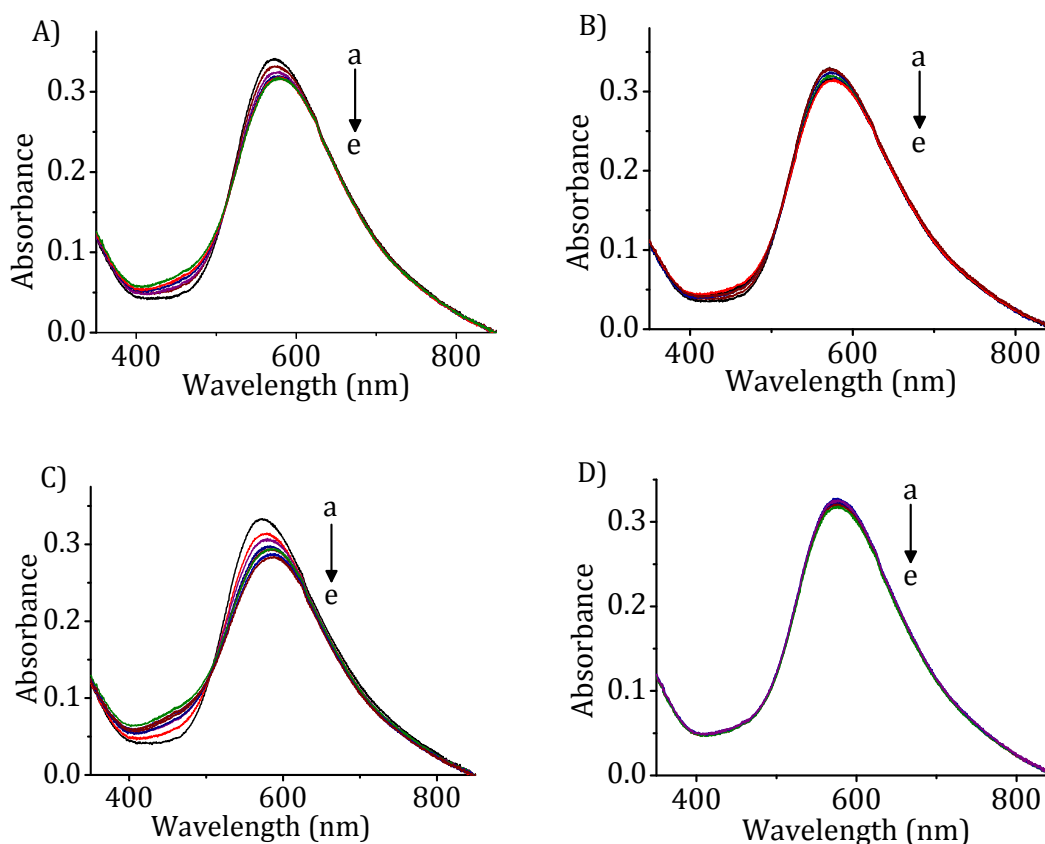


**Figure 4.6.** Absorption spectral changes showing the negligible interaction of probe **3b** (20  $\mu\text{M}$ ) in 1N HCl with the addition of various competitive anions a) 0; e) 10 mM; A) azide ( $\text{N}_3^-$ ), B) carbonate ( $\text{CO}_3^{2-}$ ), C) nitrate ( $\text{NO}_3^-$ ) and D) sulphate ( $\text{SO}_4^{2-}$ ) ions.

from these studies that only  $\text{NO}_2^-$  ions induced the bathochromic shift and decreased absorbance of the probe **3b** (Figure 4.7). Also, the probe **3b** can selectively detect the presence of nitrite ions from a mixture of other competitive anions.

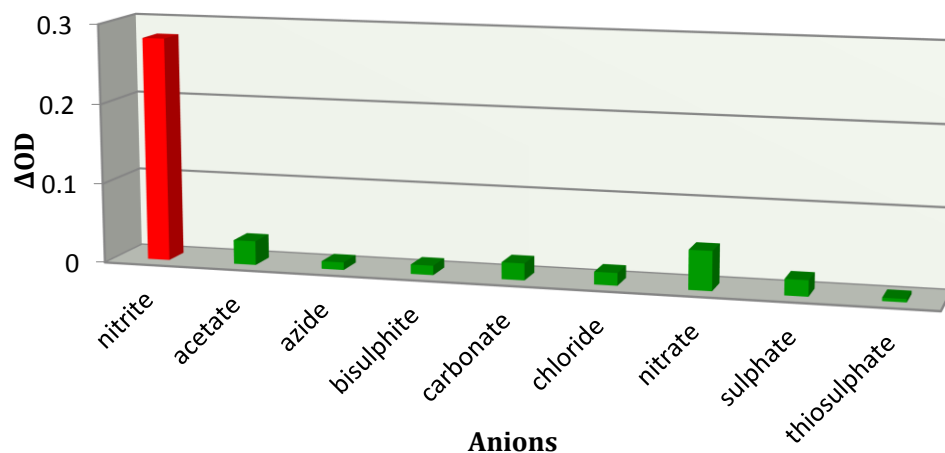


**Figure 4.7.** Selectivity plot showing the changes in absorbance of the aza-BODIPY probe **3b** (20  $\mu\text{M}$ ) in 1N HCl at 570 nm by the addition of various competitive anions such as  $\text{NO}_2^-$ ,  $\text{CH}_3\text{COO}^-$ ,  $\text{N}_3^-$ ,  $\text{HSO}_3^-$ ,  $\text{CO}_3^{2-}$ ,  $\text{Cl}^-$ ,  $\text{NO}_3^-$ ,  $\text{SO}_4^{2-}$ ,  $\text{S}_2\text{O}_3^{2-}$  under identical conditions.

#### 4.3.3.2. Estimation of Nitrite Ions in Natural Water Resources

The  $\text{NO}_2^-$  ion contamination in water causes several health problems and hence it is important to estimate these ions in natural water resources. We explored the ability of the probe **3b** to quantify the amount of  $\text{NO}_2^-$  ions present in complex environmental water resources such as lake, sea and river and also in the presence of the mixture of other anions. We have collected the samples from Arabian Sea, Lake Vellayani and River Karamana, located in Trivandrum, Kerala. To evaluate the potential of probe **3b** in the determination of  $\text{NO}_2^-$  concentration, the probe was treated with  $\text{NO}_2^-$  ions at various concentrations. The probe concentration was kept constant at 30  $\mu\text{M}$ , while the concentration of the  $\text{NO}_2^-$  ions was varied from 0 to 2 ppm. The amount of  $\text{NO}_2^-$  ions can

be estimated from the linear plot obtained between the changes in absorbance of the probe **3b** at 570 nm and the  $\text{NO}_2^-$  ion concentration.

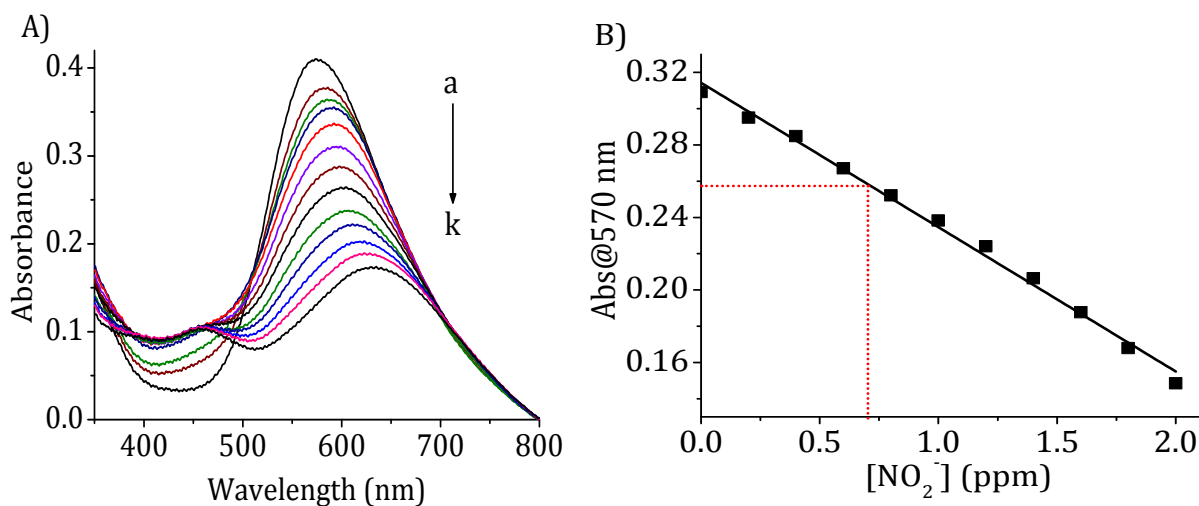


**Figure 4.8.** A) Changes in the absorption spectra of probe **3b** (30  $\mu\text{M}$ ) by the successive addition of nitrite ions, a) 0 k) 2 ppm. B) Linear plot between the absorbance of probe **3b** at 570 nm vs  $\text{NO}_2^-$  concentration.

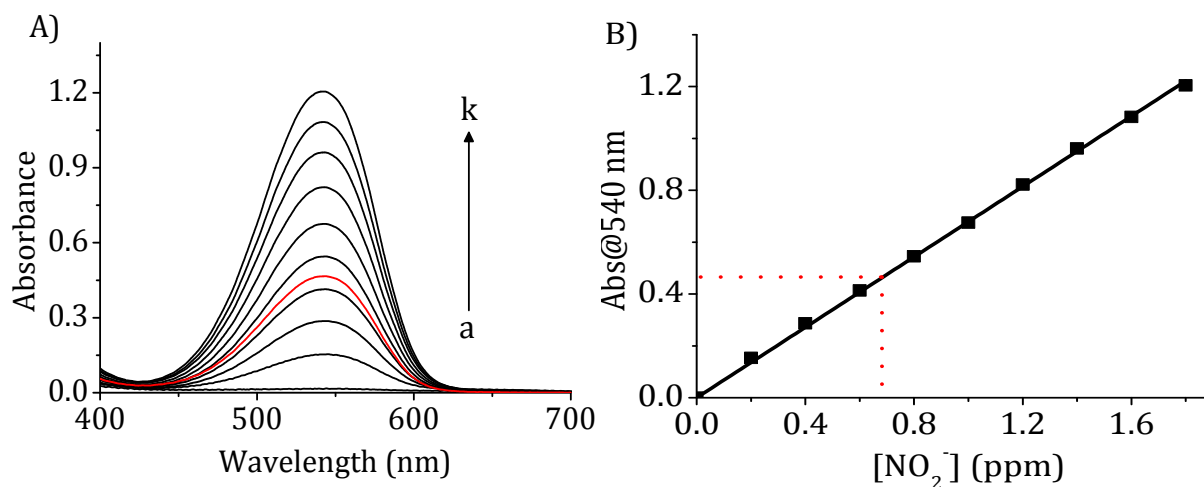


**Figure 4.9.** A) Changes in the absorption spectra of Griess reagent by the addition of nitrite ions, a) 0 k) 2 ppm. B) Linear plot between the absorbance at 540 nm vs nitrite concentration.

We observed that the aza-BODIPY probe **3b** gave accurate results in the quantification of  $\text{NO}_2^-$  ions in both distilled water as well as natural water sources like sea, lake and river (Table 4.2, Figure 4.8) even in the presence of other competitive anions. The control experiments were carried out with the commercial nitrite sensor, Griess reagent under identical conditions (Figure 4.9). The Griess reagent involves the diazotization reaction and coupling of the *in situ* generated diazonium ion with *N*-(1-naphthyl)ethylenediamine, thereby generating azochromophore, having absorption at 540 nm. Our results demonstrated that the aza-BODIPY probe, **3b** could accurately estimate the presence of the nitrite ions in natural water samples both qualitatively and quantitatively.

**Table 4.2.** Estimation of  $\text{NO}_2^-$  ions in the environmental samples.\*

Sample source	$[\text{NO}_2^-]^a$ (ppb)	$[\text{NO}_2^-]^b$ (ppb)	$[\text{NO}_2^-]^c$ (ppb)
Distilled water	262	$264 \pm 2$	$263 \pm 3$
Sea water	262	$262 \pm 2$	$258 \pm 2$
Lake water	262	$265 \pm 4$	$265 \pm 3$
River water	262	$266 \pm 3$	$265 \pm 4$
Mixture of anions <sup>d</sup>	262	$266 \pm 4$	$267 \pm 3$

The values given are the average of more than three independent experiments. Concentration of the  $\text{NO}_2^-$  <sup>a</sup>spiked, <sup>b</sup>estimated by probe **3b**, <sup>c</sup>estimated by Griess reagent, \*Arabian Sea, Lake Vellayani and River Karamana are located in Trivandrum, India. <sup>d</sup>Mixture of anions contained  $\text{SO}_4^{2-}$ ,  $\text{Cl}^-$ ,  $\text{HSO}_3^-$ ,  $\text{CO}_3^{2-}$ ,  $\text{CH}_3\text{COO}^-$ ,  $\text{NO}_3^-$ ,  $\text{S}_2\text{O}_3^{2-}$ , and  $\text{N}_3^-$  of 10 ppm each.

#### 4.3.3.3. Mechanism and Kinetics of Detection of Nitrite Ions

The addition of dilute acid (1N HCl) to the probe **3b** afforded the protonated species, which was characterized by a blue-shift in the absorption spectra from 750 nm to 570 nm. The pH of the medium was kept constant (pH <1) throughout the experiment. Interestingly, the protonated form of the probe **3b** showed a broad absorption band, shifted hypsochromically to 570 nm with an intense blue color (Figure 4.10A). The blue color of the protonated species turned to green in the presence of nitrite ions (Figure 4.10B). The possible mechanism for these changes can be attributed to the diazotization reaction between the protonated form of the probe **3b** and the nitrite ions present in the water. The diazonium salt thus formed *in situ* undergoes hydrolysis in the aqueous medium to give green hydroxyl substituted product, **3b-OH** (Scheme 4.3), which was isolated and characterized on the basis of spectral and analytical evidence. The IR spectrum of the hydroxy derivative **3b-OH** showed a broad band at 3298  $\text{cm}^{-1}$  and the FAB-MS showed a characteristic peak at 650.87, which confirmed the formation of the

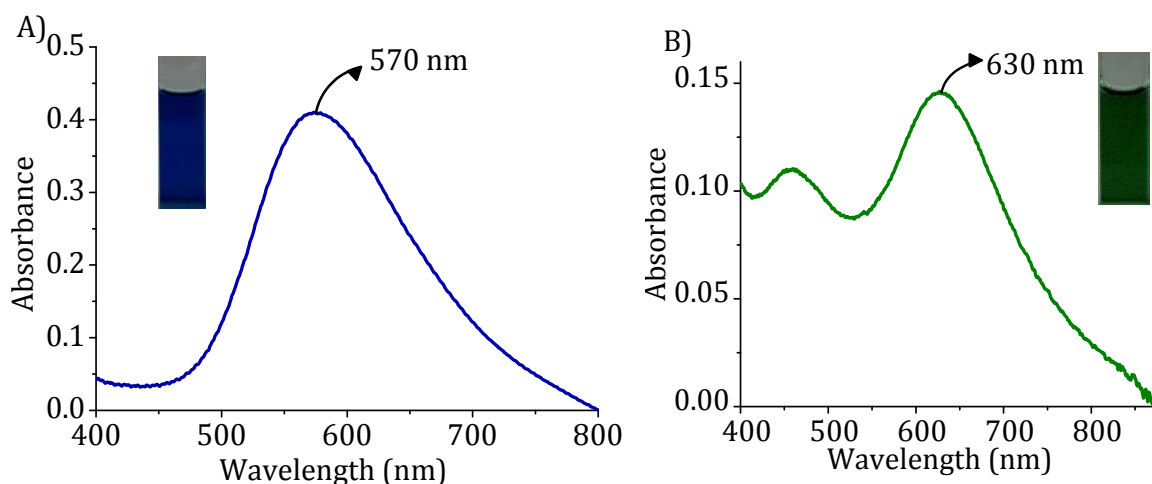
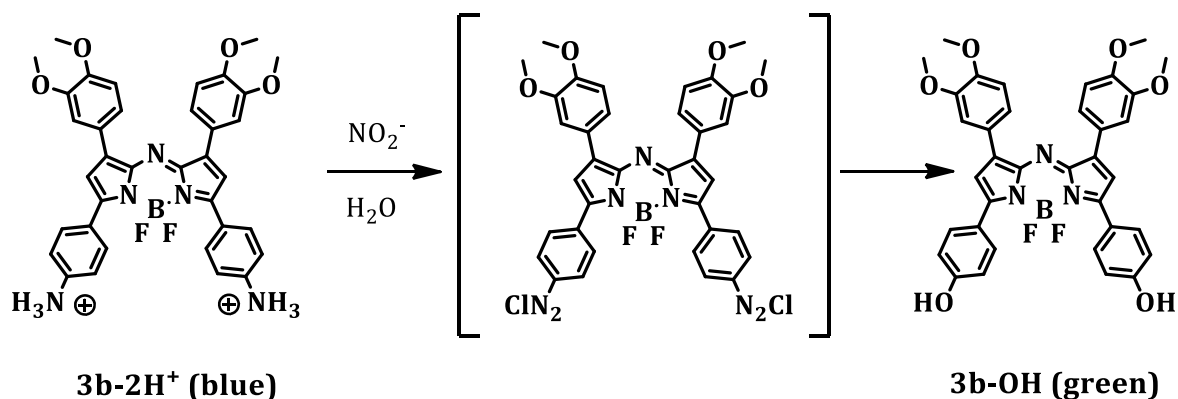


**Figure 4.10.** A) Absorption spectra of the protonated form of the probe **3b** (30  $\mu\text{M}$ ) (pH = 0.2) and B) the hydroxy derivative **3b-OH**.



hydroxyl substituted product **3b-OH**. The concentration dependent absorption spectra of the protonated form of **3b** showed a linear dependence even at higher concentrations, which ruled out the formation of the aggregates under these conditions (Figure 4.11).



**Scheme 4.3.** Possible mechanism for the nitrite sensing using aza-BODIPY probe **3b**.

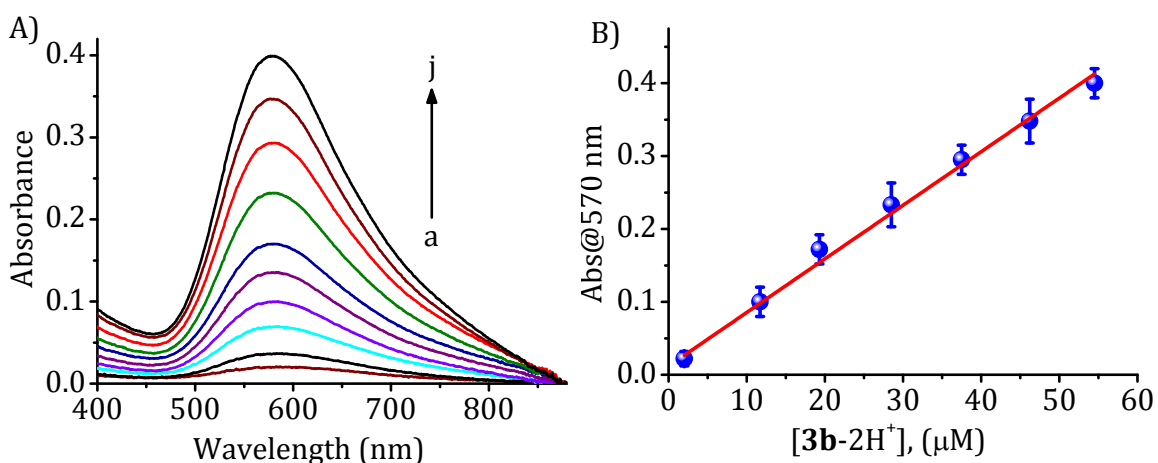


**Figure 4.11.** A) Concentration dependent absorption spectra of the probe **3b** in 1N HCl a) 2 and j) 60  $\mu\text{M}$ . B) Linear plot between the absorbance of the protonated form of the probe **3b** at 570 nm vs concentration. Data points represent the mean of more than three independent experiments ( $\pm\text{SD}$ ).

As the detection strategy requires a fast response to the practical applications, it was of our interest to investigate the kinetics of the reaction between the aza-BODIPY

probe, **3b** and nitrite ions. We have monitored the changes in absorbance of the probe at 570 nm in presence of about ten equivalents of  $\text{NO}_2^-$  ions. The time-dependent absorption changes (Figure 4.12 A) showed that the reaction was completed within a rapid period of 5 s. The rate constant ( $k'$ ) for the reaction was calculated by applying the pseudo-first order approximation from the slope of the straight line between time and the relative changes in absorbance. The value is found to be  $0.142 \pm 0.013 \text{ s}^{-1}$  (Figure 4.12 B).

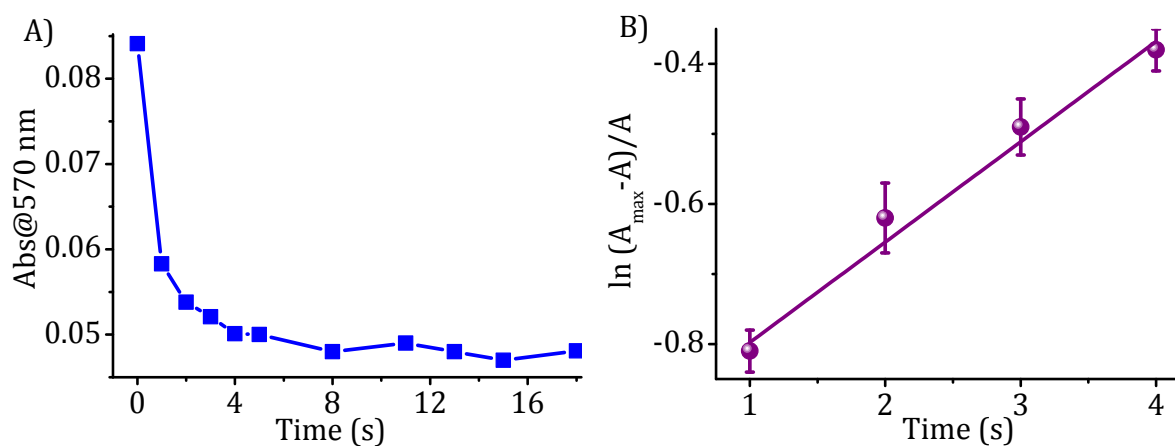


**Figure 4.12.** A) The temporal profile of absorbance at  $\lambda_{\text{abs}} = 570 \text{ nm}$  observed from the reaction between protonated form of the probe **3b** ( $20 \mu\text{M}$ ) and nitrite ions. B) Pseudo first-order kinetic plot of reaction of **3b** ( $5 \mu\text{M}$ ) with  $\text{NO}_2^-$  ions ( $50 \mu\text{M}$ ) in acetonitrile.

#### 4.3.3.4. Estimation of Nitrate Ions by the Reduction Method

In addition to the nitrite ions ( $\text{NO}_2^-$ ), the presence of the nitrate ( $\text{NO}_3^-$ ) ions also can be estimated using the aza-BODIPY dye, **3b** by the application of a simple reduction step using hydrazine sulphate as the reducing agent. To facilitate this reduction, the nitrate ions in water were mixed with hydrazine sulphate and its cofactors (See Experimental section for the details of the reduction) and then incubated at room

temperature, to generate nitrite ions *in situ*. The reduced nitrite ions in the samples behaved the same as that of the direct titrations (Figure 4.13). We observed a decrease in absorbance of **3b** at 570 nm with a bathochromic shift as in the case of direct nitrite detection. The complete reduction was ensured by the treatment of the reducing agent with an equimolar nitrite-nitrate mixture and the concentration of the nitrite ions estimated was found to be almost doubled after the reduction as compared to the original concentration, which evidenced the complete reduction (Figure 4.14). The accurate estimation of the nitrite and nitrate ions would be useful for the estimation of the highly reactive nitrogen species such as nitric oxide (NO) in the aqueous as well as the biological samples since the nitric oxide is known to undergo rapid oxidation to nitrite and nitrate ions.

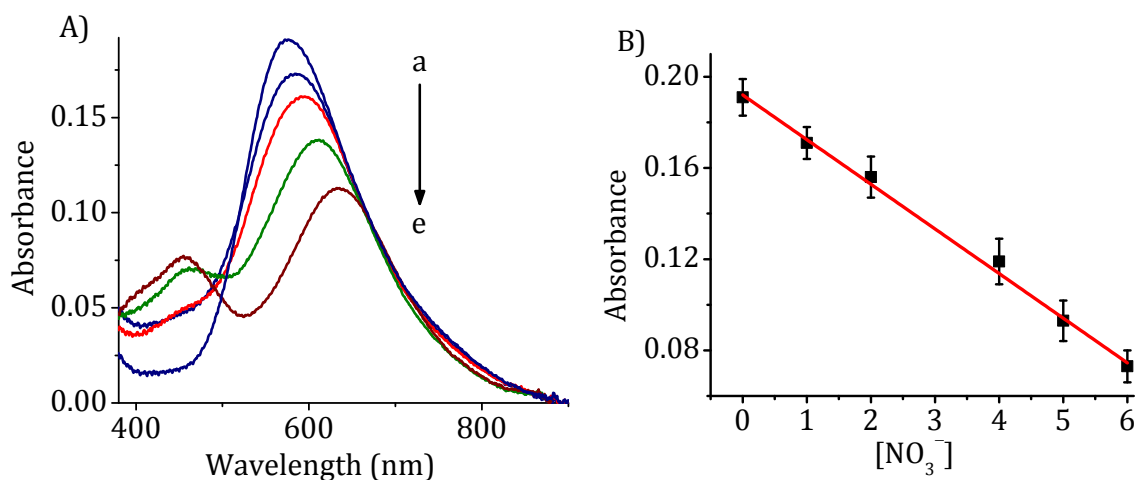


**Figure 4.13.** A) Changes in the absorption spectra of probe **3b** (20  $\mu\text{M}$ , protonated) by the successive addition of  $\text{NO}_3^-$  ions after treating with hydrazine sulphate a) 0 e) 2 ppm. B) Linear plot between the absorbance of probe **3b** (20  $\mu\text{M}$ ) vs nitrate ion ( $\text{NO}_3^-$ ) concentration. Data points represent the mean of more than three independent experiments ( $\pm\text{SD}$ ).

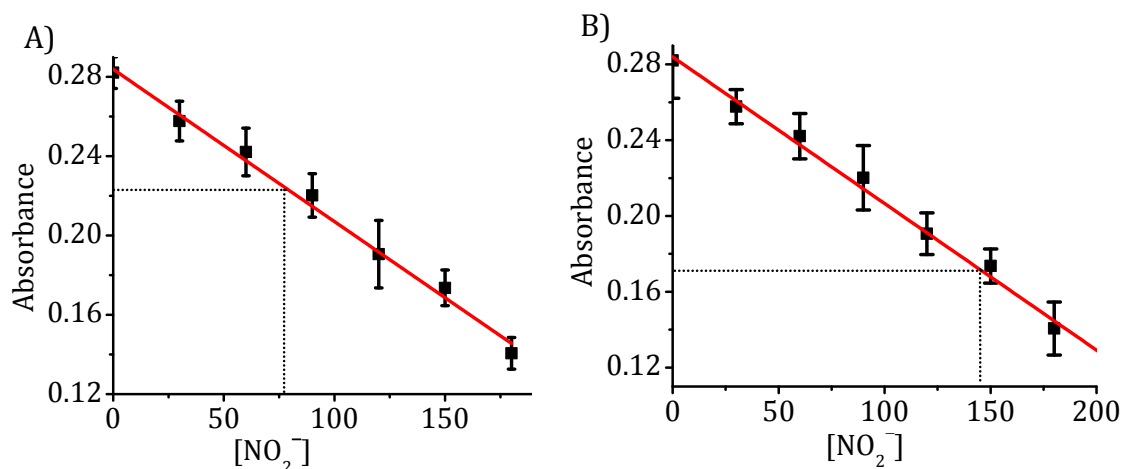


**Figure 4.14.** Quantitative estimation of nitrate ions in presence of nitrite ions by the probe **3b** (20  $\mu\text{M}$ , protonated). A) Determination of the amount of nitrite ions present initially in the solution. B) Determination of the amount of nitrite ions after the reduction of nitrate ions using hydrazine sulphate. Data points represent the mean of more than three independent experiments ( $\pm\text{SD}$ ).

#### 4.3.3.5. Direct Detection of Freshly Generated Nitric Oxide

The diazotization reaction is known to be 100 times more sensitive to nitric oxide (NO) and labile nitroso compounds than for  $\text{NO}_2^-$  ions (Keefer *et al.*, 1996; Hrabie *et al.*, 1993; Maragos *et al.*, 1991), and hence we have further investigated the efficiency of the probe **3b**, for the estimation of freshly generated NO in water. We used diethylamine NONOate sodium as a precursor to release NO in the aqueous medium. At neutral pH, each one of these precursor molecules underwent hydrolysis to generate two molecules of NO, following a first order reaction kinetics with a half-life time of *ca.* 2 min. We observed a regular decrease in the absorption spectra at 570 nm along with a bathochromic shift of *ca.* 60 nm with the successive additions of nitric oxide (Figure 4.15A). The concentration dependent absorbance followed a linear response to **3b** for

nitric oxide in the range of 0–200 nM (Figure 4.15B), which enabled its accurate quantification in the aqueous medium. The lowest level of detection (LOD) of NO by the dye **3b** was found to be 5 nM, which is *ca.* 100-fold sensitive than that of nitrite ions (LOD[NO<sub>2</sub><sup>-</sup>] = 0.5 μM).

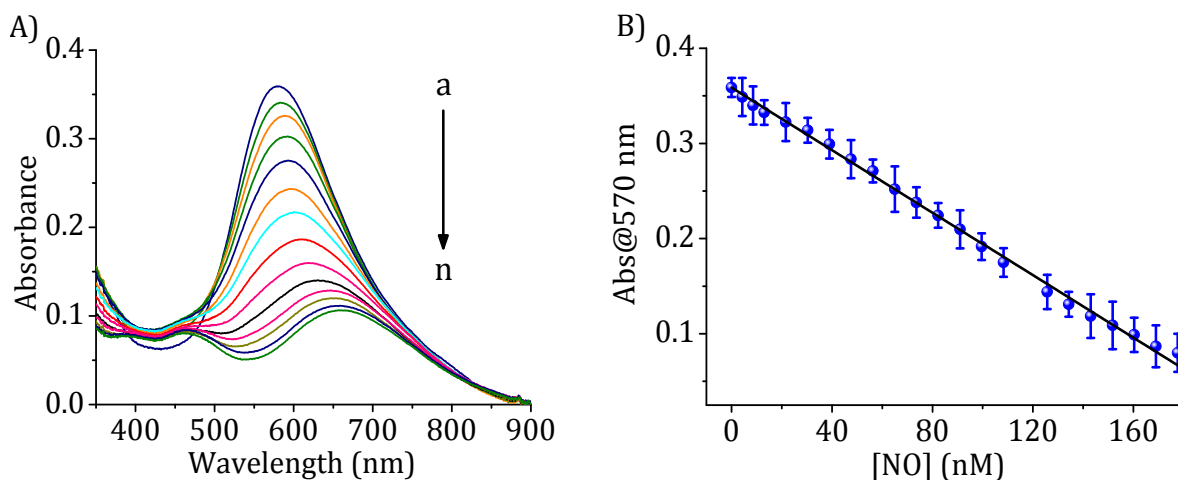


**Figure 4.15.** A) Changes in absorption spectra of the probe **3b** (20 μM, protonated) by the successive addition of NO in water; a) 0 n) 200 nM. B) Linear response of the absorption changes of **3b** vs the concentration of NO. Data points represent the mean of more than three independent experiments ( $\pm$ SD).

#### 4.3.3.6. Development of a “Dipstick” for Detection of Nitrite Ions

To develop a simple and convenient device that can be used for the selective and sensitive on the spot visual detection of the nitrite ions, we have developed a dip-stick by coating the alumina slurry of the probe **3b**, on a glass stick support (Figure 4.16A). The prepared stick was exposed to hydrogen chloride vapors (10% v/v) to give the protonated form (Figure 4.16B), which was blue in color and was used for the detection. The performance of the stick was examined by dipping it into a solution of various competitive anions and the nitrite ions in water. We observed a visual color change

from blue to intense green, wherever the dip-stick came into contact with the solution of the nitrite ions (Figure 4.16C). In solution the detection limit of the probe **3b** towards the nitrite ions was in the range of 20 ppb ( $5 \times 10^{-7}$  M), whereas with the dip-stick strategy, we observed the visible detection limit in the range of 1 ppm ( $2 \times 10^{-5}$  M). Thus, our results demonstrate that the aza-BODIPY dye **3b**, having two amino groups at the peripheral positions, is a highly selective, sensitive and environmentally viable molecular probe that can be used for the on-site detection and quantification of the nitrite ( $\text{NO}_2^-$ ), nitrate ( $\text{NO}_3^-$ ) and nitric oxide (NO) in the laboratory practical experiments as well as under the environmental conditions.

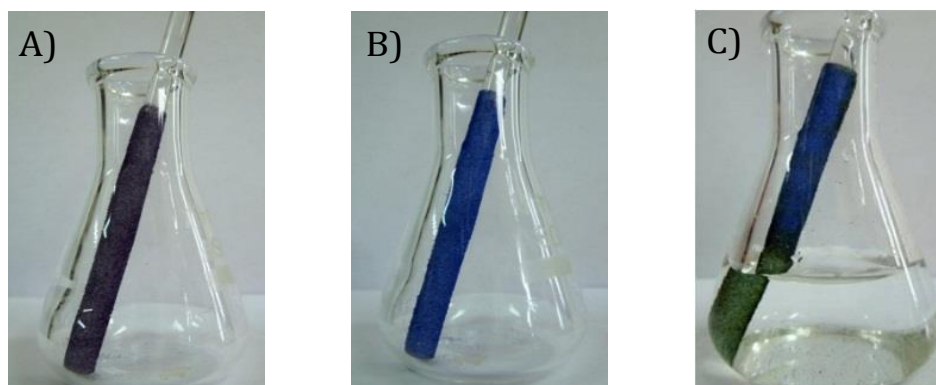


**Figure 4.16.** Photographs of the dipstick device showing its performance in aqueous solution of nitrite ions (1 ppm). A) The purple colored aza-BODIPY, **3b** coated over a glass support. B) The dipstick after exposing to the hydrogen chloride vapors turned to intense blue in color. C) The color change of the dipstick from intense blue to bright green by dipping into a solution containing nitrite ions (1 ppm).

#### 4.3.4. Aza-BODIPY (**3a**) as a Probe for Neutral Molecules

The aza-BODIPY **3a** having intense absorption and fluorescence maxima at 700 and 750 nm is expected to have interactions with hydrogen sulfide ( $\text{H}_2\text{S}$ ) due to the

presence of two chemically responsive azido groups at the peripheral phenyl rings. To investigate the potential of the aza-BODIPY derivative, **3a** as the selective and sensitive probe for H<sub>2</sub>S, we have studied its interactions with various anions and neutral molecules. The chromogenic behavior of **3a** was tested in THF upon addition of different concentrations of freshly generated H<sub>2</sub>S in water (Na<sub>2</sub>S in water was used as the source). Interestingly, the gradual addition of H<sub>2</sub>S (end concentration = 40 μM) to the probe **3a** (1.0 × 10<sup>-5</sup> M) induced *ca.* 50% hypochromicity at 700 nm, with a concomitant bathochromic shift of *ca.* 50 nm, through an isosbestic point at 726 nm. These observations correspond to the formation of purple colored and reduced amino aza-BODIPY derivative **3b** (Figure 4.17). The product was characterized by comparing with the authentic sample as described in the following sections.

Introduction of H<sub>2</sub>S elicited a significant fluorescence quenching of the probe **3a** (*ca.* 97-fold) at 750 nm. We observed that, the emission of the probe **3a** exhibited a red-

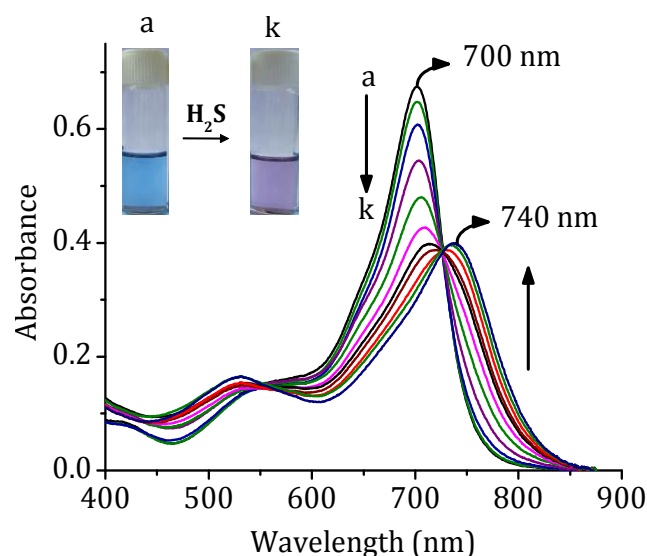


**Figure 4.17.** Changes in the absorption spectrum of **3a** (12 μM) in THF by the successive additions of hydrogen sulfide (Na<sub>2</sub>S in water). [H<sub>2</sub>S] a) 0, k) 40 μM.

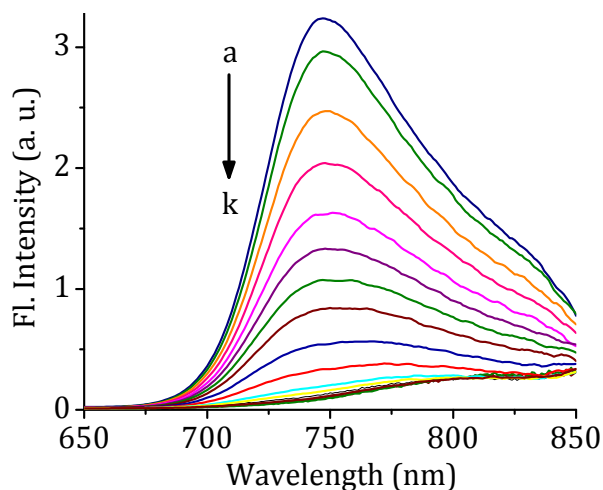


**Figure 4.18.** Changes in the fluorescence spectrum of **3a** (12  $\mu\text{M}$ ) by the successive additions of hydrogen sulfide ( $\text{Na}_2\text{S}$  in water).  $[\text{H}_2\text{S}]$  a) 0, k) 40  $\mu\text{M}$ .  $\lambda_{\text{ex}} = 640 \text{ nm}$ .

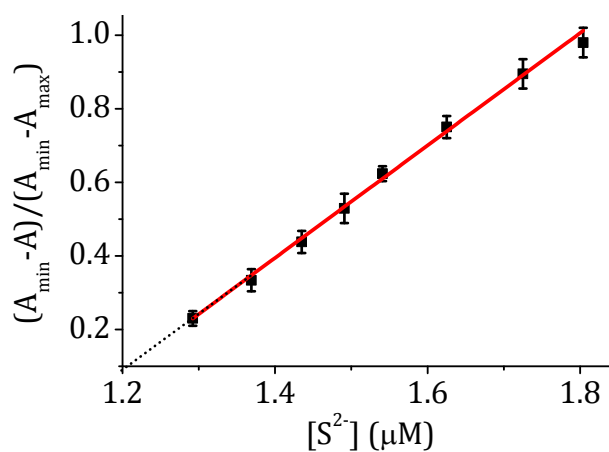


**Figure 4.19.** Linear plot for the estimation of limit of detection (LOD) of **3a** (12  $\mu\text{M}$ ) from the absorption changes with hydrogen sulfide ( $\text{H}_2\text{S}$ ). Data points represent the mean of more than three independent experiments ( $\pm\text{SD}$ ).

shift with the addition of  $\text{H}_2\text{S}$  and finally the saturated emission spectrum showed a maximum at 815 nm. The extent of fluorescence quenching was low at the initial additions (5-10  $\mu\text{M}$ ), while significant effect was observed at higher concentrations (20  $\mu\text{M}$ ) of  $\text{H}_2\text{S}$  and got saturated after the addition of 40  $\mu\text{M}$  of  $\text{H}_2\text{S}$  (Figure 4.18). Analysis of the concentration dependent absorbance at 700 nm revealed a linear response of **3a**



with H<sub>2</sub>S (Figure 4.19) and hence it can be used for the accurate quantification of H<sub>2</sub>S in the aqueous medium. The lowest level of detection (LOD) of **3a** towards H<sub>2</sub>S was found to be 0.5 ppm which is *ca.* 20 times sensitive than the allowed exposure levels (10 ppm) of H<sub>2</sub>S by EPA.

#### 4.3.4.1. Selectivity of the Detection of H<sub>2</sub>S

The selectivity of the aza-BODIPY probe **3a** towards different anions was investigated through UV-Vis and fluorescence spectroscopy (Figure 4.20). In contrast to H<sub>2</sub>S (Na<sub>2</sub>S in water), the addition of sodium salt of competitive anions such as SO<sub>4</sub><sup>2-</sup>, HSO<sub>3</sub><sup>-</sup>, S<sub>2</sub>O<sub>3</sub><sup>2-</sup>, NO<sub>3</sub><sup>-</sup>, NO<sub>2</sub><sup>-</sup>, N<sub>3</sub><sup>-</sup>, CO<sub>3</sub><sup>2-</sup>, HCO<sub>3</sub><sup>-</sup> and HPO<sub>4</sub><sup>2-</sup> in water caused virtually no changes

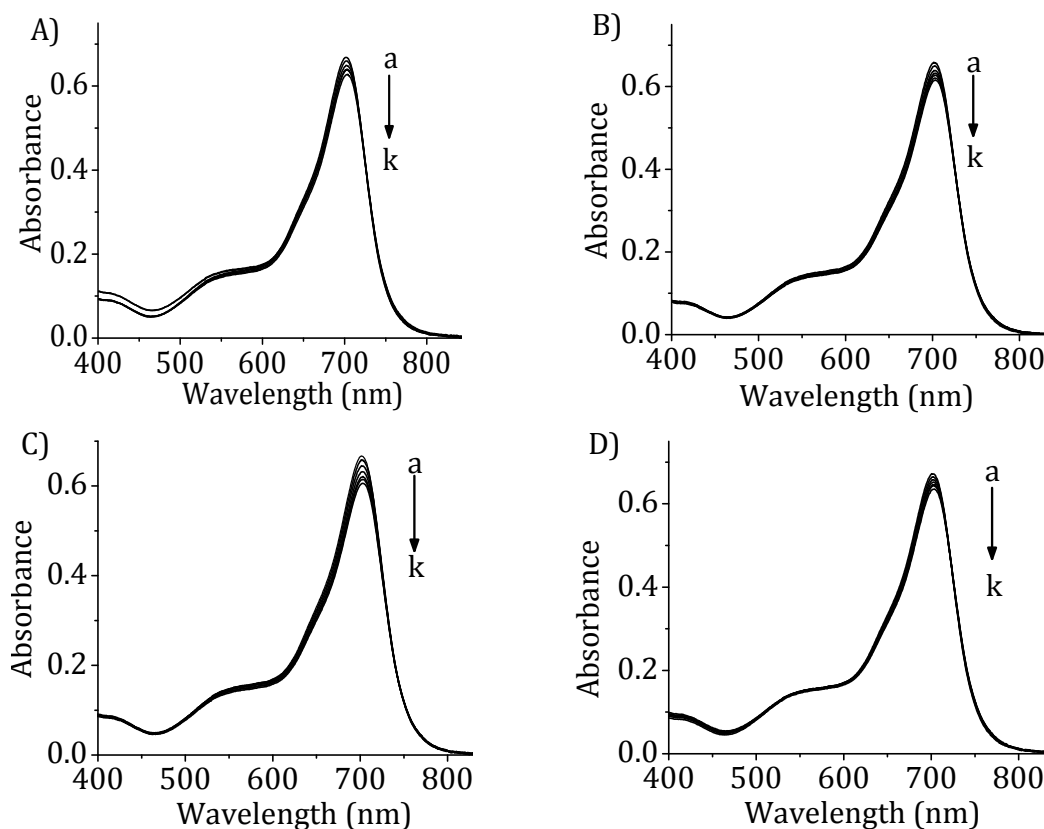


**Figure 4.20.** Absorption spectral changes of the probe **3a** (12 μM) in THF with the addition of A) SO<sub>4</sub><sup>2-</sup>, B) HSO<sub>3</sub><sup>-</sup>, C) (S<sub>2</sub>O<sub>3</sub><sup>2-</sup>), and D) (NO<sub>3</sub><sup>-</sup>) ions. [H<sub>2</sub>S] a) 0 and k) 40 mM.

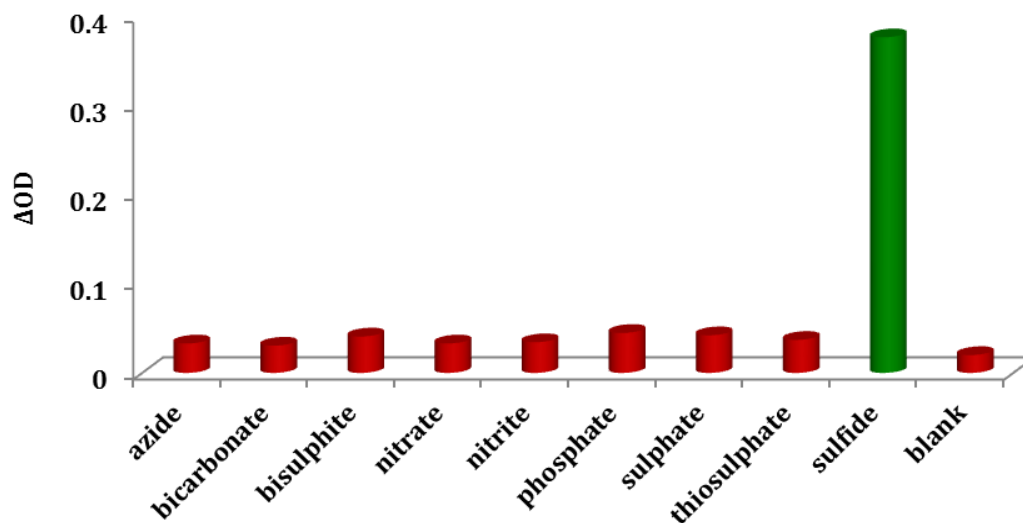


**Figure 4.21.** Selectivity plot showing the changes in absorbance of probe **3a** ( $12 \mu\text{M}$ ) at  $700 \text{ nm}$  by the addition of various anions such as  $\text{N}_3^-$ ,  $\text{HCO}_3^-$ ,  $\text{HSO}_3^-$ ,  $\text{NO}_3^-$ ,  $\text{NO}_2^-$ ,  $\text{HPO}_4^{2-}$ ,  $\text{SO}_4^{2-}$ ,  $\text{S}_2\text{O}_3^{2-}$ ,  $\text{S}^{2-}$  and blank under identical conditions.

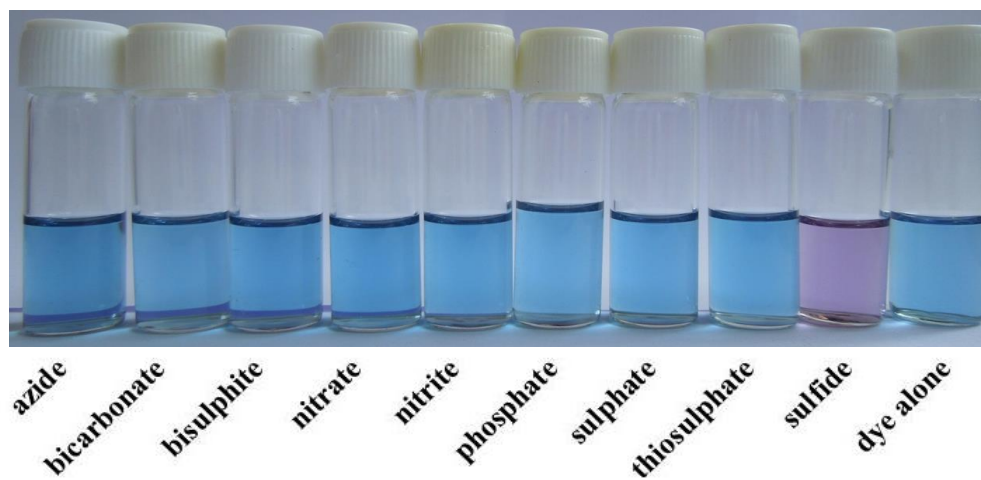


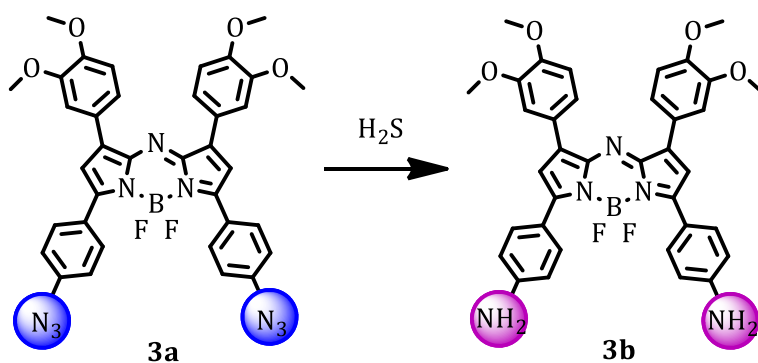
**Figure 4.22.** Colorimetric response of the probe **3a** ( $12 \mu\text{M}$ ) towards various competitive anions.

in the absorption as well as fluorescence spectra of probe **3a** even at *ca.* 100- fold higher concentrations than that of the  $\text{H}_2\text{S}$  (Figure 4.21). These results revealed that probe **3a** shows excellent selectivity as well as sensitivity towards the  $\text{H}_2\text{S}$  over the other tested anions. The sensing event can be visually monitored without the use of sophisticated

instruments and the strategy is simple and useful in practical laboratories. Compared with the blue colored probe **3a**, the deep purple colored product **3b** was found to be highly visible, which indicates the practical utility of the aza-BODIPY probe for on-spot visual detection of H<sub>2</sub>S. The presence of H<sub>2</sub>S can also be selectively detected among the mixture of anions demonstrating the versatility of the probe **3a** (Figure 4.22).

#### 4.3.4.2. Mechanism and Kinetics of Detection of H<sub>2</sub>S

To understand the sensing mechanism, the purple colored derivative obtained was isolated independently by the reaction of **3a** with Na<sub>2</sub>S in THF at room temperature for 10 min. The product was unambiguously characterized, by IR, NMR and ESI-MS, as the amino derivative, **3b** (Scheme 4.4) and compared with the authentic sample synthesized through a different method. To investigate the kinetics of the reaction between **3a** and H<sub>2</sub>S, we employed pseudo-first order approximation. We have monitored the changes in the absorption of the probe **3a** at 700 nm with respect to time upon addition of excess equivalents of H<sub>2</sub>S, which revealed that the reaction was completed within a rapid period of 30 s. The reaction was found to proceed *via* a pseudo



**Scheme 4.4.** H<sub>2</sub>S sensing mechanism of the azido-aza-BODIPY, **3a** (azide to amine transformation through reduction).

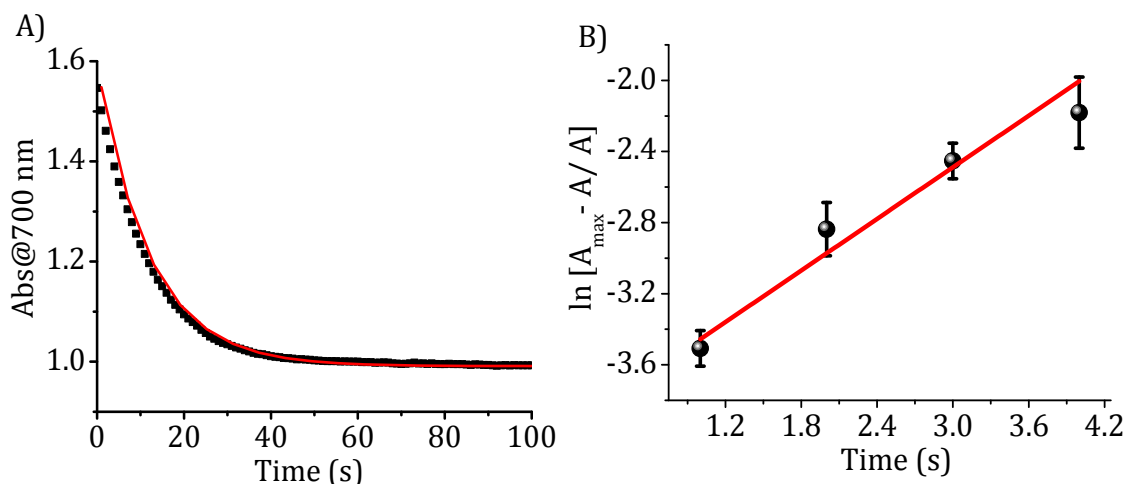


**Figure 4.23.** A) The temporal profile of absorbance at  $\lambda_{\text{abs}} = 700$  nm observed from the reaction between probe **3a** and  $\text{H}_2\text{S}$ . B) Pseudo-first-order kinetic plot of reaction of the probe **3a** ( $5 \mu\text{M}$ ) with  $\text{H}_2\text{S}$  ( $50 \mu\text{M}$ ). Data points represent the mean of more than three independent experiments ( $\pm\text{SD}$ ).

first order kinetics. The rate constant ( $k'$ ) for the reaction was calculated from the slope of the straight line between time and relative changes in the absorbance and the obtained value is found to be  $0.083 \pm 0.021 \text{ S}^{-1}$  (Figure 4.23).

## 4.4. CONCLUSIONS

In summary, we have synthesized three novel NIR absorbing aza-BODIPY derivatives, **3a-c** and have investigated their photophysical properties as well as their use as probes for various biologically important molecules. The substitution of different functionalities such as azido, amino and dimethylamino groups on the aza-BODIPY dyes rendered their absorption in the red region of 700-800 nm. The fluorescence spectra of these derivatives exhibited a regular shift towards the NIR region from azido (**3a**) to amino (**3b**) to dimethylamino (**3c**) aza-BODIPY derivatives. The results of interactions

of these molecules with various analytes revealed that, the amino aza-BODIPY, **3b** could selectively detect nitrite ions ( $\text{NO}_2^-$ ) by a distinct visual color change from bright blue to intense green with a detection limit of 20 ppb. Interestingly, this probe can be employed for the sensitive detection of the nitrate ions ( $\text{NO}_3^-$ ) through a simple reduction step and freshly generated nitric oxide (NO) in the aqueous medium. In contrast, the azido aza-BODIPY dye, **3a** exhibited selective interactions with  $\text{H}_2\text{S}$  via the reduction of azido group to amino group. Uniquely, this probe can be utilized for the visual detection and on-site analysis of  $\text{H}_2\text{S}$  and also in practical laboratory experiments through a distinct color change from bright blue to purple with a sensitivity of 0.5 ppm. Thus, the photophysical properties and sensing applications of aza-BODIPY dyes demonstrate that these systems can be effectively employed as probes for the on-site detection and analysis of  $\text{NO}_2^-$ ,  $\text{NO}_3^-$ , NO and  $\text{H}_2\text{S}$  in the aqueous medium.

## **4.5. EXPERIMENTAL SECTION**

### **4.5.1. General Techniques**

The melting points of the derivatives were determined on a Mel-Temp II melting point apparatus. The IR spectra were recorded on a Perkin Elmer Model 882 infrared spectrometer. The electronic absorption spectra were recorded on a Shimadzu UV-3101 or 2401 PC UV-VIS-NIR scanning spectrophotometer. The fluorescence spectra were recorded on a SPEX-Fluorolog F112X spectrofluorimeter.  $^1\text{H}$  and  $^{13}\text{C}$  NMR were recorded on a 500 MHz Bruker advanced DPX spectrometer. The mass spectra were recorded on Thermo Scientific Exactive ESI-MS spectrophotometer. All the solvents

used were purified and distilled before use. Quantum yields of fluorescence were measured by the relative methods using optically dilute solutions.

#### 4.5.2. Materials and Methods

**Starting materials.** 3,4-Dimethoxybenzaldehyde, 4-aminoacetophenone, nitromethane, potassium carbonate, ammonium acetate, borontrifluoride diethyletherate, N,N-diisopropyl-ethylamine, sodium sulfide, sodium nitrite, sodium nitrate, sodium azide, sodium sulphate, sodium thiosulphate, sodium carbonate and sodium bicarbonate were purchased from Aldrich and S. D. Fine Chemicals, India.

#### 4.5.3. Synthesis of Starting Materials and Aza-BODIPY Dyes 3a-c

##### 4.5.3.1. General Procedure for the Synthesis of 1a-c

*i) Synthesis of 1b:* To a solution of the parent amino chalcone (5.76 mmol) dissolved in methanol (80 mL) was added activated  $K_2CO_3$  and nitromethane (2 mL) and refluxed for 15 h. The mixture was washed with water and extracted with chloroform. Removal of the solvent gave a residue which was purified by column chromatography over silica gel. Elution of the column with a mixture (1:4) of ethyl acetate and hexane gave the product **1b** in good yield.

**1-(4-Aminophenyl)-3-(3,4-dimethoxyphenyl)-4-nitrobutan-1-one (1b):** 85%, mp 139-140 °C, IR (KBr)  $\nu_{max}$  3400, 1658, 1598  $cm^{-1}$ ;  $^1H$  NMR ( $CDCl_3$ , 500 MHz)  $\delta$  7.78 (2H, d, J = 8.5 Hz), 6.81 (2H, s), 6.77 (1H, s), 6.63 (2H, d, J = 8.5 Hz), 4.84 (1H, q, J = 8 Hz), 4.65 (1H, q, J = 8 Hz), 4.18 (2H, s), 4.16 (1H, t, J = 2.5 Hz), 3.86 (3H, s), 3.84 (3H, s), 3.36 (2H, m);  $^{13}C$  NMR ( $CDCl_3$ , 125 MHz)  $\delta$  194.9, 151.6, 149.3, 148.6, 132.4, 130.6, 127.0,

119.3, 113.8, 111.7, 111.2, 79.9, 56.1, 41.1, 39.4; FAB-MS  $m/z$  Calcd for  $C_{18}H_{18}INO_5$ : 344.14; Found: 344.75 ( $M^+$ ).

**ii) Synthesis of 1a:** To a suspension of **1b** (3 g) in water was added concentrated HCl (5.8 mL). A solution of sodium nitrite (750 mg) in water was added drop wise to the stirred suspension at a rate to maintain the reaction temperature  $<5$  °C. The reaction mixture was allowed to stir at 0 °C for 0.5 h followed by the slow addition of sodium azide (750 mg). The reaction mixture was protected from light and allowed to warm to room temperature. After 4 h, the resulting precipitate was dissolved in ethyl acetate (100 mL), washed with water, dried over sodium sulphate and concentrated under reduced pressure. The crude viscous product obtained was chromatographed over silica gel with a mixture of ethyl acetate and hexane (1:4) to yield the product **1a**.

**1-(4-Azidophenyl)-3-(3,4-dimethoxyphenyl)-4-nitrobutan-1-one (1a):** 90%; mp 92-94°C; IR (KBr)  $\nu_{max}$  2124, 1598, 1495  $cm^{-1}$ ;  $^1H$  NMR ( $CDCl_3$ , 500 MHz)  $\delta$  7.93 (2H,d,  $J = 8$  Hz), 7.08 (2H, d,  $J = 8.5$  Hz), 6.81 (1H,d,  $J = 18.5$  Hz), 4.82 (1H, q,  $J = 12$  Hz), 4.69 (1H, q,  $J = 12.5$  Hz), 4.18 (1H, m), 3.87 (3H, s), 3.84 (3H, s), 3.44 (2H, m);  $^{13}C$  NMR ( $CDCl_3$ ,125 MHz):  $\delta$  195.4, 149.2, 148.6, 145.4, 133.0, 131.4, 130.0, 119.1, 119.1, 111.5, 111.0, 79.7, 55.9, 55.8, 41.5, 39.1; ESI-MS  $m/z$  Calcd for  $C_{18}H_{18}O_5N_4$ : 370.13; Found: 371.13 ( $M+1^+$ ).

**iii) Synthesis of 1c:** To a solution of **1b** (3 g) in anhydrous DMF (30 mL) was added activated  $K_2CO_3$ , and methyl iodide and the solution was heated to 50 °C for 24 h. The reaction mixture was allowed to cool to room temperature and poured on crushed ice. The precipitated product was filtered, washed with water, dried and

chromatographed over silica gel with a mixture (1:4) of ethyl acetate and hexane to yield the product **1c**.

**3-(3,4-Dimethoxyphenyl)-1-(4-(dimethylamino)phenyl)-4-nitrobutan-1-one (1c):** 80%, mp 80-82 °C; IR (KBr)  $\nu_{\max}$  2801, 1683, 1595, 1298, 1205  $\text{cm}^{-1}$ ;  $^1\text{H-NMR}$  ( $\text{CDCl}_3$ , 500 MHz)  $\delta$  7.84 (2H, d,  $J = 9$  Hz), 6.81 (2H, s), 6.78 (1H, s), 6.64 (2H, d,  $J = 9$  Hz), 4.86 (1H, dd,  $J = 12$  Hz), 4.67 (1H, q,  $J = 8$  Hz), 4.15 (1H, t,  $J = 7$  Hz), 3.87 (6H, d,  $J = 11$  Hz), 3.37 (2H, m), 3.06 (6H, s);  $^{13}\text{C NMR}$  ( $\text{CDCl}_3$ , 125 MHz)  $\delta$  196.6, 155.5, 149.5, 147.0, 141.7, 129.7, 126.2, 119.4, 112.1, 111.7, 79.1, 56.1, 46.6, 41.3, 39.0; FAB-MS  $m/z$  Calcd for  $\text{C}_{20}\text{H}_{24}\text{N}_2\text{O}_5$ : 372.41; Found: 372.29 ( $\text{M}^+$ ).

#### 4.5.3.2. General Procedure for the Synthesis of **2a-c**

The nitromethane adducts **1a-c** (2 g) and ammonium acetate (24 g) were dissolved in ethanol (40 mL) and heated under reflux for 48 h. The precipitated product was washed with water and extracted using DCM (50 mL x 2). The organic extracts were dried over sodium sulphate and concentrated under reduced pressure. The product thus obtained was chromatographed over silica gel (100-200 mesh). Elution of the column with a mixture of ethyl acetate and hexane (1:4) yielded the product **2a-c**.

**(Z)-5-(4-Azidophenyl)-N-(5-(4-azidophenyl)-3-(3,4-dimethoxyphenyl)-2H-pyrrol-2-ylidene)-3-(3,4-dimethoxyphenyl)-1H-pyrrol-2-amine (2a):** 25%, mp > 250 °C; IR (KBr)  $\nu_{\max}$  2126, 1598, 1503, 1257, 805  $\text{cm}^{-1}$ ;  $^1\text{H NMR}$  ( $\text{CDCl}_3$ , 500 MHz)  $\delta$  7.89 (4H, d,  $J = 8.5$  Hz), 7.58 (2H, d,  $J = 8$  Hz), 7.49 (2H, s), 7.17 (4H, d,  $J = 8.5$  Hz), 7.04 (2H, s), 6.91 (2H, d,  $J = 8$  Hz), 3.94 (6H, s), 3.75 (6H, s);  $^{13}\text{C NMR}$  ( $\text{CDCl}_3$ , 125 MHz)  $\delta$  164.4, 160.6, 150.4, 149.0, 146.3, 144.0, 141.5, 136.8, 135.8, 133.1, 130.9, 129.6, 125.5,



122.6, 116.5, 115.5, 112.8, 106.9, 56.1, 55.9; ESI-MS (negative mode)  $m/z$  Calcd for  $C_{18}H_{18}O_5N_2$ : 651.23; Found: 650.23 ( $M-1^+$ ).

**(Z)-5-(4-Aminophenyl)-N-(5-(4-aminophenyl)-3-(3,4-dimethoxyphenyl)-2H-pyrrol-2-ylidene)-3-(3,4-dimethoxyphenyl)-1H-pyrrol-2-amine (2b)**: 40%, mp 170-171°C; IR (KBr)  $\nu_{max}$  3362, 1600, 1506  $cm^{-1}$ ;  $^1H$  NMR ( $CDCl_3$ , 300 MHz)  $\delta$  7.79 (4H, d,  $J = 8$  Hz), 7.61 (2H, d,  $J = 8$  Hz), 7.53 (2H, s), 6.99 (2H, s), 6.92 (2H, d,  $J = 8$  Hz), 6.81 (4H, d,  $J = 8.5$  Hz), 4.06 (4H, s), 3.93 (6H, s), 3.74 (6H, s);  $^{13}C$  NMR ( $CDCl_3$ , 75 MHz)  $\delta$  153.9, 149.2, 148.9, 148.8, 148.3, 127.5, 121.8, 115.2, 113.2, 112.4, 111.0, 56.0, 55.8; FAB-MS  $m/z$  Calcd for  $C_{36}H_{31}N_3O_4$ : 599.23; Found: 599.26 ( $M^+$ ).

**(Z)-3-(3,4-Dimethoxyphenyl)-N-(3-(3,4-dimethoxyphenyl)-5-(4-(dimethylamino)phenyl)-2H-pyrrol-2-ylidene)-5-(4-(dimethylamino)phenyl)-1H-pyrrol-2-amine (2c)**: 50%, mp 245-246°C; IR (KBr)  $\nu_{max}$  2833, 1600, 1510, 1462, 1258  $cm^{-1}$ ;  $^1H$ -NMR ( $CDCl_3$ , 500 MHz)  $\delta$  7.86 (4H, d,  $J = 8.5$  Hz), 7.63 (2H, d,  $J = 8.5$  Hz), 7.57 (2H, s), 7.02 (2H, s), 6.92 (2H, d,  $J = 8.5$  Hz), 6.83 (4H, d,  $J = 8.5$  Hz), 3.94 (6H, s), 3.76 (6H, s), 3.09 (12H, s);  $^{13}C$  NMR ( $CDCl_3$ , 125 MHz)  $\delta$  160.8, 155.3, 153.4, 150.3, 149.8, 141.5, 136.8, 130.7, 128.3, 125.3, 122.4, 116.5, 115.9, 113.6, 112.8, 111.9, 106.0, 56.1, 55.6, 41.3; FAB-MS  $m/z$  Calcd for  $C_{40}H_{41}N_5O_4$ : 655.32; Found: 655.51 ( $M^+$ ).

#### 4.5.3.3. General Procedure for the Synthesis of 3a-c

The azadipyrromethene derivatives **2a-c** (0.45 mmol) were dissolved in dry dichloromethane (80 mL) were treated with diisopropylethylamine (DIEA) (0.8 mL, 4.6 mmol) and stirred for 10 min at 30 °C. To this reaction mixture, boron trifluoride diethyletherate (1 mL, 8.13 mmol) was added and stirred at 25 °C for 15-24 h. The

solvent was evaporated, washed with water (2 × 50 mL) and extracted with chloroform. Removal of the solvent gave a residue, which was purified by column chromatography over basic alumina. Elution of the column with a mixture (1:1) ethyl acetate and hexane gave the aza-BODIPY dyes **3a-c** in good yields.

**3,7-Bis(4-azidophenyl)-1,9-bis(3,4-dimethoxyphenyl)-5,5-difluoro-5H-dipyrrolo[1,2-c:2',1'-f][1,3,5,2]triazaborinin-4-ium-5-uide (3a):** 75%, mp > 300°C; IR (KBr)  $\nu_{\max}$  2123, 1598, 1493, 1263, 1105, 1034, 808  $\text{cm}^{-1}$ ;  $^1\text{H}$  NMR ( $\text{CDCl}_3$ , 500 MHz)  $\delta$  8.08 (4H, d, J = 8.5 Hz), 7.65 (2H, d, J = 8 Hz), 7.55 (2H, s), 7.15 (4H, d, J = 9 Hz), 6.96 (4H, d, J = 8 Hz), 3.96 (6H, s), 3.82 (6H, s);  $^{13}\text{C}$  NMR ( $\text{CDCl}_3$ , 125 MHz)  $\delta$  157.4, 150.7, 149.1, 145.5, 144.0, 142.5, 131.2, 128.3, 125.6, 122.8, 119.2, 117.8, 112.3, 111.2, 100.0, 56.1, 55.9; ESI-MS (-ve mode) m/z Calcd for  $\text{C}_{36}\text{H}_{38}\text{BF}_2\text{N}_9\text{O}_4$ : 699.21; Found: 698.20 (M-1<sup>+</sup>).

**3,7-Bis(4-aminophenyl)-1,9-bis(3,4-dimethoxyphenyl)-5,5-difluoro-5H-dipyrrolo[1,2-c:2',1'-f][1,3,5,2]triazaborinin-4-ium-5-uide (3b):** 75%, mp 192-193°C; IR (KBr)  $\nu_{\max}$  3360, 1600, 1498  $\text{cm}^{-1}$ ;  $^1\text{H}$  NMR ( $\text{CDCl}_3$ , 500 MHz)  $\delta$  8.00 (4H, d, J = 8.5 Hz), 7.64 (2H, dd, J = 8 Hz), 7.55 (2H, d, J = 2 Hz), 6.94 (4H, d, J = 6.5 Hz), 6.75 (4H, d, J = 8.5 Hz), 4.09 (4H, s), 3.95 (6H, s), 3.81 (6H, s);  $^{13}\text{C}$  NMR ( $\text{CDCl}_3$ , 125 MHz)  $\delta$  156.3, 154.2, 150.8, 149.2, 137.1, 136.9, 130.9, 130.8, 130.3, 129.5, 125.7, 122.9, 122.8, 117.6, 112.2, 111.2, 56.1, 55.9; ESI-MS (+ve mode) m/z Calcd for  $\text{C}_{36}\text{H}_{30}\text{BF}_2\text{N}_3\text{O}_4$ : 647.25; Found: 648.25 (M+1<sup>+</sup>).

**1,9-Bis(3,4-dimethoxyphenyl)-3,7-bis(4-(dimethylamino)phenyl)-5,5-difluoro-5H-dipyrrolo[1,2-c:2',1'-f][1,3,5,2]triazaborinin-4-ium-5-uide (3c):** 80%, mp 184-185°C; IR (KBr)  $\nu_{\max}$  2930, 1602, 1498, 1421, 1263  $\text{cm}^{-1}$ ;  $^1\text{H}$  NMR ( $\text{CD}_3\text{COCD}_3$ ,

500 MHz)  $\delta$  8.24 (4H, d,  $J = 9$  Hz), 7.83 (2H, d,  $J = 8.5$  Hz), 7.73 (2H, s), 7.38 (2H, s), 7.09 (2H, d,  $J = 8.5$  Hz), 6.87 (4H, d,  $J = 8.5$  Hz), 3.92 (6H, s), 3.81 (6H, s), 3.15 (12H, s);  $^{13}\text{C}$  NMR ( $\text{CDCl}_3$ , 125 MHz)  $\delta$  153.6, 151.3, 148.8, 148.7, 141.1, 127.9, 127.7, 121.7, 120.3, 113.0, 112.4, 112.2, 110.9, 56.0, 55.8, 40.3; FAB-MS  $m/z$  Calcd for  $\text{C}_{40}\text{H}_{40}\text{BF}_2\text{N}_5\text{O}_4$ : 703.58; Found: 704.56 ( $\text{M}+1^+$ ).

#### 4.5.3.4. Characterization of the Hydroxyl Product 3b-OH

The product formed during the sensing event was isolated and characterized through various spectroscopic techniques. Mp 160-161 °C; IR (KBr)  $\nu_{\text{max}}$  3298 (broad), 1496, 1254  $\text{cm}^{-1}$ ;  $^1\text{H}$  NMR ( $\text{CDCl}_3$ , 500 MHz)  $\delta$  8.01 (4H, d,  $J = 8.5$  Hz), 7.65 (2H, d,  $J = 8$  Hz), 7.54 (5H, m), 6.96 (5H, m), 5.21 (2H, broad, -OH peak), 3.95 (6H, s), 3.82 (6H, s);  $^{13}\text{C}$  NMR ( $\text{CDCl}_3$ , 125 MHz)  $\delta$  159.6, 156.3, 150.8, 149.2, 141.1, 136.1, 130.9, 130.5, 130.3, 129.6, 126.7, 122.8, 116.2, 113.4, 111.2, 56.3, 56.1; FAB-MS  $m/z$  Calcd for  $\text{C}_{36}\text{H}_{30}\text{BF}_2\text{N}_3\text{O}_6$ : 650.52; Found: 650.87 ( $\text{M}^+$ ).

#### 4.5.4. Electrochemical Measurements

Redox potentials of the aza-BODIPY dyes were recorded using a BAS CV50W voltammetric analyzer. Solutions of **3a-c** ( $1 \times 10^{-3}$  M) in acetonitrile containing 0.1 M tetra-*n*-butylammonium hexafluorophosphate as supporting electrolyte were thoroughly deaerated before use. A platinum disc electrode was used as working electrode and a platinum wire was used as counter electrode and the potentials were referenced to saturated calomel electrode (SCE).

#### 4.5.5. Procedure for the Preparation of the Dipstick

Thermoplastic or glass support was cut having the dimensions of 10 x 0.4 cm. The probe **3b** was dissolved in dichloromethane and made to a uniform slurry containing silica/alumina and was carefully fixed over the surface of the support using glue. This gave the solid-state device, dipstick, which can be used on demand. The stick was exposed to HCl gas followed by dipping into a solution taken in a beaker containing nitrite ions ( $2 \times 10^{-5}$  M). Wherever the analyte came in contact with the stick, it resulted in a color change from blue to bright green, thereby indicating the presence of  $\text{NO}_2^-$  ions.

#### 4.5.6. Detection of Nitrate Ions- Hydrazine Sulphate Reduction Method

The detection of nitrate ion ( $\text{NO}_3^-$ ) was achieved by employing a simple reduction step from nitrate to nitrite using hydrazine sulphate method. Initially, the buffer reagent was prepared by adding 25 mL of the phenol solution (4.3 mL in 100 mL distilled water) to 25 mL of the freshly prepared NaOH solution (1.5 g in 100 mL water) and shaken well. The reducing agent was prepared by mixing 25 mL solution of hydrazine sulphate (0.725 g in 100 mL) and 25 mL copper sulphate solution (0.010 g in 100 mL) in a dark bottle. The buffer reagent (2 mL) was added to 50 mL nitrate solution. After rapidly adding 1 mL of the reducing agent to the solution, the flask was protected from sunlight for 10 h, which quantitatively reduces nitrate to nitrite ions.

#### 4.5.7. Generation of NO in Solution

NO solution was prepared by dissolving NO precursor [2-(N,N-diethylamino)-diazonolate 2-oxide sodium salt hydrate (diethylamine NONOate)] in 10 mM PBS

(pH=7.4), following a protocol developed earlier (Keefer *et al.*, 1996; Hrabie *et al.*, 1993; Maragos *et al.*, 1991). The NO-containing PBS solutions were allowed to set for at least 10 min before experiment. Griess test was used to confirm the concentration of NO generated by diethylamine NONOate.

#### 4.5.8. Calculation of Reaction Rates

Kinetic studies were performed at  $25\pm 1^{\circ}\text{C}$  using a Shimadzu UV-Vis spectrophotometer (UV-2600). The experiments were carried out using the kinetic mode of the instrument, where the absorption of the aza-BODIPY derivatives **3a** and **3b** (1 equivalent) at their respective maximum were monitored with respect to time after the addition of analyte (10 equivalents). The slope of the straight line between time and relative changes in absorbance gave the pseudo-first-order rate constant for the reaction.

#### 4.5.9. Theoretical Calculations

The structure optimizations of the aza-BODIPY derivatives **3a-c** were performed with the Gaussian 03 package using B3LYP density functional theory (DFT). The 6-31G\* basis set was used to treat all the atoms. The contours of the HOMO and LUMO orbitals of **3a-c** were plotted using Gauss View. On the basis of ground-state optimization, the density functional theory approach was applied to predict their absorption.

---

## REFERENCES

---

- Abe, K.; Kimura, H. "The Possible Role of Hydrogen Sulfide as an Endogenous Neuromodulator", *J. Neurosci.*, **1996**, *16*, 1066-1071.
- Adams, M. L.; Lavasanifar, A.; Kwon, G. S. "Amphiphilic Block Copolymers for Drug Delivery", *J. Pharm. Sci.*, **2003**, *92*, 1343-1355.
- Albini, A.; Fagnoni, M. "Green Chemistry and Photochemistry were Born at the Same Time", *Green Chem.*, **2004**, *6*, 1-6.
- Ashok, B.; Arleth, L.; Hjelm, R. P.; Rubinstein, I.; Onyuksel, H. "In Vitro Characterization of PEGylated Phospholipid Micelles for Improved Drug Solubilization: Effects of PEG Chain Length and PC Incorporation", *J. Pharm. Sci.*, **2004**, *93*, 2476-2487.
- Atilgan, S.; Ekmekci, Z.; Dogan, A. L.; Gucb, D.; Akkaya, E. U. "Water Soluble Distyryl-Boradiazaindacenes as Efficient Photosensitizers for Photodynamic Therapy", *Chem. Commun.*, **2006**, 4398-4400.
- Atilgan, S.; Ozdemir, T.; Akkaya, E. U. "A Sensitive and Selective Ratiometric Near IR Fluorescent Probe for Zinc Ions Based on the Distyryl-BODIPY Fluorophore", *Org. Lett.*, **2008**, *10*, 4065-4067.
- Avirah, R. R.; Jayaram, D. T.; Adarsh, N.; Ramaiah, D. "Squaraine Dyes in PDT: From Basic Design to In Vivo Demonstration", *Org. Biomol. Chem.*, **2012**, *10*, 911-920.
- Avirah, R. R.; Jyothish K.; Ramaiah D. "Infrared Absorbing Croconaine Dyes: Synthesis and Metal Ion Binding Properties", *J. Org. Chem.*, **2008**, *73*, 274-279.
- Awuah, S. G.; You, Y. "Boron Dipyrromethene (BODIPY)-Based Photosensitizers for Photodynamic Therapy", *RSC Adv.*, **2012**, *2*, 11169-11183.

- Baruah, M.; Qin, W. W.; Vallee, R. A. L.; Beljonne, D.; Rohand, T.; Dehaen, W.; Boens, N. "A Highly Potassium-Selective Ratiometric Fluorescent Indicator Based on BODIPY Azacrown Ether Excitable with Visible Light", *Org. Lett.*, **2005**, *7*, 4377-4380.
- Basu, U.; Khan, I.; Hussain, A.; Kondaiah, P.; Chakravarty, A. R. "Photodynamic Effect in Near-IR Light by a Photocytotoxic Iron(III) Cellular Imaging Agent", *Angew. Chem., Int. Ed.*, **2012**, *51*, 2658-2661.
- Batat, P.; Cantuel, M.; Jonusauskas, G.; Scarpantonio, L.; Palma, A.; O'Shea, D. F.; McClenaghan, N. D. "BF<sub>2</sub>-Azadipyromethenes: Probing the Excited-State Dynamics of a NIR Fluorophore and Photodynamic Therapy Agent", *J. Phys. Chem. A.*, **2011**, *115*, 14034-14039.
- Bellier, Q.; Dalier, F.; Jeanneau, E.; Maury, O.; Andraud, C. "Thiophene Substituted Aza-BODIPY as a Strategic Synthone for the Design of Near-infrared Dyes", *New J. Chem.*, **2012**, *36*, 768-773.
- Bellier, Q.; Pegaz, S.; Aronica, C.; Guennic, B. L.; Andraud, C.; Maury, O. "Near-Infrared Nitrofluorene Substituted Aza-Boron-dipyromethenes Dyes", *Org. Lett.*, **2011**, *13*, 22-25.
- Boehning, D.; Snyder S. H. "Novel Neural Modulators", *Annu. Rev. Neurosci.*, **2003**, *26*, 105-131.
- Boens, N.; Leen, V.; Dehaen, W. "Fluorescent Indicators Based on BODIPY", *Chem. Soc. Rev.*, **2012**, *41*, 1130-1172.
- Bonesi, S. M.; Manet, H.; Freccero, M.; Fagnoni M.; Albini, A. "Photosensitized Oxidation of Sulfides: Discriminating Between the Singlet-Oxygen Mechanism and Electron Transfer Involving Superoxide Anion or Molecular Oxygen", *Chem. Eur. J.*, **2006**, *12*, 4844-4857.

- Bonnett, R. "Photosensitizers of the Porphyrin and Phthalocyanine Series for Photodynamic Therapy", *Chem. Soc. Rev.*, **1995**, *24*, 19-33.
- Bonnett, R.; Djelal, B. D.; Nguyen, A. "Physical and Chemical Studies Related to the Development of *m*-THPC (FOSCAN®) for the Photodynamic Therapy (PDT) of Tumors", *J. Porphyrins Phthalocyanines*, **2001**, *5*, 652-661.
- Bonnett, R. in *Chemical Aspects of Photodynamic Therapy*, Gordon and Breach Science Publishers, The Netherlands, **2000**.
- Bouit, P. A.; Kamada, K.; Feneyrou, P.; Berginc, G.; Toupet, L.; Maury, O.; Andraud, C. "Two-Photon Absorption-Related Properties of Functionalized BODIPY Dyes in the Infrared Range up to Telecommunication Wavelengths", *Adv. Mater.*, **2009**, *21*, 1151-1154.
- Bozdemir, O. A.; Cakmak, Y.; Sozmen, F.; Ozdemir, T.; Siemiarczuk, A.; Akkaya, E. U. "Synthesis of Symmetrical Multichromophoric BODIPY Dyes and Their Facile Transformation into Energy Transfer Cassettes", *Chem. Eur. J.*, **2010**, *16*, 6346-6351.
- Brender, J. D.; Olive, J. M.; Felkner, M.; Suarez, L.; Marckwardt, W. M.; Hendricks, K. A. "Dietary Nitrites and Nitrates, Nitrosatable Drugs, and Neural Tube Defects", *Epidemiology*, **2004**, *15*, 330-336.
- Buldt, A.; Karst, U. "Determination of Nitrite in Waters by Microplate Fluorescence Spectroscopy and HPLC with Fluorescence Detection", *Anal. Chem.*, **1999**, *71*, 3003-3007.
- Burroughes, J. H.; Bradley, D. D. C.; Brown, A. R.; Marks, R. N.; Mackay, K.; Friend, R. H.; Burns, P. L.; Holmes, A. B. "Light-emitting Diodes Based on Conjugated Polymers", *Nature*, **1990**, *347*, 539-541.



- Cakmak, Y.; Akkaya, E. U. "Phenylethynyl-BODIPY Oligomers: Bright Dyes and Fluorescent Building Blocks", *Org. Lett.*, **2009**, *11*, 85-88.
- Carreno, M. C. "Applications of Sulfoxides to Asymmetric Synthesis of Biologically Active Compounds", *Chem. Rev.*, **1995**, *95*, 1717-1760.
- Carreira, E.; Zhao, W. "Aza-dipyrromethene Dyes Compatible with Diode Lasers, and Their Processes of Preparation", PCT Patent WO 2006/058448, **2006**.
- Chen, C.-Q; Xin, H.; Zhu, Y.-Z. "Hydrogen Sulfide: Third Gaseous Transmitter, But with Great Pharmacological Potential", *Acta Pharmacol Sin.*, **2007**, *28*, 1709-1716.
- Chen, L.; Yang, Y.; Jiang, D. "CMPs as Scaffolds for Constructing Porous Catalytic Frameworks: A Built-in Heterogeneous Catalyst with High Activity and Selectivity Based on Nanoporous Metalloporphyrin Polymers", *J. Am. Chem. Soc.*, **2010**, *132*, 9138-9143.
- Chen, Z.; Zhang, Z.; Qu, C.; Pana, D.; Chen, L. "Highly Sensitive Label-free Colorimetric Sensing of Nitrite Based on Etching of Gold Nanorods", *Analyst*, **2012**, *137*, 5197-5200.
- Coskun, A.; Yilmaz, M. D.; Akkaya, E. U. "Bis(2-pyridyl)-Substituted Boratriazaindacene as an NIR-Emitting Chemosensor for Hg(II)", *Org. Lett.*, **2007**, *9*, 607-609.
- Crouse, D. J.; Wheeler, M. M.; Goemann, M.; Tobin, P. S.; Basu, S. K.; Wheeler, D. M. S. "Oxidation of 1,5-Naphthalenediol and its Methyl Ether: Preparation of Juglone Methyl Ether Monoacetal", *J. Org. Chem.*, **1981**, *46*, 1814-1817.
- Dadova, J.; Svobodova, E.; Sikorski, M.; König B.; Cibuka, R. "Photooxidation of Sulfides to Sulfoxides Mediated by Tetra-O-Acetylriboflavin and Visible Light", *ChemCatChem.*, **2012**, *4*, 620-623.

- Daniel, W. L.; Han, M. S.; Lee, J.-S.; Mirkin, C. A. "Colorimetric Nitrite and Nitrate Detection with Gold Nanoparticle Probes and Kinetic End Points", *J. Am. Chem. Soc.*, **2009**, *131*, 6362–6363.
- Davies, W. H.; Rogers, M. A. T. "4-Diarylpyrroles. Part IV. The Formation of Acylated 5-Amino-2, 4-diphenylpyrroles from  $\beta$ -Benzoyl- $\alpha$ -phenylpropionitrile and Some Notes on the Leuckart reaction", *J. Chem. Soc.*, **1944**, 126-131.
- DeRosa, M. C.; Crutchley, R. J. "Photosensitized Singlet Oxygen and Its Applications", *Coord. Chem. Rev.*, **2002**, *233–234*, 351–371 and references therein.
- Detty, M. R.; Merkel P. B. "Chalcogenapyrylium Dyes as Potential Photochemotherapeutic Agents: Solution Studies of Heavy Atom Effects on Triplet Yields, Quantum Efficiencies of Singlet Oxygen Generation. Rates of Reaction with Singlet Oxygen and Emission Quantum Yields", *J. Am. Chem. Soc.*, **1990**, *112*, 3845-3855.
- Devi, D. G.; Cibin, T. R.; Ramaiah, D.; Abraham, A. "Bis(3,5-diiodo-2,4,6-trihydroxyphenyl) squaraine: A Novel Candidate in Photodynamic Therapy for Skin Cancer Models *In Vivo*", *J. Photochem. Photobiol. B.*, **2008**, *92*, 153-159.
- Diring, S.; Puntoriero, F.; Nastasi, F.; Champagna, S.; Zeissel, R. "Star-Shaped Multichromophoric Arrays from BODIPY Dyes Grafted on Truxene Core", *J. Am. Chem. Soc.*, **2009**, *131*, 6108-6110.
- Djurovich, P. I.; Mayo, E. I.; Forrest, S. R.; Thompson, M. E. "Measurement of the Lowest Unoccupied Molecular Orbital Energies of Molecular Organic Semiconductors", *Organic Electronics*, **2009**, *10*, 515–520.
- Dou, L.; You, J.; Hong, Z.; Xu, Z.; Li, G.; Street, R. A.; Yang, Y. "25<sup>th</sup> Anniversary Article: A Decade of Organic/Polymeric Photovoltaic Research", *Adv. Mater.*, **2013**, *25*, 6642-6671.

- Dougherty, T. J.; MacDonald, I. J. "Basic Principles of Photodynamic Therapy", *J. Porphyrins Phthalocyanines*, **2001**, *5*, 105–129.
- Dougherty, T. J.; Marcus, S. L. "Photodynamic Therapy", *Eur. J. Cancer*, **1992**, *28*, 1734-1742.
- D'Souza, F.; Amin, A. N.; El-Khouly, M. E.; Subbaiyan, N. K.; Zandler, M. E.; Fukuzumi, S. "Control over Photoinduced Energy and Electron Transfer in Supramolecular Polyads of Covalently linked aza BODIPY-Bisporphyrin 'Molecular Clip' Hosting Fullerene", *J. Am. Chem. Soc.*, **2012**, *134*, 654–664.
- Durchstein, H.-J.; Wurm, G. "Juglone Formation in Indicator Reaction for Molecular Activated Oxygen in the Singlet State", *Arch. Pharm. (Weinheim)*, **1984**, *317*, 809-812.
- Esser, P.; Pohlmann, B.; Scharf, H.-D. "Photochemical Synthesis of Fine Chemicals with Sunlight", *Angew. Chem.*, **1994**, *106*, 2093-2108.
- European Standard, Water quality-Determination of Nitrites-Molecular Absorption Spectrometric Method. **1993**, EN 26777.
- Fernandez, I.; Khiar, N. "Recent Developments in the Synthesis and Utilization of Chiral Sulfoxides", *Chem. Rev.*, **2003**, *103*, 3651–3706.
- Flavin, K.; Lawrence, K.; Bartelmess, J.; Tasiar, M.; Navio, C.; Bittencourt, C.; O'Shea, D. F.; Guldi, D. M.; Giordani S. "Synthesis and Characterization of Boron Aza-dipyrromethene Single-Wall Carbon Nanotube Electron Donor-Acceptor Conjugates", *ACS Nano*, **2011**, *5*, 1198–1206.
- Focazio, M. J.; Tipton, D.; Shapiro, S. D.; Geiger, L. H. "The Chemical Quality of Self-Supplied Domestic Well Water in the United States", *Ground Water Monit. R.*, **2006**, *26*, 92–104.

- Foote, C. S. "Definition of Type I and Type II Photosensitized Oxidation", *Photochem. Photobiol.*, **1991**, *54*, 659.
- Fox, J. B. "Kinetics and Mechanisms of the Griess Reaction", *Anal. Biochem.*, **1979**, *51*, 1493-1502.
- Fudickar, W.; Linker, T. "Reversible Photooxygenation of Alkynylanthracenes: Chemical Generation of Singlet Oxygen under Very Mild Conditions", *Chem. Eur. J.*, **2011**, *17*, 13661-13664.
- Gallagher, W. M.; Allen, L. T.; O'Shea, C.; Kenna, T.; Hall, M. J.; Killoran, J.; O'Shea, D. F. "A Potent Nonporphyrin Class of Photodynamic Therapeutic Agent: Cellular Localisation, Cytotoxic Potential and Influence of Hypoxia", *Br. J. Cancer*, **2005**, *92*, 1702-1710.
- Golovkova, T. A.; Kozlov, D. V.; Neckers, D. C. "Synthesis and Properties of Novel Fluorescent Switches", *J. Org. Chem.*, **2005**, *70*, 5545-5549.
- Gorman, A.; Killoran, J.; O'Shea, C.; Kenna, T.; Gallagher, W. M.; O'Shea, D. F. "In Vitro Demonstration of the Heavy-Atom Effect for Photodynamic Therapy", *J. Am. Chem. Soc.*, **2004**, *126*, 10619-10631.
- Goze, C.; Ulrich, G.; Ziessel, R. "Unusual Fluorescent Monomeric and Dimeric Dialkynyl Dipyrrromethene-Borane Complexes", *Org. Lett.*, **2006**, *8*, 4445-4448.
- Greer, A. "Christopher Foote's Discovery of the Role of Singlet Oxygen [ $^1\text{O}_2$  ( $^1\Delta_g$ )] in Photosensitized Oxidation Reactions", *Acc. Chem. Res.*, **2006**, *39*, 797-804.
- Greer, F. R.; Shannon, M. "Infant Methemoglobinemia: The Role of Dietary Nitrate in Food and Water", *Pediatrics*, **2005**, *116*, 784-786.

- Griesbeck, A. G.; Johannes, U.; Thomas, S.; Lhoussaine, B.; Reinhard, S.; Grundler, P. V.; Helm, L.; Alberto, R.; Merbatch, A. E. "Singlet Oxygen Photo-Oxygenation in Water/Pluronic F-127 Hydrogels: Increased Reaction Efficiency Coupled with a Switch in Regioselectivity", *Chem. Eur. J.*, **2012**, *18*, 16161–16165.
- Griesbeck, A. G.; Cho, M. "9-Mesityl-10-methylacridinium: An Efficient Type II and Electron-Transfer Photooxygenation Catalyst", *Org. Lett.*, **2007**, *9*, 611-613.
- Griesbeck, A. G.; El-Idressy, T. T.; Bartoschek, A. "Photooxygenation in Polystyrene Beads with Covalently and Non-Covalently Bound Tetraarylporphyrin Sensitizers", *Adv. Synth. Catal.*, **2004**, *346*, 245-251.
- Griesbeck, A. G.; Miranda, M. A.; Uhlig, J. "Sweet Chiral Porphyrins as Singlet Oxygen Sensitizers for Asymmetric Type II Photooxygenation", *Photochem. Photobiol. Sci.*, **2011**, *10*, 1431 –1435.
- Griesbeck, A. G.; Schafer, M.; Uhlig, J. "Photooxygenation Catalysis with a Polyol-Decorated Disc-Shaped Porphyrin Sensitizer: Shell-Recognition Effects", *Adv. Synth. Catal.*, **2008**, *350*, 2104-2108.
- Griffiths, J.; Chu, K. -Y.; Hawkins, C. "Photosensitised Oxidation of 1-Naphthols", *J. Chem. Soc., Chem. Commun.*, **1976**, *17*, 676-677.
- Grimsdale, A. C.; Chan, K. L.; Martin, R. E.; Jokisz, P. G.; Holmes, A. B. "Synthesis of Light-Emitting Conjugated Polymers for Applications in Electroluminescent Devices", *Chem. Rev.*, **2009**, *109*, 897-1091.
- Grossi, M.; Palma, A.; McDonnell, S. O.; Hall, M. J.; Rai, D. K.; Muldoon, J.; O'Shea, D. F. "Mechanistic Insight into the Formation of Tetraarylazadipyrromethenes", *J. Org. Chem.*, **2012**, *77*, 9304–9312.

- Haefele, A.; Zedde, C.; Retailleau, P.; Ulrich, G.; Ziessel, R. "Boron Asymmetry in a BODIPY Derivative", *Org. Lett.*, **2010**, *12*, 1672-1675.
- Haggiage, E.; Coyle, E. E.; Joyce, K.; Oelgemoller, M. "Green Photochemistry: Solar Chemical Synthesis of 5-amido-1,4-naphthoquinones", *Green Chem.*, **2009**, *11*, 318-321.
- Hajimohammadi, M.; Safari, N.; Mofakham, H.; Deyhimi, F. "Highly Selective, Economical and Efficient Oxidation of Alcohols to Aldehydes and Ketones by Air and Sunlight or Visible Light in the Presence of Porphyrins Sensitizers", *Green Chem.*, **2011**, *13*, 991-997.
- Halliwell, B.; Gutteridge, J. M. C. "Free Radicals in Biology and Medicine", 3<sup>rd</sup> Ed, Oxford University Press, Oxford, **1999**
- Hanajiri, R. K.; Martin, R. S.; Lunte, S. M. "Indirect Measurement of Nitric Oxide Production by Monitoring Nitrate and Nitrite Using Microchip Electrophoresis with Electrochemical Detection", *Anal. Chem.*, **2002**, *74*, 6370-6377.
- Haugland, R. P. *Handbook of Fluorescent Probes and Research Chemicals, 6th ed.*; Molecular Probes: Eugene, OR, **1996**.
- Haughland, R. P.; Kang, H. C. "Chemically Reactive Dipyrromethene Boron Difluoride Dyes", US Patent US4774339, **1988**.
- Heather, J. B.; Mittal R. S. D.; Sih, C. J. "Total Synthesis of d1-Strigol", *J. Am. Chem. Soc.*, **1974**, *96*, 1976-1977.
- He, H.; Lo, P.-C.; Yeung, S.-L.; Fong, W.-P.; Ng, D. K. P. "Preparation of Unsymmetrical Distyryl BODIPY Derivatives and Effects of the Styryl Substituents on their *In Vitro* Photodynamic Properties," *Chem. Commun.*, **2011**, *47*, 4748-4750.

- Hill, M. J. *Nitrates and Nitrites in Food and Water, 1st Ed.*, Woodhead Publishing Limited, England, **1996**.
- Hoffmann, N. "Photochemical Reactions as Key Steps in Organic Synthesis", *Chem. Rev.*, **2008**, *108*, 1052–1103.
- Hong, Z. R.; Lessmann, R.; Maennig, B.; Huang, Q.; Harada, K.; Riede, M.; Leo, K. "Antenna Effects and Improved Efficiency in Multiple Heterojunction Photovoltaic Cells Based on Pentacene, Zinc Phthalocyanine, and C<sub>60</sub>", *J. Appl. Phys.*, **2009**, *106*, 064511.
- Hrabie, J. A.; Klose, J. R.; Wink, D. A.; Keefer L. K. "New Nitric Oxide-releasing Zwitterions Derived from Polyamines", *J. Org. Chem.*, **1993**, *58*, 1472–1476.
- Ishii, K. "Functional Singlet Oxygen Generators Based on Phthalocyanines", *Coord. Chem. Rev.*, **2012**, *256*, 1556-1568.
- Jisha, V. S.; Arun, K. T.; Hariharan, M.; Ramaiah, D. "Site-Selective Interactions: Squaraine Dye-Serum Albumin Complexes with Enhanced Fluorescence and Triplet Yields", *J. Phys. Chem. B*, **2010**, *114*, 5912-5919.
- Johan, E. V.; Hongjian, T.; Hasrat, A.; Nicole, C.; Haroutioun, H. M. "Trisulfonated Porphyrazines: New Photosensitizers for the Treatment of Retinal and Subretinal Edema", *J. Med. Chem.*, **2009**, *52*, 4107–4110.
- Kamkaew, A.; Lim, S. H.; Lee, H. B.; Kiew, L. V.; Chung, L. Y.; Burgess, K. "BODIPY Dyes in Photodynamic Therapy", *Chem. Soc. Rev.*, **2013**, *42*, 77-88.
- Kanazawa, A.; Kotsuki H.; Tokoroyama, T. "Total Synthesis of Portulal", *Tetrahedron Lett.*, **1975**, *42*, 3651-3654.

- Kang P.; Foote C. S. "Formation of Transient Intermediates in Low-Temperature Photosensitized Oxidation of an 8-<sup>13</sup>C-Guanosine Derivative", *J. Am. Chem. Soc.*, **2002**, *124*, 4865–4873.
- Karunakaran, S. C.; Babu, P. S. S.; Madhuri, B.; Marydasan, B.; Paul, A. K.; Nair, S. A.; Rao, K. S.; Srinivasan, A.; Chandrashekar, T. K.; Ch. Rao, M.; Pillai, M. R.; Ramaiah, D. "In Vitro Demonstration of Apoptosis Mediated Photodynamic Activity and NIR Nucleus Imaging through a Novel Porphyrin", *ACS Chem. Biol.*, **2013**, *8*, 127–132.
- Kastantin, M.; Ananthanarayanan, B.; Karmali, P.; Ruoslahti, E.; Tirrell M. "Effect of the Lipid Chain Melting Transition on the Stability of DSPE-PEG(2000) Micelles", *Langmuir*, **2009**, *25*, 7279–7286.
- Keefer, L. K.; Nims, R. W.; Davies, K. M.; Wink, D. A. "NONOates-(1-substituted diazen-1-ium-1,2-diolates) as Nitric Oxide Donors: Convenient Nitric Oxide Dosage Forms", *Methods Enzymol.*, **1996**, *268*, 281–293.
- Kelkar, S. S.; Reineke, T. M. "Theranostics: Combining Imaging and Therapy", *Bioconjugate Chem.*, **2011**, *22*, 1879–1903.
- Kilfoy, B. A.; Zhang, Y.; Park, Y.; Holford, T. R.; Schatzkin, A.; Hollenbeck, A.; Ward, M. H. "Dietary Nitrate and Nitrite and the Risk of Thyroid Cancer in the NIH-AARP Diet and Health Study", *Int. J. Cancer*, **2011**, *129*, 160-172.
- Killoran, J.; Allen, L.; Gallagher, J. F.; Gallagher, W. M.; O'Shea, D. F. "Synthesis of BF<sub>2</sub> Chelates of Tetraarylazadipyrromethenes and Evidence for their Photodynamic Therapeutic Behaviour", *Chem. Commun.*, **2002**, 1862–1863.
- Killoran, J.; McDonnell, S. O.; Gallagher, J. F.; O'Shea, D. F. "A Substituted BF<sub>2</sub>-Chelated Tetraarylazadipyrromethene as an Intrinsic Dual Chemosensor in the 650–850 nm Spectral Range", *New J. Chem.*, **2008**, *32*, 483-489.



- Killoran, J.; O'Shea, D. F. "Impact of a Conformationally Restricted Receptor on the BF<sub>2</sub> Chelated Azadipyrrromethene Fluorosensing Platform", *Chem. Commun.*, **2006**, *14*, 1503–1505.
- Kim, H. J.; Kim, Y. K. "Determination of Nitrite in Drinking Water and Environmental Samples by Ion Exclusion Chromatography with Electrochemical Detection", *Anal. Chem.*, **1989**, *61*, 1485-1489.
- Kim, T. Y.; Kim, D. W.; Chung, J. Y.; Shin, S. G.; Kim, S. C.; Heo, D. S.; Kim, N. K.; Bang, Y. J. "Phase I and Pharmacokinetic Study of Genexol-PM, A Cremophor-free, Polymeric Micelle-Formulated Paclitaxel, in Patients with Advanced Malignancies", *Clin. Cancer Res.*, **2004**, *10*, 3708–16.
- Knott, E. B. "β-Cycloylpropionitriles. Part II. Conversion into Bis-2-(5-cyclylpyrrole)azamethin Salts", *J. Chem. Soc.*, **1947**, 1196-2001.
- Koziar, J. C.; Cowan, D. O. "Photochemical Heavy-Atom Effects", *Acc. Chem. Res.*, **1978**, *11*, 334-341.
- Kumar C. V.; Qin L.; Das P. K. "Aromatic Thioketone Triplets and Their Quenching Behaviour Towards Oxygen and Di-t-butylnitroxy Radical. A Laser-Flash-Photolysis Study", *J. Chem. Soc. Faraday Trans. 2*, **1984**, *80*, 783-793.
- Lakshmi, V.; Ravikanth, M. "Synthesis of Sterically Crowded Polyarylated Boron-Dipyrrromethenes", *J. Org. Chem.*, **2011**, *76*, 8466–8471.
- Lattmann, E.; Coombs, J.; Hoffmann, H. M. R. "Pyranofuranones via Lewis Acid Mediated Hetero-Diels-Alder Reactions of 4-Furan-2(5H)-ones: A Convergent Route to the Manoalide Substructure", *Synthesis*, **1996**, *1*, 171-177.
- Lawrence, N. S.; Davis, J.; Jiang, L.; Jones, T. G. J.; Davies, S. N.; Compton, R. G. "The Electrochemical Analog of the Methylene Blue Reaction: A Novel Amperometric

- Approach to the Detection of Hydrogen Sulfide”, *Electroanalysis*, **2000**, *12*, 1453-1460.
- Lawrence, N. S.; Deo, R. P.; Wang, J. “Electrochemical Determination of Hydrogen Sulfide at Carbon Nanotube Modified Electrodes”, *Anal. Chim. Acta*, **2004**, *517*, 131-137.
- Li, W.; Li, L.; Xiao, H.; Qi, R.; Huang, Y.; Xie, Z.; Jing, X.; Zhang, H. “Iodo-BODIPY: A Visible-light-driven, Highly Efficient and Photostable Metal-free Organic Photocatalyst”, *RSC Adv.*, **2013**, *3*, 13417-13421.
- Li, W.; Xie, Z.; Jing, X. “BODIPY Photocatalyzed Oxidation of Thioanisole Under Visible Light”, *Catalysis Commun.*, **2011**, *16*, 94-97.
- Lin, Z.; Xue, W.; Chen, H.; Lin, J. M. “Peroxy-nitrous-Acid-Induced Chemiluminescence of Fluorescent Carbon Dots for Nitrite Sensing”, *Anal. Chem.*, **2011**, *83*, 8245- 8251.
- Lindsey, J. S.; “Synthesis of Meso-Substituted Porphyrins”, *The Porphyrin Handbook*, Edited by Kadish, K. M.; Smith K. M.; Guilsard, R., Academic Press, San Diego, Vol. **11**, **2000**.
- Lippert, A. R.; New, E. J.; Chang, C. J. “Reaction-Based Fluorescent Probes for Selective Imaging of Hydrogen Sulfide in Living Cells”, *J. Am. Chem. Soc.*, **2011**, *133*, 10078-10080.
- Liras, M.; Prieto, J. B.; Pintado-Sierra, M.; Arbeloa, F. L.; Garcia-Moreno, I.; Costela, A.; Infantes, L.; Sastre, R.; Amat-Guerri, F. “Synthesis, Photophysical Properties, and Laser Behavior of 3-Amino and 3-Acetamido BODIPY Dyes”, *Org. Lett.*, **2007**, *9*, 4183-4186.
- Liu, H.; Mack, J.; Guo, Q.; Lu, H.; Kobayashi, N.; Shen, Z. “A Selective Colorimetric and Fluorometric Ammonium Ion Sensor Based on the H-Aggregation of an Aza-BODIPY with Fused Pyrazine Rings”, *Chem. Commun.*, **2011**, *47*, 12092-12094.

- Loudet, A.; Bandichhor, R.; Burgess, K.; Palma, A.; McDonnell, S. O.; Hall, M. J.; O'Shea, D. F. "B,O-Chelated Azadipyrromethenes as Near-IR Probes", *Org. Lett.*, **2008**, *10*, 4771-4774.
- Loudet, A.; Burgess, K. "BODIPY Dyes and Their Derivatives: Syntheses and Spectroscopic Properties", *Chem. Rev.*, **2007**, *107*, 4891-4932 and references therein.
- Lovell, J. F.; Liu, T. W.; Chen, J.; Zheng, G. "Activatable Photosensitizers for Imaging and Therapy", *Chem. Rev.*, **2010**, *110*, 2839-2857.
- Lower, S. K.; El-Sayed, M. A. "The Triplet State and Molecular Electronic Processes in Organic Molecules", *Chem. Rev.*, **1966**, *66*, 199-241.
- Lu, H.; Shimizu, S.; Mack, J.; Shen, Z.; Kobayashi, N. "Synthesis and Spectroscopic Properties of Fused-Ring-Expanded Aza-Boradiazaindacenes", *Chem. Asian J.*, **2011**, *6*, 1026-1037.
- Lukyanov, A. N.; Gao, Z.; Mazzola, L.; Torchilin, V. P. "Polyethylene Glycoldiacyllipid Micelles Demonstrate Increased Accumulation in Subcutaneous Tumors in Mice", *Pharm. Res.*, **2002**, *19*, 1424-1429.
- Lv, P. C.; Sun, J.; Luo, Y.; Yang, Y.; Zhu, H. L. "Design, Synthesis, and Structure-activity Relationships of Pyrazole Derivatives as Potential FabH Inhibitors", *Bioorg. Med. Chem. Lett.*, **2010**, *20*, 4657-4660.
- Maeda, H. "Tumor-Selective Delivery of Macromolecular Drugs via the EPR Effect: Background and Future Prospects", *Bioconjug. Chem.*, **2010**, *21*, 797-802.
- Manassaram, D. M.; Backer, L. C.; Moll, D. M. "A Review of Nitrates in Drinking Water: Maternal Exposure and Adverse Reproductive and Developmental Outcomes", *Environ. Health Perspect.*, **2006**, *114*, 320-324.

- Maragos, C. M.; Morley, D.; Wink, D. A.; Dunams, T. M.; Saavedra, J. E.; Hoffman, A.; Bove, A. A.; Isaac, L.; Hrabie, J. A.; Keefer, L. K. "Complexes of NO with Nucleophiles as Agents for the Controlled Biological Release of Nitric Oxide. Vasorelaxant Effects", *J. Med. Chem.*, **1991**, *34*, 3242–3247.
- Mark, N.; Michael, S. P.; Brian, C. W. "Direct Near-infrared Luminescence Detection of Singlet Oxygen Generated by Photodynamic Therapy in Cells *In Vitro* and Tissues *In Vivo*", *Photochem. Photobiol.*, **2002**, *75*, 382–391.
- Marydasan, B.; Nair, A. K.; Ramaiah, D. "Optimization of Triplet Excited State and Singlet Oxygen Quantum Yields of Picolylamine–Porphyrin Conjugates Through Zinc Insertion", *J. Phys. Chem. B*, **2013**, *117*, 13515-13522.
- Mathai, S.; Smith, T. A.; Ghiggino, K. P. "Singlet Oxygen Quantum Yields of Potential Porphyrin-Based Photosensitisers for Photodynamic Therapy", *Photochem. Photobiol. Sci.*, **2007**, *6*, 995-1002.
- McClure, D. S. "Triplet-Singlet Transitions in Organic Molecules. Lifetime Measurements of the Triplet State", *J. Chem. Phys.*, **1949**, *17*, 905-913.
- McCulloch, I.; Heeney, M.; Bailey, C.; Genevicius, K.; Macdonald, I.; Shkunov, M.; Sparrowe, D.; Tierney, S.; Wagner, R.; Zhnag, W. M.; Chabiny, M. L.; Kline, R. J.; McGehee, M. D.; Toney, M. F. "Liquid-Crystalline Semiconducting Polymers with High Charge Carrier Mobility", *Nat. Mater.*, **2006**, *5*, 328-333.
- McDonnell, S. O.; Hall, M. J.; Allen, L. T.; Byrne, A.; Gallagher, W. M.; O'Shea, D. F. "Supramolecular Photonic Therapeutic Agents", *J. Am. Chem. Soc.*, **2005**, *127*, 16360-16361.
- McDonnell, S. O.; O'Shea, D. F. "Near-Infrared Sensing Properties of Dimethylamino-Substituted BF<sub>2</sub>-Azadipyromethenes", *Org. Lett.*, **2006**, *8*, 3493-3496.

- Meyers, I. A.; Nolen, R. L.; Collington, E. W.; Norwid T. A.; Strickland, R. C. "Total Synthesis of Camptothecin and Desethyldeoxycamptothecin", *J. Org. Chem.*, **1973**, *38*, 1974-1982.
- Min, J.; Ameri, T.; Gresser, R.; Lorenz-Rothe, M.; Baran, D.; Troeger, A.; Sgobba, V.; Leo, K.; Riede, M.; Guldi, D. M.; Brabec C. J. "Two Similar Near-Infrared (IR) Absorbing Benzannulated Aza-BODIPY Dyes as Near-IR Sensitizers for Ternary Solar Cells", *ACS Appl. Mater. Interfaces*, **2013**, *5*, 5609–5616.
- Mirenda, M.; Strassert, C. A.; Dicello, L. E.; Roman, E. S. "Dye-Polyelectrolyte Layer-by-Layer Self-Assembled Materials: Molecular Aggregation, Structural Stability, and Singlet Oxygen Photogeneration", *Appl. Mater. Interfaces*, **2010**, *2*, 1556-1560.
- Möller, S.; Perlov, C.; Jackson, W.; Taussig, C.; Forrest, S. F. A. "A Polymer/Semiconductor Write Once Read Many Times Memory", *Nature*, **2003**, *426*, 166-169.
- Monsma, F. J.; Barton, A. C.; Kang, H. C.; Brassard, D. L.; Haughland, R. P.; Sibley, D. R. "Characterization of Novel Fluorescent Ligands with High Affinity for D1 and D2 Dopaminergic Receptors", *J. Neurochem.*, **1989**, *52*, 1641-1644.
- Moorcroft, M. J.; Davis, J.; Compton, R. G. "Detection and Determination of Nitrate and Nitrite: A Review", *Talanta*, **2001**, *54*, 785-803.
- Morone, M.; Beverina, L.; Abbotto, A.; Silvestri, F.; Collini, E.; Ferrante, C.; Bozio, R.; Pagani, G. A. "Enhancement of Two-Photon Absorption Cross-Section and Singlet-Oxygen Generation in Porphyrins upon  $\beta$ -Functionalization with Donor–Acceptor Substituents", *Org. Lett.*, **2006**, *8*, 2719-2722.
- Mueller, T.; Gresser, R.; Leo, K.; Riede, M. "Organic Solar Cells Based on a Novel Infrared Absorbing Aza-BODIPY Dye", *Sol. Energy Mater. Sol. Cells*, **2012**, *99*, 176-181.

- Nasongkla, N.; Bey, E.; Ren, J.; Ai, H.; Khemtong, C.; Guthi, J. S.; Chin, S. F.; Sherry, A. D.; Boothman, D. A.; Gao, J. "Multifunctional Polymeric Micelles as Cancer-Targeted, MRI Ultrasensitive Drug Delivery Systems", *Nano Lett.*, **2006**, *6*, 2427–2430.
- Nemoto, M.; Kokubun, H.; Koizumi, M. "Determination of the S\*–T Transition Probabilities of Some Xanthene and Thiazine Dyes on the Basis of the T-Energy Transfer. I. Experiment in Ethanol Solutions", *Bull. Chem. Soc. Jpn.*, **1969**, *42*, 1223-1230.
- Oelgemoller, M.; Jung, C.; Ortner, J.; Mattay, J.; Zimmermann, E. "Green Photochemistry: Solar Photooxygenations with Medium Concentrated Sunlight", *Green Chem.*, **2005**, *7*, 35–38.
- Ogilby, P. R.; Foote, C. S. "Chemistry of Singlet Oxygen. 42. Effect of Solvent, Solvent Isotopic Substitution, and Temperature on the Lifetime of Singlet Molecular Oxygen ( $^1\Delta_g$ )", *J. Am. Chem. Soc.*, **1983**, *105*, 3423–3430.
- Ogilby, P. R. "Singlet oxygen: There is Indeed Something New Under the Sun", *Chem. Soc. Rev.*, **2010**, *39*, 3181–3209 and references therein.
- Oki, A. R.; Morgan, R. J. "An Efficient Preparation of 4, 4'-Dicarboxy-2, 2'-Bipyridine", *Synth. Commun.*, **1995**, *25*, 4093-4097.
- Orfanopoulos, M.; Smonou, I.; Foote, C. S. "Intermediates in the Ene Reactions of Singlet Oxygen and N-Phenyl-1,2,4-triazoline-3,5-dione with Olefins", *J. Am. Chem. Soc.*, **1990**, *112*, 3607–3614.
- Ozlem, S.; Akkaya, E. U. "Thinking Outside the Silicon Box: Molecular AND Logic As an Additional Layer of Selectivity in Singlet Oxygen Generation for Photodynamic Therapy", *J. Am. Chem. Soc.*, **2009**, *131*, 48-49.

- Palma, A.; Alvarez, L. A.; Scholz, D.; Frimannsson, D. O.; Grossi, M.; Quinn, S. J.; O'Shea D. F. "Cellular Uptake Mediated Off/On Responsive Near-Infrared Fluorescent Nanoparticles", *J. Am. Chem. Soc.*, **2011**, *133*, 19618–19621.
- Palmisano, G.; Augugliaro, V.; Pagliaro, M.; Palmisano, L. "Photocatalysis: A Promising Route for 21st Century Organic Chemistry", *Chem. Commun.*, **2007**, 3425-3437.
- Patrice, T. In *Photodynamic Therapy*, The Royal Society of Chemistry, *Vol 2*, **2003**.
- Peng, H.; Cheng, Y.; Dai, C.; King, A. L.; Predmore, B. L.; Lefer, D. J.; Wang, B. H. "A Fluorescent Probe for Fast and Quantitative Detection of Hydrogen Sulfide in Blood", *Angew. Chem., Int. Ed.*, **2011**, *50*, 9672-9675.
- Perkins, W. R.; Ahmad, I.; Li, X.; Hirsh, D. J.; Masters, G. R.; Fecko, C.J.; Lee, J.; Ali, S.; Nguyen, J.; Schupsky, J.; Herbert, C.; Janoff, A. S.; Mayhew, E. "Novel Therapeutic Nano-particles (lipocores): Trapping Poorly Water Soluble Compounds", *Int. J. Pharm.*, **2000**, *200*, 27–39.
- Peters, C.; Billich, A.; Ghobrial, M.; Hoegenauer, K.; Ullrich, T.; Nussbaumer, P. "Synthesis of Borondipyrrromethene (BODIPY)-Labeled Sphingosine Derivatives by Cross-metathesis Reaction", *J. Org. Chem.*, **2007**, *72*, 1842-1845.
- Protti, S.; Dondi, D.; Fagnoni, M.; Albini, A. "Photochemistry in Synthesis: Where, When, and Why", *Pure Appl. Chem.*, **2007**, *79*, 1929–1938.
- Pushpan, S. K.; Venkatraman, S.; Anand, V. G.; Sankar, J.; Parmeswaran, D.; Ganesan, S.; Chandrashekar, T. K. "Porphyrins in Photodynamic Therapy - a Search for Ideal Photosensitizers", *Curr. Med. Chem. - Anti-Cancer Agents*, **2002**, *2*, 187-207.
- Qian, Y.; Karpus, J.; Kabil, O.; Zhang, S.; Zhu, H.; Banerjee, R.; Zhao, J.; He, C. "Selective Fluorescent Probes for Live-Cell Monitoring of Sulphide", *Nat. Commun.*, **2011**, *2*, 495.

- Quimby, D. J.; Longo, F. R. "Luminescence Studies on Several Tetraarylporphins and Their Zinc Derivatives", *J. Am. Chem. Soc.*, **1975**, *97*, 5111-5117.
- Radford-Knaery, J.; Cutter, G. A. "Determination of Carbonyl Sulfide and Hydrogen Sulfide Species in Natural Waters Using Specialized Collection Procedures and Gas Chromatography with Flame Photometric Detection", *Anal. Chem.*, **1993**, *65*, 976-982.
- Ramaiah, D.; Joy, A.; Chandrasekhar, N.; Eldho, N. V.; Das, S.; George, M. V. "Halogenated Squaraine Dyes as Potential Photochemotherapeutic Agents. Synthesis and Study of Photophysical Properties and Quantum Efficiencies of Singlet Oxygen Generation", *Photochem. Photobiol.*, **1997**, *65*, 783-790.
- Randy, P. S.; Theresa, M. M.; Theodore, L.; Kristina, C. W.; Richard, E.; David, W. M. "Intersystem Crossing in Halogenated BODIPY Chromophores Used for Solar Hydrogen", *J. Phys. Chem. Lett.*, **2011**, *2*, 223-227.
- Ravelli, D.; Dondi, D.; Fagoni, M.; Albini, A. "Photocatalysis. A Multi-Faceted Concept for Green Chemistry", *Chem. Soc. Rev.*, **2009**, *38*, 1999-2011.
- Ribeiro, A. O.; Tome, J. P. C.; Neves, M. S.; Cavaleiro, J. A. S.; Iamamoto, Y.; Torres, T. "[1,2,3,4-Tetrakis( $\alpha/\beta$ -d-galactopyranos-6-yl)phthalocyaninato]zinc(II): A Water Soluble Phthalocyanines", *Tetrahedron Lett.*, **2006**, *47*, 9177-9180.
- Ribeiro, S.; Serra, A. C.; Rocha Gonsalves A. M. A. "Efficient Solar Photooxygenation with Supported Porphyrins as Catalysts", *ChemCatChem*, **2013**, *5*, 134-137.
- Richardson, C. J.; Magee, E. A. M.; Cummings, J. H. "A New Method for the Determination of Sulphide in Gastrointestinal Contents and Whole Blood by Microdistillation and Ion Chromatography", *Clin. Chim. Acta*, **2000**, *293*, 115-125.



- Rogers, M. A. T. "4-Diarylpyrroles. Part I. Synthesis of 2 : 4-Diarylpyrroles and 2 : 2' : 4 : 4'-Tetra-arylazadipyrromethines", *J. Chem. Soc.*, **1943**, 590-596.
- Rossi, L. M.; Silva, P. R.; Vono, L. L. R.; Fernandes, A. U.; Tada, D. B.; Baptista, M. S. "Protoporphyrin IX Nanoparticle Carrier: Preparation, Optical Properties, and Singlet Oxygen Generation", *Langmuir*, **2008**, *24*, 12534-12538.
- Rousseau, T.; Cravino, A.; Bura, T.; Ulrich, G.; Ziessel, R.; Roncali, J. "Multi-donor Molecular Bulk Heterojunction Solar Cells: Improving Conversion Efficiency by Synergistic Dye Combinations", *J. Mater. Chem.*, **2009**, *19*, 2298-2300.
- Rurack, K.; Spieles, M. "Fluorescence Quantum Yields of a Series of Red and Near-Infrared Dyes Emitting at 600–1000 nm", *Anal. Chem.*, **2011**, *83*, 1232–1242.
- Samtsov, M. P.; Tikhomirov, S. A.; Buganov, O. V.; Kaplevsky, K. N.; Melnikov, D. G.; Lyashenko, L. S. "Fast Photoprocesses in a Symmetric Indotricarbocyanine Dye (HITC) in Solutions", *Journal of Applied Spectroscopy*, **2009**, *76*, 783-790.
- Sathyamoorthi, G.; Soong, M.-L.; Ross, T. W.; Boyer, J. H., "Fluorescent Tricyclic  $\beta$ -Azavinamidine–BF<sub>2</sub> Complexes", *Heteroatom Chem.*, **1993**, *4*, 603–608.
- Schmidt, R. "Photosensitized Generation of Singlet Oxygen", *Photochem. Photobiol.*, **2006**, *82*, 1161-1177.
- Scott, W.; Davorin, P.; Honghua, H.; Lazaro, A. P.; Olga, V. P.; Artem, E. M.; Andriy, O. G.; Alexey, D. K.; Yurii, L. S.; Alexey, I. T.; Vladimir, V. K.; Olexander, O. V.; Emma, B.; Richard, L.; David, J. H.; Eric, W. V. S. "Near-Unity Quantum Yields for Intersystem Crossing and Singlet Oxygen Generation in Polymethine like Molecules: Design and Experimental Realization", *J. Phys. Chem. Lett.*, **2010**, *1*, 2354–2360.

- Sens, R.; Drexhage, K. H. "Fluorescence Quantum Yield of Oxazine and Carbazine Laser Dyes. *J. Luminesc.*, **1981**, *24*, 709-712.
- Sharman, W. M.; Allen, C. M.; Van Lier, J. E. "Photodynamic Therapeutics: Basic Principles and Clinical Applications", *Drug Discov. Today*, **1999**, *4*, 507-517.
- Shi, W.-J.; Menting, R.; Ermilov, E. A.; Lo, P.-C.; Röder, B.; Ng, D. K. P. "Formation and Photoinduced Processes of the Host-Guest Complexes of a  $\beta$ -cyclodextrin-Conjugated Aza-BODIPY and Tetrasulfonated Porphyrins", *Chem. Commun.*, **2013**, *49*, 5277-5279.
- Shimizu, S.; Iino, T.; Arakib, Y.; Kobayashi, N. "Pyrrolopyrrole Aza-BODIPY Analogues: A Facile Synthesis and Intense Fluorescence", *Chem. Commun.*, **2013**, *49*, 1621-1623.
- Skovsen, E. J.; Snyder, W.; Lambert, J. D. C.; Ogilby, P. R. "Lifetime and Diffusion of Singlet Oxygen in a Cell". *J. Phys. Chem. B*, **2005**, *109*, 8570-8573.
- Suchard, O.; Kane, R.; Roe, B. J.; Zimmermann, E.; Jung, C.; Waske, P. A.; Mattay, J.; Oelgemoller, M. "Photooxygenations of 1-Naphthols: An Environmentally Friendly Access to 1,4-Naphthoquinone", *Tetrahedron*, **2006**, *62*, 1467-1473.
- Takaguchi, Y.; Yanagimoto, Y.; Fujima, S.; Tsuboi S. "Photooxygenation of Olefins, Phenol, and Sulfide Using Fullerodendrimer as Catalyst", *Chemistry Letters*, **2004**, *33*, 1142-1143.
- Takechi, K.; Kamat, P. V.; Avirah, R. R.; Jyothish, K.; Ramaiah, D. "Harvesting Infrared Photons with Croconate Dyes", *Chem. Mater.*, **2008**, *20*, 265-272.
- Tanizawa, K. "Production of H<sub>2</sub>S by 3-Mercaptopyruvate Sulphurtransferase", *J. Biochem.*, **2011**, *149*, 357-359.

- Tasior, M.; Murtagh, J.; Frimannsson, D. O.; McDonnell, S. O.; O'Shea, D. F. "Water-Solubilised BF<sub>2</sub>-Chelated Tetraarylazadipyrromethenes", *Org. Biomol. Chem.*, **2010**, *8*, 522–525.
- Thomas, A. P.; Babu, P. S. S.; Nair, S. A.; Ramakrishnan, S.; Ramaiah, D.; Chandrashekar, T. K.; Srinivasan, A.; Pillai, M. R. "Meso-tetrakis(p-sulfonatophenyl)N-confused Porphyrin Tetrasodium Salt: A Potential Sensitizer for Photodynamic Therapy", *J. Med. Chem.*, **2012**, *55*, 5110–5120.
- Thomson, R. H. "Naturally Occurring Quinones IV: Recent Advances, 4<sup>th</sup> Edition", Blackie, London, UK, **1997**.
- Timothy, W. S.; Fuckel, B.; Roberts, D. A.; Yuen, Y. C.; Raphae, G. C.; Roland, B. P.; Ekins-Daukes, N. J.; Maxwell, J. C. "Singlet Oxygen Mediated Photochemical Upconversion of NIR Light", *J. Phys. Chem. Lett.*, **2011**, *2*, 966–971.
- Torchilin, V. P. "Micellar Nanocarriers: Pharmaceutical Perspectives", *Pharm. Res.*, **2007**, *24*, 1–16.
- Treibs, A.; Kreuzer, F. H. "Difluorboryl-Komplexe von Di- und Tripyrrylmethenen", *Liebigs Ann. Chem.*, **1968**, *718*, 208–223.
- Trieflinger, C.; Rurack, K.; Daub, J. "Turn ON/OFF your LOV light": Borondipyrromethene–Flavin Dyads as Biomimetic Switches Derived from the LOV Domain" *Angew. Chem., Int. Ed.*, **2005**, *44*, 2288–2291.
- Turfan, B.; Akkaya, E. U. "Modulation of Boradiazaindacene Emission by Cation-Mediated Oxidative PET", *Org. Lett.*, **2002**, *4*, 2857–2859.
- Turro, N. J. "Modern Molecular Photochemistry". **1978**, Benjamin/Cummings, Menlo Park, CA.

- Ulrich, G.; Ziessel, R.; Harriman, A. "The Chemistry of Fluorescent Bodipy Dyes: Versatility Unsurpassed", *Angew. Chem. Int. Ed.*, **2008**, *47*, 1184-1201 and references therein.
- United States Environmental Protection Agency, *National Primary Drinking Water Regulations: Contaminant Specific Fact Sheets, Inorganic Chemicals*, Consumer Version, Washington, DC, **1995**.
- Urano, Y.; Asanuma, D.; Hama, Y.; Koyama, Y.; Barrett, T.; Kamiya, M.; Nagano, T.; Watanabe, T.; Hasegawa, A.; Choyke, P. L.; Kobayashi, H. "Selective Molecular Imaging of Viable Cancer Cells with pH Activatable Fluorescence Probes", *Nat Med.*, **2009**, *15*, 104-109.
- Wainwright, M. in *Photosensitizers in Biomedicine*, Wiley-Blackwell, A John Wiley & Sons, Ltd. Publication, West Sussex, **2009**.
- Wainwright, M. "Photodynamic Therapy: The Development of New Photosensitisers. Anti-Cancer Agents", *Med. Chem.*, **2008**, *8*, 280– 291.
- Wakamatsu, T.; Nishi, T.; Ohnuma, T.; Ban, Y. "A Convenient Synthesis of Juglone Via Neutral Salcomine Oxidation", *Synth. Commun.*, **1984**, *14*, 1167-1173.
- Wan, C.-W.; Burghart, A.; Chen, J.; Bergstrom, F.; Johansson, L. B.-A.; Wolford, M. F.; Kim, T. G.; Topp, M. R.; Hochstrasser, R. M.; Burgess, K. "Anthracene–BODIPY Cassettes: Syntheses and Energy Transfer", *Chem. Eur. J.*, **2003**, *9*, 4430-4441.
- Wang, M.; Gartel, A. L. "Micelle-Encapsulated Thiostrepton as an Effective Nanomedicine for Inhibiting Tumor Growth and for Suppressing FOXM1 in Human Xenografts", *Mol. Cancer Ther.*, **2011**, *10*, 2287-2297.

- Wang, N.; Cao, X.; Cai, X.; Xu, Y.; Guo, L. "Porous Cuprite Films: Facile Solution Deposition and their Application for Nitrite Sensing", *Analyst*, **2010**, *135*, 2106-2110.
- Wories, H. J.; Koek, J. H.; Lodder, G.; Lugtenburg, J.; Fokkens, R.; Driessen, O.; Mohn, G. R., "A Novel Water-soluble Fluorescent Probe: Synthesis, Luminescence and Biological Properties of Sodium Salt of the 4-Sulfonato-3,3',5,5'-tetramethyl-2,2'-pyrromethen-1,1'-BF<sub>2</sub> Complex", *Recl. Trav. Chim. Pays-Bas.*, **1985**, *104*, 288-291.
- World Health Organization. *Guidelines for Drinking Water Quality: Incorporating 1st and 2nd Addenda, Vol.1, Recommendations – 3rd Ed.*, WHO Press, Geneva, Switzerland, **2008**.
- Wu, W.; Guo, H.; Wu, W.; Ji, S.; Zhao, J. "Organic Triplet Sensitizer Library Derived from a Single Chromophore (BODIPY) with Long-Lived Triplet Excited State for Triplet-Triplet Annihilation Based Upconversion", *J. Org. Chem.*, **2011**, *76*, 7056-7064.
- Wurm, G.; Geres, U. "Studies on 1,4-Naphthoquinones 10. Mitt. Reactions of Methyl Ethers of 1,5-Dihydroxynaphthalene with Singlet Oxygen", *Arch. Pharm. (Weinheim)*, **1985**, *318*, 931-937.
- Xiao, N.; Yu, C. "Rapid-Response and Highly Sensitive Noncross-Linking Colorimetric Nitrite Sensor Using 4-Aminothiophenol Modified Gold Nanorods", *Anal. Chem.*, **2010**, *82*, 3659-3663.
- Ye, D.; Luo, L.; Ding, Y.; Chen, Q.; Liu, X. "A Novel Nitrite Sensor Based on Graphene /polypyrrole/chitosan Nanocomposite Modified Glassy Carbon Electrode", *Analyst*, **2011**, *136*, 4563-4569.
- Yilmaz, M. D.; Bozdemir, O. A.; Akkaya, E. U. "Light Harvesting and Efficient Energy Transfer in a Boron-dipyrrin (BODIPY) Functionalized Perylenediimide Derivative", *Org. Lett.*, **2006**, *8*, 2871-2873.

- Yuster, P.; Weissman, S. I. "Effects of Perturbations on Phosphorescence: Luminescence of Metal Organic Complexes", *J. Chem. Phys.*, **1949**, *17*, 1182.
- Zen, J. M.; Liou, S. L.; Kumar, A. S.; Hsia, M. S. "An Efficient and Selective Photocatalytic System for the Oxidation of Sulfides to Sulfoxides", *Angew. Chem. Int. Ed.*, **2003**, *42*, 577–579.
- Zhang, X.; Zhang, H. -S. "Design, Synthesis and Characterization of a Novel Fluorescent Probe for Nitric Oxide Based on Difluoroboradiaza-s-indacene Fluorophore", *Spectrochim. Acta, Part A*, **2005**, *61*, 1045–1049.
- Zhang, X.; Yu, H.; Xiao Y. "Replacing Phenyl Ring with Thiophene: An Approach to Longer Wavelength Aza-dipyrromethene Boron Difluoride (Aza-BODIPY) Dyes", *J. Org. Chem.*, **2012**, *77*, 669–673.
- Zhao, W.; Carreira, E. M. "Conformationally Restricted Aza-BODIPY: A Highly Fluorescent, Stable, Near-Infrared-Absorbing Dye", *Angew. Chem. Int. Ed.*, **2005**, *44*, 1677 –1679.
- Zhao, W.; Carreira, E. M. "Conformationally Restricted Aza-BODIPY: Highly Fluorescent, Stable Near-Infrared Absorbing Dyes", *Chem. Eur. J.*, **2006**, *12*, 7254–7263.
- Ziessel, R.; Goze, C.; Ulrich, G.; Cesario, M.; Retailleau, P.; Harriman, A.; Rostron J. P. "Intramolecular Energy Transfer in Pyrene–BODIPY Molecular Dyads and Triads", *Chem. Eur. J.*, **2005**, *11*, 7366 – 7378.
- Ziessel, R.; Ulrich, G.; Harriman, A.; Alamiry, M. A. H.; Stewart, B.; Retailleau P. "Solid-State Gas Sensors Developed from Functional Difluoroboradiaza-indacene Dyes", *Chem. Eur. J.*, **2009**, *15*, 1359–1369.

## LIST OF PUBLICATIONS AND PATENTS

1. Sensitive Naked Eye Detection of Hydrogen Sulfide (H<sub>2</sub>S) and Nitric Oxide (NO) by Aza-BODIPY Dyes in Aqueous Medium, **N. Adarsh**, M. S. Krishnan and D. Ramaiah, *Anal. Chem.* **2014**, *86*, 9335–9342 (**IF: 5.825**).
2. Efficient Reaction Based Colorimetric Probe for Sensitive Detection, Quantification, and On-Site Analysis of Nitrite Ions in Natural Water Resources, **N. Adarsh**, M. Shanmugasundaram and D. Ramaiah, *Anal. Chem.* **2013**, *85*, 10008–10012 (**IF: 5.825**).
3. Aza-BODIPY Derivatives: Enhanced Quantum Yields of Triplet Excited State and Singlet Oxygen Generation and their Role as Facile Green Photooxygenation Catalyst, **N. Adarsh**, M. Shanmugasundaram, R. R. Avirah and D. Ramaiah, *Chem. Eur. J.* **2012**, *18*, 12655-12662 (**Highlighted as Cover Page of the Journal- IF: 5.696**).
4. Squaraine Dyes in PDT: From Basic Design to *In Vivo* Demonstration, R. R. Avirah, D. T. Jayaram, **N. Adarsh** and D. Ramaiah, *Org. Biomol. Chem.* **2012**, *10*, 911-920 (**Highlighted as Hot Perspective Research Article-IF: 3.568**).
5. Tuning the Photosensitized Singlet Oxygen Generation of Aza- BODIPY Dyes, **N. Adarsh**, R. R. Avirah and D. Ramaiah, *Org. Lett.* **2010**, *12*, 5720–5723 (**IF: 6.324**).
6. A Novel Aza BODIPY Derivative for the Selective Detection of Nitrite ions in Water: A Process Thereof and its Application in Waste Water Management, D. Ramaiah, **N. Adarsh**, M. Shanmugasundaram, Patent No. PCT/IN2014/000067, WO2014/115176, **2014**.
7. Aza-BODIPY-DSPE Nano Medicine for Photodynamic Therapy: *In Vitro* Demonstration of Apoptosis Mediated Cell Death, **N. Adarsh**, P. S. Saneesh Babu, R. R. Avirah, S. A. Nair, M. R. Pillai and D. Ramaiah, *ACS Nano*, **2015** (Communicated).
8. A Green and Sustainable Aza-BODIPY Catalyst for the Oxidation of Naphthols, Thioanisoles and Furans, **N. Adarsh** and D. Ramaiah (To be communicated).
9. Aza-BODIPY Dyes: Unveiling the “Hidden” Versatility, **N. Adarsh**, R. R. Avirah, M. Shanmugasundaram and D. Ramaiah ( Review article under preparation).

## PAPERS/POSTERS PRESENTED IN CONFERENCE PROCEEDINGS

1. “Aza-BODIPY Dyes: Novel Optical Probes for H<sub>2</sub>S and Nitrite Ions”, **N. Adarsh**, M. Shanmugasundaram and D. Ramaiah, A **Paper** Presented at the *10<sup>th</sup> JNC Research Conference on Chemistry of Materials*, Trivandrum, Kerala, India, **2014**, October 11–13 (**Received Best Oral Presentation Award**).
2. “Aza-BODIPY Dyes: Versatile Optical Chemodosimeters for Selective Detection and Analysis of NO<sub>2</sub><sup>-</sup> & H<sub>2</sub>S in Aqueous Medium”, **N. Adarsh**, M. Shanmugasundaram and D. Ramaiah, A **Poster** Presented at the *8<sup>th</sup> Asian Photochemistry Conference (APC-2014)*, Trivandrum, Kerala, India, **2014**, November 10–13.
3. “Efficient Reaction Based Colorimetric Probe for Sensitive Detection, Quantification, and On-Site Analysis of Nitrite Ions in Natural Water Resources”, **N. Adarsh**, M. Shanmugasundaram and D. Ramaiah, A **Poster** Presented at the *16<sup>th</sup> CRSI National Symposium in Chemistry (NSC-16)*, IIT Bombay, Mumbai, India, **2014**, February 07–09.
4. “Aza-BODIPY Dyes: Novel Sensitizers for Singlet Oxygen Generation”, **N. Adarsh**, M. Shanmugasundaram, R. R. Avirah and D. Ramaiah, A **Paper** Presented at the *8<sup>th</sup> JNC Research Conference on Chemistry of Materials*, Trivandrum, Kerala, India, **2012**, October 01–03.